Semi-active SOBEN suspensions modeling and control

Sébastien Aubouet

Institut National Polytechnique de Grenoble

No. attribué par la bibliothèque

THESE

pour obtenir le grade de

DOCTEUR de l'Université de Grenoble

délivré par l'Institut polytechnique de Grenoble

Spécialité : **AUTOMATIQUE-PRODUCTIQUE**

préparée au GIPSA-lab, Département automatique

dans le cadre de l'École Doctorale :
Électronique, Électrotechnique, Automatique, Traitement du Signal

présentée et soutenue publiquement

par

Sébastien AUBOUET

le 25 Octobre 2010

Modélisation et commande de suspensions semi-actives SOBEN

JURY :

Président:	Michel BASSET
Rapporteurs:	Sergio SAVARESI
	Xavier MOREAU
Examinateurs:	Brigitte d'ANDREA-NOVEL
	Ricardo RAMIREZ-MENDOZA
	Benjamin TALON
Directeurs de thèse:	Luc DUGARD
	Olivier SENAME

Contents

Remerciements

Je tiens tout d'abord à remercier mes directeurs de thèse, Olivier Sename et Luc Dugard, pour leur disponibilité, leur aide et leur suivi régulier, sans lesquels cette thèse n'aurait pas pu se dérouler aussi bien.

Je remercie particulièrement Benjamin Talon, le PDG de SOBEN, pour la liberté et la confiance qu'il m'a accordées pendant trois ans, malgré les contraintes très fortes liées à l'activité de l'entreprise. Sans cela, la collaboration entre SOBEN et le laboratoire aurait été bien plus difficile et bien moins intéressante.

Je tiens également à exprimer ma gratitude pour ma famille, qui a fait l'effort de traverser le pays pour la soutenance, et qui m'a toujours soutenu et aidé.

Je souhaite également remercier chaleureusement mon grand ami, Cyril, pour son soutien, pour m'avoir logé, pour avoir cuisiné et fait la vaisselle pendant que je lisais Le Figaro. Sans toi, je ne sais même pas où j'aurais logé, ni ce que j'aurais mangé! Tous ces bons moments ne peuvent jamais s'oublier. Je n'oublie pas non plus les bons moments passés avec Sylvain au labo, ses petites visites-éclairs, cherchant désespérément son directeur de thèse, et les séances de dégustation au restaurant universitaire en sa compagnie, ça n'est jamais bien triste!

Je remercie également Mehdi, pour son aide dans la réalisation des essais, et le temps qu'il m'a fait gagner avec ses cartes électroniques qui marchent du premier coup! Enfin, je dois bien reconnaître que Corentin et Charles m'ont apporté une aide précieuse, et de nombreux conseils utiles, pour la programmation comme pour la rédaction de la thèse. Merci pour tes librairies Charles, qui m'ont évité des heures de programmation fastidieuse!

Je remercie mes collègues mexicains, Aline, Ricardo et Jorge, car ils m'ont accueilli chaleureusement, aidé à trouver un logement, aidé à découvrir les bons restaurants ou bien les bars les plus intéressants! Grâce à vous j'ai pu tout simplement découvrir, comprendre et apprécier votre pays d'une manière unique. Il m'est impossible de l'oublier.

Enfin, je remercie tout le personnel du GIPSA-lab, Marie-Thérèse, Virginie, Daniel, et Patricia.

Notations

$\mathbb{R}$	Field of real numbers
$\mathbb{C}$	Field of complex numbers
M^*	Complex transpose conjugate of $M \in \mathbb{C}$
M^T	Transpose of $M \in \mathbb{R}$
M^+	Moore-Penrose pseudoinverse matrix of M
$\sigma(M)$	Singular values of M
j	Imaginary unit
$*$	Symmetric element in a given matrix
$\mathcal{R}e(.)$	Real part of a complex number
$\mathcal{I}m(.)$	Imaginary part of a complex number
$\det(M)$	Determinant of the square matrix M
$rank(M)$	Rank of the matrix M
$Tr(M)$	Trace of the square matrix M
$\otimes$	Kronecker product
$M \prec (\preceq)$	Matrix M is symmetric and negative (semi-)definite
$M \succ (\succeq)$	Matrix M is symmetric and positive (semi-)definite
$\mathcal{I}_i$	Identity matrix of dimension (i, i)
$\mathcal{O}_{i,j}$	Null matrix of dimension (i, j)
s	Laplace variable
LTI	Linear Time Invariant
LPV	Linear Parameter Varying
LMI	Linear Matrix Inequality
BMI	Bilinear Matrix Inequality
SDP	Semi-Definite Programming
DOF	Degree Of Freedom
COG	Center Of Gravity
iff.	if and only if
UIO	Unknown Input Observer
w.r.t.	with respect to
s.t.	such that
resp.	respectively

List of Figures

List of Tables

Chapter 1

Résumé

1.1 Introduction

Les suspensions semi-actives sont des suspensions dont l'amortissement est réglable par le biais d'un actionneur. Ce type de suspensions fait l'objet de nombreuses études depuis plusieurs années, tant dans la recherche académique que dans la recherche industrielle, car elles sont à la fois moins coûteuses et moins consommatrices d'énergie que les suspensions actives, et plus performantes que les suspensions passives. Plusieurs stratégies de commande ont déjà été développées dans de précédentes études pour piloter ce type de suspension. Cependant, le nombre et le coût des capteurs nécessaires, ainsi que les technologies d'actionneurs utilisées, ont précédemment limité l'utilisation de ce type d'amortisseurs aux véhicules haut de gamme.

Les constructeurs automobiles se sont récemment focalisés sur le développement de ce type de suspensions, grâce à une demande de plus en plus forte de performances, de confort et de sécurité très élevés, mais également grâce aux progrès de l'électronique et de l'automatique. Ainsi, en quelques années les systèmes électroniques de contrôle sont devenus omniprésents dans les véhicules automobiles. Cette thèse s'inscrit dans cette tendance, puisqu'elle consiste à piloter, par des lois de commandes automatiques, les suspensions conçues par SOBEN, afin d'améliorer leurs performances en termes de confort et de tenue de route.

De nombreuses stratégies de commande de suspensions actives ont été développées par le passé, tant dans le milieu académique qu'industriel. Cependant, lorsqu'elles sont appliquées sans modification à des suspensions semi-actives, ni les performances, ni la stabilité ne peuvent être garanties, et les résultats sont imprévisibles. Il est donc nécessaire de prendre en compte les limitations dues aux actionneurs de suspensions directement dans la synthèse afin de concevoir des stratégies de commandes semi-actives adaptées

aux suspensions telles que celle développée par SOBEN. Il s'agit de l'un des objectifs majeurs de cette thèse.

D'autre part, quelques stratégies de commande semi-actives ont récemment été développées pour améliorer le confort et la tenue de route. Cependant, de nombreuses mesures, parfois très difficiles à réaliser, ainsi qu'une connaissance très pointue du modèle sont nécessaires. L'un des enjeux majeurs pour les constructeurs automobiles et les équipementiers comme SOBEN, concerne donc le choix des mesures à réaliser, l'emplacement des capteurs et la réduction du nombre de capteurs nécessaires, afin d'obtenir un système dont la mise en œuvre est possible sur des véhicules de série bon marché.

Les objectifs de la stratégie de commande des suspensions peuvent être résumés ainsi:

- améliorer le confort et la tenue de route du véhicule,
- prendre en compte les limitations des actionneurs,
- être robuste vis-à-vis des non linéarités et des variations paramétriques telles que la variation des masses, des raideurs des pneumatiques, ou le bruit de mesure,
- être réglable en fonction des performances attendues par le conducteur,
- être adaptable à toutes les technologies d'amortisseurs,
- utiliser un nombre réduit de capteurs,
- permettre aux constructeurs automobiles d'adapter facilement la loi de commande en fonction des capteurs disponibles,
- être implantable dans une application temps réel embarquée utilisant des micro-contrôleurs bon marché.

Objectifs et contribution:

Cette thèse synthétise le travail de trois années, réalisé en collaboration avec le département automatique du GIPSA-lab (équipe S. L. R.), et l'entreprise SOBEN, qui conçoit et fabrique des amortisseurs entre-autres semi-actifs. Ce travail vise d'une part à développer des méthodologies de commande de suspensions, et d'autre part à faire bénéficier l'entreprise de différents résultats issus du milieu académique. La contribution repose essentiellement sur les deux aspects suivants:

- synthèse d'observateurs pour l'estimation de modèles de véhicules:

une méthodologie de synthèse d'observateurs est proposée dans un premier temps, permettant d'estimer des variables du véhicules non mesurées ou non mesurables. La méthode de mise au point permet en outre de considérer lors de la synthèse, les contraintes pratiques liées à la mise en œuvre du contrôleur, notamment en termes de placement de pôles,

- conception de lois de commandes adaptées aux suspensions semi-actives:

  une stratégie de commande de suspensions semi-actives de type LPV (Linéaire à Paramètres Variants) est développée pour contrôler les quatre suspensions du véhicule. Grâce à une loi d'adaptation appropriée, le contrôleur génère directement une commande semi-active prenant en compte les limitations de l'amortisseur telles que sa plage d'effort ou sa bande passante. La méthodologie proposée permet de construire des lois de commande facilement implantables et adaptées à tous les types de suspensions semi-actives, proportionnelles ou ON/OFF.

L'enjeu principal pour SOBEN concerne le développement d'un amortisseur hydraulique haute performance à coût réduit, par rapport notamment aux amortisseurs semi-actifs magnéto-rhéologiques de la concurrence. Les programmes et librairies issus de ce travail de thèse fournissent à l'entreprise les moyens de concevoir simplement et efficacement des stratégies de commande et d'estimation adaptées à ses technologies.

1.2 Modélisation du véhicule

Dans un premier temps, les différentes ressources matérielles utilisées sont présentées, ainsi que les essais réalisés. Enfin, les différents modèles de véhicules et d'amortisseurs utilisés dans la suite de cette thèse pour la synthèse d'observateurs et de contrôleurs sont présentés.

1.2.1 Ressources matérielles et essais

SOBEN utilise plusieurs bancs d'essais et cartes électroniques pour étudier et contrôler le comportement des amortisseurs. Ces équipements ont été utilisés pour étudier le comportement des amortisseurs et tester certaines lois de commande.

Banc d'essais pour amortisseur

Ce banc d'essais, représenté sur la Figure 1.1 est composé d'un vérin hydraulique piloté par un PC et une carte d'acquisition/contrôle. Différents types de signaux, tels que

des déplacements sinusoïdaux, peuvent être appliqués à l'amortisseur afin d'étudier son comportement. L'effort et le débattement sont mesurés et enregistrés.

Figure 1.1: Banc d'essais

Prototypes d'amortisseurs semi-actifs

Quatre prototypes d'amortisseurs semi-actifs ont été construits par SOBEN et montés sur un véhicule d'essais. Ces amortisseurs peuvent être contrôlés par le biais d'une servovalve qui permet le réglage du débit d'huile interne de chaque amortisseur, et par conséquence, celui de l'amortissement. La Figure 1.2 représente un amortisseur avant, installé sur le véhicule d'essais (Renault Laguna GT).

Véhicule d'essais

Ce véhicule a été équipé de sept accéléromètres permettant de mesurer trois des quatre accélérations verticales de la caisse au niveau des suspensions, ainsi que les quatre accélérations verticales des masses non suspendues. Les mesures disponibles et les capteurs

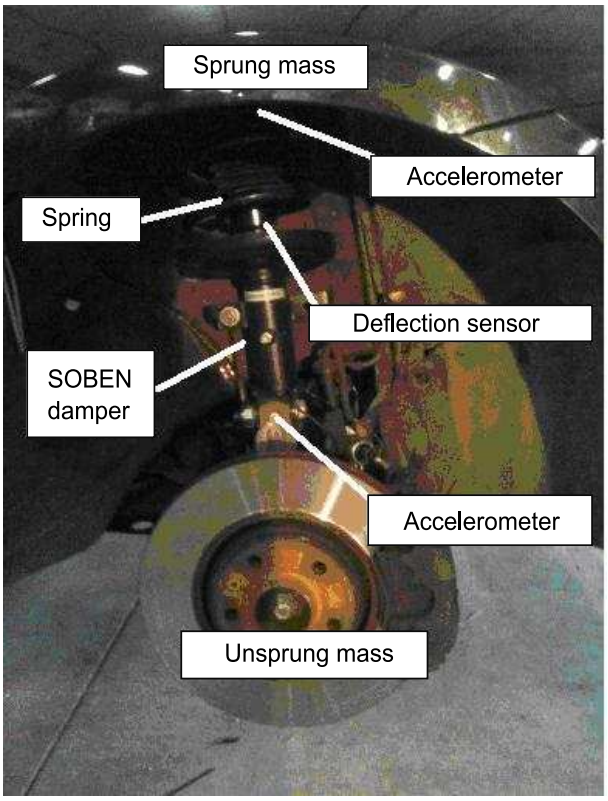

Figure 1.2: Nouvel amortisseur semi-actif SOBEN

sont donnés dans le Tableau 1.1. Ces mesures sont utilisées en ligne pour la commande-estimation du châssis.

Notation	Description	Plage
$\ddot{z}_{us_1}$	Accélération masse non suspendue avant gauche	+/- 50g
$\ddot{z}_{us_2}$	Accélération masse non suspendue avant droite	+/- 50g
$\ddot{z}_{us_3}$	Accélération masse non suspendue arrère gauche	+/- 50g
$\ddot{z}_{us_4}$	Accélération masse non suspendue arrère droite	+/- 50g
$\ddot{z}_{s_1}$	Accélération masse suspendue avant gauche	+/- 5g
$\ddot{z}_{s_2}$	Accélération masse suspendue avant droite	+/- 5g
$\ddot{z}_{s_3}$	Accélération masse suspendue arrère gauche	+/- 5g
$z_{def_1} = z_{s_1} - z_{us_1}$	Débattement de la suspension avant gauche	0-20cm
$z_{def_2} = z_{s_2} - z_{us_2}$	Débattement de la suspension avant droite	0-20cm
$z_{def_3} = z_{s_3} - z_{us_3}$	Débattement de la suspension arrière gauche	0-20cm
$z_{def_4} = z_{s_4} - z_{us_4}$	Débattement de la suspension arrière droite	0-20cm
F_i, $i = 1, .., 4$	Force produite par les amortisseurs	Confidentiel

Table 1.1: Véhicule d'essais: variables mesurées et capteurs

Cartes d'acquisition et de commande

L'acquisition des mesures présentées ci-dessus, est réalisée par un ensemble de quatre cartes déportées, installées au niveau de chaque amortisseur, ainsi que d'une carte centrale, communiquant les unes avec les autres par l'intermédiaire d'un bus de terrain CAN[1].

Essais réalisés

Le matériel présenté dans la section précédente a été utilisé pour réaliser les essais suivants:

- Essais 1-2: L'amortisseur semi-actif SOBEN a été soumis à différents débattements sinusoïdaux d'amplitude et de fréquence variables grâce au banc d'essais, pour une tension de commande constante minimale et maximale, afin de déterminer la plage de variation complète de l'amortisseur.
- Essai 3: Les essais précédents on été effectués pour différentes valeurs intermédiaires constantes de la commande. Ces essais seront utilisés par la suite pour modéliser l'influence de la commande sur le fonctionnement de l'amortisseur.
- Essai 4: L'amortisseur a été soumis à un déplacement en rampe et à un échelon de commande, afin de mesurer son temps de réponse.
- Essai 5: L'amortisseur étant toujours soumis à des déplacements en rampe, une commande sinusoïdale d'amplitude constante et de fréquence croissante lui a été appliquée. L'atténuation de l'effort produit permet de calculer sa bande passante.

1.2.2 Modèles d'amortisseurs

Dans cette section, un modèle d'amortisseur, donné par l'Équation (1.2.1), est identifié à partir des essais décrits précédemment. Ce modèle simplifié statique permet de modéliser les non linéarités de l'amortisseur ainsi que son comportement hystérétique. Il permet de modéliser aussi bien un amortisseur continument variable qu'un amortisseur ON/OFF. De plus, sa simplicité le rend facilement utilisable dans une application temps réel embarquée.

$$F_c = (A_1 u_d + A_2)\tanh(A_3 v + A_4 x) + A_5 v + A_6 x + A_7 \tag{1.2.1}$$

[1] Controller Area Network

où F_c est la force produite par l'amortisseur, x le débattement, v la vitesse de débattement, $u_d \in [-1, 1]$ le signal de commande, et les coefficients A_j, $j \in [1, 7]$ sont les paramètres identifiés.

Ce modèle permet de donner l'effort produit par l'amortisseur en fonction du débattement et de la vitesse de débattement. Cependant, le comportement dynamique de l'actionneur n'est pas pris en compte. Les résultats des essais 4 et 5 ont été utilisés pour modéliser le comportement dynamique de l'amortisseur. La réponse de l'amortisseur à un échelon de commande, obtenue dans l'Essai 4, montre que le système se comporte comme un système linéaire du second ordre G_d, d'entrée I et de sortie F, l'effort produit par l'amortisseur. En complétant le modèle (1.2.1), on obtient le modèle d'amortisseur (1.2.2) qui représente à la fois les comportements statiques et dynamiques.

$$\begin{cases} F(t) &= (A_1 u_d + A_2)\tanh(A_3 v + A_4 x) + A_5 v + A_6 x + A_7 \\ \dfrac{I(s)}{u_d(s)} &= \dfrac{G}{\left(\dfrac{s}{\omega_d}\right)^2 + 2m_d\dfrac{s}{\omega_d} + 1} \end{cases} \tag{1.2.2}$$

où $I(s)$ est le courant dans l'amortisseur, u_d est la tension de commande de l'amplificateur, $F(t)$ est la force fournie par l'amortisseur, $x = x(t)$ est le débattement, $v(t)$ est la vitesse de débattement, $\omega_d = 12$Hz est la bande passante de l'amortisseur, m_d =0.6 est le coefficient d'amortissement, et les coefficients A_j, $j \in [1, 7]$ sont les paramètres du modèle identifié.

1.2.3 Modèle de véhicule

Dans cette partie, nous présentons un modèle de véhicule complet vertical à 7 degrés de liberté. Ce modèle, représenté sur la Figure 1.3, a été utilisé pour la synthèse des contrôleurs et observateurs développés dans la suite.

Les équations de ce modèle de véhicule sont données par (1.2.3) et (1.2.4).

$$\begin{cases} m_s\ddot{z}_s &= -(F_{s_1} + F_{s_2} + F_{s_3} + F_{s_4} + F_z) \\ m_{us_1}\ddot{z}_{us_1} &= (F_{s_1} - F_{t_1}) \\ m_{us_2}\ddot{z}_{us_2} &= (F_{s_2} - F_{t_2}) \\ m_{us_3}\ddot{z}_{us_3} &= (F_{s_3} - F_{t_3}) \\ m_{us_4}\ddot{z}_{us_4} &= (F_{s_4} - F_{t_4}) \\ I_x\ddot{\theta} &= (F_{s_1} - F_{s_2})t_f + (F_{s_3} - F_{s_4})t_r + M_x \\ I_y\ddot{\phi} &= (F_{s_4} + F_{s_3})l_r - (F_{s_2} + F_{s_1})l_f + M_y \end{cases} \tag{1.2.3}$$

Les forces verticales produites par les suspensions et les pneus sont données par

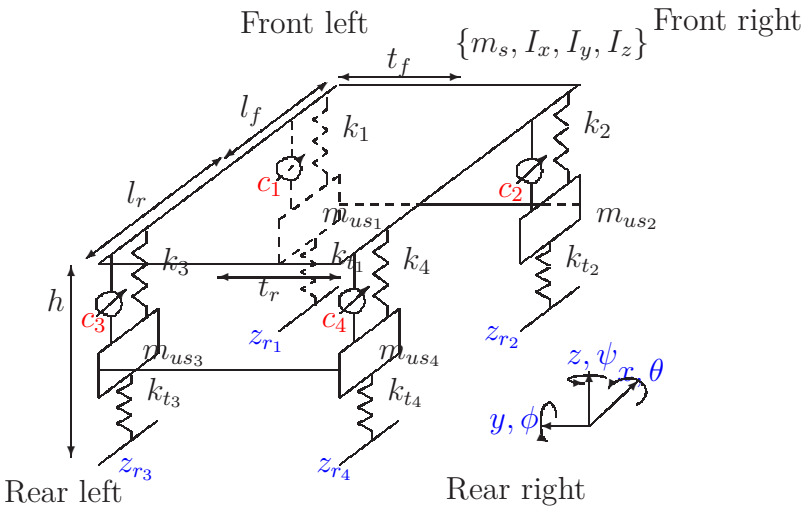

Figure 1.3: Modèle de véhicule complet vertical à 7 DDL

l'Équation (1.2.4), où u_i est la force supplémentaire devant être fournie par l'amortisseur i en plus de la force nominale $c_i \cdot (\dot{z}_{s_i} - \dot{z}_{us_i})$.

$$\begin{cases} F_{si} &= k_i \cdot (z_{s_i} - z_{us_i}) + c_i \cdot (\dot{z}_{s_i} - \dot{z}_{us_i}) + u_i \\ F_{ti} &= k_{t_i} \cdot (z_{us_i} - z_{r_i}) \end{cases} \tag{1.2.4}$$

Les modèles d'amortisseur et de véhicule présentés dans cette partie seront utilisés dans la suite pour synthétiser des contrôleurs et observateurs afin d'améliorer les performances du véhicule.

1.3 Méthodologie pour la synthèse d'observateurs

L'objectif principal de ce chapitre est d'estimer les variables d'état du modèle de véhicule complet vertical décrit dans la section précédente, afin de piloter les suspensions du véhicule. L'observateur doit permettre au constructeur automobile de réduire le nombre de capteurs et de choisir les grandeurs mesurées ainsi que l'emplacement des capteurs. Une méthodologie complète est donc proposée pour adapter au mieux l'observateur en fonction des contraintes industrielles, ce qui constitue la contribution principale de ce chapitre. Ici, les mesures données sont celles utilisées par l'observateur.

Notons que l'approche proposée dans cette partie, pour la synthèse d'observateurs à entrée inconnue est très générale et peut être utilisée pour un grand nombre de systèmes. Elle permet d'obtenir un découplage parfait ou approché, entre l'erreur d'estimation et l'entrée inconnue (perturbation due aux irrégularités du sol). De plus, une méthode de placement de pôles [Chilali et al., 1999] est proposée pour que les contraintes liées à

la mise en œuvre du contrôleur puissent être prises en compte lors de la synthèse de l'observateur.

1.3.1 Définition du problème

Considérons le système (1.3.1) à observer, représentant le modèle de véhicule présenté précédemment.

$$\begin{cases} \dot{x} = A \cdot x + D_x \cdot v \\ y = C \cdot x + D_y \cdot v \end{cases} \tag{1.3.1}$$

où x est le vecteur d'état, v la perturbation du sol, y les mesures.

La structure choisie pour l'observateur est la suivante:

$$\begin{cases} \dot{z} = N \cdot z + L \cdot y \\ \hat{x} = z - E \cdot y \end{cases} \tag{1.3.2}$$

où $z \in \mathbb{R}^{n \times n}$ représente le vecteur d'état de l'observateur, et $\hat{x} \in \mathbb{R}^{n \times n}$ les états estimés.

En définissant les matrices $P = \mathcal{I}_n + EC$ et $K = L + NE$, l'erreur d'estimation est régie par:

$$\begin{aligned} \dot{e} &= \dot{x} - \dot{\hat{x}} \\ &= Ne + (PA - KC - N)x + (PD_x - LD_y)v + ED_y\dot{v} \end{aligned} \tag{1.3.3}$$

Ainsi l'estimé $\hat{x}$, converge asymptotiquement vers l'état x du système si et seulement si les conditions suivantes sont satisfaites:

Stabilité:

$$\begin{cases} N \text{ is Hurwitz} \\ N = PA - KC \end{cases} \tag{1.3.4}$$

Découplage de la perturbation:

$$\begin{cases} LD_y - PD_x = 0 \\ ED_y = 0 \end{cases} \tag{1.3.5}$$

La synthèse de l'observateur implique donc le calcul des matrices N, L et E vérifiant, si possible, les conditions de découplage et de stabilité. Cependant ces conditions ne sont pas suffisantes d'un point de vue pratique. En effet, l'observateur calculé peut ne pas être utilisable en pratique, à cause de dynamiques trop rapides, ou bien si les pôles sont en limite de stabilité. Ainsi, des contraintes concernant le placement des pôles doivent être prises en compte, si possible lors de la synthèse, pour éviter de tels problèmes, c'est l'objectif de la méthodologie proposée dans la suite de cette étude.

Definition 1.3.1 (*Observateur exact et $\mathcal{H}_\infty$*)

Un observateur d'état d'ordre plein de la forme (1.3.2) est appelé,

- *un observateur exact si N, L et E sont solutions de (1.3.4) et (1.3.5). Dans de cas, un découplage exact est obtenu puisque les états estimés ne dépendent pas de la perturbation.*
- *un observateur $\mathcal{H}_\infty$ si N, L et E sont obtenus par minimisation de l'influence de la perturbation sur les états estimés, i.e. le problème (1.3.6) a été résolu,*

$$\min \gamma_\infty \; s.\; t.\; ||e||_2 < \gamma_\infty \cdot ||v||_2 \tag{1.3.6}$$

Dans ce chapitre, les conditions d'existence de l'observateur exact, définies ci-dessus, sont analysées et rappelées, afin d'obtenir un découplage exact entre la perturbation inconnue et les états estimés. Puis, une solution est proposée pour obtenir ce découplage approché lorsque les conditions de découplage parfait ne sont pas vérifiées, ou bien lorsque l'observateur exact calculé possède des pôles inadaptés compromettant la mise en œuvre ou l'efficacité en pratique. Le découplage de cette perturbation est approché par minimisation de la norme $\mathcal{H}_\infty$ du transfert (1.3.7) entre la perturbation inconnue et les états estimés, ce qui correspond au problème (1.3.6).

$$\dot{e} \;=\; Ne + (PA - KC - N)x + (PD_x - LD_y)v + ED_y\dot{v} \tag{1.3.7}$$

De plus, la méthode décrite pour la synthèse d'un observateur $\mathcal{H}_\infty$, permet de spécifier une région où les pôles de l'observateur doivent être situés. Cette région, représentée sur la Figure 1.4, est l'intersection de deux demi-plans permettant de borner la partie réelle des pôles p $(\mathcal{R}](p) \in [-p_{max}, -p_{min}]$, et d'un cône de demi-angle θ et centré en 0, permettant de borner la partie imaginaire des pôles.

1.3.2 Solution

La procédure pour le calcul de l'observateur est synthétisée par la proposition suivante:

Proposition:

Considérons le système (1.3.1) et l'observateur (1.3.2). Etant donné un scalaire positif

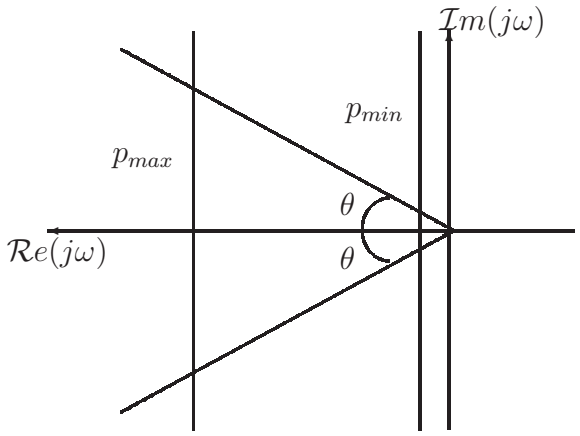

Figure 1.4: LMI regions in complex plane

γ_∞, s'il existe $\mathbf{X} = \mathbf{X}^T \succ 0$, $\tilde{\mathbf{Y}} = \mathbf{XY}$ vérifiant les inégalités (1.3.8), (1.3.9) et (1.3.10),

$$\begin{pmatrix} \mathcal{M}_{11} & \mathcal{M}_{12} & \mathcal{M}_{13} \\ * & \mathcal{M}_{22} & \mathcal{M}_{23} \\ * & * & \mathcal{M}_{33} \end{pmatrix} \prec 0 \tag{1.3.8}$$

$$\begin{pmatrix} Q\Psi_1 + \Psi_1^T Q^T + 2p_{min}\mathbf{X} & Q\Psi_2 & \mathcal{I}_n \\ * & -\gamma_\infty \mathcal{I}_d & \mathcal{O}_{d,n} \\ * & * & -\gamma_\infty \mathcal{I}_n \end{pmatrix} \prec 0 \tag{1.3.9}$$

$$\begin{pmatrix} -Q\Psi_1 - \Psi_1^T Q^T - 2p_{max}\mathbf{X} & Q\Psi_2 & -\mathcal{I}_n \\ * & -\gamma_\infty \mathcal{I}_d & \mathcal{O}_{d,n} \\ * & * & -\gamma_\infty \mathcal{I}_n \end{pmatrix} \prec 0 \tag{1.3.10}$$

où

$$\begin{aligned} \mathcal{M}_{11} &= \begin{pmatrix} \sin(\theta)(Q\Psi_1 + \Psi_1^T Q^T) & \cos(\theta)(Q\Psi_1 - \Psi_1^T Q^T) \\ -\cos(\theta)(Q\Psi_1 - \Psi_1^T Q^T) & \sin(\theta)(Q\Psi_1 + \Psi_1^T Q^T) \end{pmatrix} \\ \mathcal{M}_{12} &= \begin{pmatrix} Q\Psi_2 & \mathcal{O}_{n,d} \\ \mathcal{O}_{n,d} & Q\Psi_2 \end{pmatrix} \\ \mathcal{M}_{13} &= \begin{pmatrix} \sin(\theta)\mathcal{I}_n & -\cos(\theta)\mathcal{I}_n \\ \cos(\theta)\mathcal{I}_n & \sin(\theta)\mathcal{I}_n \end{pmatrix} \\ \mathcal{M}_{22} &= -\gamma_\infty \mathcal{I}_{2d} \\ \mathcal{M}_{23} &= \mathcal{O}_{2d,2n} \\ \mathcal{M}_{33} &= -\gamma_\infty \mathcal{I}_{2n} \end{aligned} \tag{1.3.11}$$

et $Q = \mathbf{X}\Psi\Theta^+ + \tilde{\mathbf{Y}}(\mathcal{I}_{2n+2m} - \Theta\Theta^+)$, alors l'observateur (1.3.2) est un observateur $\mathcal{H}_\infty$ selon la Définition 1.3.6, avec le niveau de découplage γ_∞ de la perturbation et dont les pôles sont situés dans la région spécifiée. Les matrices de l'observateur sont alors données par,

$[N, P, K, Y_E] = \Psi\Theta^+ + Y_\Omega(\mathcal{I}_{2n+2m} - \Theta\Theta^+)$

où

$$Y_\Omega = X^{-1}\tilde{Y},\ \Theta = \begin{bmatrix} -\mathcal{I}_n & \mathcal{O}_n \\ A & \mathcal{I}_n \\ -C & \mathcal{O}_{m,n} \\ \mathcal{O}_{m,n} & -(\mathcal{I}_m - D_y D_y^+)C \end{bmatrix} \text{ and } \Psi = [\mathcal{O}_n, \mathcal{I}_n]. \blacksquare$$

Cette méthode est utilisée pour estimer le modèle de véhicule (1.3.1) à partir des mesures données dans le Tableau 1.1 disponibles sur le véhicule. La procédure et les résultats de la synthèse sont présentés, ainsi que des résultats expérimentaux obtenus grâce au véhicule d'essais et aux cartes d'acquisition. Les résultats obtenus permettent d'illustrer d'une part l'efficacité de la méthodologie proposée, et d'autre part les performances de l'observateur synthétisé.

1.4 Synthèse de lois de commande

Dans ce chapitre, une stratégie de commande des suspensions est proposée, fondée d'une part sur l'observateur développé dans le chapitre précédent et d'autre part sur une architecture de commande hiérarchique à deux niveaux, incluant un contrôle global du véhicule et un contrôle local de chaque amortisseur. Des résultats expérimentaux et de simulation sont présentés dans les domaines temporel et fréquentiel pour illustrer l'intérêt de la stratégie de commande développée.

1.4.1 Introduction

Les objectifs académiques et industriels du contrôle des suspensions peuvent être résumés ainsi:

1. synthèse de lois de commande semi-actives prenant en compte la plage d'effort et la bande passante de l'amortisseur,
2. synthèse de lois de commandes pour des amortisseurs continument variables et de type ON/OFF, prenant en compte les non linéarités de l'amortisseur,
3. performances du véhicule ajustables en fonction de spécifications données sur le confort et la tenue de route,
4. stratégie de commande nécessitant peu de capteurs, et adaptable facilement en fonction des mesures disponibles.

Les différents problèmes engendrés par les quatre points précédents rendent l'utilisation des suspensions semi-actives coûteuse et complexe. Ils doivent donc être résolus pour que les constructeurs automobiles puissent en équiper des véhicules de série.

La contribution principale de ce chapitre concerne le développement d'une stratégie de commande complète, incluant un observateur, un contrôleur global du véhicule et un contrôleur local pour chaque amortisseur. L'observateur présenté précédemment permet d'estimer les variables non mesurées du modèle de véhicule complet. Un contrôleur global par retour d'état statique $\mathcal{H}_\infty$/LPV calcule les consignes d'effort pour chaque amortisseur, afin d'améliorer le confort et la tenue de route du véhicule. La méthode LPV est utilisée pour garantir la dissipativité de la loi de commande, de telle sorte que la consigne d'effort calculée soit directement semi-active et incluse dans la plage d'effort que l'amortisseur peut fournir, cette plage étant donnée par un modèle d'amortisseur non linéaire. Enfin, un contrôleur local pour chaque amortisseur, par retour de sortie dynamique $\mathcal{H}_\infty/\mathcal{H}_2$ LPV, permet de prendre en compte les non linéarités et les limitations des amortisseurs dans la loi de commande.

1.4.2 Architecture de commande

L'architecture de la stratégie de commande est représentée sur la Figure 1.5. Le bloc V représente le modèle de véhicule piloté, incluant le modèle de véhicule complet vertical, et quatre modèles d'amortisseurs dynamiques non linéaires (1.2.2). Ce modèle est perturbé par les irrégularités du sol $z_r \in \mathbb{R}^4$ sous chaque roue, ainsi que par les moments M_x et M_y dus aux transferts de charge. Les quatre amortisseurs semi-actifs peuvent être contrôlés par les signaux de commande $u_d \in \mathbb{R}^{n_u}$, $n_u = 4$. Le bloc O représente l'observateur d'ordre plein développé dans le chapitre précédent. Il estime en temps réel les états du modèle de véhicule complet linéaire. Le contrôleur K_v est un retour d'état statique LPV qui reçoit en entrée, les états estimés $\hat{x}$ et calcule les forces u que les amortisseurs doivent fournir en plus de la force nominale $c_0 z_{def}$, afin d'améliorer les performances du véhicule. Ce contrôleur s'adapte en fonction du paramètre ρ_v qui impose une contrainte plus ou moins forte au signal de commande, de telle manière que la force de consigne F^* calculée, reste dans la plage d'effort que l'amortisseur peut produire. Ceci sera détaillé plus tard. Les quatre contrôleurs K_d calculent les quatre signaux de commande u_{d_i} des amortisseurs qui leur permettent de fournir l'effort de consigne F^*. Les efforts F réellement produits par les amortisseurs, sont calculés à partir des mesures M par une méthode confidentielle qui ne peut être décrite ici. Dans cette thèse, les efforts réels sont donc supposés disponibles.

Considérons le modèle de véhicule (1.2.3), mis sous forme de représentation d'état:

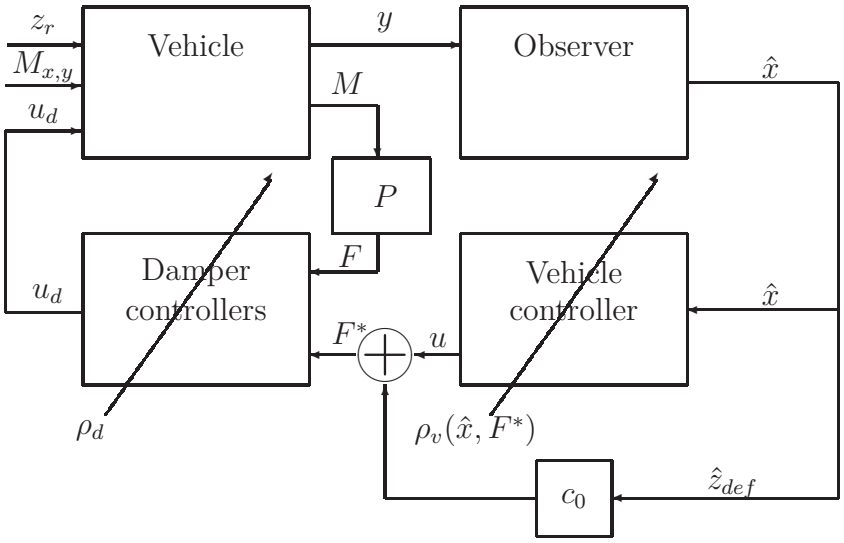

Figure 1.5: Control architecture

$$\begin{cases} \dot{x} = A \cdot x + B_1 \cdot w + B_2 \cdot u \\ y = C \cdot x + D_w \cdot w + D_u u \end{cases} \tag{1.4.1}$$

où le vecteur x représente les états du véhicule, w les perturbations du sol et y les variables mesurées, données dans le Tableau 1.1.

1.4.3 Contrôle global du véhicule

Dans cette section, un contrôleur est proposé pour calculer les efforts de consigne de chaque amortisseur afin d'améliorer les performances du véhicule selon certains critères fréquentiels spécifiques, établis notamment par les constructeurs automobiles. La synthèse de ce contrôleur est basée sur une approche $\mathcal{H}_\infty$/LPV, permettant d'une part la minimisation de certaines variables sur certaines zones fréquentielles, et d'autre part d'adapter automatiquement le comportement du contrôleur pour que les efforts de consigne restent dans la plage d'effort accessible. Ce contrôleur est synthétisé à partir du modèle (1.4.1). Les paramètres variants sont calculés proportionnellement à la différence entre la force d'amortissement de consigne et la force extrémale que l'amortisseur peut fournir. Cette solution permet au contrôleur par retour d'état statique K_v, représenté sur la Figure 1.5, de calculer une force de consigne réaliste et semi-active pour chaque amortisseur, à partir du modèle d'amortisseur identifié présenté précédemment. La plage d'effort accessible de l'amortisseur SOBEN est donnée par la Zone 3 représentée sur la Figure 1.7. Le système généralisé utilisé pour la synthèse, incluant les filtres de pondérations représentant les performances, est représenté sur la Figure 1.6. Les filtres sont

donnés dans le Tableau 1.2.

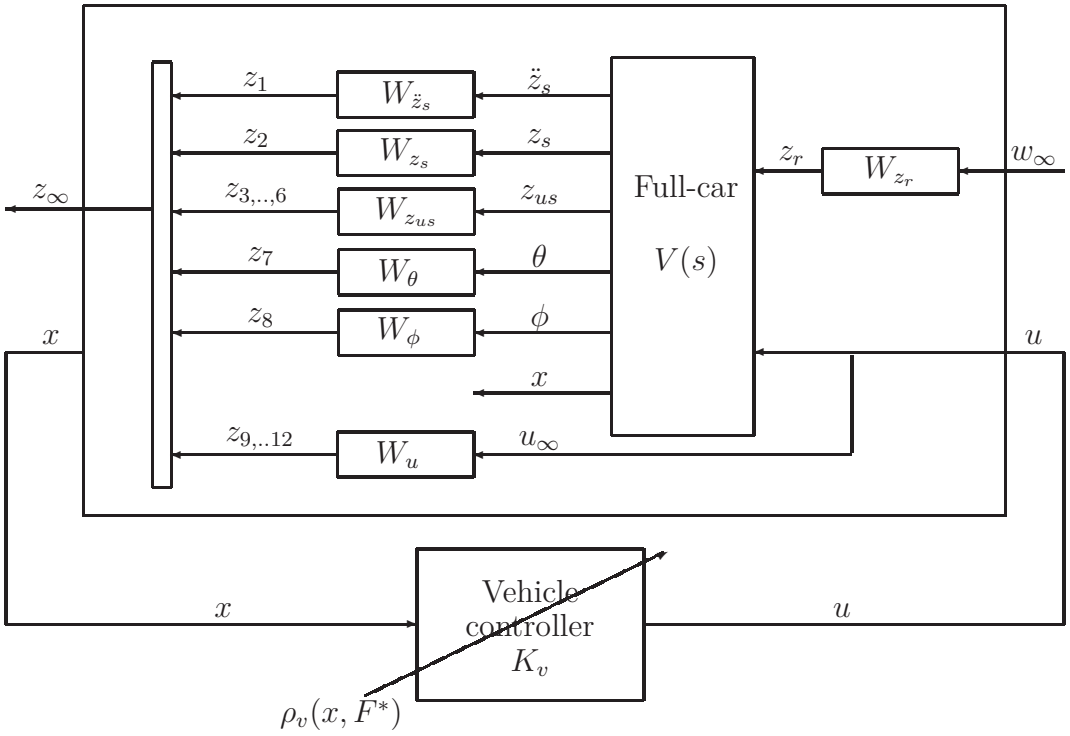

Figure 1.6: Schéma généralisé et filtres de pondération

Système	**Filtre** (Unité de fréquence: Hz)	
$\ddot{z}_s \mapsto z_1$	$W_{\ddot{z}_s}(s) = G_{\ddot{z}_s} \frac{s}{s+2\pi f_{\ddot{z}_s}}$	$f_{\ddot{z}_s} = 4$
		$G_{\ddot{z}_s} = 0.01$
$z_s \mapsto z_2$	$W_{z_s}(s) = G_{z_s} \frac{2\pi f_{z_s}}{s+2\pi f_{z_s}}$	$f_{z_s} = 5$
		$G_{z_s} = 2$
$\theta \mapsto z_7$	$W_\theta(s) = G_\theta \frac{2\pi f_\theta}{s+2\pi f_\theta}$	$f_\theta = 5$
		$G_\theta = 2$
$\phi \mapsto z_8$	$W_\phi(s) = G_\phi \frac{2\pi f_\phi}{s+2\pi f_\phi}$	$f_\theta = 5$
		$G_\theta = 2$
$z_{us_i} \mapsto z_j$	$W_{z_{us}}(s) = G_{z_{us}} \frac{2\pi f_{z_{us}}}{s+2\pi f_{z_{us}}}$	$f_{z_{us}} = 20$
$i \in [1,4]$, $j \in [3,6]$		$G_{z_{us}} = 1$
$w_\infty \mapsto z_{r_i}$	$W_{z_r}^{-1}(s) = G_{z_r} \frac{2\pi f_{z_r}}{s+2\pi f_{z_r}}$	$f_{z_{r_i}} = 20$
$i \in [1,4]$		$G_{z_{r_i}} = 1$
$u \mapsto z_j$	$W_{u_i}(\rho_{v_i})(s) = \rho_{v_i}$	
$i \in [1,4]$, $j \in [9,12]$		

Table 1.2: Filtres de pondération pour le contrôle global

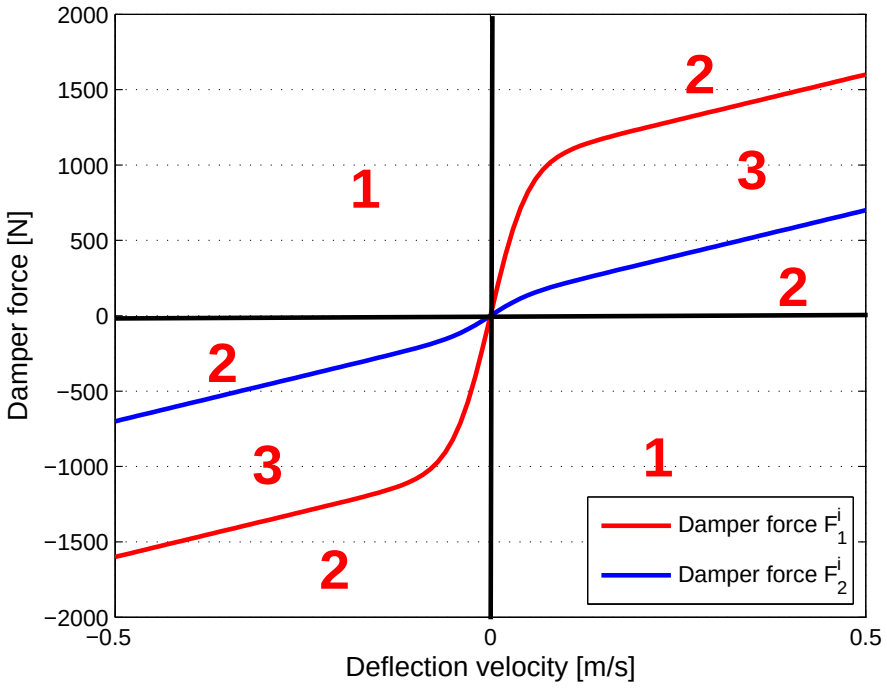

Figure 1.7: Plage d'effort de l'amortisseur

Le contrôleur $K_v(\rho)$ devant être calculé, est un retour d'état statique LPV. Ainsi, avec $u = K_v(\rho) \cdot x$, où x représente les variables d'état du modèle de véhicule complet vertical, le système en boucle fermée est donné par l'Équation (1.4.2).

$$\begin{pmatrix} \dot{x} \\ \dot{x}_f \\ z_\infty \end{pmatrix} = \begin{pmatrix} A + B_2 K_v & \mathcal{O} & B_f \\ B_f + B_{f2} K_v & A_f & B_{f1} \\ D_f + D_{f2} K_v & C_f & D_{f1} \end{pmatrix} \begin{pmatrix} x \\ x_f \\ w_\infty \end{pmatrix} \tag{1.4.2}$$

L'objectif est de résoudre le problème $\mathcal{H}_\infty$ en minimisant γ_∞, le gain $\mathcal{L}_2$ du système d'entrée z_r et de sortie z_∞. La solution à ce problème est donnée par la Proposition suivante:

Proposition:

Considérons le système en boucle fermée (1.4.2) et un scalaire positif γ_∞. Le contrôleur $K_v(\rho_v)$ est un retour d'état statique $\mathcal{H}_\infty$/LPV garantissant que la norme $\mathcal{H}_\infty$ du système (1.4.2) est inférieure à γ_∞ s'il existe $X = X^T \succ 0$ et $U(\rho_v)$ vérifiant (1.4.3-1.4.5) à chaque sommet du polytope défini par les valeurs extrémales des paramètres: $\rho_v = [\rho_{v_1}, \rho_{v_2}, \rho_{v_3}, \rho_{v_4}]$, $\rho_{v_i} = \rho_{min}$ ou ρ_{max}.

$$\begin{pmatrix} Q_1 + Q_1^T & B_{1a} & Q_2^T(\rho_v) \\ * & -\mathcal{I} & D_{f1}^T \\ * & * & -\gamma_\infty^2 \mathcal{I} \end{pmatrix} \prec 0 \tag{1.4.3}$$

$$\begin{cases} Q1 = \begin{pmatrix} A\mathbf{X_1} + B_2\mathbf{U}(\rho_\mathbf{v}) & \mathcal{O} \\ B_f\mathbf{X_1} + B_{f2}\mathbf{U}(\rho_\mathbf{v}) & A_f\mathbf{X_2} \end{pmatrix} \\ Q2(\rho_v) = \begin{pmatrix} D_f\mathbf{X_1} + D_{f2}(\rho_v)\mathbf{U}(\rho_\mathbf{v}) & C_f\mathbf{X_2} \end{pmatrix} \end{cases} \tag{1.4.4}$$

$$X = \begin{pmatrix} \mathbf{X_1} & \mathcal{O} \\ \mathcal{O} & \mathbf{X_2} \end{pmatrix} \quad B_{1a} = \begin{pmatrix} B_1 \\ B_{f1} \end{pmatrix} \tag{1.4.5}$$

où les inconnues sont $\mathbf{X_1}$, $\mathbf{X_2}$, $\mathbf{U}(\rho_\mathbf{v})$.

Le contrôleur $K(\rho_v)$ est déduit de $K(\rho_v) = U(\rho_v)X_1^{-1}$. ■

Ce contrôleur n'a pas encore été testé expérimentalement. Cependant, différentes simulations sont présentées et permettent d'analyser les performances de la loi de commande proposée.

1.4.4 Contrôle local de l'amortisseur

L'objectif est de concevoir un contrôleur local K_d, permettant à chaque amortisseur d'être asservi en effort. Chaque contrôleur local est un retour de sortie dynamique $\mathcal{H}_\infty/\mathcal{H}_2$ basé sur le modèle d'amortisseur non linéaire (1.2.2), dont la partie statique peut être décomposée comme suit:

$$\begin{aligned} F_i &= A_1 \tanh(A_3 v_i + A_4 x_i) \cdot u_{d_i} + A_2 \tanh(A_3 v_i + A_4 x_i) + A_5 v_i + A_6 x_i + A_7 \\ &= \rho_{d_i}(x_i, v_i) \cdot u_{d_i} + F_{0_i} \end{aligned} \tag{1.4.6}$$

où x_i, v_i et u_{d_i} représentent respectivement le débattement, la vitesse de débattement et le signal de commande de l'amortisseur $i = 1, .., 4$. Ce gain non linéaire peut être pris en compte dans le modèle dynamique de l'amortisseur:

$$D_i(s) = \frac{F_i(s)}{U_{d_i}(s)} = \frac{\rho_{d_i}(x_i, v_i)}{\left(\frac{s}{\omega_d}\right)^2 + 2m_d\frac{s}{\omega_d} + 1} \tag{1.4.7}$$

où ω_d et m_d représentent respectivement la bande passante et le coefficient d'amortissement. Ce modèle a été utilisé pour synthétiser le contrôleur LPV. Le

paramètre $\rho_{d_i}(x_i, v_i)$ permet d'adapter le gain du contrôleur afin de compenser les non linéarités de l'amortisseur. Le schéma généralisé, utilisé pour la synthèse, incluant les contraintes de performance sous forme de filtres de pondération, est représenté sur la Figure 1.8.

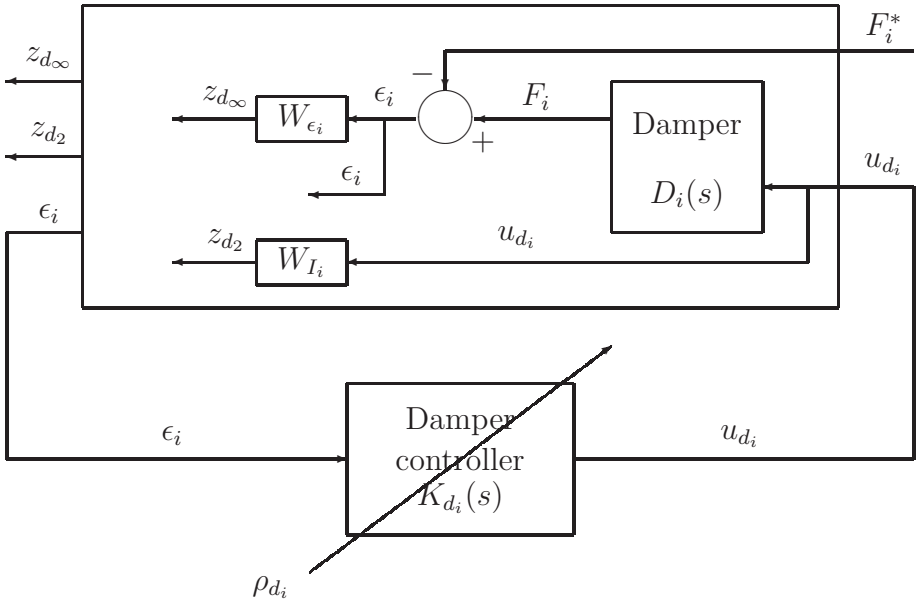

Figure 1.8: Synthèse du contrôleur local de l'amortisseur: schéma généralisé et filtres de pondération

La stratégie proposée inclut des contraintes $\mathcal{H}_\infty$ et $\mathcal{H}_2$, permettant d'assurer les performances de l'asservissement en effort d'une part, et de limiter l'énergie du signal de commande d'autre part. Ce problème de synthèse multi-objectifs consiste donc à:

- assurer la stabilité et prendre en compte les non linéarités de l'amortisseur grâce à l'approche LPV,
- borner la norme $\mathcal{H}_\infty$ du système $F_i^* \mapsto z_{d_\infty}$ par une valeur γ_0: ceci permet de spécifier les performances de l'asservissement,
- borner la norme $\mathcal{H}_2$ du système $F_i^* \mapsto z_{d_2}$ par une valeur σ_0: ceci permet de limiter l'énergie du signal de commande,
- placer les pôles du système en boucle fermée dans une région appropriée à la bande passante du système et aux contraintes liées à la mise en œuvre pratique de la loi de commande.

Les filtres de pondération utilisés lors de la synthèse pour atteindre ces objectifs de performance, sont donnés dans le Tableau 1.3.

Relation	**Filtre** (Unité de fréquence: Hz)	
$\epsilon_i \mapsto z_{d_\infty}$	$W_{\epsilon_i} = G_{\epsilon_i} \frac{2\pi f_{\epsilon_i}}{s+2\pi f_{\epsilon_i}}$	$f_{\epsilon_i} = 20$
		$G_{\epsilon_i} = 2$
$u_{d_i} \mapsto z_{d_2}$	$W_{I_i} = G_I \frac{2\pi f_I}{s+2\pi f_I}$	$f_I = 20$
		$G_I = 0.5$

Table 1.3: Contrôle local de l'amortisseur: filtres de pondération

Les performances de ce contrôleur ont été testées à la fois en simulation et expérimentalement. Les résultats sont présentés et analysés.

1.5 Conclusion

Ce travail vise à apporter une contribution méthodologique dans le domaine du contrôle des suspensions automobiles semi-actives, avec également pour objectif d'assurer un transfert de la recherche académique vers l'industrie. Les principaux résultats de ce travail sont décrits brièvement ci-dessous:

- **Modèles d'amortisseurs:**

  Les modèles d'amortisseurs proposés peuvent être utilisés pour représenter le comportement non linéaire de nombreux amortisseurs. Ils peuvent également être utilisés pour la synthèse de contrôleurs ou d'observateurs, car ils sont utilisables facilement dans une application temps réel embarquée.

- **Estimation du véhicule:**

  Une méthodologie de synthèse d'observateurs a été proposée, permettant de synthétiser et de régler des observateurs adaptés à ce type d'application. Les variables estimées peuvent ensuite être utilisées pour piloter les suspensions à partir d'un nombre de capteurs réduit. La méthodologie inclut à la fois les spécifications de performance en terme de découplage de la perturbation, et le placement de pôles pour que la dynamique de l'observateur soit adaptée au système et permette le filtrage des bruits de mesure. Elle fournit donc tous les outils pour résoudre les principaux problèmes pratiques.

- **Contrôle des suspensions:**

  Une méthode complète de contrôle des suspensions a été développée. Les résultats de Poussot-Vassal [2008], concernant le contrôle d'un modèle quart de véhicule

équipé d'une suspension semi-active, ont été étendus au modèle de véhicule complet, et complétés par une méthode de placement de pôles, ainsi que par une prise en compte des limitations réelles de l'amortisseur, grâce à un modèle identifié d'amortisseur. Finalement, la méthode permet de prendre en compte toutes les contraintes industrielles et technologiques, et fournit des contrôleurs efficaces, pouvant être mis en œuvre facilement, et permettant d'améliorer le confort et la tenue de route du véhicule. De plus la stratégie proposée étant facilement réglable, elle peut être facilement adaptée à toutes les technologies d'amortisseurs.

Les principales perspectives permettant de compléter et d'améliorer ce travail sont données ci-dessous.

Perspectives à court terme

Les perspectives à court terme concernent l'étude des performances du contrôle global du véhicule de manière expérimentale, ainsi que la synthèse d'un observateur d'ordre réduit, puis la discrétisation et la mise en œuvre des contrôleurs et observateurs sur processeur de signaux (DSP).

Perspectives à long terme

Les perspectives à long terme concernent l'amélioration du modèle de véhicule, la conception d'une stratégie de commande globale du châssis, incluant les systèmes de freinage et de direction, la conception d'une stratégie de commande incluant un terme d'anticipation à partir de la mesure du profil de la route, l'utilisation d'un ressort pneumatique piloté, la conception d'une stratégie de détection de défauts, et la supervision, détection de cas d'urgence.

Chapter 2

General introduction

In this chapter, a brief history of automotive suspensions, widely inspired from [Eckermann, 2001, Rajput, 2007, Gillepsie, 1992, Wong, 2001, Miliken and Miliken, 1995], is presented in Section 2.1 in order to recall and emphasize the interest of the various suspension types developed by car manufacturers for road vehicles. Then this chapter focuses on semi-active suspensions. Some previous works on suspension control applications are discussed. Finally, the industrial and methodological issues of this thesis, and its contribution as well, are detailed in Section 2.2.

2.1 Historical facts on suspensions

Since the first steam car, represented in Figure 2.1, invented in 1770 by Cugnot, many suspension technologies have been used to improve the comfort of the vehicles without deteriorating the road-holding drastically. In this section, various front and rear suspension technologies, used in the past or still used, are presented.

2.1.1 First suspension

The first automobile suspension system was invented by William Brush in 1904. His car, called the Brush Two-Seat Runabout, finally appeared in 1906. It featured a revolutionary suspension system that incorporated two innovations never before assembled together: front coil springs and devices at each wheel that dampened spring bounce, mounted on a flexible wood axle. Some European car-makers tried coil springs. However, most manufacturers stood fast with leaf springs. They were less expensive, and by simply adding leaves or changing the shape from full elliptic to three-quarter or half elliptic, the spring could be made to support varying weights. Leaf springs have been

Figure 2.1: First steam car

used since the Romans suspended a two-wheeled vehicle called a Pilentum on elastic wooden poles. The first steel spring put on a vehicle was a single flat plate installed on carriages in the 18th century. The leaf spring, represented in Figure 2.2, which some manufacturers still use in rear suspensions today, was invented by Obadiah Elliot in 1804.

Figure 2.2: Model T Ford: leaf spring (left) and coil spring (right)

The coil spring, also represented in Figure 2.2, is quite an old technology too. The first patent for such a spring was issued to R. Tredwell in 1763. The main advantage of coil springs is that they do not have to be spread apart and lubricated periodically to keep them from squeaking, as leaf springs do. Henry Ford's 1908 Model T Ford featured leaf springs with a novel twist. He used only one spring at each axle, mounted

transversely, instead of one at each wheel. Ford's adaptation of high-strength vanadium steel from a racing car allowed him to save weight and cut costs in many areas of the Model T without compromising its durability. With some exceptions, independent coil spring front suspension remained quite rare for 25 years after the introduction of the Brush Runabout. Then in 1934, some manufacturers such as General Motors, Chrysler and Hudson, reintroduced coil spring front suspension, this time with each wheel sprung independently. Suspending each wheel individually lessened the effects of spring bounce. Not all cars used coil springs at first. Some had independently suspended leaf springs, but soon after World War II, all manufacturers switched to coil springs for the front wheels. Nowadays, large, heavy cars are generally equipped with leaf springs, while small light cars have coil springs. Independent rear suspension became popular on the rough and twisty roads of Europe because it can offer improved ride and handling. The cheapest method is the swing axle, for which early Volkswagen cars were infamous.

Then car manufacturers began introducing dampers in vehicles. Since early motor cars were limited to the same speed as carriages, leaf springs for them could be made of the right proportion to provide relatively jolt-free rides. As roads were improved and speeds shot up, a 1909 edition of Automobile Engineering noted: "When springs are made sufficiently stiff to carry the load properly over the small inequalities of ordinary roads, they are too stiff to respond readily to the larger bumps. The result is a shock to the passengers. When the springs are made lighter and more flexible in order to minimize the larger shocks, the smaller ones have a too large influence, thus keeping the car body and its passengers in motion all the time." These two contradictory conditions have created the field for the shock absorber.

2.1.2 First shock absorber

The first recorded shock absorber is the invention of A. Gimmig in 1897. He attached rubber blocks to the top of each leaf spring. When the suspension was compressed sufficiently, the rubber bumpers hit bolts that were attached to the frame. Rubber bump stops are still used in many modern suspensions, but their effect on ride control is minimal.

The first true shock absorbers were fitted to a racing bicycle in 1898 by J. M. Truffault. The front fork was suspended on springs, and incorporated a friction device that kept the bike from oscillating constantly. In 1899, an Oldsmobile was equipped by Hartford with a variation of Truffault's device. This first automobile shock absorber consisted of two levers that were hinged together with a pad of rubber placed at the pivot point. One of the lever arms was attached to the frame, while the other was bolted to the leaf spring. A bolt placed at the hinge point could be tightened or loosened to increase or decrease the friction, providing a stiffer or softer ride. The Truffault-Hartford unit was,

therefore, not only the first automotive shock absorber, but also the first adjustable one. This interesting device was later installed on the 1906 Brush Runabout. The ride given by the car was called "magnificent" in a critique written by Hugh Dolnar for Cycle and Automobile Trade Journal.

2.1.3 Hydraulic dampers

The first workable hydraulic shock absorber was designed by Houdaille in 1908. Hydraulic shock absorbers avoid spring oscillations by forcing fluid through small passages. In the popular tubular shock, a piston with small orifices is attached to the chassis and a cylindrical oil reservoir is attached to the suspension or axle. When the suspension moves up and down, the piston is forced through the oil, resisting the action of the spring. One-way valves allow different orifices to be used to control suspension bound and rebound. This is called a double-acting shock. Another chamber of compressible gas can also be added at one end of the fluid reservoir to cushion the damping action. Monroe built the first original equipment hydraulic shocks for Hudson in 1933. By the late 1930s, the double-acting tubular shock absorber became common on cars made in the United States. In Europe, lever-type hydraulic shocks prevailed into the '60s. They resembled the Hartford friction shock, but used hydraulic fluid instead of a friction pad.

2.1.4 MacPherson struts

With the advent of front-wheel-drive cars, manufacturers in the 1970s and '80s started using MacPherson struts. MacPherson, a General Motors engineer, developed this unit in the 1960s. It combines the coil spring, hydraulic shock absorber, and upper suspension arm into a single compact device. The main advantage is that it allows the necessary space for positioning the front-drive transaxle.

2.1.5 Active and semi-active suspensions

Externally controlled suspensions, reacting according to measured or estimated signals, are referred to as semi-active or active suspensions. Semi-active suspensions include devices such as air springs and switchable shock absorbers, various self-leveling solutions, as well as systems like Hydropneumatic, Hydrolastic, and Hydragas suspensions. In 1954, Citroën developed an hydropneumatic suspension made up with two adjustable elements, controlled by a pump: an air spring and an hydraulic damper, allowing a self-levelling of the chassis, and improved comfort performance compared to basic suspensions based on a coil spring and a passive hydraulic damper. Mitsubishi also developed semi-active electronically controlled suspension system in passenger cars. The system was

first incorporated in the 1987 Galant model. Delphi currently sells shock absorbers filled with a magneto-rheological fluid manufactured by Lord, whose viscosity can be changed through an electromagnetic field [Goncalves and Carlson, 2007, Carlson, 2003, Lord, 2008], thereby giving variable control without switching valves, which is faster and thus more effective [Kern, 2008, Lozoya-Santos et al., 2009].

Fully active suspension systems use electronic monitoring of vehicle conditions, coupled with the means to impact vehicle suspension and behavior in real time to directly control the motion of the car. Lotus Cars developed several prototypes, from 1982 onwards, and introduced them to Formula 1, where they have been fairly effective. Nissan introduced a low-bandwidth active suspension in circa 1990 as an option that added an extra 20% to the price of luxury models. Citroën has also developed the so-called Hydractive suspension, which is a low frequency active suspension system allowing to correct the static vertical position of the chassis. The CRONE[1] approach, developed more recently, has been implemented to control these suspensions on a Citroën BX experimental car. It is based on the fractional derivative and consists of ensuring a constant open loop transfer phase around the frequency of the unitary gain [Moreau et al., 2009, Moreau, 1995, Oustaloup and Mathieu, 1999, Oustaloup et al., 1996]. A recently publicized fully active system from Bose Corporation uses linear electric motors, i.e. solenoids, in place of hydraulic or pneumatic actuators that have generally been used up until recently. The most advanced active suspension system is Active Body Control, introduced in 1999 on the top-of-the-line Mercedes-Benz CL-Class.

Several Japanese cars now feature struts with shock valving that can be adjusted from soft to firm by electric motors while the car is moving. The driver has a choice of three settings, but a signal from the speedometer usually overrides the manual control at highway speeds to set the shocks on firm.

The Nissan Maxima, integrated in 1985, had electronically controlled shock absorbers that automatically provided a soft, medium, or firm ride depending upon road conditions, speed, and driving style. A sonar unit under the bumper monitored the road surface, while other sensors checked speed, acceleration, steering angle, and brake use. Data were fed to a central processing unit that decided if you were driving gently or aggressively, then activated shafts in the shock absorbers that altered the size of fluid passages.

2.2 Introduction

This general introduction firstly provides a brief state of the art in the automotive suspension control field. Then the methodological and indutrial objectives are presented, and the main contribution is described.

[1] Commande RObuste Non Entière (Robust Control methodology using Non Full Derivative)

2.2.1 State of the art

Electronically controlled semi-active suspensions are under study since many years by various car manufacturers, and as seen later, in the academic world. They indeed provide an interesting compromise between cost and performance compared to passive and active suspensions. Their industrial advantage is that classical passive damper technologies with constant damping characteristics can be transformed into semi-active dampers while adding an actuator to control the damping rate. This is rather economic and requires a pretty low amount of power compared to active suspensions. With the help of control systems, various semi-active suspensions achieve an improved design compromise among different vibrations modes of the vehicle, namely bounce, roll and pitch modes. However, the applications of these advanced suspensions are constrained by the cost, packaging, weight and reliability of both sensors and actuators. Some control strategies have already been developed in the past few years, but the required technological solutions, in terms of sensors and actuators, are very expensive and, as a consequence, they have been used only for specific up-market vehicles for many years.

More recently, most car manufacturers turned their attention to this kind of suspensions. This can be explained by the growing demand for vehicles with ever better safety and comfort performances, but also by the advances in sensors technologies, in terms of cost, packaging and reliability, and by the advances in electronics as well. Indeed the embedded Digital Signal Processing (DSP) technology allows advanced control strategies to be implemented, since they tend more and more to provide low-cost solutions for embedded real-time applications, with high computation performances, low latency, and without specialized cooling or large batteries. Therefore many of the technological limitations that prevented the development of semi-active suspensions for middle of the range vehicles have been recently solved. These advances open many doors in automotive control systems and allow car manufacturers to electronically control many elements, like braking or steering systems, engines and suspensions. All these automobile components tend to be controlled so as to improve the performance of the vehicle in terms of comfort and safety. This thesis stands in these new trends since the objective is to develop a suspension control strategy for SOBEN dampers.

In the past few years, many active control strategies were developed in both academic and industrial frameworks. However most developed controllers assume active dampers, whereas active dampers are not mounted on mass-produced cars because of their cost and huge energy consumption. Therefore active control strategies are often saturated to control semi-active dampers. Unfortunately, in this case, both performances and stability are not ensured and the results may be unpredictable [Canale et al., 2006]. That is why semi-active strategies have to be tackled to make good use of the semi-active technologies. This thesis aims at designing such control strategies, suiting to the abilities of, for instance, SOBEN damper.

Some semi-active strategies have already been designed to improve comfort or road-holding. However, no complete methodology has been proposed yet to design a controller fulfilling given performance specifications for a given damper, which is the main challenge of this thesis. Therefore adjusting the controller is often difficult. Furthermore many proposed controllers require many sensors and an accurate knowledge of the model. Unfortunately, these conditions are very difficult to fulfill in practice. The developed control strategies indeed have to control the suspensions using a reduced number of sensors. This is one of the main challenges since many car or equipment manufacturers like SOBEN currently aim at equipping cheap mass-produced cars with controlled suspensions to improve comfort and road-holding performances. However, due to the number and the cost of the required sensors, this is not yet possible. Furthermore, car manufacturers need to choose the number, the kind and the location of sensors in the vehicle.

The specifications of the control strategy to be developed can be summarized as follows:

- improve the comfort and road-holding of the vehicle,
- take the limitations of the actuators into account,
- be robust with respect to nonlinearities, parameter variations such as mass variations or tire stiffness, and measurement noise,
- be adjustable according to the performance expected by the customer (sport, comfort, commercial or city cars, heavy goods vehicles...)
- be adapted to various damper technologies,
- use a reduced number of sensors,
- allow car manufacturers to easily adapt the control strategy according to the available sensors,
- be implemented in real-time embedded applications using low-cost microcontrollers.

2.2.2 Objectives and contribution

This dissertation synthesizes the three years PhD work, under the supervision of O. Sename and L. Dugard, in collaboration with SOBEN company, within a CIFRE frame-

work. Furthermore, it stands in the MCOS[2] international project, of the PCP[3] franco-mexican program. This thesis has been carried out partly in Monterrey, Mexico, in collaboration with Professor Ramirez-Mendoza, Dr. Morales-Menèndez and J. J. Lozoya-Santos, a PhD student, from the TEC of Monterrey.

This work aims both at providing some methodological advances in suspension control, and carrying out transfers from academical research to industry. The contribution mainly relies on two fields:

- vehicle observer design,
- suspension control strategies.

An observer design methodology is firstly proposed, allowing the suspension designer to build and adjust an appropriate observer, estimating the non-measured variables. Various previous works on unknown input observers are adapted to vehicle estimation. The developed methodology includes both the performance specifications in terms of unknown road disturbance decoupling, pole placement for implementation issues and measurement noise filtering. Therefore the proposed methodology is a complete observer synthesis tool allowing the suspension designer to overcome the main practical problems. This work led to various publications, as detailed in the next section.

Then, a complete suspension control design methodology is proposed. The previous results of Poussot-Vassal [2008], for semi-active suspension control, are extended to the full vertical car, and completed with both a pole placement method, a scheduling strategy based on a damper model, and a local damper control. Indeed, the scheduling strategy is improved using an identified damper model in order to take the real abilities of the damper into account. The expected behavior of the vehicle, for instance the roll movements, and the characteristics of the dampers, such as its bandwidth and force range, can be easily specified by the designer while following the proposed design methodology. Control solutions are developed both for continuously variable and switched two-state dampers, so that the most widespread types of dampers can be controlled. Finally, this methodology leads to taking the whole set of industrial constraints and technologies into account, and provides efficient and implementable controllers.

The industrial issues of this thesis concern the development of a new high-performance product. SOBEN is specialized in hydraulic systems, and designs shock absorbers in various fields such as automotive, motorcycling or aerospace. Some innovative valve technologies, developed by SOBEN, have been patented and allow dampers to provide improved performances compared to existing technologies. One of the main development

[2]Méthodologies et applications pour la modélisation et la commande de suspensions automobiles pilotées

[3]Programme de Coopération Post-gradué Franco-Mexicain

and research activity concerns the development of high-performance semi-active suspensions. In the past few months, SOBEN designed both a semi-active damper prototype, equipped with an electro-mechanical actuator, and its electronic control board. While combining its hydraulic technologies with a semi-active control system, SOBEN aims at developing a high-performance product, both for up-market and economical mass-produced vehicles. Therefore the cost of this technology has to be restricted. The reduced cost of this hydraulic technology is supposed to be an advantage, for instance compared to expensive magneto-rheological dampers. Therefore designing a control strategy using few and cheap sensors while improving the performances of the vehicle is the main challenge for SOBEN since it amounts to designing a competitive product.

The various programs and libraries resulting from this work form a complete tool that can be used by damper manufacturers to design efficient semi-active control strategies fulfilling the various specifications in terms of comfort and road-holding performance, available sensors, closed-loop bandwidth, damper abilities, robustness and measurement noise filtering.

2.3 Publications and patents

2.3.1 Publications

International conference papers with proceedings

- *"Experimental results of an $\mathcal{H}_\infty$ observer for an industrial semi-active suspension"* (S. Aubouet, L. Dugard and O. Sename).
  In Proceeding of the **IFAC Symposium Advances in Automotive Control**, Munich, Germany, July, 2010.

- *"Semi-active $\mathcal{H}_\infty$/*LPV *control for an industrial hydraulic damper"* (S. Aubouet, L. Dugard, O. Sename, C. Poussot-Vassal and B. Talon).
  In Proceedings of the **European Control Conference**, Budapest, Hungary, August, 2009.

- *"$\mathcal{H}_\infty$/*LPV *observer for industrial semi-active suspension"* (S. Aubouet, L. Dugard and O. Sename).
  In Proceedings of the **IEEE Multi-Conference on Systems and Control**, Saint-Petersburg, Russia, July, 2009.

- *"Performance analysis and simulation of a new industrial semi-active damper"* (S. Aubouet, O. Sename, B. Talon, C. Poussot-Vassal and L. Dugard).
  In Proceedings of the 17*th* **IFAC World Congress**, Seoul, Korea, July, 2008.

- *"A LPV control approach for a semi-active hydraulic damper"* (S. Aubouet, L. Dugard, O. Sename and C. Poussot-Vassal).
  In Proceeding of the **11th Mini Conference on Vehicle System Dynamics, Identification and anomalies**, Budapest, Hungary, November, 2008.

- *"Simulation performance of a quarter of vehicle including a* MR *damper model with hysteresis"* (J-J Lozoya-Santos, S. Aubouet, R. Morales-Menendez, O. Sename, R. Ramirez-Mendoza, L. Dugard).
  In Proceeding of the **7th EUROSIM Congress on modeling and simulation**, Prague, Czech Republic, September, 2010.

National conference papers with proceedings

- *"Analyse des performances et simulation d'un amortisseur semi-actif industriel"* (S. Aubouet, L. Dugard and O. Sename).
  In Proceeding of the "**Journées Automatique et Automobile**" (JAA GRD-MACS), Bordeaux, France, November, 2007.

2.4 Structure of the thesis

In Chapter 3, the main theoretical tools used in this thesis to design both controllers or observers are recalled: LTI (Linear Time Invariant) and LPV (Linear Parameter Varying) systems, $\mathcal{H}_\infty$, $\mathcal{H}_2$ and mixed $\mathcal{H}_\infty/\mathcal{H}_2$ control synthesis, LPV control, pole placement in LMI regions and robustness analysis.

In Chapter 4, widespread suspension and damper technologies are presented. Then the material resources and the experiments used in this dissertation are presented. Then two different kinds of models are developed for the SOBEN damper. An identified damper model is proposed from the experimental results. Finally, some well-known vehicle models, used in the next chapters, are presented.

In Chapter 5, a methodology to design observers for vehicle estimation is developed in order to estimate some non-measured variables, using a small number of sensors. This methodology has been applied to the vehicle and the synthesized observer has been tested experimentally using a SOBEN testing car. The experimental set-up and results are presented and analyzed in order to emphasize the performance of the proposed observer.

In Chapter 6, some performance criteria are defined for the full-car. Then, the developed control architecture including the observer, the damper controller and the vehicle controller is described. The controllers are designed, and finally, their performance are

studied using some simulations and experimental results obtained with a damper testing bench.

Chapter 3

Theoretical background

This chapter deals with existing theoretical tools, definitions and results for robust control and analysis, LMI formulation and pole placement. These problems have been widely developed in the past and still are. Furthermore, these topics are not the core of this thesis. Therefore this chapter only recalls some mathematical elements used in the next chapters. It is widely inspired from previous works such as [Scherer and Weiland, 1999, Scherer et al., 1997, Scherer, 2000, Doyle et al., 1994, Chilali and Gahinet, 1996, Scorletti, 2004, Gahinet and Apkarian, 1994]. For a mature reader in LMI and LPV approaches, this chapter may be viewed as short and incomplete, but the objective is to present the main ideas and concepts. Conversely, an unfamiliar reader should refer to the provided bibliography for more details.

This chapter is organized as follows: some definitions on linear dynamical systems are given in Section 3.1, the LMI and convex constraints are presented in Section 3.2. Then some signal and system norms are defined in Section 3.3. The bounded real lemma is recalled in Section 3.4, and the $\mathcal{H}_\infty$, $\mathcal{H}_2$ and mixed $\mathcal{H}_\infty/\mathcal{H}_2$ problems are firstly stated in Section 3.5, and then, they are solved in the LTI and LPV case respectively in Section 3.6 and 3.7. A pole placement method in LMI regions is proposed in Section 3.8, and finally, some robustness analysis tools, based on the structured singular value are presented in Section 3.9.

3.1 Linear dynamical systems

Definition 3.1.1 (*Linear systems*)

Given some matrix functions $A(.) : \mathbb{R}^p \mapsto \mathbb{R}^{n\times n}$, $B(.) : \mathbb{R}^p \mapsto \mathbb{R}^{n\times n_e}$, $C(.) : \mathbb{R}^p \mapsto \mathbb{R}^{m\times n}$ *and* $D(.) : \mathbb{R}^p \mapsto \mathbb{R}^{m\times n_e}$, *where*

- p *denotes the size of the parameter vector* ρ,

- n_e *denotes the number of system* Σ *inputs,*
- m *denotes the number of system* Σ *outputs,*

and the following system Σ*,*

$$\Sigma : \begin{cases} \dot{x}(t) &= A(\rho)x(t) + B(\rho)e(t) \\ y(t) &= C(\rho)x(t) + D(\rho)e(t) \end{cases} \tag{3.1.1}$$

the system is said to be:

- ***Linear Time Invariant*** *if* ρ *is constant,*
- ***Quasi Linear Parameter Varying*** *(QLPV) if* ρ *is defined over the state variables* $x(t)$*, i.e.* $\rho = \rho(x(t))$*,*
- ***Linear Parameter Varying*** *(LPV) if* ρ *is defined over the time, i.e.* $\rho = \rho(t)$*.*

3.2 LMI and convex constraints

Here a definition of the Linear Matrix Inequalities is given, based on the book of Boyd et al. [1994]. Many convex problems can be written using LMI. This is interesting since these inequalities can be solved in an efficient and reliable way using the powerful convex optimization theory. Various algorithms for solving optimization problems have already been proposed [Scorletti, 2004, Ciarlet, 1998], and some efficient toolboxes allow to deal with such problems [Sturm, 1998, Benson et al., 1998].

Definition 3.2.1 (*Linear Matrix Inequality*)

A linear matrix inequality is defined as,

$$F(x) \triangleq F_0 + x_1F_1 + ... + x_nF_n \prec 0 \tag{3.2.1}$$

where

- $x = (x_1, ..., x_n)$ *is a vector of* n *real numbers called the decision variables,*
- $F_0, ..., F_n$ *are real symmetric matrices, i.e.,* $F_j = F_j^T$ *, for* $j = 0, ..., n$*,*
- *the inequality* $\prec$ *in (3.2.1) means "negative definite" i.e.* $u^TF(x)u < 0$ *for all non-zero real vectors* u*. This is equivalent to* $\lambda_{max}(F(x)) < 0$*, where* λ_{max} *denotes the maximal eigenvalue.*

The linear matrix inequality (3.2.1) defines a convex constraint on x. That is, the set $\mathcal{S} \triangleq \{x|F(x) \prec 0\}$ is convex. Indeed, if $y, z \in \mathcal{S}$ and $\alpha \in [0,1]$, then

$$F(\alpha y + (1-\alpha)z) = \alpha F(y) + (1-\alpha)F(z) \prec 0 \tag{3.2.2}$$

where the inequality follows from the fact that F is affine, $\alpha > 0$ and $(1-\alpha) > 0$.

This formulation has a major interest. Indeed, semi-definite programming (SDP) belongs to the class of complex programming for which a well-rounded theory exists [Boyd et al., 1994]. Such optimization problems can be efficiently solved using interior-point algorithm [Nesterov and Nemirovskii, 1994, Boyd et al., 1994], as implemented in the Sedumi toolbox [Sturm, 1998].

Remark 3.2.1 (*Optimization software*)

The $\mathcal{H}_\infty$ and $\mathcal{H}_2$ problems can be formulated using LMI. Then, for instance, the Yalmip interface described in [Lofberg, 2004] can be used to solve them.

3.3 Signal and system norms

In this section, various norms applying both to signals and systems are presented, since they will be used in the next chapters.

3.3.1 Signal norms

Definition 3.3.1 ($\mathcal{L}_2$-*norm*)

Given a function $x(t) : \mathbb{R} \to \mathbb{C}$, the $\mathcal{L}_2$-norm is defined as,

$$||x(t)||_2 \triangleq \sqrt{\int_0^{+\infty} x^*(t)x(t)dt} \tag{3.3.1}$$

where x^* denotes the transpose complex conjugate of x.

Definition 3.3.2 ($\mathcal{L}_\infty$-*norm*)

Given a complex function $x(t))$, the $\mathcal{L}_\infty$-norm of $x(t)$ is defined as,

$$||x(t)||_\infty \triangleq \begin{cases} \sup_{t\in\mathbb{R}} |x(t)| \\ \sup_{t\in\mathbb{R}} \sqrt{x^T x} \end{cases} \tag{3.3.2}$$

.

3.3.2 System norms

Definition 3.3.3 (*Generalized $\mathcal{H}_2$-norm*)

Given a strictly proper system G from input w to output z, and its unit impulse response g, the $\mathcal{H}_2$-norm of G is the energy ($\mathcal{L}_2$-norm) of $g(t)$ defined as,

$$||G(j\omega)||_2 \triangleq \sqrt{\int_{-\infty}^{+\infty} g^*(t)g(t)dt} = \sqrt{\frac{1}{2\pi}\int_{-\infty}^{+\infty} Tr(G(j\omega)^*G(j\omega))d\omega} \tag{3.3.3}$$

where G denotes the Laplace transform of g. The norm $\mathcal{H}_2$ is finite if and only if G is strictly proper.

For SISO systems, the $\mathcal{H}_2$-norm represents the surface located below the Bode diagram, whereas for MIMO systems, the $\mathcal{H}_2$-norm is the impulse-to-energy gain of the output $z(t)$ in response to a white noise input $w(t)$. This norm is also called the generalized $\mathcal{H}_2$-norm, and can be defined as,

$$||G(j\omega)||_2 \triangleq \frac{||z||_2}{||w||_\infty}$$

Definition 3.3.4 (*$\mathcal{H}_\infty$-norm*)

The $\mathcal{H}_\infty$-norm of a proper and real rational stable transfer function G from the input w to the output z is the $\mathcal{L}_2$-induced norm [Scherer and Weiland, 1999] and coincides with,

$$||G(j\omega)||_\infty \triangleq \begin{cases} \sup_{\omega\in\mathbb{R}} \bar{\sigma}(G(j\omega)) & \textit{(LTI systems only)} \\ \max_{w(t)} \dfrac{||z||_2}{||w||_2} & \textit{(LTI and LPV systems)} \end{cases} \tag{3.3.4}$$

where $\bar{\sigma}(G(j\omega))$ represents the maximal singular value of G, and w is any 2-power integrable function .

Remark 3.3.1

Using the $\mathcal{H}_\infty$-norm for LPV systems is common but this is a misuse of language since the $\mathcal{H}_\infty$-norm is not defined for LPV systems. Indeed, for LPV systems, the $\mathcal{L}_2$-induced norm has to be considered, as given in the previous definition.

This norm represents the maximal gain of the frequency response of the system. It is also called the worst case attenuation level in the sense that it measures the maximum energy amplification. For SISO (resp. MIMO) systems, it represents the maximal peak value on the Bode magnitude (resp. singular value) of $G(j\omega)$, $\omega \in \mathbb{R}$.

3.4 Bounded Real Lemma

The Bounded Real Lemma (BRL) allows to compute the $\mathcal{H}_\infty$-norm of a given linear system. This result can be proved using dissipativity theory.

Lemma 3.4.1 (*Bounded Real Lemma*)

Suppose that the system described by (3.1.1) is controllable and has transfer function H. Let $s(w,z) = \gamma w^T w - z^T \gamma^{-1} z$, $\gamma \geq 0$ be a supply function. Then the considered system is asymptotically stable if there exists a symmetric positive definite matrix P such that the LMI

$$\begin{pmatrix} A^T P + PA & PB & C^T \\ * & -\gamma\mathcal{I} & D^T \\ * & * & -\gamma\mathcal{I} \end{pmatrix} \prec 0 \tag{3.4.1}$$

holds for all $\omega \in \mathbb{R}$. Then, we have $||H||_\infty < \gamma^2$.

3.5 $\mathcal{H}_\infty$, $\mathcal{H}_2$ and mixed $\mathcal{H}_\infty/\mathcal{H}_2$ problems

In this section, the $\mathcal{H}_\infty$, $\mathcal{H}_2$ and mixed $\mathcal{H}_\infty/\mathcal{H}_2$ control problems are presented using LMI formulations, both for state-feedback and output-feedback controller synthesis. These problems have already been studied in many previous works such as [Gahinet and Apkarian, 1994, Iwasaki and Skelton, 1994, Scherer and Weiland, 1999, Scherer et al., 1997, Scherer, 2000] for $\mathcal{H}_\infty$ control, [Abedor et al., 1994, Rotea, 1993, Masubuchi et al., 1995] for $\mathcal{H}_2$ control, [Scherer, 2000, Scherer et al., 1997, Khargonekar and Rotea, 1991, Doyle et al., 1994] for $\mathcal{H}_\infty/\mathcal{H}_2$ control, and [Bambang et al., 1993] for $\mathcal{H}_\infty/\mathcal{H}_2$ control with pole placement.

Consider the generalized plant P to be controlled, and the controller K, respectively given by (3.5.1) and (3.5.2), are represented in Figure 3.1.

$$P : \begin{pmatrix} \dot{x} \\ z \\ y \end{pmatrix} = \begin{pmatrix} A & B_1 & B_2 \\ C_1 & D_{11} & D_{12} \\ C_2 & D_{21} & \mathcal{O} \end{pmatrix} \begin{pmatrix} x \\ w \\ u \end{pmatrix} \tag{3.5.1}$$

where $x \in \mathbb{R}^n$ is the state vector, $y \in \mathbb{R}^m$ are the measured variables, $z \in \mathbb{R}^{n_z}$ are the outputs to be controlled, $u \in \mathbb{R}^{n_u}$ are the control signals, $w \in \mathbb{R}^{n_w}$ are the exogenous inputs.

Remark 3.5.1

Here only strictly proper systems are considered since D_{22} is assumed to be zero.

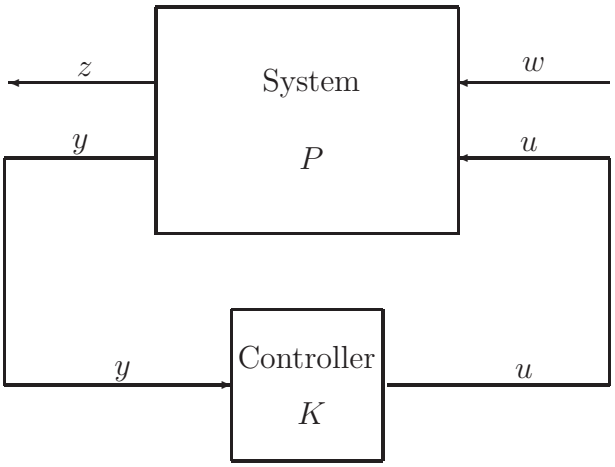

Figure 3.1: Generalized plant and controller

$$K : \begin{pmatrix} \dot{\zeta} \\ u \end{pmatrix} = \begin{pmatrix} A_K & B_K \\ C_K & D_K \end{pmatrix} \begin{pmatrix} \zeta \\ y \end{pmatrix} \tag{3.5.2}$$

where $A_K \in \mathbb{R}^{n_K \times n_K}$, $B_K \in \mathbb{R}^{n_K \times m}$, $C_K \in \mathbb{R}^{n_u \times n_K}$, $D_K \in \mathbb{R}^{n_u \times n_m}$ represent the matrices of the controller to be designed and ζ are the state variables of the controller.

The closed-loop system (3.5.3) can be derived from the generalized plant (3.5.1) and the controller (3.5.2).

$$\begin{pmatrix} \dot{x}_{cl} \\ z \end{pmatrix} = \begin{pmatrix} A_{cl} & B_{cl} \\ C_{cl} & D_{cl} \end{pmatrix} \begin{pmatrix} x_{cl} \\ w \end{pmatrix} \tag{3.5.3}$$

where the state vector $x_{cl} = (x^T, \zeta^T)^T$ of the closed-loop system contains both the state vector of the system and of the controller. The matrices A_{cl}, B_{cl}, C_{cl} and D_{cl} of the closed-loop system are given by (3.5.4).

$$\begin{cases} A_{cl} = \begin{pmatrix} A + B_2 D_K C_2 & B_2 C_K \\ B_K C_2 & A_K \end{pmatrix} \\ B_{cl} = \begin{pmatrix} B_1 + B_2 D_K D_{21} \\ B_K D_{21} \end{pmatrix} \\ C_{cl} = \begin{pmatrix} C_1 + D_{12} D_K C_2 & D_{12} C_K \end{pmatrix} \\ D_{cl} = D_{11} + D_{12} D_K D_{21} \end{cases} \tag{3.5.4}$$

The $\mathcal{H}_\infty$ control synthesis is a disturbance attenuation problem and consists of finding a stabilizing controller that minimizes the impact of the input disturbances on the

controlled output. In the case of the $\mathcal{H}_\infty$ control, this impact is measured thanks to the induced $\mathcal{L}_2$-norm.

Definition 3.5.1 ($\mathcal{H}_\infty$ *optimal and suboptimal problems*)

The $\mathcal{H}_\infty$ problem consists of finding a controller that minimizes the induced $\mathcal{L}_2$-norm of the system T_{zw} between the exogenous input w and the controlled output z, while stabilizing the closed-loop system. The optimal problem consists of finding a stabilizing controller that solves

$$\min_{\gamma>0} \gamma \ s.t. \ ||T_{zw}(s)||_\infty = ||C_{cl}(p\mathcal{I} - A)^{-1}B_{cl} + D_{cl}||_\infty < \gamma \tag{3.5.5}$$

The minimal $\mathcal{H}_\infty$-norm γ_∞ of the closed-loop transfer T_{zw} is defined by

$$\gamma_\infty = \min_{A_K, B_K, C_K, D_K} ||T_{zw}(s)||_\infty \tag{3.5.6}$$

where A_K, B_K, C_K, D_K are the matrices of stabilizing controllers.
The suboptimal problem consists of bounding γ to a given value $\gamma_0 > \gamma_\infty$.

The $\mathcal{H}_\infty$-norm gives the system gain when input and output are measured using the $\mathcal{L}_2$-norm. Rather than bounding the output energy, it may be desirable to keep the peak amplitude of the controlled output below a certain level, e.g. to avoid actuator saturations. This corresponds to the $\mathcal{H}_2$ problem.

Definition 3.5.2 ($\mathcal{H}_2$ *optimal and suboptimal problems*)

The $\mathcal{H}_2$ problem consists of finding a controller that minimizes the $\mathcal{H}_2$-norm of the system between the exogenous input w and the controlled output z, while stabilizing the closed-loop system. This optimization problem consists of finding a stabilizing controller that minimizes σ, the $\mathcal{H}_2$-norm of the transfer T_{zw} from w to z. This problem can be written as

$$\min \sigma \ s.t. \ ||T_{zw}(s)||_2 = ||C_{cl}(p\mathcal{I} - A)^{-1}B_{cl} + D_{cl}||_2 < \sigma \tag{3.5.7}$$

The minimal $\mathcal{H}_2$-norm σ_2 of the closed-loop transfer T_{zw} is defined by

$$\sigma_2 = \min_{A_K, B_K, C_K, D_K} ||T_{zw}(s)||_2 \tag{3.5.8}$$

where A_K, B_K, C_K, D_K are the matrices of stabilizing controllers.
The suboptimal problem consists of bounding σ to a given value $\sigma_0 > \sigma_2$.

The mixed $\mathcal{H}_\infty/\mathcal{H}_2$ synthesis consists of giving different constraints on the controlled system outputs. The transfers between the input w to the output z_∞ and z_2 are respectively associated with an $\mathcal{H}_\infty$ and $\mathcal{H}_2$ performance criteria.

Definition 3.5.3 (*Mixed $\mathcal{H}_\infty/\mathcal{H}_2$ problem*)

Consider the outputs $z = (z_\infty, z_2)$ to be controlled. The mixed $\mathcal{H}_\infty/\mathcal{H}_2$ problem consists of finding a controller which

- *stabilizes the closed-loop system,*
- *bounds the $\mathcal{H}_\infty$-norm of the transfer between the input disturbances w and the output z_∞ to a given level γ_∞,*
- *the $\mathcal{H}_2$-norm of the transfer between the input disturbances w and the output z_2 to a given level σ_2.*

Remark 3.5.2

The $\mathcal{H}_\infty$ and $\mathcal{H}_2$-norms cannot be minimized simultaneously since this problem is non-convex. Therefore two different methods are usually used to deal with this problem:

- *Minimize $\gamma_{\mathcal{H}_\infty/\mathcal{H}_2} = \alpha \cdot \gamma_\infty + (1-\alpha) \cdot \sigma_2$, the linear combination of γ_∞ and σ_2, where $\alpha \in [0,1]$ is a chosen weighting parameter.*
- *Minimize γ_∞ for a fixed σ_2, or vice-versa.*

3.6 LTI design

In this section, the solutions of the $\mathcal{H}_\infty$, $\mathcal{H}_2$ and mixed $\mathcal{H}_\infty/\mathcal{H}_2$ design problems presented in Section 3.5 are given using LMI formulations. Only a brief summary of these results is given, therefore the reader should refer to [Gahinet and Apkarian, 1994, Iwasaki and Skelton, 1994, Scherer and Weiland, 1999, Scherer et al., 1997, Scherer, 2000] for $\mathcal{H}_\infty$ control, [Abedor et al., 1994, Rotea, 1993, Masubuchi et al., 1995] for $\mathcal{H}_2$ control, [Scherer, 2000, Scherer et al., 1997, Khargonekar and Rotea, 1991, Doyle et al., 1994] for $\mathcal{H}_\infty/\mathcal{H}_2$ control, and [Bambang et al., 1993] for $\mathcal{H}_\infty/\mathcal{H}_2$ control with pole placement.

3.6.1 LTI design: dynamic output-feedback control

The solution of the $\mathcal{H}_\infty$ problem is given in the dynamic output-feedback case. The controller to be designed and the closed-loop system are respectively given by (3.5.2) and (3.5.3-3.5.4). The $\mathcal{H}_\infty$ and $\mathcal{H}_2$ dynamic output-feedback control problems can be solved respectively according to Propositions 3.6.1 and 3.6.2. Note that here K is chosen to be of the same order than the generalized plant P.

Proposition 3.6.1 (*Dynamic $\mathcal{H}_\infty$ output-feedback control*)

Consider the closed-loop system (3.5.4). Given a scalar $\gamma > 0$ (γ fixed), K is a stabilizing $\mathcal{H}_\infty$ dynamic output-feedback controller solving the problem of the Definition 3.5.1, if there exist $\mathbf{R}$, $\mathbf{S}$, $\mathcal{A}_\mathbf{K}$, $\mathcal{B}_\mathbf{K}$, $\mathcal{C}_\mathbf{K}$ and $\mathbf{D}_\mathbf{K}$ satisfying (3.6.1).

$$\begin{pmatrix} \mathcal{M}_{11} & \mathcal{M}_{21}^T & \mathcal{M}_{31}^T & \mathcal{M}_{41}^T \\ \mathcal{M}_{21} & \mathcal{M}_{22} & \mathcal{M}_{32}^T & \mathcal{M}_{42}^T \\ \mathcal{M}_{31} & \mathcal{M}_{32} & \mathcal{M}_{33} & \mathcal{M}_{43}^T \\ \mathcal{M}_{41} & \mathcal{M}_{42} & \mathcal{M}_{43} & \mathcal{M}_{44} \end{pmatrix} \prec 0 \quad \begin{pmatrix} \mathbf{R} & \mathcal{I}_n \\ \mathcal{I}_n & \mathbf{S} \end{pmatrix} \succ 0 \tag{3.6.1}$$

$$\begin{array}{ll} \mathcal{M}_{11} = A\mathbf{R} + \mathbf{R}A^T + B_2\mathcal{C}_\mathbf{K} + \mathcal{C}_\mathbf{K}{}^T B_2^T & \mathcal{M}_{21} = \mathcal{A}_\mathbf{K} + A^T + C_2^T \mathbf{D}_\mathbf{K}{}^T B_2^T \\ \mathcal{M}_{22} = A^T\mathbf{S} + \mathbf{S}A + \mathcal{B}_\mathbf{K}C_2 + C_2^T\mathcal{B}_\mathbf{K}{}^T & \mathcal{M}_{31} = B_1^T + D_{21}^T\mathbf{D}_\mathbf{K}{}^T B_2^T \\ \mathcal{M}_{32} = B_1^T\mathbf{S} + D_{21}^T\mathcal{B}_\mathbf{K}{}^T & \mathcal{M}_{33} = -\mathcal{I}_{n_u} \\ \mathcal{M}_{41} = C_1\mathbf{R} + D_{12}\mathcal{C}_\mathbf{K} & \mathcal{M}_{42} = C_1 + D_{12}\mathbf{D}_\mathbf{K}C_2 \\ \mathcal{M}_{43} = D_{11} + D_{12}\mathbf{D}_\mathbf{K}D_{21} & \mathcal{M}_{44} = -\gamma^2\mathcal{I}_m \end{array}$$

The controller K is then given by the following transformations,

$$\begin{cases} C_K = (\mathcal{C}_\mathbf{K} - \mathbf{D}_\mathbf{K}C_2\mathbf{R})M^{-T} \\ B_K = N^{-1}(\mathcal{B}_\mathbf{K} - \mathbf{S}B_2\mathbf{D}_\mathbf{K}) \\ A_K = N^{-1}(\mathcal{A}_\mathbf{K} - \mathbf{S}A\mathbf{R} - \mathbf{S}B_2\mathbf{D}_\mathbf{K}C_2\mathbf{R} - NB_KC_2\mathbf{R} - \mathbf{S}B_2C_KM^T)M^{-T} \end{cases}$$

where M and N are defined such that $MN^T = I_n - RS$. This equation can be solved using a singular value decomposition and a Cholesky factorization.
The optimal problem is solved if the previous inequality holds and $\gamma = \gamma_\infty$.

Proof 3.6.1

For detailed proof, see [Scherer and Weiland, 1999, Scherer et al., 1997, Scherer, 2000].

Remark 3.6.1 (*Numerical issues*)

For practical issues, the LMI (2.95) is solved a first time to find γ_∞, the optimal attenuation level. Then, the LMI resolution can be played a second time with a fixed higher attenuation level. Furthermore, the second LMI of (3.6.1) should be replaced by,

$$\begin{pmatrix} R & \alpha\mathcal{I}_n \\ \alpha\mathcal{I}_n & S \end{pmatrix} \succ 0$$

where $\alpha > 0$, and the optimization to be done consists of maximizing α. This procedure maximizes the minimal eigenvalue of RS, and hence pushes it away from $\mathcal{I}_n$, avoiding bad conditioning when inverting M and N during the transformations. This procedure avoids numerical problems and should be used in practice for all the controller synthesis given in this chapter.

Proposition 3.6.2 (*Dynamic $\mathcal{H}_2$ output-feedback control*)

Consider the closed-loop system (3.5.4). Given a scalar $\sigma > 0$ (σ fixed), the controller K is a stabilizing $\mathcal{H}_2$ dynamic output-feedback controller solving the suboptimal problem of the Definition 3.5.2 if there exist $\mathbf{X}$, $\mathbf{Y}$, $\mathbf{Z}$, $\mathcal{A}_\mathbf{K}$, $\mathcal{B}_\mathbf{K}$, $\mathcal{C}_\mathbf{K}$ and $\mathbf{D}_\mathbf{K}$ satisfying (3.6.2).

$$\begin{pmatrix} \mathcal{M}_{11} & \mathcal{M}_{21}^T & \mathcal{M}_{31}^T \\ \mathcal{M}_{21} & \mathcal{M}_{22} & \mathcal{M}_{32}^T \\ \mathcal{M}_{31} & \mathcal{M}_{32} & \mathcal{M}_{33} \end{pmatrix} \prec 0 \quad \begin{pmatrix} \mathcal{N}_{11} & \mathcal{N}_{21}^T & \mathcal{N}_{31}^T \\ \mathcal{N}_{21} & \mathcal{N}_{22} & \mathcal{N}_{32}^T \\ \mathcal{N}_{31} & \mathcal{N}_{32} & \mathcal{N}_{33} \end{pmatrix} \succ 0 \quad Tr(\mathbf{Z}) < \sigma \tag{3.6.2}$$

$$\begin{array}{ll} \mathcal{M}_{11} = A\mathbf{X} + \mathbf{X}A^T + B_2\mathcal{C}_\mathbf{K}{}^T B_2^T & \mathcal{M}_{21} = \mathcal{A}_\mathbf{K} + A^T + C_2^T \mathbf{D}_\mathbf{K}{}^T B_2^T \\ \mathcal{M}_{22} = A^T\mathbf{Y} + \mathbf{Y}A + \mathcal{B}_\mathbf{K} C_2 + C_2^T \mathcal{B}_\mathbf{K}{}^T & \mathcal{M}_{31} = B_1^T + D_{21}^T \mathbf{D}_\mathbf{K}{}^T B_2^T \\ \mathcal{M}_{32} = B_1^T\mathbf{Y} + D_{21}^T \mathcal{B}_\mathbf{K}{}^T & \mathcal{M}_{33} = -\mathcal{I}_{n_u} \\ \mathcal{N}_{11} = \mathbf{X} & \mathcal{N}_{21} = \mathcal{I}_n \\ \mathcal{N}_{22} = \mathbf{Y} & \mathcal{N}_{31} = C1\mathbf{X} + D_{12}\mathbf{C}_\mathbf{K} \\ \mathcal{N}_{32} = C_1 + D_{12}D_K C_2 & \mathcal{N}_{33} = \mathbf{Z} \end{array}$$

The controller K is then given by the following transformations,

$$\begin{cases} C_K = (\mathcal{C}_\mathbf{K} - \mathbf{D}_\mathbf{K} C_2 \mathbf{X}) M^{-T} \\ B_K = N^{-1}(\mathcal{B}_\mathbf{K} - \mathbf{Y} B_2 \mathbf{D}_\mathbf{K}) \\ A_K = N^{-1}(\mathcal{A}_\mathbf{K} - \mathbf{Y}A\mathbf{X} - \mathbf{Y}B_2\mathbf{D}_\mathbf{K}C_2\mathbf{X} - NB_K C_2\mathbf{X} - \mathbf{Y}B_2 C_K M^T) M^{-T} \end{cases}$$

where M and N are defined such that $MN^T = I_n - RS$. This equation can be solved using a singular value decomposition and a Cholesky factorization.
The optimal problem is solved if the previous inequality holds and $\sigma = \sigma_2$.

Proof 3.6.2

For detailed proof, see [Scherer and Weiland, 1999, Scherer et al., 1997, Scherer, 2000].

In order to tackle the mixed $\mathcal{H}_\infty/\mathcal{H}_2$ synthesis problem, described in the previous section, the generalized plant (3.6.3) has to be considered. It includes both the $\mathcal{H}_\infty$ and $\mathcal{H}_2$ performance objectives, as represented in Figure 3.2.

$$\begin{pmatrix} \dot{x} \\ z_\infty \\ z_2 \\ y \end{pmatrix} = \begin{pmatrix} A & B_1 & B_2 \\ C_\infty & D_{\infty 1} & D_{\infty 2} \\ C_2 & D_{21} & D_{22} \\ C_y & D_{y1} & \mathcal{O} \end{pmatrix} \begin{pmatrix} x \\ w \\ u \end{pmatrix} \tag{3.6.3}$$

where the outputs z_∞ and z_2 represent the outputs to be controlled, corresponding to the $\mathcal{H}_\infty$ and $\mathcal{H}_2$ performance specifications respectively.

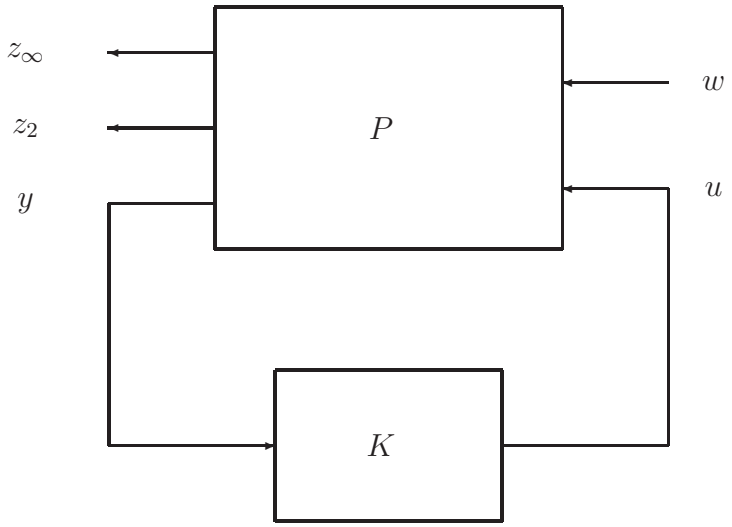

Figure 3.2: Generalized plant for mixed $\mathcal{H}_\infty/\mathcal{H}_2$ design

Given the controller (3.5.2) to be designed, the closed-loop system can be expressed as in (3.6.4).

$$\begin{pmatrix} \dot{x}_{cl} \\ z_\infty \\ z_2 \end{pmatrix} = \begin{pmatrix} A_{cl} & B_{cl} \\ C_{cl_1} & D_{cl_1} \\ C_{cl_2} & D_{cl_2} \end{pmatrix} \begin{pmatrix} x_{cl} \\ w \end{pmatrix} \tag{3.6.4}$$

where the state vector $x_{cl} = (x^T, \zeta^T)^T$ of the closed-loop system contains both the state vector of the system and of the controller. The matrices A_{cl}, B_{cl}, C_{cl_2}, C_{cl_1}, D_{cl_1} and D_{cl_2} of the closed-loop system are given by (3.6.5).

$$\begin{cases} A_{cl} = \begin{pmatrix} A + B_2 D_K C_y & B_2 C_K \\ B_K C_y & A_K \end{pmatrix} & B_{cl} = \begin{pmatrix} B_1 + B_2 D_K D_{y1} \\ B_K D_{y1} \end{pmatrix} \\ C_{cl_1} = \begin{pmatrix} C_\infty + D_{\infty 2} D_K C_y & D_{\infty 2} C_K \end{pmatrix} & C_{cl_2} = \begin{pmatrix} C_2 + D_{22} D_K C_y & D_{22} C_K \end{pmatrix} \\ D_{cl_1} = (D_{\infty 1} + D_{\infty 2} D_K D_{y1}) & D_{cl_2} = (D_{21} + D_{22} D_K D_{y1}) \end{cases} \tag{3.6.5}$$

Proposition 3.6.3 (*Dynamic $\mathcal{H}_\infty/\mathcal{H}_2$ output-feedback control*)

Consider the closed-loop system (3.6.4) and two scalars $\gamma > 0$ and $\sigma > 0$. The controller (3.5.2) is a dynamic output-feedback $\mathcal{H}_\infty/\mathcal{H}_2$ controller solving the problem of the Definition 3.5.3 if there exist $\mathbf{R}$, $\mathbf{S}$, $\mathbf{Q}$, $\mathcal{A}_\mathbf{K}$, $\mathcal{B}_\mathbf{K}$, $\mathcal{C}_\mathbf{K}$, $\mathbf{D}_\mathbf{K}$ satisfying (3.6.6-3.6.8).

$$\begin{pmatrix} \mathcal{P}_{11} & \mathcal{P}_{12} & \mathcal{P}_{13} & \mathcal{P}_{41}^T \\ \mathcal{P}_{12}^T & \mathcal{P}_{22} & \mathcal{P}_{23} & \mathcal{P}_{42}^T \\ \mathcal{P}_{13}^T & \mathcal{P}_{23}^T & \mathcal{P}_{33} & \mathcal{P}_{43}^T \\ \mathcal{P}_{41} & \mathcal{P}_{42} & \mathcal{P}_{43} & \mathcal{P}_{44} \end{pmatrix} \prec 0 \tag{3.6.6}$$

$$\begin{aligned}
\mathcal{P}_{11} &= A\mathbf{R} + \mathbf{R}A^T + B_2\mathcal{C}_\mathbf{K} + \mathcal{C}_\mathbf{K}{}^T B_2^T \\
\mathcal{P}_{12} &= \mathcal{A}_\mathbf{K}{}^T + A + B_2\mathbf{D}_\mathbf{K}C_y \\
\mathcal{P}_{13} &= B_1 + B_2\mathbf{D}_\mathbf{K}D_{y1} \\
\mathcal{P}_{22} &= A^T\mathbf{S} + \mathbf{S}A + \mathcal{B}_\mathbf{K}C_y + C_y^T\mathcal{B}_\mathbf{K} \\
\mathcal{P}_{23} &= \mathbf{S}B_1 + \mathcal{B}_\mathbf{K}D_{y1} \\
\mathcal{P}_{33} &= -\mathcal{I} \\
\mathcal{P}_{41} &= C_\infty\mathbf{R} + D_{\infty 2}\mathcal{C}_\mathbf{K} \\
\mathcal{P}_{42} &= C_\infty + D_{\infty 2}\mathbf{D}_\mathbf{K}C_y \\
\mathcal{P}_{43} &= D_{\infty 1} + D_{\infty 2}\mathbf{D}_\mathbf{K}D_{y1} \\
\mathcal{P}_{44} &= -\gamma^2\mathcal{I}
\end{aligned}$$

$$\begin{pmatrix} \mathbf{Q} & C_2\mathbf{R} + D_{22}\mathcal{C}_\mathbf{K} & C_2 + D_{22}\mathbf{D}_\mathbf{K}C_y \\ * & \mathbf{R} & \mathcal{I} \\ * & \mathcal{I} & S \end{pmatrix} \succ 0 \tag{3.6.7}$$

$$\begin{aligned} Trace(\mathbf{Q}) &< \sigma^2 \\ D_{21} + D_{22}\mathbf{D}_\mathbf{K}D_{y1} &= 0 \end{aligned} \tag{3.6.8}$$

The controller K is then given by the following transformations,

$$\begin{cases} C_K = (\mathcal{C}_\mathbf{K} - \mathbf{D}_\mathbf{K}C_y\mathbf{X})M^{-T} \\ B_K = N^{-1}(\mathcal{B}_\mathbf{K} - \mathbf{Y}B_2\mathbf{D}_\mathbf{K}) \\ A_K = N^{-1}(\mathcal{A}_\mathbf{K} - \mathbf{Y}A\mathbf{X} - \mathbf{Y}B_2\mathbf{D}_\mathbf{K}C_y\mathbf{X} - NB_KC_y\mathbf{X} - \mathbf{Y}B_2C_KM^T)M^{-T} \end{cases}$$

where M and N are defined such that $MN^T = I_n - RS$. This equation can be solved using a singular value decomposition and a Cholesky factorization.

Proof 3.6.3

For detailed proof, see [Scherer and Weiland, 1999, Scherer et al., 1997, Scherer, 2000].

3.6.2 LTI design: state-feedback control

In this section, the objective is to design a stabilizing $\mathcal{H}_\infty$ state-feedback controller $K \in \mathbb{R}^{n_u \times n}$. Therefore a full-state measurement is assumed: $C_2 = \mathcal{I}_n$ and $D_{21} = \mathcal{O}$ in the system (3.5.1). The control signal is given by $u = K \cdot x$, where K is the static gain of the controller. Therefore the corresponding closed-loop system is given by (3.6.9).

$$\begin{cases} A_{cl} = A + B_2 K \\ B_{cl} = B_1 \\ C_{cl} = C_1 + D_{12} K \\ D_{cl} = D_{11} \end{cases} \tag{3.6.9}$$

Then the $\mathcal{H}_\infty$ and $\mathcal{H}_2$ controllers can be computed according to the following LMI based results respectively given in Propositions 3.6.4 and 3.6.5.

Proposition 3.6.4 ($\mathcal{H}_\infty$ *state-feedback control*)

Consider the closed-loop system (3.6.9). Given a scalar $\gamma > 0$ (γ fixed), K is a stabilizing $\mathcal{H}_\infty$ static state-feedback controller solving the problem of the Definition 3.5.1 if there exist a symmetric matrix $\mathbf{X} \succ 0$, and $\mathbf{Y}$ satisfying (3.6.10).

$$\begin{pmatrix} (A\mathbf{X} + B_2\mathbf{Y}) + (A\mathbf{X} + B_2\mathbf{Y})^T & B_1 & (C_1\mathbf{X} + D_{12}\mathbf{Y})^T \\ B_1^T & -\mathcal{I} & D_{11}^T \\ C_1\mathbf{X} + D_{12}\mathbf{Y} & D_{11} & -\gamma^2\mathcal{I} \end{pmatrix} \prec 0 \tag{3.6.10}$$

The controller K is then given by $K = \mathbf{Y}\mathbf{X}^{-1}$.
The optimal problem is solved if the previous inequality holds and $\gamma = \gamma_\infty$.

Proof 3.6.4

For detailed proof, see [Scherer and Weiland, 1999, Scherer et al., 1997, Scherer, 2000].

Proposition 3.6.5 ($\mathcal{H}_2$ *state-feedback control*)

Consider the closed-loop system (3.6.9) determined by (3.6.9). Given a scalar $\sigma > 0$ (σ fixed), K is a stabilizing $\mathcal{H}_2$ static state-feedback controller solving the problem of the Definition 3.5.2 if there exist $\mathbf{X} = \mathbf{X}^T$, $\mathbf{Q} = \mathbf{Q}^T$ and $\mathbf{Y}$ satisfying (3.6.11).

$$\begin{gathered} \begin{pmatrix} (A\mathbf{X} + B_2\mathbf{Y}) + (A\mathbf{X} + B_2\mathbf{Y})^T & B_1^T \\ B_1^T & -\mathcal{I} \end{pmatrix} \prec 0 \\ \begin{pmatrix} \mathbf{Q} & (C_1\mathbf{X} + D_{12}\mathbf{Y}) \\ (C_1\mathbf{X} + D_{12}\mathbf{Y})^T & \mathbf{X} \end{pmatrix} \succ 0 \\ Tr(\mathbf{Q}) < \sigma^2 \end{gathered} \tag{3.6.11}$$

The controller K is given by $K = \mathbf{Y}\mathbf{X}^{-1}$.
The optimal problem is solved if the previous inequality holds and $\sigma = \sigma_2$.

Proof 3.6.5

For detailed proof, see [Scherer and Weiland, 1999, Scherer et al., 1997, Scherer, 2000].

Remark 3.6.2

The mixed $\mathcal{H}_\infty/\mathcal{H}_2$ static state-feedback controller can be easily derived from the two previous Propositions 3.6.4 and 3.6.5, as in the dynamic output-feedback case.

3.7 LPV design

The results presented in Section 3.6 allow to design $\mathcal{H}_\infty/\mathcal{H}_2$ controllers for LTI systems only. This could be restrictive since most systems are nonlinear and may have time-varying parameters. In this section, the previous results are extended to LPV systems. As many systems can be represented as LPV systems, the results given in this section are very interesting since they allow to take nonlinearities or parameter variations into account in the synthesis of the controller, and to use the powerful linear control theory as well. These results will be used in the next chapters to design "gain-scheduled" suspension controllers. This section is based on LPV control results presented in [Scherer and Weiland, 1999, Apkarian et al., 1995].

3.7.1 Problem statement

Let us consider the following LPV system (3.7.1) to be controlled, whose matrices depend on a given parameter ρ.

$$\left\{ \begin{array}{rcl} \dot{x}(t) & = & A(\rho)x(t) + B(\rho)e(t) \\ y(t) & = & C(\rho)x(t) + D(\rho)e(t) \end{array} \right. \tag{3.7.1}$$

where $\rho = (\rho_1, \rho_2, ..., \rho_p)$, $\rho_i \in [\underline{\rho}_i, \overline{\rho}_i]$; $\underline{\rho}_i$ and $\overline{\rho}_i$ denote respectively the minimal and maximal values of the parameter ρ_i. The corresponding generalized parameter-dependent plant is given by (3.7.2).

$$P(\rho) : \left(\begin{array}{c} \dot{x} \\ z \\ y \end{array} \right) = \left(\begin{array}{ccc} A(\rho) & B_1(\rho) & B_2(\rho) \\ C_1(\rho) & D_{11}(\rho) & D_{12}(\rho) \\ C_2(\rho) & D_{21}(\rho) & \mathcal{O} \end{array} \right) \left(\begin{array}{c} x \\ w \\ u \end{array} \right) \tag{3.7.2}$$

where $x \in \mathbb{R}^n$ is the state vector, $y \in \mathbb{R}^m$ are the measured variables, $z \in \mathbb{R}^{n_z}$ are the outputs to be controlled, $u \in \mathbb{R}^{n_u}$ are the control signals, $w \in \mathbb{R}^{n_w}$ are the exogenous

inputs. Here, only strictly proper systems are considered since D_{22} is assumed to be zero.

The parameter-dependent dynamic output-feedback controller to be designed can be expressed as,

$$K : \begin{pmatrix} \dot{\zeta} \\ u \end{pmatrix} = \begin{pmatrix} A_K(\rho) & B_K(\rho) \\ C_K(\rho) & D_K(\rho) \end{pmatrix} \begin{pmatrix} \zeta \\ y \end{pmatrix} \tag{3.7.3}$$

where $A_K \in \mathbb{R}^{n\times n}$, $B_K \in \mathbb{R}^{n\times m}$, $C_K \in \mathbb{R}^{n_u\times n}$, $D_K \in \mathbb{R}^{n_u\times m}$ represent the matrices of the controller and ζ denotes the state variables of the controller.

Remark 3.7.1

The set of parameters used respectively in the controller and in the system could be different.

Then the closed-loop system can be written as,

$$\begin{pmatrix} \dot{x}_{cl} \\ z \end{pmatrix} = \begin{pmatrix} A_{cl}(\rho) & B_{cl}(\rho) \\ C_{cl}(\rho) & D_{cl}(\rho) \end{pmatrix} \begin{pmatrix} x_{cl} \\ w \end{pmatrix} \tag{3.7.4}$$

where the state-vector $x_{cl} = (x^T, \zeta^T)^T$ of the closed-loop system contains the state-vector of the system and the state vector of the controller. The matrices of the closed-loop system are defined by,

$$\begin{cases} A_{cl}(\rho) = \begin{pmatrix} A(\rho) + B_2(\rho)D_K(\rho)C_2(\rho) & B_2(\rho)C_K(\rho) \\ B_K(\rho)C_2(\rho) & A_K(\rho) \end{pmatrix} \\ B_{cl}(\rho) = \begin{pmatrix} B_1(\rho) + B_2(\rho)D_K(\rho)D_{21}(\rho) \\ B_K(\rho)D_{21}(\rho) \end{pmatrix} \\ C_{cl}(\rho) = \begin{pmatrix} C_1(\rho) + D_{12}(\rho)D_K(\rho)C_2(\rho) & D_{12}(\rho)C_K(\rho) \end{pmatrix} \\ D_{cl}(\rho) = D_{11}(\rho) + D_{12}(\rho)D_K(\rho)D_{21}(\rho) \end{cases} \tag{3.7.5}$$

The solution of the $\mathcal{H}_\infty$ problem in the LPV case, according to Definition 3.5.1 is given in the Proposition 3.7.1.

Proposition 3.7.1 (*Dynamic LPV/$\mathcal{H}_\infty$ output-feedback control*)

Consider the closed-loop system (3.7.5). Given a scalar $\gamma > 0$ (γ fixed), $K(\rho)$ is a stabilizing $\mathcal{H}_\infty$ dynamic output-feedback controller solving the problem of the Definition 3.5.1 if there exist $\mathbf{R}$, $\mathbf{S}$, $\mathcal{A}_\mathbf{K}(\rho)$, $\mathcal{B}_\mathbf{K}(\rho)$, $\mathcal{C}_\mathbf{K}(\rho)$ and $\mathbf{D}_\mathbf{K}(\rho)$ according to (3.7.6).

$$\begin{pmatrix} \mathcal{M}_{11} & \mathcal{M}_{21}^T & \mathcal{M}_{31}^T & \mathcal{M}_{41}^T \\ \mathcal{M}_{21} & \mathcal{M}_{22} & \mathcal{M}_{32}^T & \mathcal{M}_{42}^T \\ \mathcal{M}_{31} & \mathcal{M}_{32} & \mathcal{M}_{33} & \mathcal{M}_{43}^T \\ \mathcal{M}_{41} & \mathcal{M}_{42} & \mathcal{M}_{43} & \mathcal{M}_{44} \end{pmatrix} \prec 0 \quad \begin{pmatrix} \mathbf{R} & \mathcal{I}_n \\ \mathcal{I}_n & \mathbf{S} \end{pmatrix} \succ 0 \tag{3.7.6}$$

$$\begin{aligned}
\mathcal{M}_{11} &= A(\rho)\mathbf{R} + \mathbf{R}A^T(\rho) + B_2(\rho)\mathcal{C}_\mathbf{K}(\rho) + \mathcal{C}_\mathbf{K}{}^T(\rho)B_2^T(\rho) \\
\mathcal{M}_{21} &= \mathcal{A}_\mathbf{K}(\rho) + A^T(\rho) + C_2^T(\rho)\mathbf{D}_\mathbf{K}{}^T(\rho)B_2^T(\rho) \\
\mathcal{M}_{22} &= A^T(\rho)\mathbf{S} + \mathbf{S}A(\rho) + \mathcal{B}_\mathbf{K}(\rho)C_2(\rho) + C_2^T(\rho)\mathcal{B}_\mathbf{K}{}^T(\rho) \\
\mathcal{M}_{31} &= B_1^T(\rho) + D_{21}^T(\rho)\mathbf{D}_\mathbf{K}{}^T(\rho)B_2^T(\rho) \\
\mathcal{M}_{32} &= B_1^T(\rho)\mathbf{S} + D_{21}^T(\rho)\mathcal{B}_\mathbf{K}{}^T(\rho) \\
\mathcal{M}_{33} &= -\mathcal{I}_{n_u} \\
\mathcal{M}_{41} &= C_1(\rho)\mathbf{R} + D_{12}(\rho)\mathcal{C}_\mathbf{K}(\rho) \\
\mathcal{M}_{42} &= C_1(\rho) + D_{12}(\rho)\mathbf{D}_\mathbf{K}(\rho)C_2(\rho) \\
\mathcal{M}_{43} &= D_{11}(\rho) + D_{12}(\rho)\mathbf{D}_\mathbf{K}(\rho)D_{21}(\rho) \\
\mathcal{M}_{44} &= -\gamma^2\mathcal{I}_m
\end{aligned}$$

The controller $K(\rho)$ can be computed using the following transformations,

$$\begin{cases}
C_K(\rho) = (\mathcal{C}_\mathbf{K}(\rho) - \mathbf{D}_\mathbf{K}(\rho)C_2(\rho)\mathbf{R})M^{-T} \\
B_K(\rho) = N^{-1}(\mathcal{B}_\mathbf{K}(\rho) - \mathbf{S}B_2(\rho)\mathbf{D}_\mathbf{K}(\rho)) \\
A_K(\rho) = N^{-1}(\mathcal{A}_\mathbf{K}(\rho) - \mathbf{S}A(\rho)\mathbf{R} - \mathbf{S}B_2(\rho)\mathbf{D}_\mathbf{K}(\rho)C_2(\rho)\mathbf{R} \\
\quad - NB_K(\rho)C_2(\rho)\mathbf{R} - \mathbf{S}B_2(\rho)C_K(\rho)M^T)M^{-T}
\end{cases}$$

where M and N are defined such that $MN^T = I_n - RS$. Note that this equation can be solved using a singular value decomposition and a Cholesky factorization. The optimal problem is solved if the previous inequality holds and $\gamma = \gamma_\infty$.

Proof 3.7.1

For detailed proof, see [Scherer and Weiland, 1999, Scherer et al., 1997, Scherer, 2000].

The solution of the $\mathcal{H}_2$ problem in the LPV case, according to Definition 3.5.2, is given in the Proposition 3.7.2.

Proposition 3.7.2 (*Dynamic LPV/$\mathcal{H}_2$ output-feedback control*)

Consider the closed-loop system (3.7.5). Given a scalar $\sigma > 0$ (σ fixed), $K(s)(\rho)$ is a stabilizing $\mathcal{H}_2$ dynamic output-feedback controller solving the problem of the Definition 3.5.2 if there exist $\mathbf{X}$, $\mathbf{Y}$, $\mathbf{Z}$, $\mathcal{A}_\mathbf{K}(\rho)$, $\mathcal{B}_\mathbf{K}(\rho)$, $\mathcal{C}_\mathbf{K}(\rho)$ and $\mathbf{D}_\mathbf{K}(\rho)$ according to (3.7.7).

$$\begin{pmatrix} \mathcal{M}_{11} & \mathcal{M}_{21}^T & \mathcal{M}_{31}^T \\ \mathcal{M}_{21} & \mathcal{M}_{22} & \mathcal{M}_{32}^T \\ \mathcal{M}_{31} & \mathcal{M}_{32} & \mathcal{M}_{33} \end{pmatrix} \prec 0 \quad \begin{pmatrix} \mathcal{N}_{11} & \mathcal{N}_{21}^T & \mathcal{N}_{31}^T \\ \mathcal{N}_{21} & \mathcal{N}_{22} & \mathcal{N}_{32}^T \\ \mathcal{N}_{31} & \mathcal{N}_{32} & \mathcal{N}_{33} \end{pmatrix} \succ 0 \quad Tr(Z) < \sigma \tag{3.7.7}$$

$$\begin{aligned}
\mathcal{M}_{11} &= A(\rho)\mathbf{X} + \mathbf{X}A^T(\rho) + B_2(\rho)\mathcal{C}_\mathbf{K}(\rho) + \mathcal{C}_\mathbf{K}(\rho)^T B_2^T(\rho) \\
\mathcal{M}_{21} &= \mathcal{A}_\mathbf{K}(\rho) + A^T(\rho) + C_2^T(\rho)\mathbf{D}_\mathbf{K}(\rho)^T B_2^T(\rho) \\
\mathcal{M}_{22} &= A^T(\rho)\mathbf{Y} + \mathbf{Y}A(\rho) + \mathcal{B}_\mathbf{K}(\rho)C_2(\rho) + C_2^T(\rho)\mathcal{B}_\mathbf{K}(\rho)^T \\
\mathcal{M}_{31} &= B_1^T(\rho) + D_{21}^T(\rho)\mathbf{D}_\mathbf{K}(\rho)^T B_2^T(\rho) \\
\mathcal{M}_{32} &= B_1^T(\rho)\mathbf{Y} + D_{21}^T(\rho)\mathcal{B}_\mathbf{K}(\rho)^T \\
\mathcal{M}_{33} &= -\mathcal{I}_{n_u} \\
\mathcal{N}_{11} &= \mathbf{X} \\
\mathcal{N}_{21} &= \mathcal{I}_n \\
\mathcal{N}_{22} &= \mathbf{Y} \\
\mathcal{N}_{31} &= C1(\rho)\mathbf{X} + D_{12}(\rho)\mathbf{C}_\mathbf{K}(\rho) \\
\mathcal{N}_{32} &= C_1(\rho) + D_{12}(\rho)\mathbf{D}_\mathbf{K}(\rho)C_2(\rho) \\
\mathcal{N}_{33} &= Z
\end{aligned}$$

The controller $K(\rho)$ can be computed using the following transformations,

$$\begin{cases}
C_K(\rho) = (\mathcal{C}_\mathbf{K}(\rho) - \mathbf{D}_\mathbf{K}(\rho)C_2(\rho)\mathbf{X})M^{-T} \\
B_K(\rho) = N^{-1}(\mathcal{B}_\mathbf{K}(\rho) - \mathbf{Y}B_2(\rho)\mathbf{D}_\mathbf{K}(\rho)) \\
A_K(\rho) = N^{-1}(\mathcal{A}_\mathbf{K}(\rho) - \mathbf{Y}A(\rho)\mathbf{X} - \mathbf{Y}B_2(\rho)\mathbf{D}_\mathbf{K}(\rho)C_2(\rho)\mathbf{X} \\
\quad - NB_K(\rho)C_2(\rho)\mathbf{X} - \mathbf{Y}B_2(\rho)C_K(\rho)M^T)M^{-T}
\end{cases}$$

where M and N are defined such that $MN^T = I_n - RS$. Note that this equation can be solved using a singular value decomposition and a Cholesky factorization. The optimal problem is solved if the previous inequality holds and $\sigma = \sigma_2$.

Proof 3.7.2

For detailed proof, see [Scherer and Weiland, 1999, Scherer et al., 1997, Scherer, 2000].

Remark 3.7.2 (*Mixed synthesis : LPV case*)

The results given for the mixed synthesis in the LTI case can be extended to the LPV case, according to the same procedure.

Remark 3.7.3 (*State-feedback control : LPV case*)

The results given for the state-feedback control in the LTI case can be extended to

the LPV case, according to the same procedure.

3.7.2 A polytopic approach to the design of LPV controllers

The Propositions 3.7.1 and 3.7.2 consist in solving various parameter-dependent sets of matrix inequalities. Since the parameter ρ varies in a compact interval $[\underline{\rho}, \overline{\rho}]$, the number of possible values is infinite. Therefore an infinite set of LMI has to be solved. Various methods exist to turn this infinite dimension problem into a finite one:

- The Polytopic approach
- The Parameter dependent approaches (grid, sum of square, polynomial,...)
- The Linear Fractional Representation approach

In this thesis, the Polytopic approach, detailed in [Apkarian et al., 1995], has been used since it is the most simple and appropriate method when the number of parameters is small. It is referred to as the "Polytopic approach" since the design method relies on a polytope whose vertices are given by the upper and lower bounds of each parameter. Then a new set of LMI is derived from the evaluation of the parameter-dependent LMI at each vertex of the polytope, which turns the infinite dimensional problem into a finite one. Finally, a single Lyapunov function that solves the relaxed problem and ensures the quadratic stability of the closed-loop system has to be found in order to solve the $\mathcal{H}_\infty$ or $\mathcal{H}_2$ problems.

Remark 3.7.4 (*Polytopic approach: application requirements*)

The Polytopic approach can be applied to an LPV system when (see [Scherer and Weiland, 1999, Scherer et al., 1997]):

- *The transfer $u \mapsto y$ is strictly proper: $D_{22} = \mathcal{O}$,*
- *The input and output matrices B_2, D_{12} and C_2, D_{21} do not depend on the varying parameter,*

Therefore the system has to be defined as,

$$P(\rho) : \begin{pmatrix} \dot{x} \\ z \\ y \end{pmatrix} = \begin{pmatrix} A(\rho) & B_1(\rho) & B_2 \\ C_1(\rho) & D_{11}(\rho) & D_{12} \\ C_2 & D_{21} & \mathcal{O} \end{pmatrix} \begin{pmatrix} x \\ w \\ u \end{pmatrix} \tag{3.7.8}$$

If the system cannot be written such that these conditions are fulfilled, a simple solution consists of filtering the input and/or the output with a strictly proper filter. This leads to parameter independent matrices B_2, D_{12} and C_2, D_{21}.

Proposition 3.7.3 (*LPV synthesis*)

If the application requirements given in Remark 3.7.4 are fulfilled, a polytopic controller can be computed by synthesizing a controller at each vertex of the polytopic system. If a single Lyapunov function can be found for all the controllers, the achieved LPV controller stabilizes the LPV system for all the possible sets of parameters. This leads to the global stability of the closed-loop LPV system. The N controllers to be computed at each vertex of the polytope are given by:

$$\left\{K_1 = \begin{pmatrix} A_{K_1} & B_{K_1} \\ C_{K_1} & D_{K_1} \end{pmatrix}, ...K_N = \begin{pmatrix} A_{K_N} & B_{K_N} \\ C_{K_N} & D_{K_N} \end{pmatrix}\right\} \tag{3.7.9}$$

Then the LPV controller is given by the convex combination (3.7.10) of these controllers as,

$$K(\rho) = \sum_{k=1}^{2^p} \alpha_k(\rho) \cdot K_k \tag{3.7.10}$$

with

$$\alpha_k(\rho) = \frac{\prod_{j=1}^{p} \mid \rho_j - \Theta_k \mid}{\prod_{j=1}^{p} \mid \overline{\rho_j} - \underline{\rho_j} \mid} \tag{3.7.11}$$

and

$$\sum_{k=1}^{2^p} \alpha_k(\rho) = 1 \tag{3.7.12}$$

where p is the number of varying parameters, $N = 2^p$ the number of vertices of the polytope, $\overline{\rho_j}$, $\underline{\rho_j}$ are respectively the upper and lower bounds of the parameter ρ_j, and Θ_k is the kth vertex of the polytope.

3.8 Pole placement in LMI regions

In this section, a pole placement method in LMI regions, developed in [Chilali et al., 1999], is presented. This method leads to LMI constraints that can be used in the synthesis of the controller to specify given pole placement objectives. The concept of LMI region is useful to formulate pole placement objectives in LMI terms.

Remark 3.8.1

The class of LMI regions is fairly general since its closure is the set of convex regions symmetric with respect to the real axis. From a practical point of view, LMI regions include useful regions such as sectors, disks, conics, strips, etc., as well as any intersection of the above.

Definition 3.8.1 (*LMI region*)

LMI regions are convex subsets $\mathcal{D}$ of the complex plane characterized by

$$\mathcal{D} = \{z \in \mathbb{C} : L + Mz + M^T z^* \prec 0\} \tag{3.8.1}$$

with $L = L^T = [\lambda_{ij}]_{i,j\in[1,m]}$ and $M = [\mu_{ij}]_{i,j\in[1,m]}$, where λ_{ij} and μ_{ij} denote respectively the entries of $L \in \mathbb{R}^{m\times m}$ and $M \in \mathbb{R}^{m\times m}$.

The LMI constraint allowing to place the poles of a given closed-loop system (3.7.5) in the LMI region (3.8.1), is given by the Proposition 3.8.1.

Proposition 3.8.1 (*Pole placement in LMI regions*)

The closed-loop poles are located in the LMI region (3.8.1) if [Chilali et al., 1999] there exists a symmetric matrix $X = X^T \succ 0$ such that

$$\left[\lambda_{ij}X + \mu_{ij}A_{cl}X + \mu_{ij}XA_{cl}^T\right]_{i,j\in[1,m]} \prec 0 \tag{3.8.2}$$

with the notation

$$[S_{ij}]_{i,j\in[1,m]} \begin{pmatrix} S_{11} & \cdots & S_{1m} \\ \vdots & \ddots & \vdots \\ S_{m1} & \cdots & S_{mm} \end{pmatrix}$$

.

Proof 3.8.1

For detailed proof, see [Chilali et al., 1999].

Note that several constraints defined by (3.8.2) can be used in the synthesis to place the poles in the intersection of several LMI regions defined by (3.8.1).

3.9 μ-analysis

In this section, some useful tools for robustness analysis are briefly presented, resulting from past studies on the structured singular value, such as [Zhou et al., 1996, Skogestad and Postlethwaite, 2005, Stein and Doyle, 1991, Packard and Doyle, 1994]. This section is also based on previous investigations on robust stability and performance analysis, such as [Young et al., 1995, Safonov, 1983, Doyle, 1982]. Here the robust stability or performance of LTI systems with linear-fractional uncertainty is studied through μ analysis tools.

3.9.1 Structured singular value

While modeling a given system to be controlled or observed, some dynamics, particularly high-frequency dynamics, are often neglected for simplicity and computation-time reasons. Furthermore some parameters might be unknown or might change with time. Therefore the models used to design controllers or observers are simple and contain some uncertainties. When these uncertainties are not taken into account during the design process, it may lead, in practice, to a loss of performance or stability. The objective is then to design a robust controller/observer ensuring both the stability and given performances of the uncertain closed-loop system. Some tools have already been developed in past studies to analyze the robust stability and performance of a given closed-loop system, or to design robust controllers. The robust stability and performance are generally studied by computing respectively the smallest uncertainty making the closed-loop system unstable, and the smallest uncertainty making the system loose given performances. According to the considered type of uncertainties (structured or unstructured), various norms can be used to measure the robustness. The small-gain theorem, based on the $\mathcal{H}_\infty$-norm, allows to compute the maximal allowable uncertainties [Zhou et al., 1996, Skogestad and Postlethwaite, 2005] for unstructured uncertainties. In the case of structured uncertainties, the μ analysis, based on the structured singular value μ, is considered. This method is briefly described in this section since it is less conservative than the small-gain theorem.

Let us define the set of complex matrices representing a given set of uncertainties and characterized by

$$\underline{\Delta} = \left\{ \begin{array}{l} \Delta = diag\left\{\Delta_1(s), \Delta_2(s), ..., \Delta_q(s), \delta_1\mathcal{I}_{r_1}, ..., \delta_r\mathcal{I}_{r_r}, \epsilon_1\mathcal{I}_{c_1}, ..., \epsilon_c\mathcal{I}_{c_c}\right\} \\ \Delta \in \mathbb{C}^{k\times k}, \Delta_i \in \mathbb{C}^{k_i\times k_i}, \delta_i \in \mathbb{R}, \epsilon_i \in \mathbb{C} \end{array} \right\} \tag{3.9.1}$$

.

Note that the uncertainties $\Delta_i(s)$ have to be normalized as follows:

$$||\Delta_i(s)||_\infty < 1, \delta_i \in]-1; +1[\,, |\epsilon_i| < 1 \tag{3.9.2}$$

Remark 3.9.1

The model uncertainties (neglected dynamics,...), the parameter uncertainties and the sensors gain or phase uncertainties are commonly represented respectively by the terms $\Delta_i(s)$, $\delta_i\mathcal{I}_{r_i}$ and $\epsilon_i\mathcal{I}_{c_i}$ [Zhou et al., 1996, Skogestad and Postlethwaite, 2005].

Let us define the various problems under study in this section.

Definition 3.9.1 (*Nominal and robust stability and performances*)

- *The nominal stability (NS) is achieved if the nominal closed-loop system is internally stable,*
- *The nominal performance (NP) is achieved if the nominal stability is achieved and if the performance specifications of the nominal system are fulfilled,*
- *The robust stability (RS) is achieved if the uncertain system is stable for all* $\Delta_r(s) \in \underline{\Delta}_r$*, where* $\underline{\Delta}_r$ *is the considered set of uncertainties, and if the nominal stability is achieved,*
- *The robust performances (RP) is achieved if the robust stability is achieved and if the performance specifications of the uncertain sytem are fulfilled for all* $\Delta_r(s) \in \underline{\Delta}_r$*, where* $\underline{\Delta}_r$ *is the considered set of uncertainties.*

Consider a given system $N(s) \in \mathbb{R}^{n \times m}$ and a block diagonal perturbation $\Delta(s) \in \underline{\Delta}$, as represented in Figure 3.3. The interconnection of the Figure 3.3 is well-posed if $\mathcal{I} - N\Delta$ is invertible. The μ analysis consists of determining the smallest amount of perturbation Δ required to render the interconnection ill-posed. The structured singular value is defined below [Stein and Doyle, 1991, Packard and Doyle, 1994].

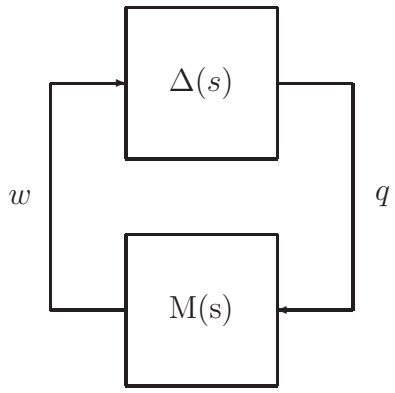

Figure 3.3: μ analysis interconnection

Definition 3.9.2 (*Structured singular value*)

Given a matrix $N \in \mathbb{C}^{k\times k}$, the structured singular value μ of the matrix N, corresponding to the set $\underline{\Delta}$ is given by,

$$\mu_{\underline{\Delta}}(N) \triangleq \begin{cases} \dfrac{1}{\min_{\Delta\in\underline{\Delta}}(\overline{\sigma}(\Delta)\ s.t.\ \det(\mathcal{I}-N\Delta)=0)} \\ \\ 0 \text{ if } \mathcal{I}-N\Delta \text{ is invertible} \end{cases} \tag{3.9.3}$$

where $\overline{\sigma}(\Delta)$ denotes the maximal singular value of Δ.

Remark 3.9.2

For each pulsation ω, it is possible to find the singular value $\mu_{\underline{\Delta}}(N)$ corresponding to the set $\underline{\Delta}$.

From the Definition 3.9.2, $\mathcal{I}-N\Delta$ remains invertible as long as Δ satisfies $\overline{\sigma}(\Delta) < 1/\mu_{\underline{\Delta}}(N)$, where $1/\mu_{\underline{\Delta}}(N)$ is called the well-posedness margin. For instance, $1/\mu_{\underline{\Delta}}(N) = 0.8$ means that well-posedness is guaranteed for perturbation sizes that do not exceed 80% of the prescribed bounds. Computing $\mu_{\underline{\Delta}}(N)$ is an NP-hard[1] problem in general. However, some upper and lower bounds can be computed by solving an LMI problem. For more details on the algorithm, see [Fan et al., 1991].

3.9.2 Robust stability and performance analysis

In this section, the methodology to analyze the robust stability and performance is presented, using various previous works on this topic [Zhou et al., 1996, Skogestad and Postlethwaite, 2005, Young et al., 1995, Safonov, 1983, Doyle, 1982]. The μ-analysis tools can be used in order to study the nominal and robust stability, and the nominal and robust performances. The Figure 3.4 represents the transfer matrix N of the nominal closed-loop system, the uncertainty matrix Δ_r of the form (3.9.1), containing all the uncertainties of the nominal system, and the matrix Δ_f representing fictive uncertainties between the outputs to be controlled and the exogenous inputs.

Remark 3.9.3

The fictive uncertainties contain the weighting functions used during the synthesis, and representing, for instance, the $\mathcal{H}_\infty$ performance specifications.

The matrix N can be written as

[1] non-deterministic polynomial-time hard

$$N(s) = \begin{pmatrix} N_{zv}(s) & N_{zw}(s) \\ N_{ev}(s) & N_{ew}(s) \end{pmatrix} \tag{3.9.4}$$

where w and e respectively represent the exogenous inputs and the outputs of the nominal system to be controlled.

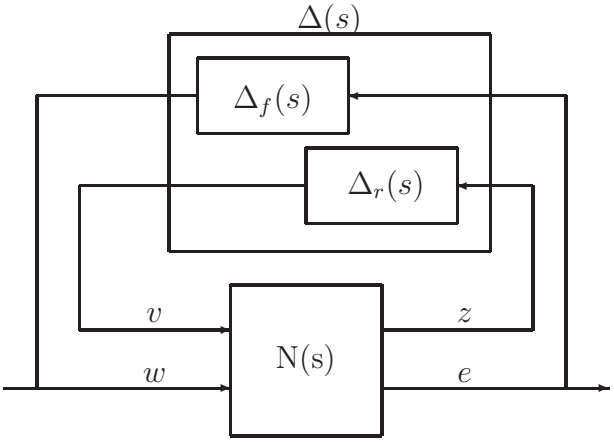

Figure 3.4: Robust performance analysis

- The nominal performance (NP) is analyzed through a μ-analysis of the stability while considering only the fictive uncertainties Δ_f [Zhou et al., 1996, Skogestad and Postlethwaite, 2005]. The structured singular value μ of the matrix N_{ew} represents the nominal performances of the system.
- The stability of the uncertain system (RS) is analyzed through the μ-analysis of the stability while considering only the real uncertainties Δ_r. If the structured singular value of the matrix N_{zv} is less than 1, then the robust stability is achieved.
- The robust performance (RP) is studied while considering both the real and fictive uncertainties:

  $$\Delta(s) = \begin{pmatrix} \Delta_f(s) & \mathcal{O} \\ \mathcal{O} & \Delta_r(s) \end{pmatrix} \tag{3.9.5}$$

  The structured singular value μ of the matrix N represents the robust performances of the uncertain system. If it is less than 1, the performances of the nominal system are achieved.

Consider the uncertainty (3.9.5), fulfilling $||\Delta(s)||_\infty < 1$, and the following required performances:

$$||T_{ew}(s)||_\infty = ||N_{ew}(s) + N_{ev}(s)\Delta(s)(\mathcal{I} - N_{zv}(s)\Delta(s))^{-1}N_{zw}(s)||_\infty \leq 1 \tag{3.9.6}$$

Remark 3.9.4

If $\Delta = 0$, it corresponds to the nominal problem.

Then for all the considered uncertainties,

- NS $\Leftrightarrow$ N is internally stable,
- NP $\Leftrightarrow \overline{\sigma}(N_{ew}(j\omega)) = \mu_{\underline{\Delta}_f}(N_{ew}(j\omega)) < 1$, $\forall\omega$, and NS,
- RS $\Leftrightarrow \mu_{\underline{\Delta}_r}(N_{zv}(j\omega)) < 1$, $\forall\omega$, and NS,
- RP $\Leftrightarrow \mu_{\underline{\Delta}}(N(j\omega)) < 1$, $\forall\omega$, $\Delta = \begin{pmatrix} \Delta_f & \mathcal{O} \\ \mathcal{O} & \Delta_r \end{pmatrix}$ and NS.

Remark 3.9.5

In this section, some tools have been presented to analyze the robust and nominal stability and performances of LTI systems. Note that these results can also be applied to LPV systems by deriving an equivalent linear-fractional representation.

3.10 Conclusion

Various theoretical definitions and results, have been briefly recalled. The $\mathcal{H}_\infty$, $\mathcal{H}_2$ and mixed $\mathcal{H}_\infty/\mathcal{H}_2$ problems have been stated, and the corresponding solutions have been given, both for state-feedback and output-feedback controller design. Furthermore, a pole placement method has been described, and the μ-analysis tools have been presented. There is no contribution in this chapter. The aim is to allow the unfamiliar reader to understand the basic ideas used in the next chapters to design various observers and controllers, i.e. to estimate the non-measured variables of the vehicle, and improve its performances.

The controller design formulation, based on LMI, and the pole placement method, have been chosen since they provide simple and flexible control synthesis tools. This leads to easily implementable controllers and observers, that the designer will be able to adjust properly in order to estimate and control the vehicle efficiently.

Chapter 4

Vehicle modeling

This chapter aims at describing the various models used in the next chapters for estimation or control purposes. Some existing vehicle models are presented, and some identified damper models are developed from experimental data. Since some parts of this work are confidential, they are not presented. For example, the physical damper model is only briefly described since its structure and parameters are confidential. Furthermore, some measurements used to estimate the damper force in the vehicle are confidential too and cannot be given. Therefore the force provided by the damper is supposed to be measured in the next chapters. Some of the presented results have been published in [Aubouet et al., 2009b, 2008].

This chapter is organized as follows: the most common automotive suspension and damper technologies are described in Section 4.1. Then the equipments and experiments used to analyze the behavior of the dampers are presented in Section 4.2. Some damper models are developed in Section 4.3, including both physical and identified models. Then the vehicle models used in this thesis are presented in Section 4.4.

4.1 Automotive suspensions

This section aims at presenting some widespread automotive suspension technologies, and the main damper types in order to understand the various vehicle and suspension models used in the next sections. Since this brief description is not exhaustive, the interested reader may refer in particular to [Miliken and Miliken, 1995, Spelta, 2008] for any further details.

4.1.1 Suspension technologies

Front suspensions

Many types of front suspensions have been used over the years in the automotive industry. Nowadays passenger cars use basically two types: the Mac Pherson Strut and the Short-Long-Arm, respectively represented in Figure 4.1 and 4.2. Most of front suspensions are equipped with one of these technologies since the other types suffer from either high-bending loads, poor geometry, high friction or a combination of these problems.

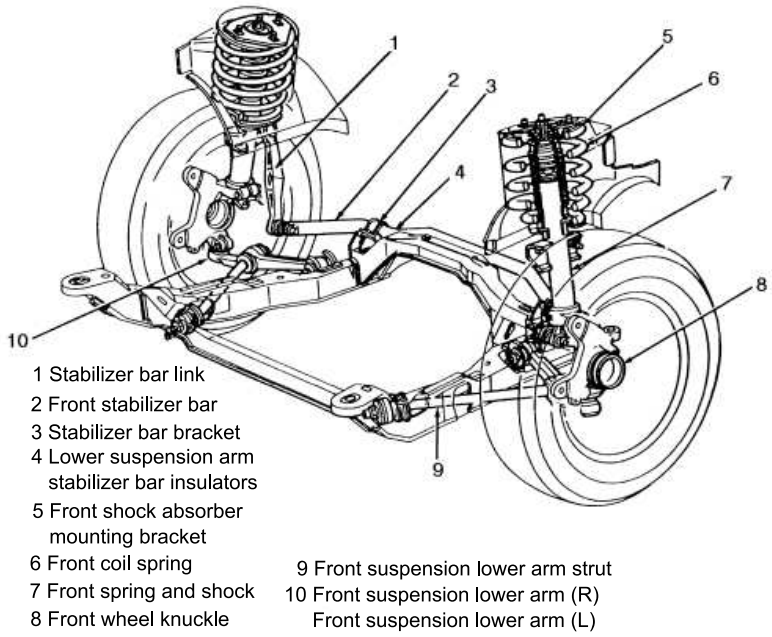

Figure 4.1: Mac Pherson front suspension

Rear suspensions

Suspension systems can be classified into two subgroups: dependent and independent. These terms refer to the ability of opposite wheels to move independently of each other. A dependent suspension normally has a beam or live axle that holds wheels parallel to each other and perpendicular to the axle. When the camber of one wheel changes, the camber of the opposite wheel changes in the same way. An independent suspension allows wheels to rise and fall without affecting the opposite wheel. Suspensions with other devices, such as anti-roll bars that link the wheels in some way are still classified as independent. In this case, the motion of one wheel affects the position of the other but they are not rigidly attached to each other.

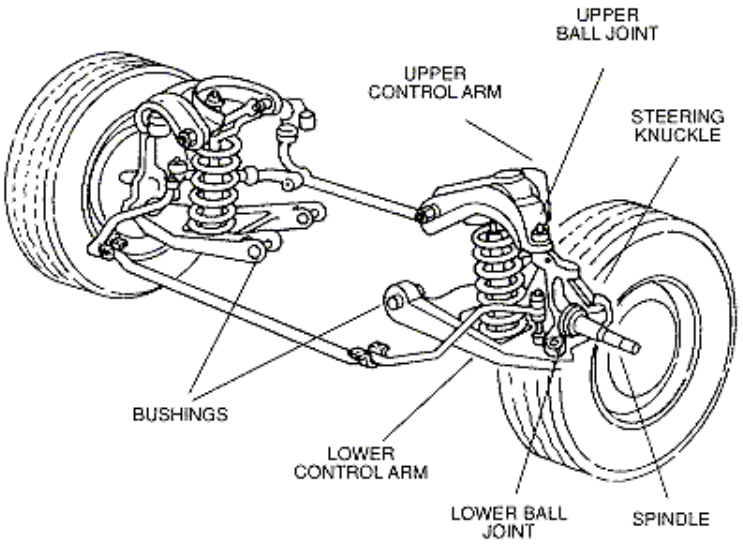

Figure 4.2: Short-Long-Arm front suspension

4.1.2 Hydraulic damper technologies

In this section, a non-exhaustive classification of various hydraulic damper types is given. Note that these dampers are all made up with oil, flowing between various hydraulic chambers through given restrictions. These restrictions can be either non-controllable mechanical valves, or electro-mechanical and externally controlled, therefore hydraulic dampers can be either passive or semi-active. Since this technology is intrinsically dissipative, hydraulic dampers cannot be active. There have been numerous variations of hydraulic dampers. The main types may be classified as,

- Lever vane,
- Lever cam in-line pistons,
- Lever cam parallel pistons,
- Lever rod piston,
- Telescopic.

The vane type is rarely used nowadays since the long seal length is prone to leakage and wear. Therefore it requires very viscous oil, which increases the temperature sensitivity.

The various lever and piston types are occasionally still used, but the construction implies use of a short piston stroke, so the forces and pressures need to be very high. This can also create leakage.

The lever types have the advantage that the damper body can be bolted firmly to the vehicle body, assisting with cooling. However, the lever type has now been almost entirely superseded by the telescopic type.

The telescopic damper has numerous detail variations, and may be classified in various ways. The main classification concerns the method by which the insertion volume of the rod is accommodated. This is a major design problem because the oil itself is nowhere near compressible enough to accept the internal volume reduction of 10% or more associated with the full stroke insertion. There are three basic types of telescopic dampers given below and represented in Figure 4.3:

- The through-rod telescopic,
- The double tube telescopic,
- The single tube telescopic.

SOBEN designs various kinds of passive and semi-active dampers. Note that equipping a damper with a single actuator, controlling both the compression and extension phases, leads to various design problems.

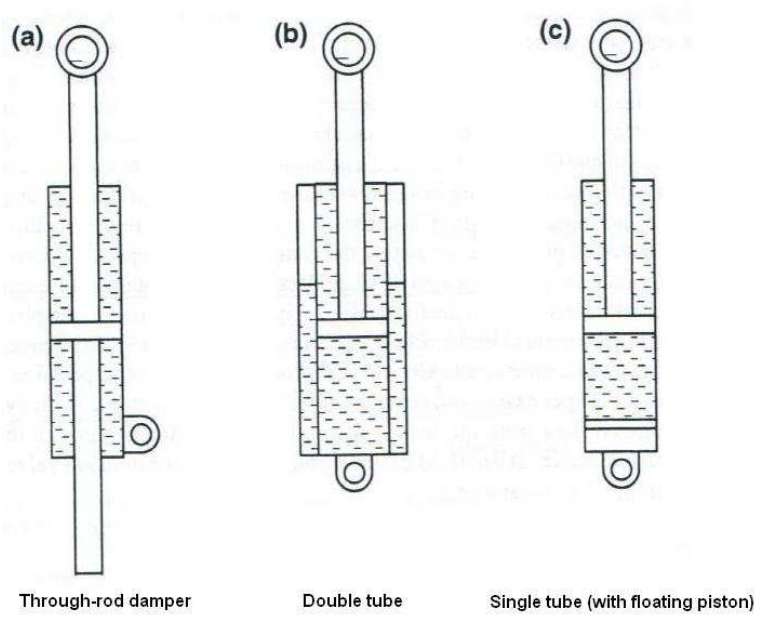

Figure 4.3: Basic types of telescopic dampers

4.2 Material resources and experiments

SOBEN uses various testing benches and electronic boards to study, control and validate the behavior of the new passive and semi-active damper prototypes. These equipments have been used during this thesis to get experimental results, build various damper models, and study the performance of some control strategies.

4.2.1 SOBEN equipments

In this section, the available SOBEN equipments, such as the testing bench, the dampers, the testing car and the acquisition and control boards are presented. These resources have been used for the various experiments described in Section 4.2.2.

Damper testing bench

The damper testing bench, represented in Figure 4.4, is made up with an hydraulic jack. A PC, equipped with an acquisition/control *National Instrument* board allows the user to specify several kinds of position disturbances to be applied to the damper, such as sine waves or ramps of different amplitudes (0 to 20cm) and frequencies (0 to 25Hz). This bench is well-known by damper manufacturers since it is generally used to typify and validate dampers while using sine wave disturbances. This testing bench is equipped with two sensors described in Table 4.1. The measured damper force and deflection are recorded over the time in a text file that can be analyzed after the experiment. The deflection velocity is also provided by the testing bench and recorded, but it is not measured, it is derived from the deflection.

Variable	Technology	Full scale
Damper force	Strain-gages	+/- 10kN
Damper deflection	Potentiometer	0-200mm

Table 4.1: Testing bench: measured variables

Semi-active damper prototypes

Four semi active damper prototypes, under study in this thesis, have been build by SOBEN and mounted on a testing car. These dampers can be controlled by the mean of a servomechanism installed on each damper to control the internal oil flow, and therefore, the damping properties. The Figure 4.5 represents a front damper prototype mounted on the SOBEN testing car.

Figure 4.4: Testing bench

Testing car

The testing car used during this thesis is a *Renault Laguna GT* and can be considered as a speeding car since the damping level of the passive original dampers is high. Such a car is represented in Figure 4.6.

Furthermore, several sensors have been mounted on the testing car, as represented in Figure 4.5. Some of them, like the accelerometers are used by the control strategy, whereas the other have been installed only to study the behavior of the suspensions, and to validate the estimated variables, as detailed in Chapter 5. Seven accelerometers have been mounted. The four vertical unsprung masses accelerations $\ddot{z}_{us_{i=1,2,3,4}}$, at each corner

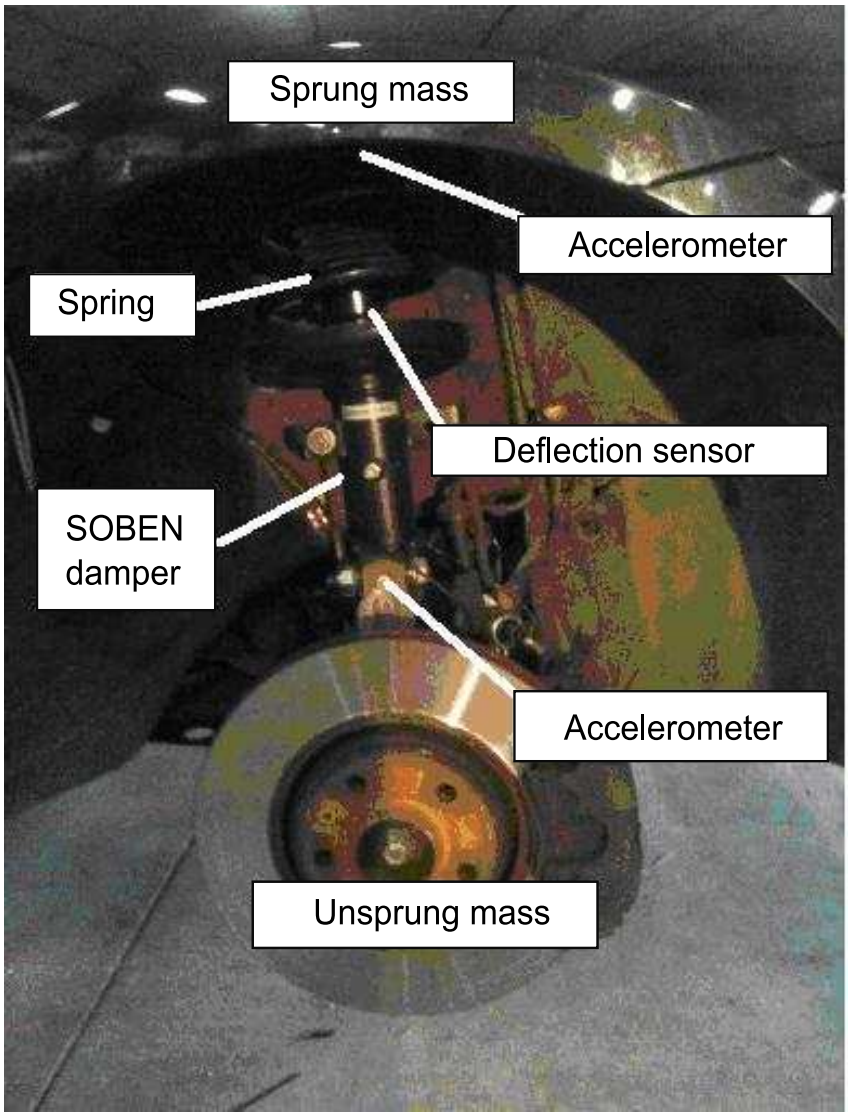

Figure 4.5: New semi-active SOBEN damper

of the vehicle, the vertical sprung mass accelerations $\ddot{z}_{s_{1,2,3}}$ at three corners, and the four suspension deflections are measured.

Remark 4.2.1

The last unsprung mass acceleration is not required since the vehicle body is supposed to be a solid having three degrees of freedom. Indeed, for example, the acceleration $\ddot{z}_{s_4}$ can be easily deduced from $\ddot{z}_{s_1}$, $\ddot{z}_{s_2}$ and $\ddot{z}_{s_3}$ using the derivatives of equations (4.4.6), as detailed later in Section 4.4.2.

The accelerometers are strain-gage based, whereas the deflection sensors are potentiometer based. They have been chosen because of their reduced cost, high reliability and small packaging. The measured variables, and used sensors, are given in Table 4.2.

Figure 4.6: Testing car (*Renault Laguna GT*)

Notation	Description	Full scale
$\ddot{z}_{us_1}$	Front left wheel vertical acceleration	+/- 50g
$\ddot{z}_{us_2}$	Front right wheel vertical acceleration	+/- 50g
$\ddot{z}_{us_3}$	Rear left wheel vertical acceleration	+/- 50g
$\ddot{z}_{us_4}$	Rear left wheel vertical acceleration	+/- 50g
$\ddot{z}_{s_1}$	Front left body vertical acceleration	+/- 5g
$\ddot{z}_{s_2}$	Front right body vertical acceleration	+/- 5g
$\ddot{z}_{s_3}$	Rear left body vertical acceleration	+/- 5g
$z_{def_1} = z_{s_1} - z_{us_1}$	Front left suspension deflection	0-20cm
$z_{def_2} = z_{s_2} - z_{us_2}$	Front right suspension deflection	0-20cm
$z_{def_3} = z_{s_3} - z_{us_3}$	Rear left suspension deflection	0-20cm
$z_{def_4} = z_{s_4} - z_{us_4}$	Rear right suspension deflection	0-20cm
F_i, $i = 1, .., 4$	Damper forces	Confidential

Table 4.2: Testing car: measured variables and sensors

Acquisition and control boards

The vehicle is equipped with various sensors for each suspension. The acquisition of these data is done by a set of five electronic boards developed by SOBEN. Each damper

is equipped with a small acquisition board, represented in Figure 4.7, that converts the analog measurements into CAN[1] frames.

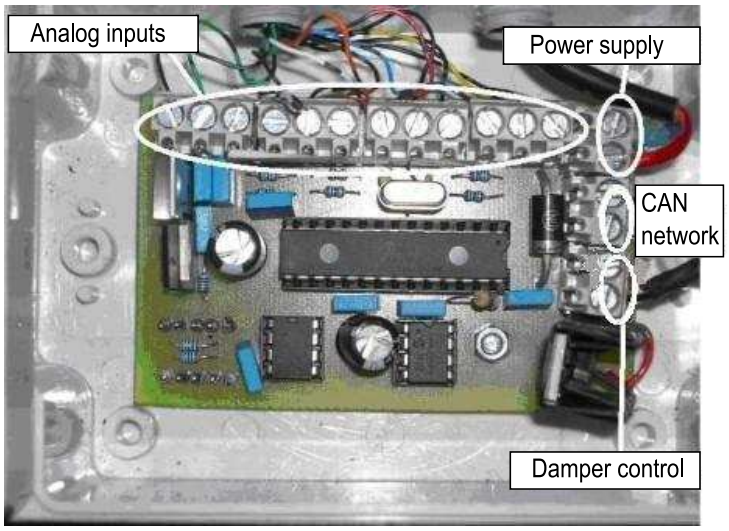

Figure 4.7: Damper control board

A central board where an observer is implemented receives the frames through the CAN network and computes on-line the control signal of each damper, and sends it to the four damper control boards through the CAN network. This architecture is described in Figure 4.8.

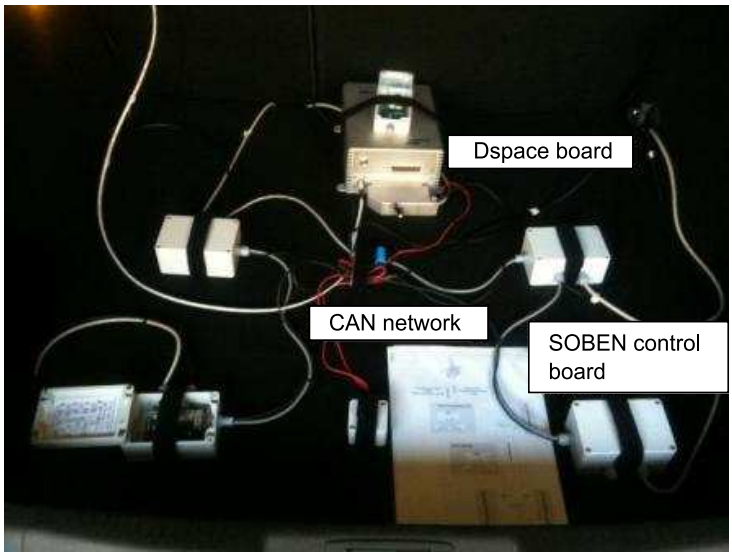

Figure 4.8: Control architecture of the four dampers

[1]Controller Area Network

The four damper boards are operational, but the central board has not been programmed yet. Therefore a *Dspace* card has been used for the experiments presented in this thesis. The implementation of the controllers is done automatically by the software provided by *Dspace*, from a *Matlab-Simulink* program. A PC can be connected to analyse and record on-line the different signals.

4.2.2 Experiments and results

The equipments presented in Section 4.2.1 have been used to run various experiments in order to analyze and model the behavior of SOBEN damper. The test procedures and the results are given in this section, and analyzed in the next chapters.

Experiment 1: damper behavior analysis

The damper testing bench, previously described in Section 4.2.1, has been used to subject the damper to various sinusoidal deflections with varying amplitudes and frequencies. Here the damper was controlled in open-loop only and the damper has been subjected to the set of sine waves described in Table 4.3 for a minimal control signal (0%), and then for a maximal one (100%). The force provided by the damper, the deflection and the deflection velocity have been measured. Here the objective is to get a complete set of measured variables, representing the behavior of the damper for various interesting disturbances. Since this experiment is very similar to the next one, the results are given only for the Experiment 2 in Figure 4.9 and 4.10.

Sine wave	**Freq. [Hz]**	**Amp. [mm]**	**Control [%]**
Sine 1	1.5	2.2	0 and 100
Sine 2	1.5	8.3	0 and 100
Sine 3	1.5	15	0 and 100
Sine 4	12	3.1	0 and 100
Sine 5	12	6.5	0 and 100
Sine 6	12	9.2	0 and 100

Table 4.3: Experiment 1: sinusoidal deflections

Remark 4.2.2

The frequencies 1.5Hz and 12Hz correspond respectively to the natural frequency of the vehicle body and of the wheel. Most damper manufacturers analyze the damper behavior at these particular frequencies since they represent the whole interesting frequency range.

Experiment 2: damper behavior analysis

This experiment is similar to the first one, but the amplitudes, given in Table 4.4, are different. The results are given in Figure 4.9 and 4.10, and give the whole achievable force range of the damper. The chosen sine deflections allow to study the damper on the whole interesting velocity range. These results emphasize the hysteretical behavior of the damper and will be used later to build an appropriate damper model, taking this behavior into account.

Sine wave	**Freq. [Hz]**	**Amp. [mm]**	**Control** [%]
Sine 1	1.5	1	0 and 100
Sine 2	1.5	10.5	0 and 100
Sine 3	1.5	21	0 and 100
Sine 4	12	1.4	0 and 100
Sine 5	12	4.1	0 and 100
Sine 6	12	6.9	0 and 100

Table 4.4: Experiment 2: sinusoidal deflections

Experiment 3: influence of the control signal

During this experiment, the damper has been subjected to the sinusoidal deflection described in Experiment 2, but with different control signals. Indeed the force provided by the damper at a given deflection velocity can be controlled by changing the input current of the servomechanism. The objective is to study the influence of this control signal on the damper behavior. A description of this experiment is given in Table 4.5, and the results are given in Figure 4.11.

Sine wave	**Control** [%]
Experiment 2	0
Experiment 2	33
Experiment 2	66
Experiment 2	100

Table 4.5: Experiment 3: sinusoidal deflections

These results give the whole achievable force range of the damper. These results will be used later to identify a damper model taking the influence of the control signal into account.

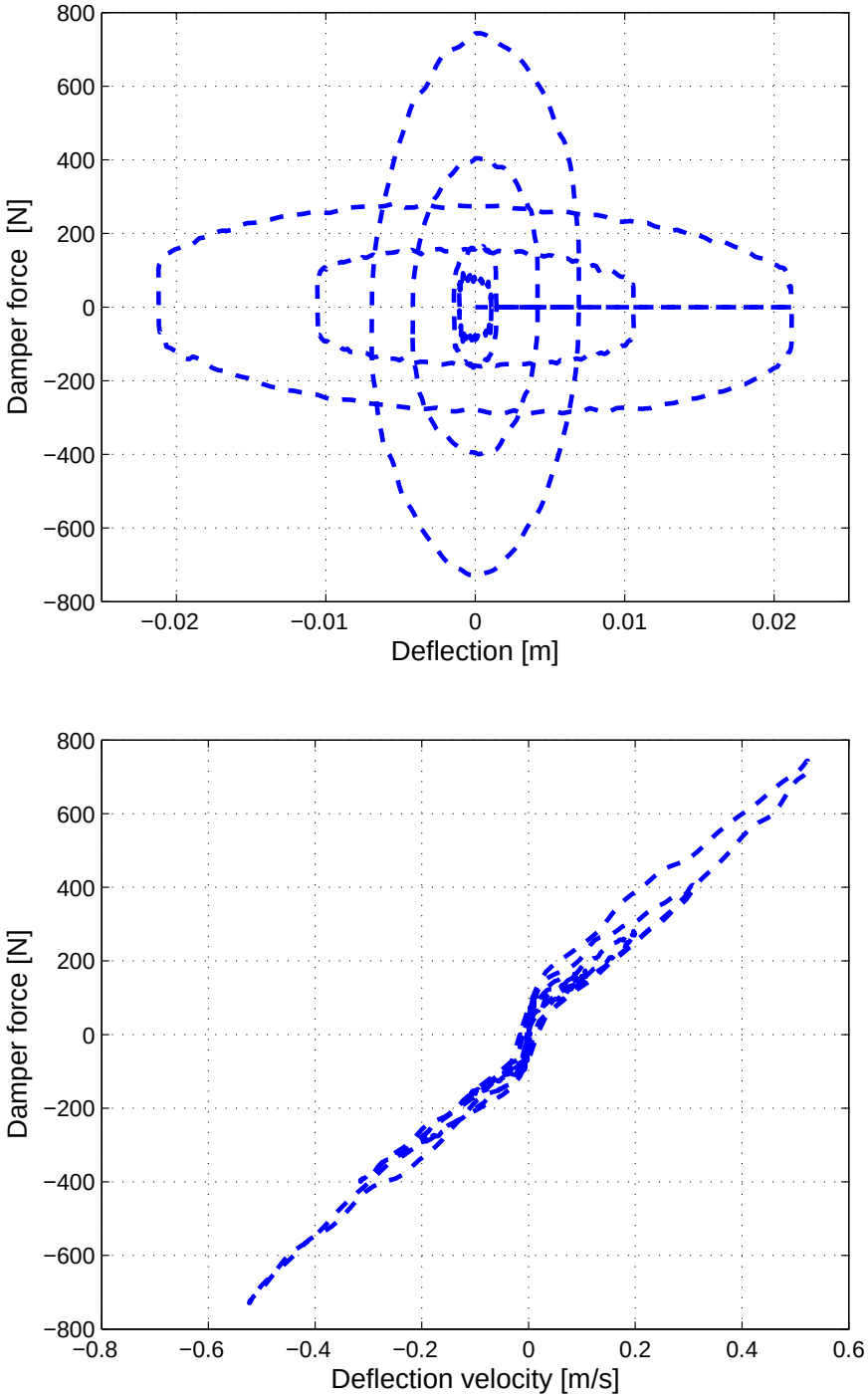

Figure 4.9: Experiment 2: minimal control signal

Experiment 4: dynamical behavior identification

The damper has been subjected to ramp deflections, corresponding to periodic and constant deflection velocities (0.1m/s and -0.1m/s) on the testing bench, and the control

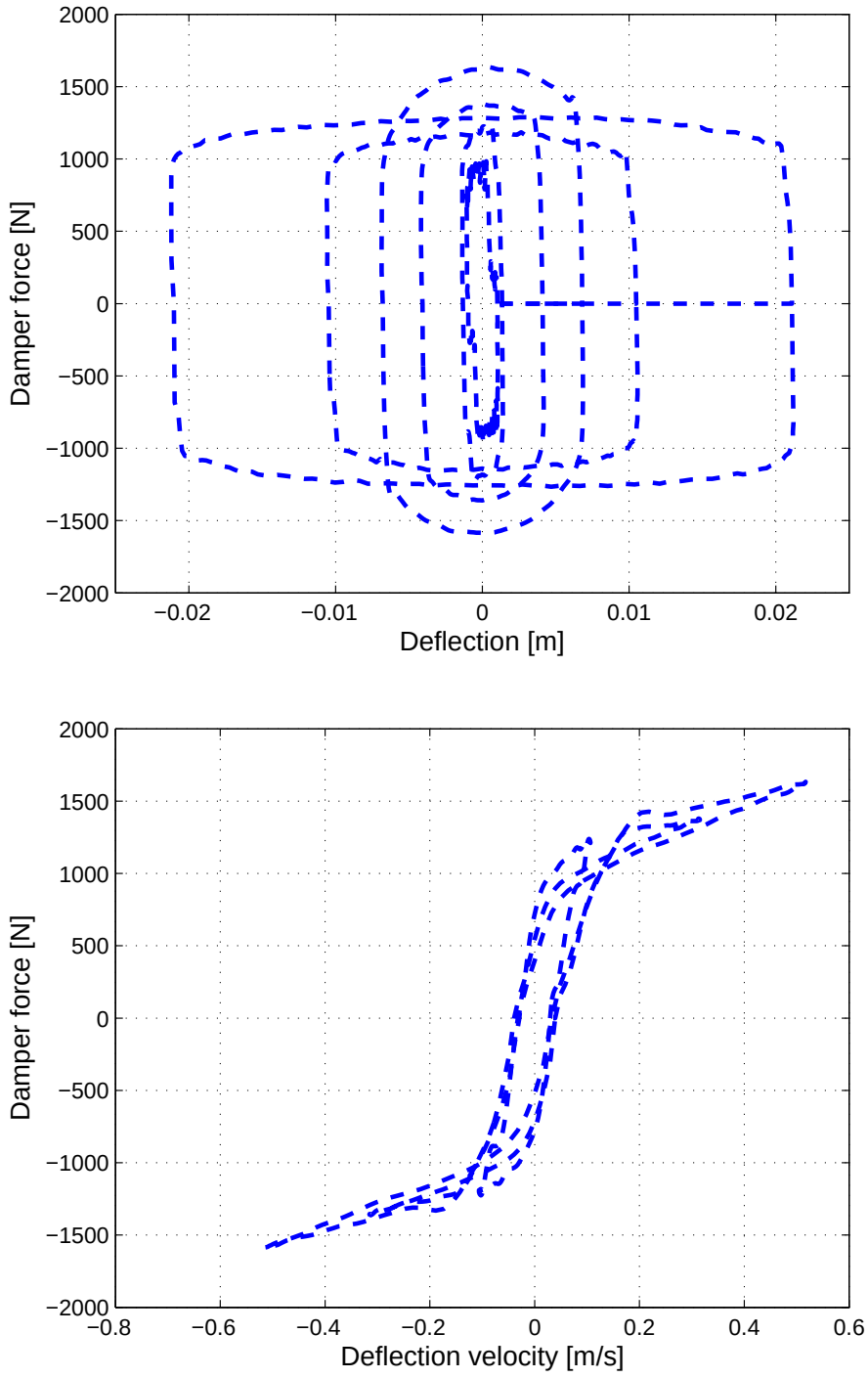

Figure 4.10: Experiment 2: maximal control signal

signal has been changed from 0% to 100% using step variations during a ramp, in order to analyze the step response of the damper. The damper force, the control signal, the deflection and the deflection velocity are measured, and the results are given in Figure

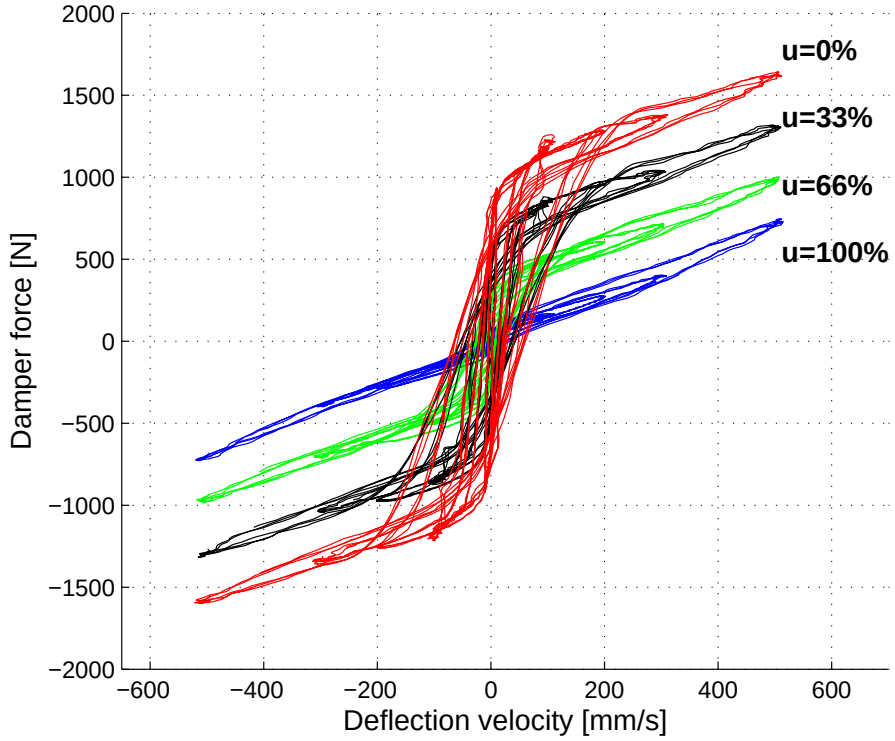

Figure 4.11: Experiment 3: influence of the control signal

4.12.

The response looks like a linear second-order system and the measured settling-time is equal to 90ms. However this is not accurate since the force provided by the damper is never constant during the experiment, even if the deflection velocity is constant. Indeed, the force also depends on the deflection because of the gas inside the damper. A better analysis is proposed in the next experiment.

Experiment 5: bandwidth identification

The damper has been subjected to a ramp deflections, corresponding to periodic and constant deflection velocities (0.1m/s and -0.1m/s), of amplitude 0.15m, with a sinusoidal control signal of varying frequency, as described in Table 4.6.

Deflection	**Amp. [m]**	**Control [%]**
Ramps	0.15	$sin(2\pi \cdot f \cdot t),\ f \in [0, 20]$Hz

Table 4.6: Experiment 5: disturbances

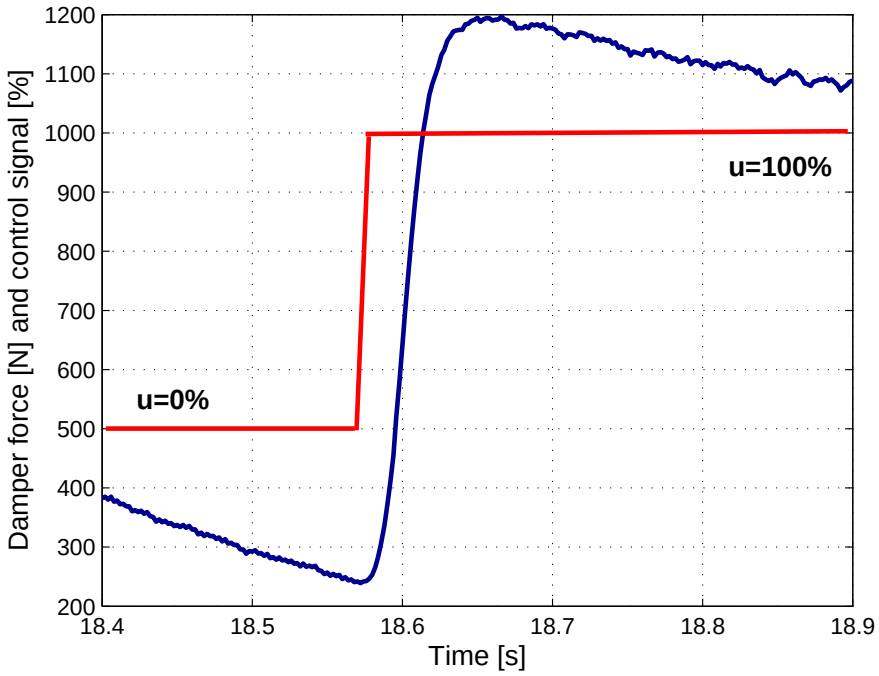

Figure 4.12: Experiment 4: step response of the damper

The results are given in Figure 4.13: the top graph represents the response of the damper, for all frequencies of the control signal between 0 and 20Hz, the middle graph gives a zoom of the top graph, and the bottom graph gives the frequency of the sine control signal over the time.

The bandwidth measured from this experiment is equal to 12Hz, which corresponds to the results of the previous experiment. These results are detailed and used in the next sections.

4.3 Damper models

In this section, some damper models are proposed, based on hydraulics equations or identified from measured data. The physical models aim at describing the real behavior of the damper and studying the influence of the various physical parameters, whereas the identified models are simplified and have been developed to be used in an embedded control strategy.

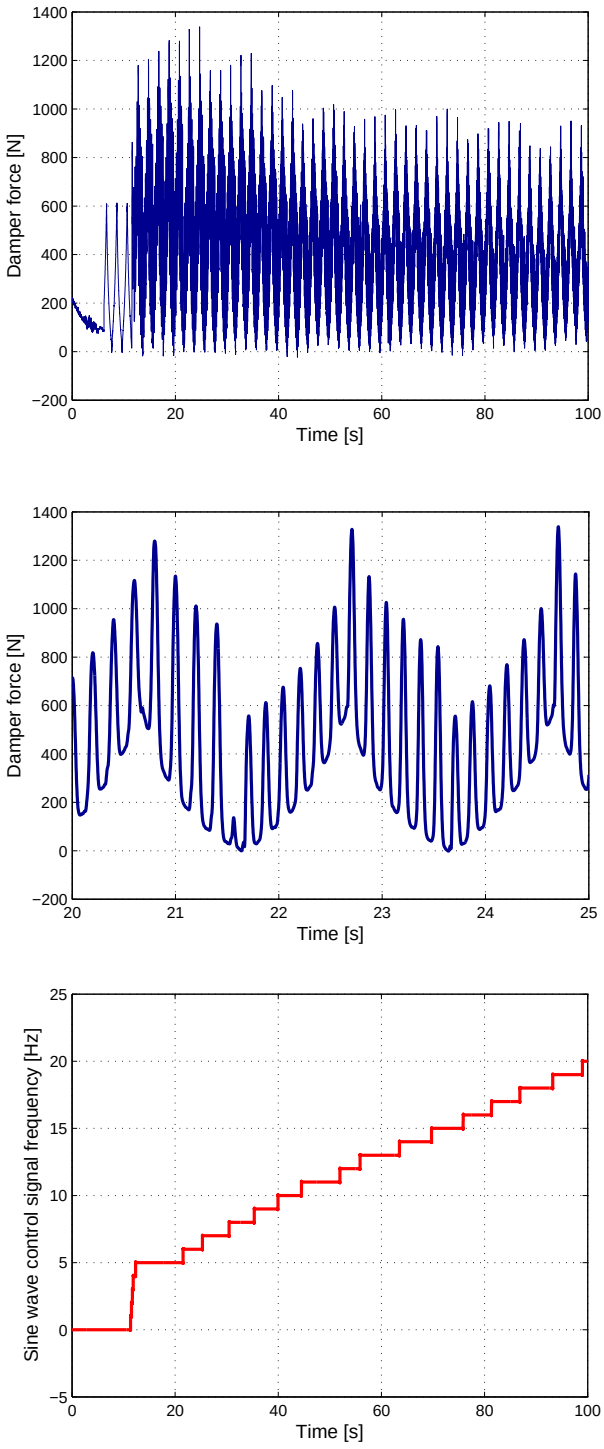

Figure 4.13: Experiment 5: bandwidth identification (top: force oscillations, middle: zoom, bottom: frequency)

4.3.1 Hydraulics-based physical model

The general form of telescopic hydraulic dampers, such as the ones designed by SOBEN, is represented in Figure 4.14. They are made up with a main body and a reservoir linked to each other by a foot-valve. The reservoir is divided into two parts: the foot chamber and the air chamber. This chamber aims at offsetting the volume of the rod when it enters the damper in compression phases. The piston, linked to the rod, is made up with several valves adjusting the oil flow between the compression and extension chambers. In passive dampers, the settings of the valves are predetermined, and the damping cannot be controlled. In variable and semi-active hydraulic dampers, these valves are replaced by an actuator, and can be adjusted. Then the damping rate can be electronically controlled. Various types of actuators can be used for semi-active dampers, like electro-valves, piezoelectric actuators, linear motors... Note that choosing or designing the damper actuator is a topical industrial problem since the actuator has to be compact, cheap to produce and have an appropriate bandwidth. Furthermore there are power-consumption, pressure, and vibration constraints for automotive applications.

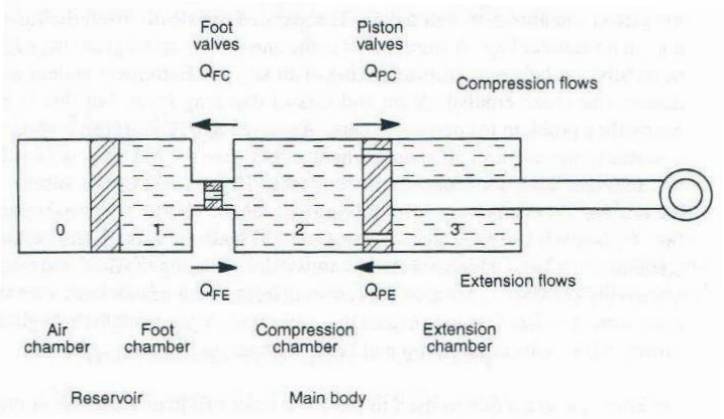

Figure 4.14: General form of telescopic dampers

The damper represented in Figure 4.14 can be modeled using fluid mechanics equations. Indeed the damper can be seen as a system made up with four chambers linked to each other by some hydraulic restrictions. The following simplifying assumptions are done:

- Laminar oil flow (non turbulent flow)
- Influence of the oil temperature negligible
- Oil non-compressible
- No cavitation phenomenon

Then the pressure P_i and the entering volumetric oil flow Q_i, for each damper chamber $i = 1, .., 4$, are ruled respectively by (4.3.1) and (4.3.2).

$$\dot{P}_i = \frac{(Q_i - \dot{V}_i) \cdot \beta}{V_i} \tag{4.3.1}$$

$$Q_i = sgn(P_{i-1} - P_i) \cdot \sqrt{\frac{\mid P_{i-1} - P_i \mid}{\rho}} \cdot S_d \tag{4.3.2}$$

where V_i denotes the volume of the chamber i, β the bulk modulus of the oil (constant parameter measuring the oil's resistance to uniform compression), P_{i-1} the pressure in the chamber uphill, ρ the volumetric mass of the oil, and S_d the section of the hydraulic restriction.

A complete damper model can be easily derived from these equations. Indeed, each chamber of the damper can be modeled by the set of equations (4.3.1) and (4.3.2). Then the force F_c provided by the damper can be derived from the pressures in the compression and extension chambers, according to (4.3.3).

$$F_c = A_p P_c - (A_p - A_r) P_d \tag{4.3.3}$$

where A_p, A_r, P_c and P_r denote respectively the section of the piston, the section of the rod, the pressure in the compression chamber ($i = 2$) and the pressure in the extension chamber ($i = 3$).

This damper model describes the physical behavior of the damper while giving the oil flow between the hydraulic chambers, and their inside pressure according to given excitations.

Parameters such as the volumetric mass of the oil, or its bulk modulus are given by the oil manufacturer in particular conditions. Since these parameters largely depend on the temperature and pressure, they also largely influence the damper behavior. Furthermore the oil flow may be turbulent, depending on the unknown ground disturbance, and for some dampers, the influence of the temperature might completely change the damping rate, depending on the vehicle ventilation, on the damper oil, on the outside temperature...

Furthermore, the major problem of this kind of model lies in the opening sections of the valves. A large majority of hydraulic dampers, passive or semi-active, are equipped with washer-based valves since it is an efficient, cheap and well-known technology. In passive dampers, the hydraulic restrictions between the chambers are most of the time such valves. In semi-active dampers, some of these valves are replaced by actuators, but some non-actuated hydraulic restrictions still require such valves, that open for instance

only when the oil pressure is very high, in order to saturate the damping force during a shock. The opening sections of these valves are variable since they depend on the inside pressures of the chambers. Their distortions over the time are highly nonlinear and neither measurable nor predictable. Therefore the parameters S_d are unknown when such a valve is used, which is very common.

Some of these phenomena could be modeled, but this would lead to a complex nonlinear and switched model, that could hardly be used for real-time control applications. However, this is an interesting research and development tool for damper manufacturers to study the influence of the various parameters on the damper behavior.

4.3.2 Identified static models

Various works dealing with damper modeling have already been proposed recently, such as [Lozoya-Santos et al., 2010, Do et al., 2010a, Lozoya-Santos et al., 2009, Kern, 2008]. These models are often nonlinear static models, providing the damping force for a given deflection and deflection velocity. The main advantage of such models lies in their simplicity compared to physical models. Therefore they can be used more easily for control purposes.

Such a simplified model of the damper is developed using the Experiments 1, 2 and 3, described in Section 4.2.2. It is based on an existing damper model firstly proposed by Guo et al. [2006] for magneto-rheological dampers and has been identified according to the following procedure:

Test procedure:

The Experiments 1 and 3 have been run, using the testing bench described in Section 4.2.1. These experiments have been chosen because they represent the behavior of the damper on its whole working range. Indeed, the experiment contains various representative disturbances, and the Experiment 3 allows the damper to be studied for various control signals. Therefore these experiments are assumed to be representative enough to identify a pertinent damper model. The following variables have been recorded over the time:

- Force provided by the damper (measured),
- Deflection (measured),
- Deflection velocity (computed from the deflection).

Method:

The Experiments 1 and 3 have been used to identify the simplified model of the damper, given by (4.3.4). This is a static nonlinear model providing the damping force from the deflection and deflection velocity. Here this equation has been adapted to model the hysteretic behavior of the hydraulic SOBEN damper, and takes the control signal into account.

$$F_c = (A_1 u_d + A_2)\tanh(A_3 v + A_4 x) + A_5 v + A_6 x + A_7 \tag{4.3.4}$$

where F_c is the damping force, x is the deflection, v the deflection velocity, $u_d \in [-1, 1]$ is the control signal, and A_j, $j \in [1, 7]$ are the identified parameters.

Remark 4.3.1

The chosen structure linearly depends on the control signal for a given deflection speed, since the influence of the control signal, described in Figure 4.11, is almost linear.

Remark 4.3.2

The proposed damper model suits both for continuously variable and switched on/off dampers. Indeed, if the control signal can be either continuously variable or on/off, allowing to model both types of dampers. Such models will be used in the Chapter 6.

The results of the Experiments 1 and 3 have been used to identify the parameters of the previous model. The optimization has been done using all the measured variables of the Experiments 1 and 3, in order to identify the model from a representative set of measurements. An identification algorithm solving the nonlinear data-fitting problem in the least squares sense has been used. The minimized criterion J is given by,

$$J(F_m - \hat{F}) = \sum_{k=1}^{n} (F_m(k) - \hat{F}(k))^2 \tag{4.3.5}$$

where n denotes the number of samples.

Results:

The identified model is defined by its parameters, given in Table 4.7.

Its performance has been tested using the results of the Experiment 2. Indeed, the force provided by the damper has been computed from the measured deflection and deflection velocity of the Experiment 2. The measured and simulated damper forces are

Parameter	A_1	A_2	A_3	A_4	A_5	A_6	A_7
Value	792	47	1328	10.5	1233	-0.27	4

Table 4.7: Identified model: parameters

compared using force-deflection and force-velocity diagrams in Figure 4.15 for a minimal control signal, and in Figure 4.16 for a maximal control signal.

Definition 4.3.1 (*Mean relative error*)

$$\epsilon_r(F_m - \hat{F}) = \frac{\sum_{k=1}^{n} |F_m(k) - \hat{F}(k)|}{F_m(k)} \tag{4.3.6}$$

where F_m and $\hat{F}$ are respectively the measured damping force (Experiment 2) and the simulated force provided by the identified damper model.

Validation:

The performance of the proposed damper model has been evaluated while computing the mean relative errors ϵ_r according to the Definition 4.3.1, for the various sine waves contained in the Experiment 2. The maximal relative error is given by (4.3.7).

$$\epsilon_r(F_m - \hat{F}) = 5.3\% \tag{4.3.7}$$

These results show that the model is accurate for the various amplitudes and frequencies of the Experiment 2 and emphasize the performance of the proposed model.

Since this damper model represents both the damper nonlinearities and its force range, for $u_d \in [-1, 1]$, it will be used in the control strategy, detailed in Chapter 6, to take the real behavior of the damper and the technological constraints into account.

4.3.3 Dynamical behavior

In the previous section, a static model of the damper has been identified. This model gives the force provided by the damper for a given deflection, deflection velocity and control signal. No dynamical behavior has been modeled. However the bandwidth of the damper drastically influences the performance of the semi-active suspensions. In this section, the dynamical response of the damper is studied and modeled, using the Experiments 4 and 5, described in Section 4.2.2.

The step response of the damper, given in Figure 4.12 (Experiment 4), shows that the damper behaves like a simple second order system G_d with the current I as input

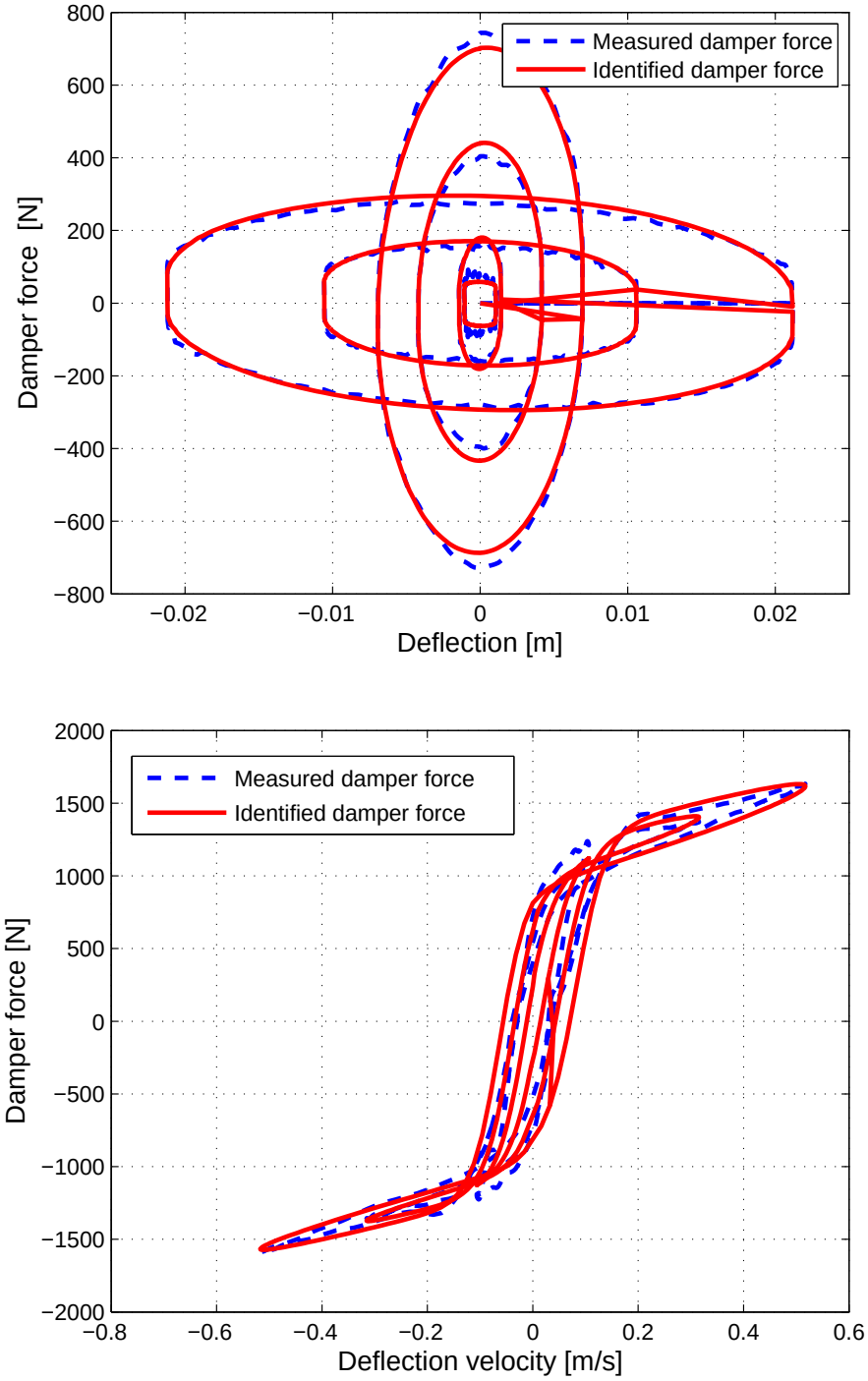

Figure 4.15: Damper identification: minimal control signal

and the force F as output, given by (4.3.8).

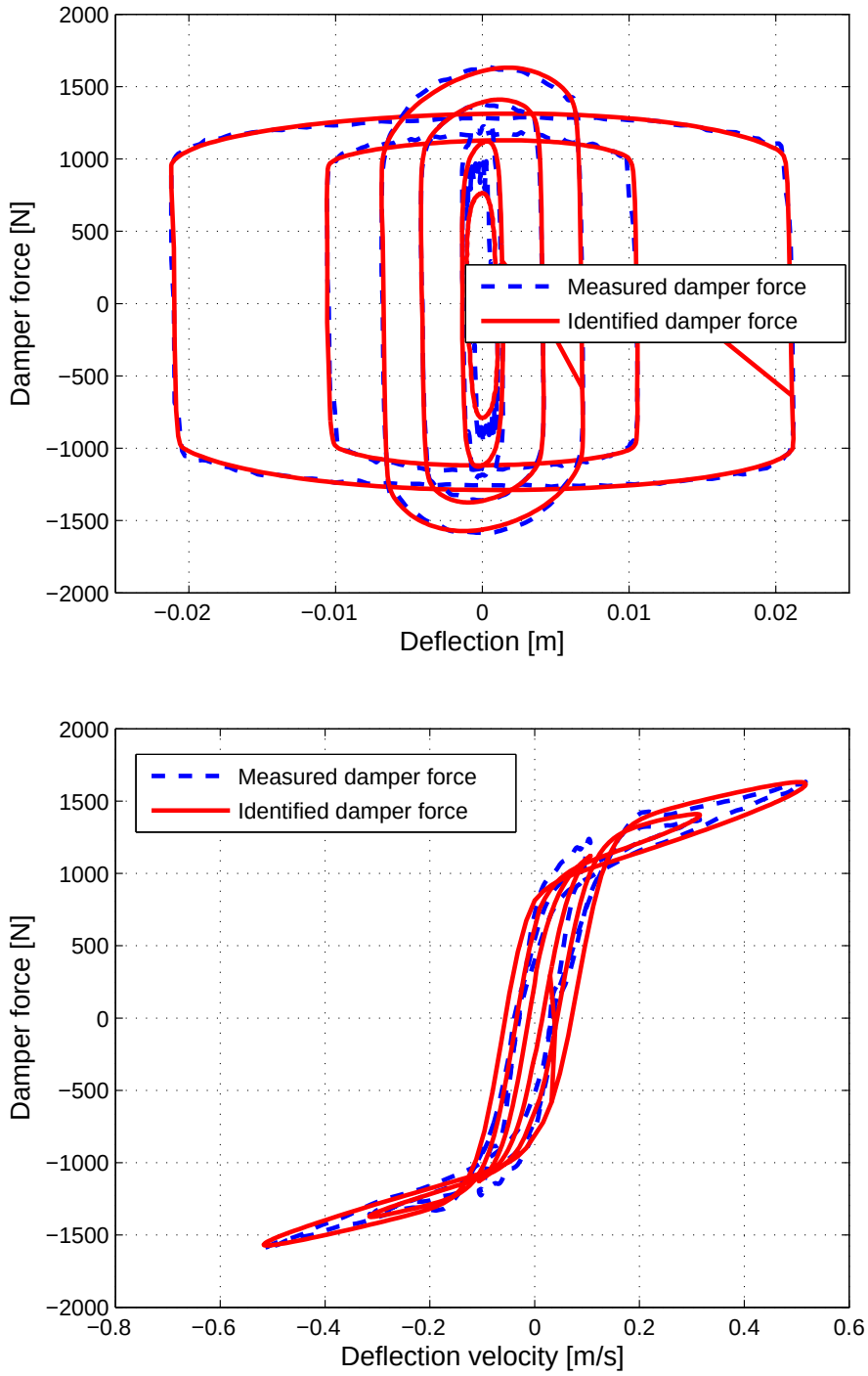

Figure 4.16: Damper identification: maximal control signal

$$G_d(s) = \frac{G}{\left(\frac{s}{\omega_d}\right)^2 + 2m_d\frac{s}{\omega_d} + 1} \tag{4.3.8}$$

where ω_d represents the natural frequency of the damper, G its static gain and m_d the damping coefficient.

The step response is not oscillating. Therefore the damping coefficient $m_d = 0.6$ has been identified. The settling-time at 5%, measured from this experiment equals 90ms.

As said before, the results of the Experiment 5, given in Figure 4.13, represent the response of the damper (top graph), for all control signal frequencies between 0 and 20Hz, a zoom of the top graph (middle graph), and the frequency of the sine control signal over the time (bottom graph). The amplitude of the force oscillations decreases when the frequency increases. The amplitude $A_{max}/\sqrt{(2)}$, where A_{max} represents the maximal amplitude of the oscillations, determines the bandwidth at 3dB of the damper. Therefore ω_d = 12Hz has been measured, which corresponds to the settling-time measured during the Experiment 4.

This dynamical behavior can be used to complete the static model (4.3.4) of the damper, identified in the previous section, as given in Figure (4.17).

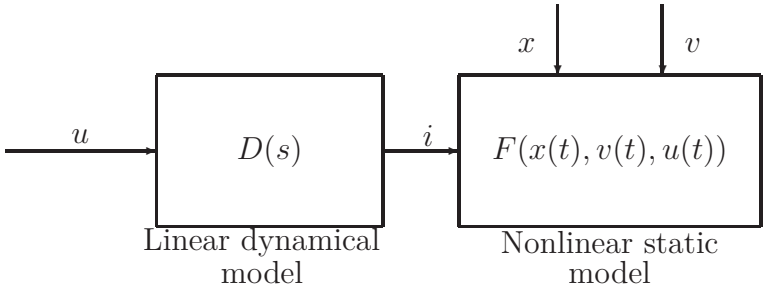

Figure 4.17: Damper model

Therefore the equation of the dynamical identified damper model turns into,

$$\begin{cases} F(t) &= (A_1 u_d + A_2)\tanh(A_3 v + A_4 x) + A_5 v + A_6 x + A_7 \\ \dfrac{I(s)}{u_d(s)} &= \dfrac{G}{\left(\dfrac{s}{\omega_d}\right)^2 + 2m_d\dfrac{s}{\omega_d} + 1} \end{cases} \tag{4.3.9}$$

where $I(s)$ is the damper input current, u_d is the control signal of the amplifier, $F(t)$ is the force provided by the damper, $x = x(t)$ is the deflection, $v(t)$ is the deflection velocity, $\omega_d = 12$Hz is the bandwidth of the damper, m_d =0.6 is the damping coefficient, and A_i are the identified parameters of the model.

This model will be used in the synthesis of the local damper controller in Chapter 6.

4.4 Vehicle models

This section aims at presenting the well-known vertical quarter and full-car models. These simplified models describe the main dynamics of the vehicle and can be used for control or estimation purposes.

4.4.1 Vertical quarter-car model

The linear quarter-car model is represented in Figure 4.18. Its equations and parameters are given respectively in Equations (4.4.1-4.4.2) and Table 4.8.

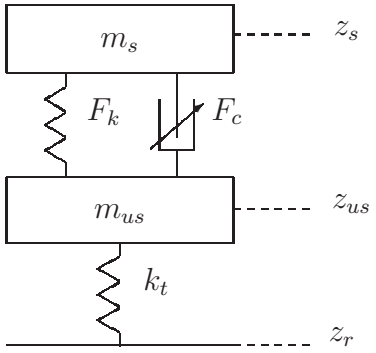

Figure 4.18: Vertical quarter-car vehicle

$$\begin{cases} m_s\ddot{z}_s &= -F_k - F_c \\ m_{us}\ddot{z}_{us} &= F_k + F_c + k_t(z_r - z_{us}) \end{cases} \tag{4.4.1}$$

$$\begin{cases} F_k &= k(z_s - z_{us}) \\ F_c &= c(\dot{z}_s - \dot{z}_{us}) \end{cases} \tag{4.4.2}$$

Remark 4.4.1

This simplified model describes the vertical behavior of a single suspension and wheel system. It has been used very often to analyze the behavior of suspensions and design controllers in suspension control applications. However, modeling or controlling the full-car with four quarter-cars amounts to ignoring that the four sprung masses are linked to each other, which leads to non-modeled or non-controlled roll and pitch angles chassis movements. If these angular dynamics have to be taken into account, the full vertical car has to be considered.

Parameter/variable	Description
m_s, m_{us}	Sprung, unsprung mass (constant)
k, k_t	Suspension, tire stiffness (constant)
z_r	Ground vertical position (variable)
$\ddot{z}_s$, $\ddot{z}_{us}$	Sprung, unsprung mass acceleration (variable)
z_s, z_{us}	Sprung, unsprung mass position (variable)
$z_{def} = z_s - z_{us}$	Suspension deflection (variable)
F_k	Spring force (variable)
F_c	Damping force (variable)

Table 4.8: Quarter-car parameters and variables

4.4.2 Vertical full-car model

The full vertical car model, firstly described by Elbeheiry et al. [1996], Esmailzadeh and Fahimi [1997], and represented in Figure 4.19, is made up with a sprung mass in vertical translation, and rotating on two horizontal axis, and the four unsprung masses, each one in vertical translation. Each unsprung mass is linked to the ground with a tire modeled by a stiffness, and to the sprung mass with a suspension made up with a linear damper and a linear spring. This model is classical and has already been used by Sammier [2001], Zin [2005], Spelta [2008]. The variables and parameters of this model are given in Table 4.9.

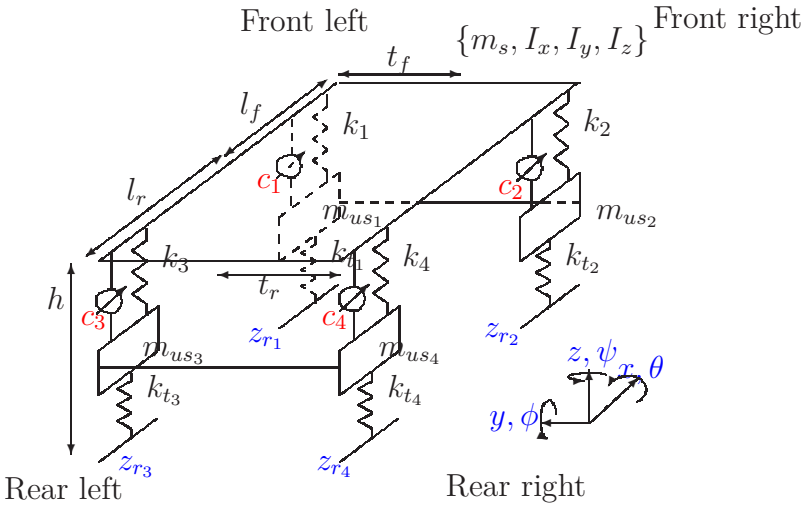

Figure 4.19: Full vertical car model with 7 DOF

The equations of the vertical full-car model presented in Figure 4.19 are given by (4.4.3) and (4.4.4).

Parameter/variable	**Description**	Value
m_s	Sprung mass	1450kg
$m_{us_{1,2}}$	Front unsprung masses	39kg
$m_{us_{3,4}}$	Rear unsprung masses	32kg
$k_{1,2}$	Front suspension stiffnesses	30000N/m
$k_{3,4}$	Rear suspension stiffnesses	18000N/m
$c_{1,2}$	Front linear damping rate	4000Ns/m
$c_{3,4}$	Rear linear damping rate	3000Ns/m
$k_{t1,2,3,4}$	Tire stiffnesses	200000N/m
I_x, I_y	Roll and pitch inertia	610, 2750kg.m^2
t_f	Distance COG[1] - front left tire	0.75m
t_r	Distance COG - rear left tire	0.75m
l_f	Distance COG - front	1.06m
l_r	Distance COG - rear	1.7m
z_{r_i}	Ground vertical positions	$i = 1..4$
z_{s_i}	Sprung mass positions	$i = 1..4$
z_{us_i}	Unsprung mass positions	$i = 1..4$
F_{s_i}	Suspension forces	$i = 1..4$
θ	Sprung mass roll angle	
ψ	Sprung mass pitch angle	
F_z	Vertical disturbance force	
M_x, M_y	Disturbance moments	
[1] Center Of Gravity		

Table 4.9: Full vertical car parameters and variables (Laguna GT)

$$\begin{cases} m_s\ddot{z}_s &= -(F_{s_1} + F_{s_2} + F_{s_3} + F_{s_4} + F_z) \\ m_{us_1}\ddot{z}_{us_1} &= (F_{s_1} - F_{t_1}) \\ m_{us_2}\ddot{z}_{us_2} &= (F_{s_2} - F_{t_2}) \\ m_{us_3}\ddot{z}_{us_3} &= (F_{s_3} - F_{t_3}) \\ m_{us_4}\ddot{z}_{us_4} &= (F_{s_4} - F_{t_4}) \\ I_x\ddot{\theta} &= (F_{s_1} - F_{s_2})t_f + (F_{s_3} - F_{s_4})t_r + M_x \\ I_y\ddot{\phi} &= (F_{s_4} + F_{s_3})l_r - (F_{s_2} + F_{s_1})l_f + M_y \end{cases} \tag{4.4.3}$$

The suspension forces are given by (4.4.4), where u_i is a control force to be added to the nominal damping force $c_i \cdot (\dot{z}_{s_i} - \dot{z}_{us_i})$, and $i = 1..4$ denotes the four suspensions.

$$\begin{cases} F_{si} &= k_i \cdot (z_{s_i} - z_{us_i}) + c_i \cdot (\dot{z}_{s_i} - \dot{z}_{us_i}) + u_i \\ F_{ti} &= k_{t_i} \cdot (z_{us_i} - z_{r_i}) \end{cases} \tag{4.4.4}$$

Then the sprung mass positions at each corner of the vehicle can be computed using the position of the sprung mass center of gravity and the pitch and roll angles. Equations (4.4.5) give the four sprung mass positions.

$$\begin{cases} z_{s_1} &= z_s + l_f \sin(\phi) - t_f \sin(\theta) \\ z_{s_2} &= z_s + l_f \sin(\phi) + t_f \sin(\theta) \\ z_{s_3} &= z_s - l_r \sin(\phi) - t_r \sin(\theta) \\ z_{s_4} &= z_s - l_r \sin(\phi) + t_r \sin(\theta) \end{cases} \tag{4.4.5}$$

Then the positions of the sprung mass can be linearized as given in (4.4.6) when θ and ϕ are small.

$$\begin{cases} z_{s_1} &\approx z_s + l_f \phi - t_f \theta \\ z_{s_2} &\approx z_s + l_f \phi + t_f \theta \\ z_{s_3} &\approx z_s - l_r \phi - t_r \theta \\ z_{s_4} &\approx z_s - l_r \phi + t_r \theta \end{cases} \tag{4.4.6}$$

This vertical full-car model (4.4.3) will be used both in the synthesis of the observer in Chapter 5 and in the design of the controller in Chapter 6. A state-space representation of this linear model is given in these chapters.

4.5 Conclusion

The most common automotive suspension and damper technologies have been briefly presented. Various SOBEN material resources have been used to run some representative experiments and study the damper behavior. Some damper models have also been developed, including both physical and simplified models, identified from the experimental results. These damper models will be used in Chapter 6 to design appropriate semi-active damper control strategies, as well as the vehicle models that will be used for control and estimation purposes in Chapters 5 and 6. Therefore this Chapter provided all the modeling tools required to build the control strategy proposed in the next chapters.

Chapter 5

Observer design

In control theory, a state-observer is usually needed to provide an estimation of the system internal state variables, given the measurements of the input and output of the real system.

This chapter deals with the estimation of some non-measured variables of the vehicle model, for suspension control objectives. Some of the results provided in this chapter has been presented in [Aubouet et al., 2009a, 2010].

5.1 Introduction

This section first presents the main objectives. Then a brief state of the art, dealing both with existing observers for suspension control applications and unknown input observers in general, is provided. Finally, the contribution of the chapter is presented.

5.1.1 Objectives

The aim is to estimate the state variables of the full-car model in order to get a complete knowledge of the vehicle dynamics for on-board suspension control applications. The developed observer has to provide the estimated state variables using a reduced number of sensors. This is one of the main challenges since many car or equipment manufacturers like SOBEN currently aim at equipping mass-produced cars with controlled suspensions to improve comfort and road-holding performances. However, due to the number and the cost of the required sensors, this is not yet possible, except for upmarket car models. Moreover even if such cars have already been equipped with controlled suspensions, the control strategies are often open-loop control strategies since closed-loop applications require many expensive sensors. Furthermore, car manufacturers need to choose the

number, the kind and the location of sensors in the vehicle. Therefore, a complete observer design methodology is of great interest to take up this challenge and meet the industrial needs.

5.1.2 State of the art

Observers for suspension control applications have already been studied [Hedrick et al., 1994, Yi, 1995, Yi and Song, 1999, Rajamani and Hedrick, 1995, Hsu and Chen, 2009]. In these previous works, bilinear observers, also based on acceleration measurements, are proposed and provide interesting results, but for quarter car estimation only. In [Yi and Song, 1999], the necessary and sufficient conditions for bilinear observer design are established. However, if these restrictive conditions for exact disturbance decoupling are not fulfilled, no result is proposed to design an approximated observer. Furthermore the location of the observer poles cannot be explicitly specified, which renders the proposed observers quite difficult to adjust in practice. In these past studies, the estimation problem is often addressed using specific sensors, and the developed methodology sometimes cannot be adapted if some other variables are measured. Furthermore, the proposed methods often do not include tuning parameters allowing the designer to easily adapt the observer behavior to the observed system. Therefore, no global and practical methodology exists to solve this problem.

The system under study is a full-car model, subject to unknown ground disturbances. Thereafter, unknown input observers (UIO) have to be considered. Such observers have already been studied by many authors [Valcher, 2000, Koenig, 2006, Darouach, 2000, Darouach et al., 1994, Hou and Muller, 1994, Tsui, 1996]. Various methods have been proposed to obtain an exact disturbance decoupling under specific conditions, or to minimize the disturbance effect on the estimated states [Koenig et al., 2008]. In [Hou and Muller, 1994], a method is proposed to design an UIO when the measured variables are also corrupted by the unknown disturbance, through some linear transformations that allow to cancel the disturbance effect on the measured outputs. Depending on the system and on the available measurements, the conditions for exact disturbance decoupling, given for example in [Darouach et al., 1994, Darouach, 2000] may not be fulfilled. These mathematical conditions are necessary and sufficient to get an exact disturbance decoupled observer, but in practice they are not necessary to get an efficient observer since they involve an exact decoupling on the whole frequency range. Indeed from a practical point of view, these conditions should be achieved on the frequency range of interest only. Furthermore, the exact disturbance decoupling may be tractable and might achieve unsuitable pole placement, leading to unusable observer. However, the trade-off between disturbance decoupling and observer pole placement has not been studied sufficiently thoroughly.

5.1.3 Contribution

The main contribution is a complete observer design methodology, based on existing results on UIO design, and moreover taking some practical implementation constraints into account, such as pole placement or $\mathcal{H}_\infty$ disturbance decoupling. The unknown disturbance effect minimization problem is formulated such that the observer matrices are determined to fulfill a global condition including all the essential objectives: stability, disturbance decoupling and pole placement, without any starting choice in the observer matrices, like in many existing studies. Therefore this method is less conservative and allows the designer to handle the compromise between disturbance decoupling and pole placement, thanks to appropriate tuning parameters and LMI regions for pole placement.

This chapter is organized as follows: the estimation problem is formulated and solved in Section 5.2, some synthesis results are given and the robustness of the observer is analyzed in Section 5.3, the experimental tests and results are presented in Section 5.4. Finally, the chapter is concluded in Section 5.5, and some future works are proposed.

5.2 Observer design

The main objective of this section is to propose a methodology to design observers for systems undergoing unknown disturbances. It is worth mentioning that the considered approach, inspired by the formulation proposed in [Koenig et al., 2008], is very general, and can be applied to a wide class of systems. In this chapter, we propose to apply this method to estimate the unmeasured state variables of a vehicle model. This section is organized as follows: the estimation problem is formulated in Section 5.2.1. Then the disturbance decoupling conditions are studied in Section 5.2.2, the proposed observer is designed in Section 5.2.3, a pole placement method is given in Section 5.2.4, and finally, the complete design methodology is summarized in Section 5.2.5.

5.2.1 General problem statement

The full-car model (4.4.3), representing the system under study, is linear with 14 state variables and 7 inputs. This model can be written as the following state-space model,

$$\begin{cases} \dot{x} = A \cdot x + D_x \cdot v \\ y = C \cdot x + D_y \cdot v \end{cases} \tag{5.2.1}$$

where x is the state vector, v the input, y the measured variables and $A \in \mathbb{R}^{n\times n}$, $D_x \in \mathbb{R}^{n\times d}$, $C \in \mathbb{R}^{m\times n}$ and $D_y \in \mathbb{R}^{m\times d}$. For the system under consideration, the state

variables, the inputs and the 7 measurements used to estimate the full-car model are given by,

$$\left\{\begin{array}{lcl} x & = & \left(\dot{z}_s, z_s, \dot{z}_{us_1}, z_{us_1}, \dot{z}_{us_2}, z_{us_2}, \dot{z}_{us_3}, z_{us_3}, \dot{z}_{us_4}, z_{us_4}, \dot{\theta}, \theta, \dot{\phi}, \phi\right) \\ v & = & (z_{r_1}, z_{r_2}, z_{r_3}, z_{r_4}, F_z, M_x, M_y) \\ y & = & (\ddot{z}_{s_1}, \ddot{z}_{s_2}, \ddot{z}_{s_3}, \ddot{z}_{us_1}, \ddot{z}_{us_2}, \ddot{z}_{us_3}, \ddot{z}_{us_4}) \end{array}\right.$$

In the synthesis of the observer, the inputs F_z, M_x and M_y will be neglected. Indeed, F_z, M_x and M_y correspond to aerodynamic forces and load transfers. These disturbances are slow, and furthermore they are indirectly measured through the accelerometers mounted on the sprung mass. Therefore it is not useful to consider them as unknown disturbances in the observer synthesis. Then v becomes $v = (z_{r_1}, z_{r_2}, z_{r_3}, z_{r_4})$ and only the ground disturbance effect is considered, which is clearly the actual unknown input in suspension systems. Furthermore, in the Equation (5.2.1), no control input is considered. This choice is explained in the next sections. However, all the results given in this chapter can be adapted if such an input is to be taken into account, as usual in observer design.

The structure of the full-order observer chosen to estimate this model is given by,

$$\left\{\begin{array}{l} \dot{z} = N \cdot z + L \cdot y \\ \hat{x} = z - E \cdot y \end{array}\right. \tag{5.2.2}$$

where $z \in \mathbb{R}^{n\times n}$ is the state variable of the observer and $\hat{x} \in \mathbb{R}^{n\times n}$ the estimated state variables. $N \in \mathbb{R}^{n\times n}$, $L \in \mathbb{R}^{n\times m}$, $E \in \mathbb{R}^{n\times m}$ are the observer matrices to be designed.

Let us define the matrices $P = \mathcal{I}_n + EC$ and $K = L + NE$. The estimation error dynamical equation can be expressed as,

$$\begin{array}{rcl} \dot{e} & = & \dot{x} - \dot{\hat{x}} \\ & = & Ax + D_x v - \dot{z} + E\dot{y} \\ & = & (A - LC + ECA)x + (D_x - LD_y + ECD_x)v + ED_y - N(Px - e) \\ & = & Ne + (A - LC + ECA - NP)x + (PD_x - LD_y)v + ED_y\dot{v} \\ & = & Ne + (PA - KC - N)x + (PD_x - LD_y)v + ED_y\dot{v} \end{array} \tag{5.2.3}$$

The estimated state variable $\hat{x}$, ruled by (5.2.3), converges asymptotically to the state x for any bounded initial conditions $\hat{x}(0)$ and $x(0)$ if and only if the following conditions hold, [Darouach, 2000, Darouach et al., 1994]

Stability:

$$\left\{\begin{array}{l} N \text{ is Hurwitz} \\ N = PA - KC \end{array}\right. \tag{5.2.4}$$

Disturbance decoupling:

$$\left\{\begin{array}{l} LD_y - PD_x = 0 \\ ED_y = 0 \end{array}\right. \tag{5.2.5}$$

The observer design involves the calculation of the matrices N, L and E satisfying both the stability and disturbance decoupling conditions (5.2.4-5.2.5). However these conditions are not sufficient from a practical point of view. Indeed, the real-time implementation of the observer may not be possible if the poles are either too fast or too close to the imaginary axis. Therefore the eigenvalues of N have to be placed in a well-chosen region fitting both the system bandwidth and the measurement noise level. These are the two main challenges to design an efficient and implementable unknown input observer. A methodology to solve this problem is proposed in the next sections.

Definition 5.2.1 (*Exact and $\mathcal{H}_\infty$-observers*)

A full state observer of the form (5.2.2) is said to be,

- *an exact observer if N, L, E are exact solutions of (5.2.4) and (5.2.5). In this case an exact disturbance decoupling is achieved since the estimated variables do not depend on the disturbance.*
- *an $\mathcal{H}_\infty$-observer if N, L, E are obtained by minimizing the disturbance effect on the estimated state variables, i.e. the problem (5.2.6) has been solved,*

$$\min \gamma_\infty \ s.\ t.\ ||e||_2 < \gamma_\infty \cdot ||v||_2 \tag{5.2.6}$$

where $||.||_2$ denotes the $\mathcal{L}_2$-norm. This norm represents the energy to energy gain ($\mathcal{L}_2$ gain) of the considered system.

5.2.2 Exact observer existence conditions

Necessary and sufficient conditions for exact observer design are recalled [Darouach, 2000, Darouach et al., 1994], and a methodology to compute the observer matrices is given in this case.

Stability conditions:
The stability conditions (5.2.4) are fulfilled if and only if (PA, C) is detectable. However, this condition depends on the matrix P. Therefore the stability conditions depend on the disturbance decoupling (5.2.5), as detailed below.

Disturbance decoupling:
Depending on the measurements, two cases have to be considered:

- Case $D_y = \mathcal{O}$:

In this case, the system (5.2.3) reduces to,

$$\dot{e} \;=\; Ne - (N - PA + KC)x + PD_x v \tag{5.2.7}$$

Since $P = \mathcal{I}_n + EC$ by definition, the disturbance decoupling condition for the exact observer design is given by,

$$PD_x = 0 \Leftrightarrow ECD_x = -D_x \tag{5.2.8}$$

This equation, where E is the unknown, is solvable [Ben-Israel and Greville, 2003] if and only if

$$rank(CD_x) = rank \begin{pmatrix} CD_x \\ D_x \end{pmatrix} \tag{5.2.9}$$

If (5.2.9) is fulfilled, there exists [Ben-Israel and Greville, 2003] an exact solution set fulfilling (5.2.8), of the form,

$$E = -D_x(CD_x)^+ + Y_E \left[\mathcal{I}_m - (CD_x)(CD_x)^+\right] \tag{5.2.10}$$

where Y_E is a free matrix of appropriate dimension.

- If E can be chosen according to (5.2.10) in such a way that (PA, C) is observable, the poles of N can be arbitrarily assigned by choosing K in the equation $N = PA - KC$. Then the last unknown matrix L can be easily derived from $K = L + NE$, leading to an exact observer according to the Definition 5.2.1.
- If E can be chosen according to (5.2.10) in such a way that (PA, C) is detectable but not observable, some of the poles cannot be placed arbitrarily. Then K can be computed to place the observable poles, and L can be derived from $K = L + NE$, leading to an exact observer according to the Definition 5.2.1, However, if some of the non observable poles are too close to the imaginary axis, or too high, the disturbance decoupling will be exact, but the observer will not be implementable. In this case, an approximated observer, according to the Definition 5.2.1, has to be found with the best possible disturbance decoupling and implementable poles. A method to solve this problem is proposed in Section 5.2.3.

- Case $D_y \neq \mathcal{O}$:
  In this case the disturbance decoupling conditions are given by,

$$\begin{cases} LD_y - PD_x = 0 \\ ED_y = 0 \end{cases} \tag{5.2.11}$$

In order to achieve an exact disturbance decoupling, E has to fulfill $ED_y = 0$. Since D_y has full column rank, this equation, where E is the unknown, can be solved and the solution set is given by [Ben-Israel and Greville, 2003],

$$E = Y_E[\mathcal{I}_m - D_y D_y^+] \tag{5.2.12}$$

where $Y_E \in \mathbb{R}^{n \times m}$ is a free matrix.

The other condition for exact disturbance decoupling is,

$$\begin{array}{rl} & LD_y - PD_x = 0 \\ \Leftrightarrow & LD_y = (\mathcal{I}_n + EC)D_x \\ \Leftrightarrow & LD_y = (\mathcal{I}_n + Y_E[\mathcal{I}_m - D_y D_y^+]C)D_x \\ \Leftrightarrow & LD_y - Y_E[\mathcal{I}_m - D_y D_y^+]CD_x = D_x \end{array} \tag{5.2.13}$$

This equation can also be parameterized as,

$$U_{LY_E} \cdot \Psi_{LY_E} = D_x \tag{5.2.14}$$

where $U_{LY_E} = \begin{bmatrix} L & Y_E \end{bmatrix}$ and $\Psi_{LY_E} = \begin{bmatrix} D_y \\ -[\mathcal{I}_m - D_y D_y^+]CD_x \end{bmatrix}$.

The Equation (5.2.14), where U_{LY_E} is the unknown, can be solved if and only if,

$$rank(\Psi_{LY_E}) = rank \begin{pmatrix} \Psi_{LY_E} \\ D_x \end{pmatrix} \tag{5.2.15}$$

If (5.2.15) is fulfilled, the solutions of (5.2.14) can be chosen among the family,

$$U_{LY_E} = D_x \Psi_{LY_E}^+ + Y_{LY_E}[\mathcal{I}_n - \Psi_{LY_E}\Psi_{LY_E}^+] \tag{5.2.16}$$

where $Y_{LY_E} \in \mathbb{R}^{n \times 2*m}$ is a free matrix.

This parameterization enables to determine both E and L such that the disturbance decoupling is perfect. However, the obtained solution set influences:

- the detectability of (PA, C), since $P = \mathcal{I}_n + EC$,
- the choice of K, allowing to place the poles of $PA - KC$, since K depends on E and L.

Therefore the disturbance decoupling conditions (5.2.11) reduce the solution set through a more restrictive detectability condition.

Furthermore, the stability condition $N = PA - KC$, with $K = L + NE$, has to be fulfilled.

$$\begin{array}{rcl} N = PA - KC & \Leftrightarrow & N = PA - LC - NEC \\ & \Leftrightarrow & NP = PA - LC \end{array} \tag{5.2.17}$$

This equation, where N is the unknown, can be solved if and only if [Ben-Israel and Greville, 2003],

$$rank(P) = rank \begin{pmatrix} PA - LC \\ P \end{pmatrix} \tag{5.2.18}$$

and the solutions of (5.2.17) are of the form,

$$N = (PA - LC)P^{+} + Y_N(\mathcal{I}_n - PP^{+}) \tag{5.2.19}$$

where $P = \mathcal{I}_n + EC$, and $Y_N \in \mathbb{R}^{n \times n}$ is a free matrix.

In (5.2.19), the matrices L and E are given by (5.2.16) and depend on Y_{LY_E}. Therefore the choice of Y_{LY_E} influences the detectability of the pair $((PA-LC)P^{+}, (\mathcal{I}_n - PP^{+}))$.

If the rank conditions (5.2.15) and (5.2.18) are fulfilled and if $((PA-LC)P^{+}, (\mathcal{I}_n - PP^{+}))$ is detectable, an exact observer can be determined and the observable poles cannot be chosen arbitrarily using Y_N.

If the rank conditions (5.2.15) and (5.2.18) are fulfilled and if $((PA-LC)P^{+}, (\mathcal{I}_n - PP^{+}))$ is observable, an exact observer can be determined and the poles can be arbitrarily chosen using Y_N.

If the rank conditions (5.2.15) and (5.2.18) are not fulfilled, the exact observer cannot be computed.

Remark 5.2.1

Choosing Y_{LY_E} such that $((PA - LC)P^{+}, (\mathcal{I}_n - PP^{+}))$ is observable, is not an easy problem, and may not be solved. Furthermore both (5.2.15) and (5.2.18) may not be fulfilled, and then no exact observer design is possible. However, an efficient approximated observer may exist and a global design methodology has to be established to help the designer find an optimal observer fulfilling all the theoretical conditions. Thereafter the solution consists in solving the whole problem including all the constraints. Such a method is proposed in Section 5.2.3.

5.2.3 $\mathcal{H}_\infty$-observer design

The system (5.2.3) will be parameterized such that the unknown observer matrices can be computed to minimize the disturbance effect on the estimated state variables. This parameterization is inspired by the formulation proposed in [Koenig et al., 2008]. The disturbance effect minimization is achieved by minimizing the $\mathcal{H}_\infty$-norm of the transfer from the unknown disturbance to the estimated state variables, which corresponds to the problem (5.2.6) given in the Definition 5.2.1.

The estimation error is ruled by the following equation,

$$\dot{e} \;=\; Ne + (PA - KC - N)x + (PD_x - LD_y)v + ED_y\dot{v} \tag{5.2.20}$$

The system (5.2.20) is corrupted by the disturbance v and its derivative $\dot{v}$, and can be rewritten as,

$$\dot{e} \;=\; Ne + (PA - KC - N)x + Fd \tag{5.2.21}$$

where $F = \begin{pmatrix} PD_x - LD_y & ED_y \end{pmatrix}$ and $d = \begin{pmatrix} v \\ \dot{v} \end{pmatrix}$.

Then the disturbance F can be minimized according to the procedure described in the next sections. However, since $\dot{v}$ may be very high, v may be less minimized. This method is possible but leads to a less efficient disturbance decoupling.

In order to avoid this problem, the observer matrix E can be chosen according to (5.2.12). Therefore $E = Y_E[\mathcal{I}_m - D_yD_y^+]$, where the matrix Y_E will be determined later, during the synthesis of the observer. Thereafter, $ED_y = \mathcal{O}$, and the system (5.2.20) can be rewritten as,

$$\dot{e} \;=\; Ne + (P(Y_E)A - KC - N)x + (P(Y_E)D_x - LD_y)v \tag{5.2.22}$$

where $P(Y_E) = \mathcal{I}_n + Y_E[\mathcal{I}_m - D_yD_y^+]C$.

The matrix $\Omega = [N, P, K, Y_E]$ is defined in order to parameterize the previous system. The following equivalence is first established,

$$\begin{cases} PA - KC - N = \mathcal{O}_n \\ P - Y_E(\mathcal{I}_m - D_yD_y^+)C = \mathcal{I}_n \end{cases} \Leftrightarrow \Omega \cdot \Theta = \Psi \tag{5.2.23}$$

where $\Theta = \begin{bmatrix} -\mathcal{I}_n & \mathcal{O}_n \\ A & \mathcal{I}_n \\ -C & \mathcal{O}_{m,n} \\ \mathcal{O}_{m,n} & -(\mathcal{I}_m - D_yD_y^+)C \end{bmatrix}$, $\Psi = [\mathcal{O}_n, \mathcal{I}_n]$, and $\mathcal{O}_n$ denotes the null matrix of size $n \times n$.

The equation $\Omega \cdot \Theta = \Psi$, where Ω is the unknown, can be solved if and only if the following condition holds,

$$rank(\Theta) = rank \begin{pmatrix} \Theta \\ \Psi \end{pmatrix} \tag{5.2.24}$$

If this condition is not fulfilled, the $\mathcal{H}_\infty$ observer design is impossible. If it is, the solutions are of the form,

$$\Omega(Y_\Omega) = \Psi\Theta^+ + Y_\Omega(\mathcal{I}_{2n+m} - \Theta\Theta^+) \tag{5.2.25}$$

where Y_Ω is a free matrix of appropriate dimension that will determined later, during the synthesis.

Then, the equality $N = PA - KC$ holds, and the system (5.2.22) can be rewritten as,

$$\dot{e} \;=\; \Omega(Y_\Omega)\Psi_1 \;\; e \;\; + \;\; \Omega(Y_\Omega)\Psi_2 \;\; v \tag{5.2.26}$$

where $\Psi_1 = \begin{bmatrix} \mathcal{I}_n \\ \mathcal{O}_n \\ \mathcal{O}_{m,n} \\ \mathcal{O}_{m,n} \end{bmatrix}$, $\Psi_2 = \begin{bmatrix} \mathcal{O}_{n,d} \\ D_x \\ -D_y \\ \mathcal{O}_{m,d} \end{bmatrix}$ and $\Omega(Y_\Omega) = \Psi\Theta^+ + Y_\Omega(\mathcal{I}_{2n+m} - \Theta\Theta^+)$.

The estimation error, ruled by the equation (5.2.26), is driven by the unknown disturbance v. If the exact observer design is not possible, and if the rank condition (5.2.24) is fulfilled, the disturbance effect can be minimized, and an efficient observer computed. The matrices of the observer can be determined by studying the stability and the $\mathcal{H}_\infty$-norm bound of the transfer $e \to v$. This problem is solved below, by minimizing γ_∞ such that (5.2.27) is verified.

$$||e||_2 < \gamma_\infty \cdot ||v||_2 \tag{5.2.27}$$

Proposition 5.2.1

Consider the system (5.2.1) and the observer (5.2.2). Given a positive scalar γ_∞, if there exist $\mathbf{X} = \mathbf{X}^T \succ 0$, $\tilde{\mathbf{Y}} = \mathbf{XY}$ satisfying the inequality (5.2.28),

$$\begin{pmatrix} Q\Psi_1 + \Psi_1^T Q^T & Q\Psi_2 & \mathcal{I}_n \\ * & -\gamma_\infty \mathcal{I}_d & \mathcal{O}_{d,n} \\ * & * & -\gamma_\infty \mathcal{I}_n \end{pmatrix} \prec 0 \tag{5.2.28}$$

$$Q = \mathbf{X}\Psi\Theta^+ + \tilde{\mathbf{Y}}(\mathcal{I}_{2n+m} - \Theta\Theta^+) \tag{5.2.29}$$

then the observer (5.2.2) is an $\mathcal{H}_\infty$-observer according to the Definition 5.2.1, where the disturbance attenuation level γ_∞ and the observer matrices are given by,

$$[N, P, K, Y_E] = \Psi\Theta^+ + Y_\Omega(\mathcal{I}_{2n+2m} - \Theta\Theta^+) \tag{5.2.30}$$

where $Y_\Omega = X^{-1}\tilde{Y}$, $\Theta = \begin{bmatrix} -\mathcal{I}_n & \mathcal{O}_n \\ A & \mathcal{I}_n \\ -C & \mathcal{O}_{m,n} \\ \mathcal{O}_{m,n} & -(\mathcal{I}_m - D_y D_y^+)C \end{bmatrix}$ *and* $\Psi = [\mathcal{O}_n, \mathcal{I}_n]$.

Proof 5.2.1

The Bounded Real Lemma [Scherer and Weiland, 1999] (BRL) applied to the system (5.2.22) gives the solution to (5.2.27) and leads to the bilinear matrix inequality (BMI) (5.2.31) where $\mathbf{X} = \mathbf{X}^T \succ 0$ and $\mathbf{Y}$ are the unknown matrices to be determined. Therefore the full-order stable and disturbance decoupled observer design problem consists in solving (5.2.31).

$$\begin{pmatrix} Q\Psi_1 + \Psi_1^T Q^T & Q\Psi_2 & \mathcal{I}_n \\ * & -\gamma_\infty \mathcal{I}_d & \mathcal{O}_{d,n} \\ * & * & -\gamma_\infty \mathcal{I}_n \end{pmatrix} \prec 0 \tag{5.2.31}$$

Where the matrix Qis given by,

$$Q = \mathbf{X}\Omega = \mathbf{X}\Psi\Theta^+ + \mathbf{XY}(\mathcal{I}_{2n+2m} - \Theta\Theta^+) \tag{5.2.32}$$

The matrix inequality (5.2.31) is a BMI since Q is bilinear in $\mathbf{X}$ and $\mathbf{Y}$. Therefore the change of variable $\tilde{\mathbf{Y}} = \mathbf{XY}$ is introduced to transform the BMI into a solvable LMI where $Q = \mathbf{X}\Psi\Theta^+ + \tilde{\mathbf{Y}}(\mathcal{I}_{2n+2m} - \Theta\Theta^+)$. Solving (5.2.31) with (5.2.32) leads to find $\mathbf{X}$, $\tilde{\mathbf{Y}}$ and thereafter $\mathbf{Y} = \mathbf{X}^{-1}\tilde{\mathbf{Y}}$.

Then Ω can be deduced using (5.2.25), which gives the observer matrices. Finally, the proposed observer is designed so that the stability conditions (5.2.4) are satisfied, and the disturbance decoupling conditions (5.2.5) are approached by minimizing γ_∞ subject to (5.2.27).

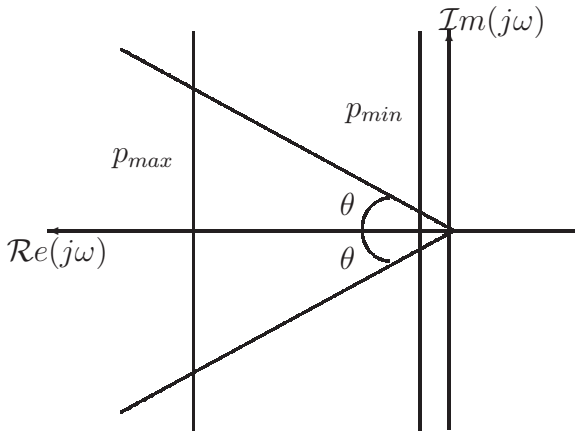

Figure 5.1: LMI regions in complex plane

5.2.4 Pole placement

The previous method ensures the stability of the observer and the minimization of the disturbance effect, but the poles of the observer are obtained through the solution of (5.2.28) and may be either very high, have high imaginary parts, or be almost unstable. Such poles may render the observer oscillating and sensitive to measurement noises or unstable in practice. In order to avoid such a behavior that may lead to implementation problems and bad estimation performances, a pole placement method using LMI regions has been introduced into the design procedure, according to the method proposed in [Chilali et al., 1999].

The poles of the observer can be placed in the intersection of the regions $\mathcal{D}_1$, $\mathcal{D}_2$ and $\mathcal{D}_3$ in the complex plane, corresponding respectively to a conic sector center with inner angle 2θ, a left half plane, and a right half plane, as represented in Figure 5.1. These regions are defined by the LMI (5.2.33), (5.2.34) and (5.2.35). The conic sector ensures that the poles lying in this region have a damping ratio at least equal to $\cos(\theta)$, which implies moderate imaginary parts. The half planes $\mathcal{D}_2$, $\mathcal{D}_3$ ensure that the poles have real parts in $[-p_{max}, -p_{min}]$.

$$\mathcal{D}_1 = \left\{ z \in \mathbb{C} : \begin{pmatrix} \sin(\theta)\cdot(z+z^*) & \cos(\theta)\cdot(z-z^*) \\ \cos(\theta)\cdot(z^*-z) & \sin(\theta)\cdot(z+z^*) \end{pmatrix} \prec 0 \right\} \tag{5.2.33}$$

$$\mathcal{D}_2 = \{ z \in \mathbb{C} : z + z^* + 2p_{min} \prec 0 \} \tag{5.2.34}$$

$$\mathcal{D}_3 = \{ z \in \mathbb{C} : -z - z^* - 2p_{max} \prec 0 \} \tag{5.2.35}$$

Proposition 5.2.2

Consider the system (5.2.1) and the observer (5.2.2). Given a positive scalar γ_∞, if there exist $\mathbf{X} = \mathbf{X}^T \succ 0$, $\tilde{\mathbf{Y}} = \mathbf{XY}$ satisfying the inequalities (5.2.36), (5.2.37) and

(5.2.38),

$$\begin{pmatrix} \mathcal{M}_{11} & \mathcal{M}_{12} & \mathcal{M}_{13} \\ * & \mathcal{M}_{22} & \mathcal{M}_{23} \\ * & * & \mathcal{M}_{33} \end{pmatrix} \prec 0 \tag{5.2.36}$$

$$\begin{pmatrix} Q\Psi_1 + \Psi_1^T Q^T + 2p_{min}\mathbf{X} & Q\Psi_2 & \mathcal{I}_n \\ * & -\gamma_\infty \mathcal{I}_d & \mathcal{O}_{d,n} \\ * & * & -\gamma_\infty \mathcal{I}_n \end{pmatrix} \prec 0 \tag{5.2.37}$$

$$\begin{pmatrix} -Q\Psi_1 - \Psi_1^T Q^T - 2p_{max}\mathbf{X} & Q\Psi_2 & -\mathcal{I}_n \\ * & -\gamma_\infty \mathcal{I}_d & \mathcal{O}_{d,n} \\ * & * & -\gamma_\infty \mathcal{I}_n \end{pmatrix} \prec 0 \tag{5.2.38}$$

where

$$\begin{aligned} \mathcal{M}_{11} &= \begin{pmatrix} \sin(\theta)(Q\Psi_1 + \Psi_1^T Q^T) & \cos(\theta)(Q\Psi_1 - \Psi_1^T Q^T) \\ -\cos(\theta)(Q\Psi_1 - \Psi_1^T Q^T) & \sin(\theta)(Q\Psi_1 + \Psi_1^T Q^T) \end{pmatrix} \\ \mathcal{M}_{12} &= \begin{pmatrix} Q\Psi_2 & \mathcal{O}_{n,d} \\ \mathcal{O}_{n,d} & Q\Psi_2 \end{pmatrix} \\ \mathcal{M}_{13} &= \begin{pmatrix} \sin(\theta)\mathcal{I}_n & -\cos(\theta)\mathcal{I}_n \\ \cos(\theta)\mathcal{I}_n & \sin(\theta)\mathcal{I}_n \end{pmatrix} \\ \mathcal{M}_{22} &= -\gamma_\infty \mathcal{I}_{2d} \\ \mathcal{M}_{23} &= \mathcal{O}_{2d,2n} \\ \mathcal{M}_{33} &= -\gamma_\infty \mathcal{I}_{2n} \end{aligned} \tag{5.2.39}$$

and $Q = \mathbf{X}\Psi\Theta^+ + \tilde{\mathbf{Y}}(\mathcal{I}_{2n+2m} - \Theta\Theta^+)$ and $*$ denotes the symmetric element, then the observer (5.2.2) is an $\mathcal{H}_\infty$-observer according to the Definition 5.2.1, with the disturbance attenuation level γ_∞ and whose poles are located in the intersection of LMI regions $\mathcal{D}_1$, $\mathcal{D}_2$ and $\mathcal{D}_3$. The observer matrices are then given by,

$[N, P, K, Y_E] = \Psi\Theta^+ + Y_\Omega(\mathcal{I}_{2n+2m} - \Theta\Theta^+)$
where

$$Y_\Omega = X^{-1}\tilde{Y},\ \Theta = \begin{bmatrix} -\mathcal{I}_n & \mathcal{O}_n \\ A & \mathcal{I}_n \\ -C & \mathcal{O}_{m,n} \\ \mathcal{O}_{m,n} & -(\mathcal{I}_m - D_y D_y^+)C \end{bmatrix} \text{ and } \Psi = [\mathcal{O}_n, \mathcal{I}_n].$$

Proof 5.2.2

In [Chilali et al., 1999], the LMI constraint allowing the pole placement in region $\mathcal{D}$ defined by (5.2.40) is given by (5.2.41).

$$\mathcal{D} = \left\{ z \in \mathcal{C} : L + zM + z^* M^T \prec 0 \right\} \tag{5.2.40}$$

$$\left(\begin{array}{c|c|c} L\otimes X + M\otimes(XA) & M_1^T\otimes(XB) & M_2^T\otimes C^T \\ +M^T\otimes(A^TX) & & \\ \hline * & -\gamma\mathcal{I} & D^T \\ \hline * & * & -\gamma\mathcal{I} \end{array}\right) \prec 0 \tag{5.2.41}$$

where $\otimes$ denotes the well-known Kronecker product and the decomposition of M is $M = M_1^T M_2$.

For the LMI region $\mathcal{D}_1$, $L^{\mathcal{D}_1}$, $M_1^{\mathcal{D}_1}$, $M_2^{\mathcal{D}_1}$ can be expressed as

$$\left\{\begin{array}{lcl} L^{\mathcal{D}_1} & = & \mathcal{O}_2 \\ M_1^{\mathcal{D}_1} & = & \mathcal{I}_2 \\ M_2^{\mathcal{D}_1} & = & \begin{pmatrix} \sin(\theta) & -\cos(\theta) \\ \cos(\theta) & \sin(\theta) \end{pmatrix} \end{array}\right. \tag{5.2.42}$$

For the LMI region $\mathcal{D}_2$, $L^{\mathcal{D}_2}$, $M_1^{\mathcal{D}_2}$, $M_2^{\mathcal{D}_2}$ can be expressed as

$$\left\{\begin{array}{lcl} L^{\mathcal{D}_2} & = & 2p_{min} \\ M_1^{\mathcal{D}_2} & = & 1 \\ M_2^{\mathcal{D}_2} & = & 1 \end{array}\right. \tag{5.2.43}$$

For the LMI region $\mathcal{D}_3$, $L^{\mathcal{D}_3}$, $M_1^{\mathcal{D}_3}$, $M_2^{\mathcal{D}_3}$ can be expressed as

$$\left\{\begin{array}{lcl} L^{\mathcal{D}_3} & = & -2p_{max} \\ M_1^{\mathcal{D}_3} & = & -1 \\ M_2^{\mathcal{D}_3} & = & -1 \end{array}\right. \tag{5.2.44}$$

Then for each region, the constraints can be expressed using (5.2.41) with (5.2.42), (5.2.43) and (5.2.44). Therefore three BMIs are obtained, that can be easily transformed into LMIs (5.2.36), (5.2.37) and (5.2.38) using the change of variable $\tilde{\mathbf{Y}} = \mathbf{XY}$. Then the solvable LMIs (5.2.36), (5.2.37) and (5.2.38) are obtained, where the unknown matrices are $\tilde{\mathbf{Y}}$ and $\mathbf{X} = \mathbf{X}^T \succ 0$.

5.2.5 Design methodology

The procedure to design the $\mathcal{H}_\infty$-observer is represented in Figure 5.2 and can be summarized as follows:

Step 1: Determine the region where the poles of the observer have to be located, and choose the pole bounds p_{min}, p_{max} and the cone angle θ.

If $D_y = 0$:

Step 2a: Check the exact disturbance decoupling condition (5.2.9).

- If (5.2.9) is fulfilled, find E according to (5.2.10), such that (PA, C) is detectable, if possible.
- If (5.2.9) is not fulfilled, the exact disturbance decoupling is impossible, but an approximated observer may be found. Go to Step 4.

Step 3a:

- If (PA, C) is detectable, place the poles using K, if possible. Then deduce the observer matrices $N = PA - KC$, $L = K - NE$ and E. Check the poles of the computed exact observer.
- If (PA, C) is not detectable, the observer design is impossible.

If $D_y \neq 0$:

Step 2b: Check the exact observer existence conditions (5.2.15).

- If (5.2.15) is fulfilled, find Y_{LYE} such that (5.2.18) is fulfilled and $((PA - LC)P^+, (\mathcal{I}_n - PP^+))$ is detectable, if possible. Then deduce the observer matrices L and E.
- If (5.2.15) is not fulfilled, the exact disturbance decoupling is impossible. Go to Step 4.

Step 3b:

- If (5.2.18) is fulfilled and $((PA-LC)P^+, (\mathcal{I}_n - PP^+))$ is detectable, place the poles of N using Y_N, if possible. Check the poles of the computed exact observer.

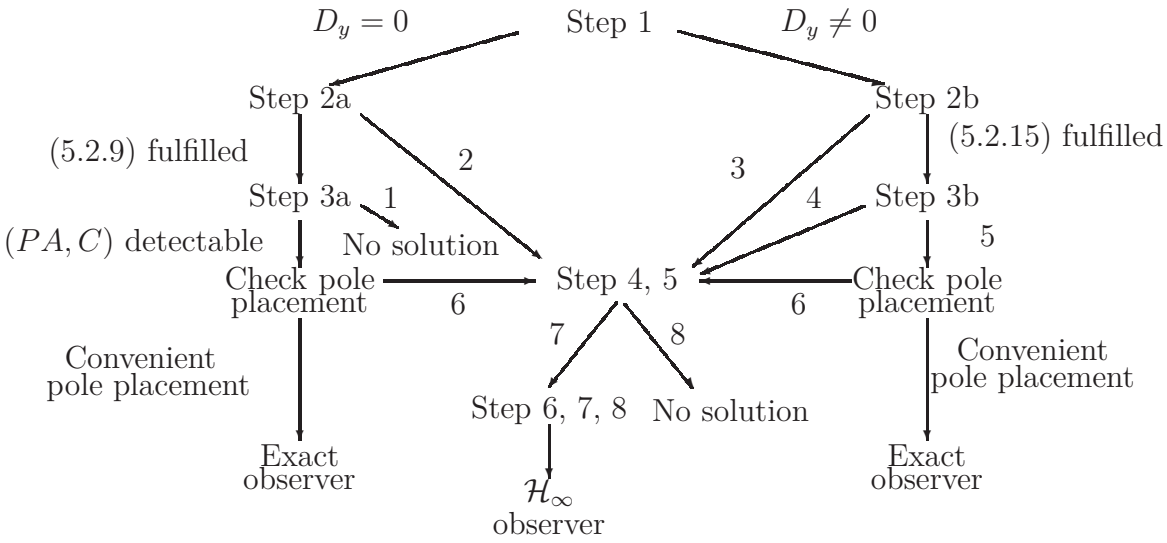

1:(PA, C) not detectable — 6: no convenient pole placement
2:(5.2.9) not fulfilled — 7: (5.2.24) fulfilled
3:(5.2.15) not fulfilled — 8: (5.2.24) not fulfilled
4:(5.2.18) not fulfilled or $((PA - LC)P^+, (I_n - PP^+))$ not detectable
5:(5.2.18) fulfilled and $((PA - LC)P^+, (I_n - PP^+))$ detectable

Figure 5.2: Observer design procedure

- If (5.2.18) is not fulfilled, or $((PA - LC)P^+, (\mathcal{I}_n - PP^+))$ is not detectable, an approximated observer may exist. Go to Step 4.

If exact decoupling is not possible or if the poles cannot be placed in the desired region, then a trade-off can be found between pole placement and disturbance decoupling according to the following procedure:

Step 4: If the rank condition (5.2.24), is fulfilled, go to Step 5. If not, the $\mathcal{H}_\infty$-observer design is impossible. **Step 5:** Minimize γ_∞ under LMI (5.2.36), (5.2.37) and (5.2.38).
Step 6: Calculate $Y_\Omega = X^{-1}\tilde{Y}$, and Ω using (5.2.25).
Step 7: Deduce the observer matrices N from Ω, E from $P = \mathcal{I} + EC$ and L from $K = L + NE$.

5.3 Synthesis results and robustness analysis

Some numerical synthesis results are given in Section 5.3.1, and a robust analysis is performed in Section 5.3.2.

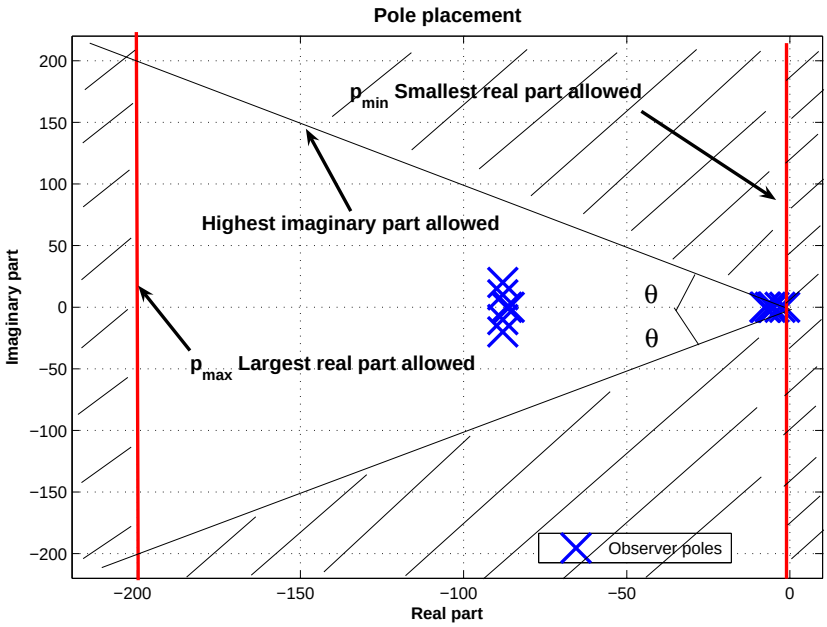

Figure 5.3: Poles of the observer and specified regions

5.3.1 Numerical synthesis results

In this paragraph, the procedure described in Section 5.2.5 is applied to design the observer.

Step 1: The LMI regions (5.2.33), (5.2.34) and (5.2.35) have been chosen and are determined by (5.3.1). This region is represented in Figure 5.3.

$$\begin{cases} \theta & = & \frac{\pi}{4} \\ p_{min} & = & 1 \\ p_{max} & = & 200 \end{cases} \tag{5.3.1}$$

Steps 2b: Here the measured unsprung mass accelerations depend on the ground disturbance, thereafter we have $D_y \neq 0$. Unfortunately, (5.2.15) is not fulfilled. The exact disturbance decoupling is not possible. Therefore the approximated observer design approach has been chosen to tackle both the disturbance decoupling and the pole placement problems.
Step 4: The rank condition (5.2.24) is fulfilled. **Step 5:** The minimal γ_∞ obtained solving the LMI problem (5.2.36-5.2.38) is $\gamma_\infty = 1.08$.
Steps 6-7: The matrices of the observer have been deduced and the poles of the observer are located in the specified region, represented in Figure 5.3.

Remark 5.3.1

The pole bounds p_{min} and p_{max} have to be chosen by the designer. The lower bound of the poles must be chosen according to the noise level. If there is almost no measurement noise, this bound can be set equal to 0, so that pure integrators are allowed. Therefore the results will be of course more accurate. But if the noise level is higher, the observer may become unstable due to very small poles, and the lower bound must be increased. Therefore a well-known compromise has to be found between performance and robustness, using this simple adjustment parameter. In the case of the experiment described in Section 5.4, the observer becomes unstable if $p_{min} < 1$, since the measurement noise is important. The upper bound has also to be chosen by the designer. It determines the bandwidth of the observer. The observer must be at least ten times faster than the system to be observed to get accurate results. However for noise filtering, this bound has to be less than the frequencies of the noise. For the application considered in this chapter, the noise is located in the frequency range $[800 - 1200Hz]$. Therefore $p_{max} = 200$ allows the observer to filter the noise.

In order to analyze the achieved disturbance decoupling, the Bode diagrams of the transfer functions between the ground disturbance v and the estimation error e on each state, have been computed for the 14 state variables. Some of them, corresponding to the analysis of the front left suspension, are given on Figure 5.4. These results emphasize the attenuation of the ground disturbance effect on the estimation error, since the largest disturbance amplification of the 14 errors, over the whole frequency range is -60dB.

5.3.2 Robustness analysis

In this section, the closed-loop system L, including the vehicle $V(s)$, given by the Equation (5.2.1), and the observer $O(s)$ defined by (5.3.2) is considered. Its output $e = x - \hat{x}$ is the state variable estimation error.

$$\left\{ \begin{array}{rcl} \dot{z} & = & Nz + Ly \\ e & = & \tilde{z} + ED_y v \end{array} \right. \tag{5.3.2}$$

The robustness of the designed $\mathcal{H}_\infty$-observer is studied using the μ-analysis tools. Here the parametric uncertainties given in Table 5.1 have been considered to define the uncertain system.

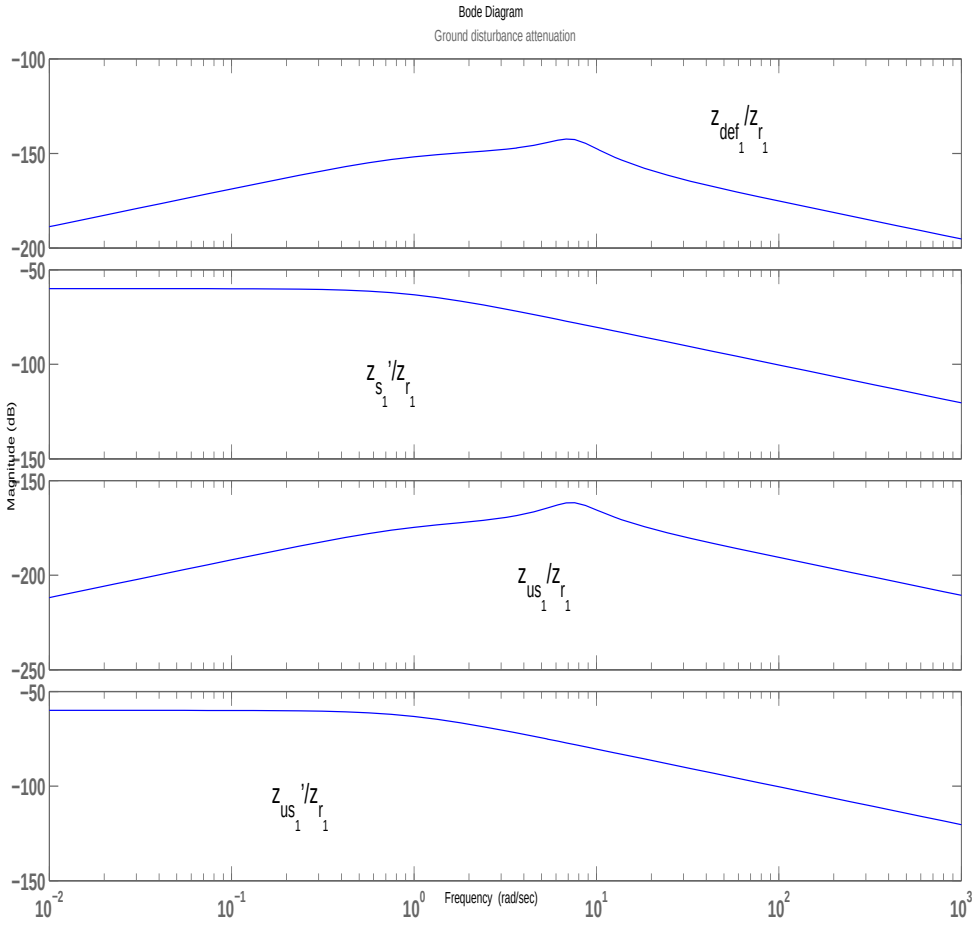

Figure 5.4: Transfer $\| e/v \|$ - Bode diagrams

Uncertain parameter	Variation	
m_s	1450	±50% [kg]
m_{us_i} , $i = 1..4$	39	±10% [kg]
k_i , $i = 1..4$	30000	±20% [N/m]
c_i , $i = 1..4$	500 to	6000 [Ns/m]
k_{ti} , $i = 1..4$	18000	±30% [N/m]
I_x	610	±30% [N*m/rad]
I_y	2750	±30% [N*m/rad]

Table 5.1: Parameter uncertainties

The main uncertainties concern the sprung mass and the damping rates. The sprung mass depends on the number and weight of passengers, quantity of fuel etc... and the damping rate depends on the control signal if the damper is controlled. It also depends on the nonlinearities of the damper, and thereafter on the damper technology. SOBEN damper is nonlinear and has a controlled damping rate varying from 500 to 6000 Ns/m. In the synthesis of the observer, a mean damping rate value has been used, but the robustness with respect to this parameter variation is very important when the observer is used in a suspension control application.

These parametric uncertainties have been considered, and used to perform a classical μ-analysis in order to study both robust stability and performances [Skogestad and Postlethwaite, 2005], where μ denotes the structured singular value.

Robust stability:

The considered uncertain system for robust stability analysis is presented in Figure 5.5 using the classical LFT form, where $\Delta_r(s)$ represents the structured uncertainties corresponding to the parametric uncertainties given in Table 5.1. $L(s)$ is the closed-loop system (5.2.3) including both the system to be observed and the observer. The robust stability is ensured if and only if the closed-loop system is stable and if the inequality (5.3.3) is fulfilled.

$$\mu_{\Delta_r(L(s))} < 1, \quad \forall s = j\omega \tag{5.3.3}$$

The structured singular value μ cannot be exactly computed. However a numerical algorithm has been used to compute the upper and lower bounds of μ. These results are given in Figure 5.6 and show that μ is less than 1 and does not depend on the frequency. Therefore the system remains stable whatever the parameters are.

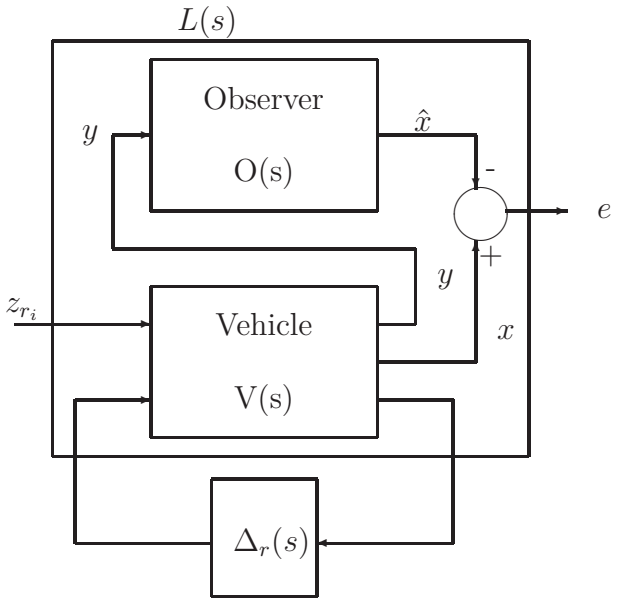

Figure 5.5: Uncertain system for robust stability analysis

Robust performance:

The considered uncertain system for robust performance analysis is presented in Figure 5.7. This system is similar to the one used for robust stability analysis, but some fictive uncertainties $\Delta_f(s)$ representing the performance objectives, given by the weighting function (5.3.4) have been added. This is a low-pass filter with cut-off frequency f_c and static gain G.

$$W(s) = G \cdot \frac{2\pi f_c}{s + 2\pi f_c} \tag{5.3.4}$$

where $f_c = 20\text{Hz}$ and $G = 1$.

This weighting filter focuses the performances objectives on the bandwidth of the system to be observed. Then using this new uncertain system including the performance objectives, the robust performance is ensured if and only if the closed-loop system is stable and if the inequality (5.3.5) is fulfilled.

$$\mu_\Delta(L(s)) < 1, \quad \forall s = j\omega \tag{5.3.5}$$

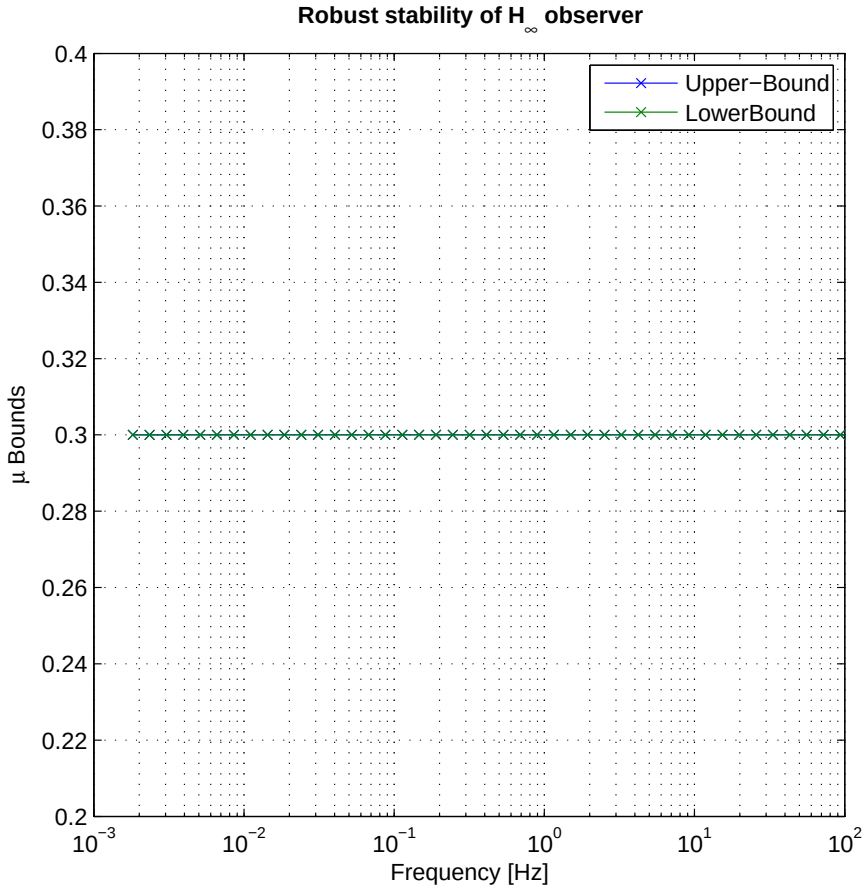

Figure 5.6: Upper and lower bounds of μ for robust stability

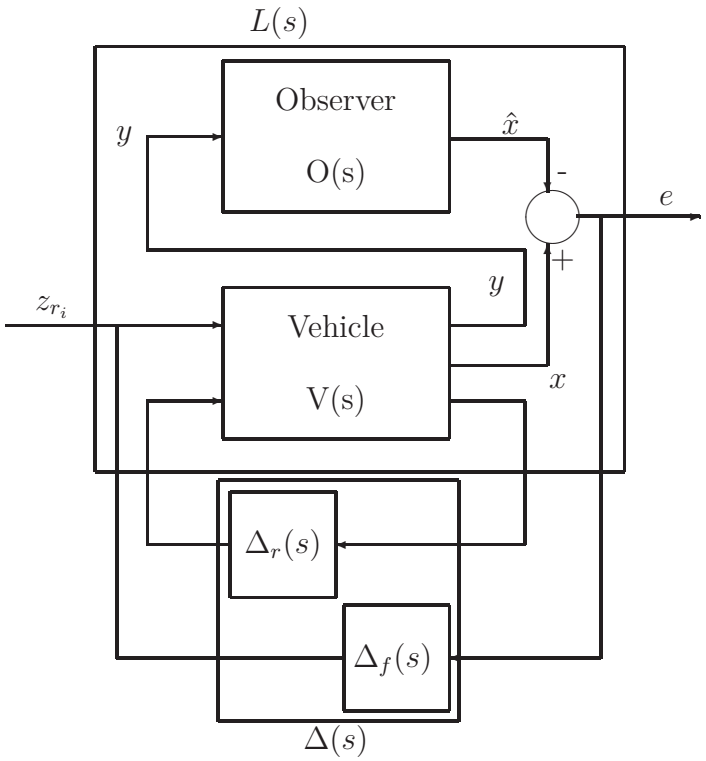

Figure 5.7: Uncertain system for robust performance analysis

where $\Delta(s)$, given by (5.3.6), includes both the real structured uncertainties and the performance objectives.

$$\Delta(s) = \begin{pmatrix} \Delta_r(s) & \mathcal{O} \\ \mathcal{O} & \Delta_f(s) \end{pmatrix} \tag{5.3.6}$$

The upper and lower bounds of μ have also been computed for the system given in Figure 5.7. These results are presented in Figure 5.8 and show that μ is always less than 1. The performance are ensured whatever the parameter uncertainties are.

These results emphasize the $\mathcal{H}_\infty$-observer robustness. The designed observer is not sensitive to the studied parametric uncertainties including all the possible parameter variations of a real vehicle equipped with controlled dampers.

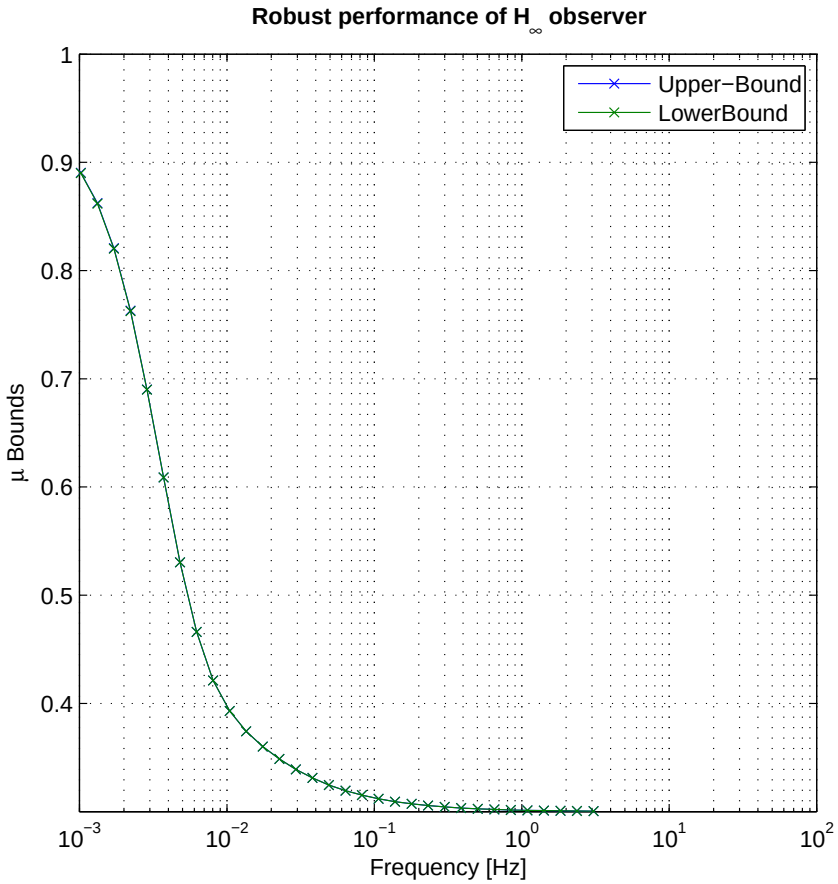

Figure 5.8: Upper and lower bounds of μ for robust performance

5.4 Experimental results

5.4.1 Description and set-up of the experiment

Four semi active damper prototypes have been built by SOBEN and mounted on a testing car, as represented in Figure 4.5. Each damper can be controlled by a servomechanism. This actuator allows the damping rate of each suspension to be controlled in real-time. The observer proposed in this chapter is to be used in a suspension control strategy, but the experiment presented here have been run to test the observer performances only. Therefore no control strategy was implemented. The influence of the damping rate on the observer performance has already been discussed in the robust analysis presented in Section 5.3.2, and the observer is robust to damping rate variations from 500 to 6000 Ns/m. In order to confirm this result, different experiments have been run with the observer proposed here, for different varying control signals (sine amplitude varying between minimal and maximal control signal), which corresponds to varying damping rates. The damping rate does not influence the accuracy of the estimations. This shows that taking these variations into account in the observer design is not useful.

The data acquisition is done by a set of five electronic boards developed by SOBEN. Each damper has a small acquisition board, represented in Figure 4.7, that converts the analog measurements into CAN (Controller Area Network) frames. A central board where the observer is implemented receives the frames through the CAN network and computes the estimated states for each damper, using the four unsprung masses accelerations and the three sprung mass accelerations. This architecture is described in Figure 4.8. The four damper boards are operational, but the central board has not been programmed yet. Therefore a Dspace board has been used for the experiments presented in this chapter. The implementation of the observer is done automatically by the software provided by Dspace. However, the implementation cannot be done if the observer is ill-conditioned. Therefore the poles of the observer have to be properly chosen.

5.4.2 Estimation results

Here the experimental results obtained with the observer designed in Section 5.2 are given. The observer has been tested while the car was traveling at 70km/h on a bad mountain road. The damper control signals were constant and nominal. During the experiment, the following variables have been estimated and measured:

- The four unsprung masses vertical accelerations (Figures 5.9, 5.10)
- The three sprung mass vertical accelerations (Figures 5.11, 5.12)

- Deflection velocities (Figure 5.13, 5.14)
- Deflections (Figure 5.15, 5.16)
- Vertical acceleration of the center of gravity (Figure 5.17)
- Pitch angular velocity (Figure 5.18)
- Roll angular velocity (Figure 5.19)
- The four unsprung masses vertical velocities (Figure 5.20, 5.21)

The measured deflection velocities have been derived from the measured deflections, and the measured unsprung masses velocities have been integrated from the measured accelerations.

Figures 5.9, 5.10, 5.11, 5.12 represent the measured and estimated sprung and unsprung masses accelerations for suspensions 1 and 4. The other ones have not been represented but the results are similar. These variables correspond to the measurements used by the $\mathcal{H}_\infty$-observer. The relative errors given by Table 5.2 and computed using the present experimental results are less than 1%. Therefore the estimated variables are very similar to the measurements, which is quite normal since these measurements are used by the observer.

Figures 5.13, 5.14, 5.15, 5.16 represent the measured and estimated deflection velocities and deflections for suspensions 1 and 4. These results emphasize the observer performance and accuracy for the $\mathcal{H}_\infty$-observer since the variables have been estimated and filtered in real-time without any delay. The relative errors of the estimated deflection velocities, given in Table 5.2 are less than 1%, which is very accurate, whereas the deflections have relative errors in the region of 15%. The estimated deflections are not as accurate as for the deflection velocities since the observer does not contain pure integrators. The minimal pole has indeed been constrained to be greater than 1 for stability reasons. However if the measurement noise could be reduced, smaller minimal poles could be allowed, and the estimated positions would be more accurate.

The deflection velocities are very important since many control strategies developed in the past few years are based on these measurements [Spelta, 2008, Sammier et al., 2003, Savaresi et al., 2005]. Furthermore the deflection sensor is very expensive and has a short life-time. The results obtained on this testing car show that the estimated deflection velocities are satisfying and can be used to control the damper.

Figure	Variable	MRE[1] [%]	RV[2] [%]
5.9	$\ddot{z}_{us_1}$	0.14	0.022
5.10	$\ddot{z}_{us_4}$	0.11	0.028
5.11	$\ddot{z}_{s_1}$	0.42	0.004
5.12	$\ddot{z}_{s_4}$	0.84	0.007
5.13	$\dot{z}_{def_1}$	0.44	1.054
5.14	$\dot{z}_{def_4}$	0.73	2.065
5.15	z_{def_1}	14.8	10.29
5.16	z_{def_4}	17.4	9.045
5.17	$\ddot{z}_s$	3.80	0.769
5.18	$\dot{\phi}$	1.76	19.75
5.19	$\dot{\theta}$	2.01	14.87
5.20	$\dot{z}_{us_1}$	0.11	0.185
5.21	$\dot{z}_{us_4}$	0.19	0.236

[1]Mean Relative Error, [2]Relative Variance

Table 5.2: Experimental results: relative mean errors and variances

The results given in Figures 5.18, 5.19, 5.20, 5.21 concern the estimations of the unsprung masses velocities and of the angular pitch and roll velocities. These figures show that the estimated variables are very similar to the measured ones. The relative errors and variances given in Table 5.2 are less than 0.2% for the unsprung masses velocities, and less than 2% for the angular velocities, therefore these estimation can be used in a control stategy to improve the vehicle behavior.

It should also be noticed that the measurements of the angular velocities, provided by the gyro meters are very noisy. The results show that the estimated variables are not corrupted by this noise. Therefore the bandwidth of the observer is appropriate, thanks to the pole placement method proposed in Section 5.2.4.

The variances given in Table 5.2 are always less than 5%, except for the deflections and angular velocities. This is due to the important measurement noise that corrupts these measured variables, but the estimated variables are not corrupted by this noise.

5.5 Conclusion

In this chapter, a methodology to design an unknown input observer for a suspension control application has been developed. This observer is based on reliable and cheap

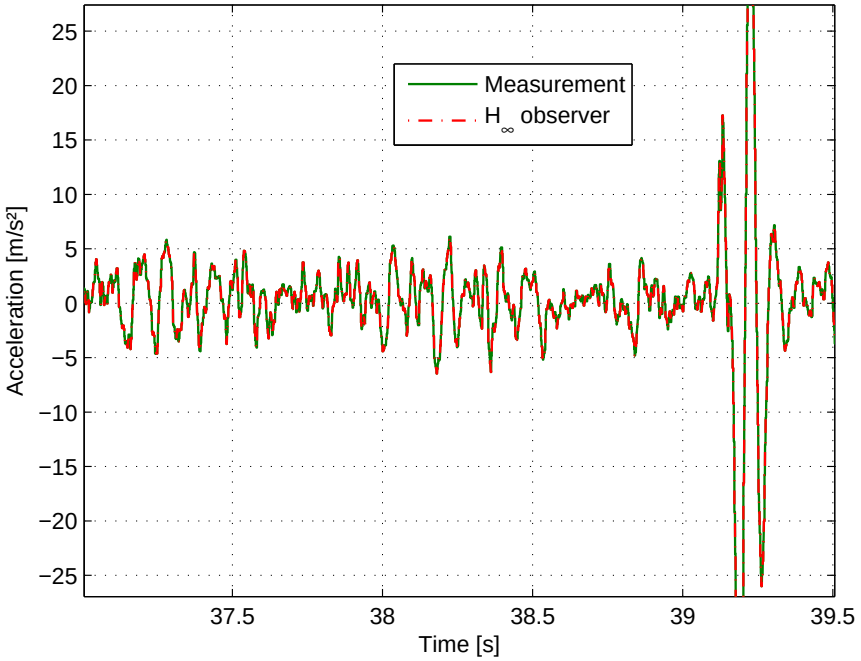

Figure 5.9: Unsprung mass 1 vertical acceleration

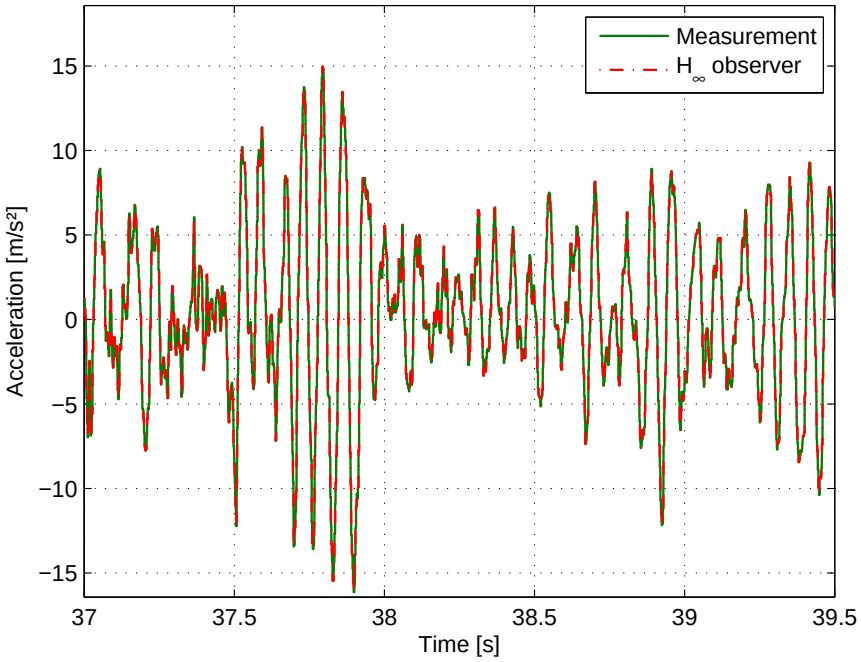

Figure 5.10: Unsprung mass 4 vertical acceleration

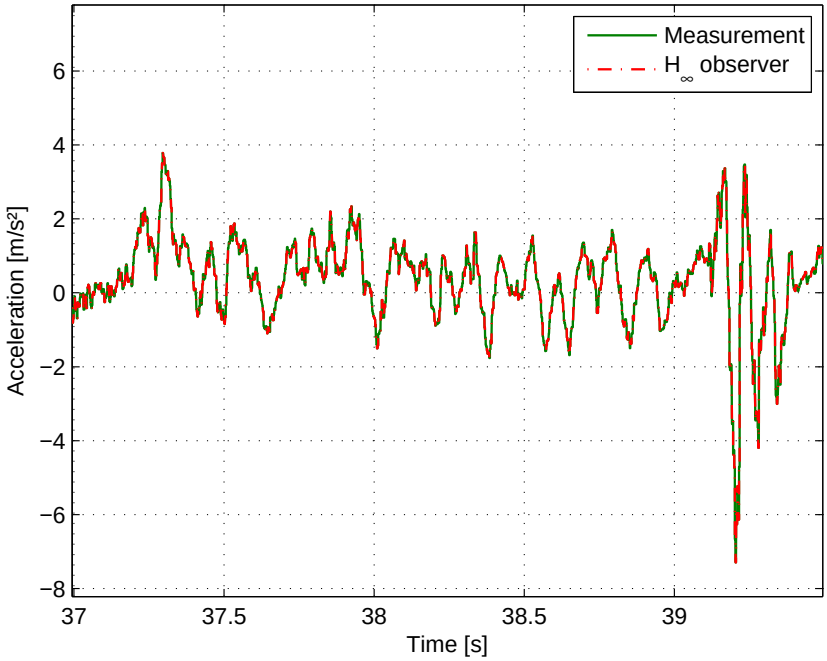

Figure 5.11: Sprung mass 1 vertical acceleration

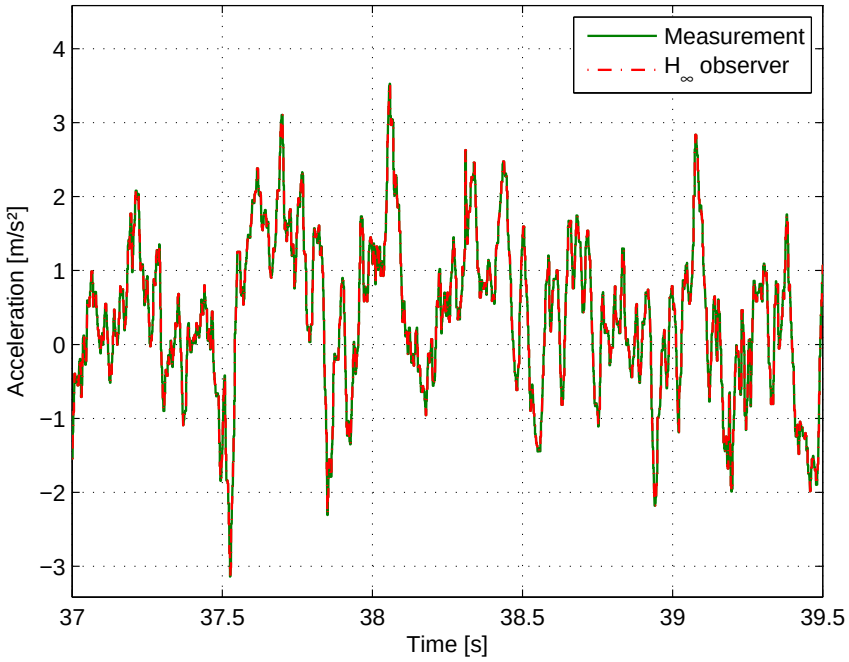

Figure 5.12: Sprung mass 4 vertical acceleration

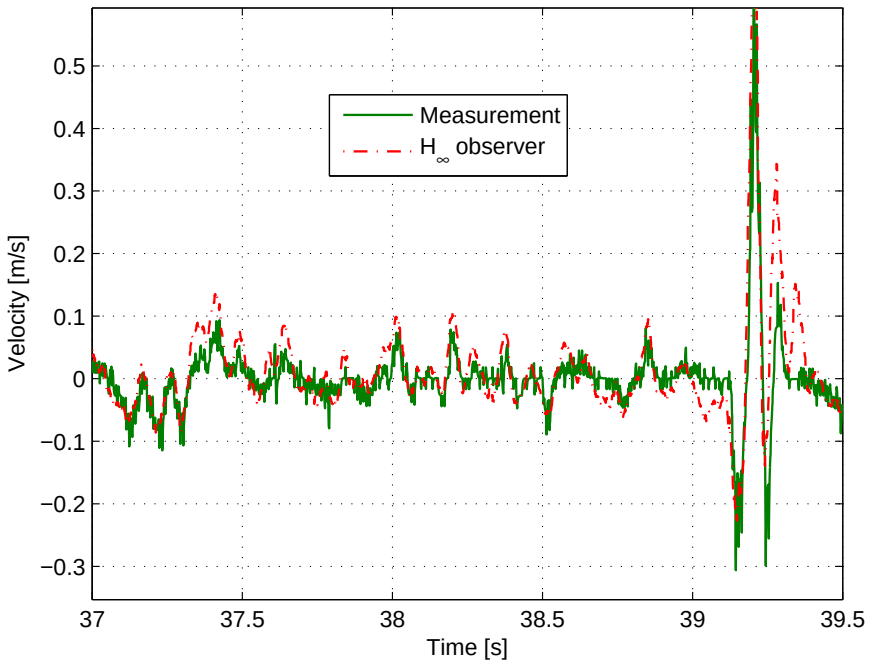

Figure 5.13: Deflection velocity 1

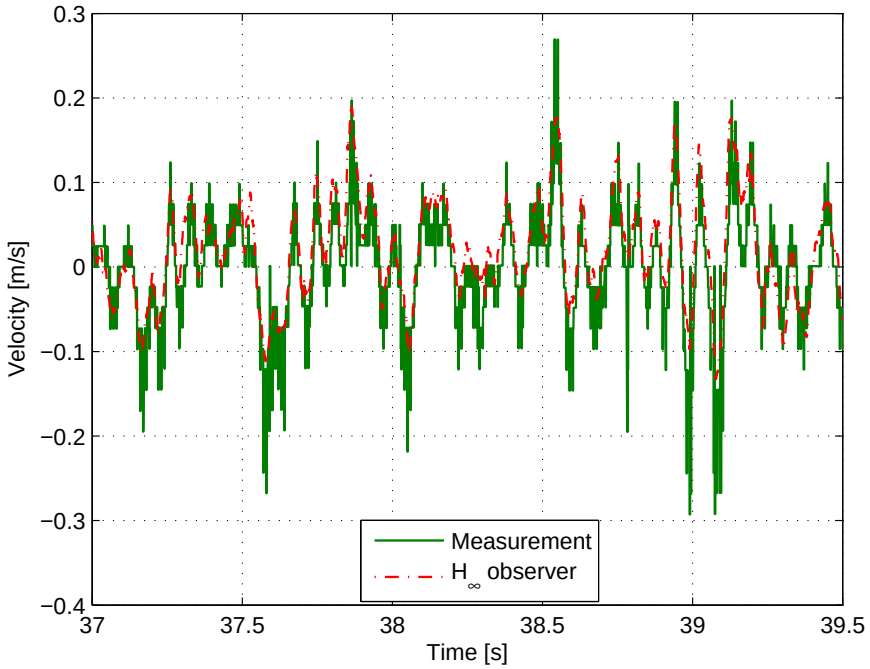

Figure 5.14: Deflection velocity 4

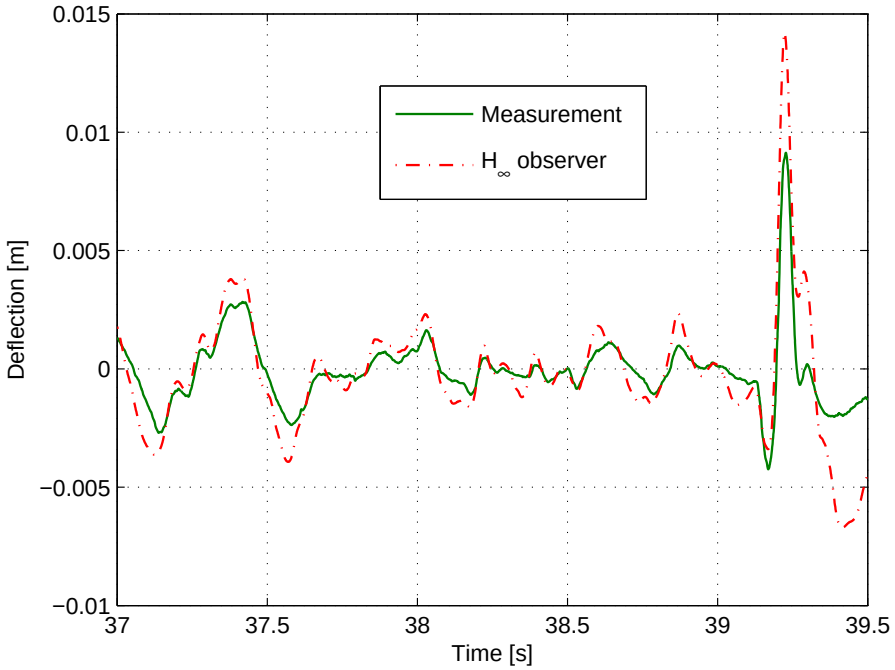

Figure 5.15: Deflection 1

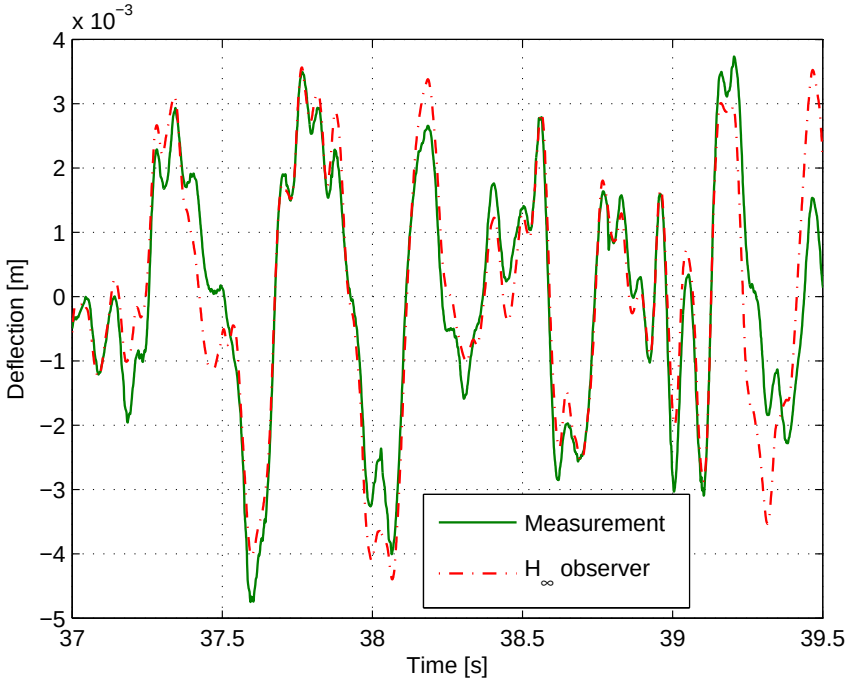

Figure 5.16: Deflection 4

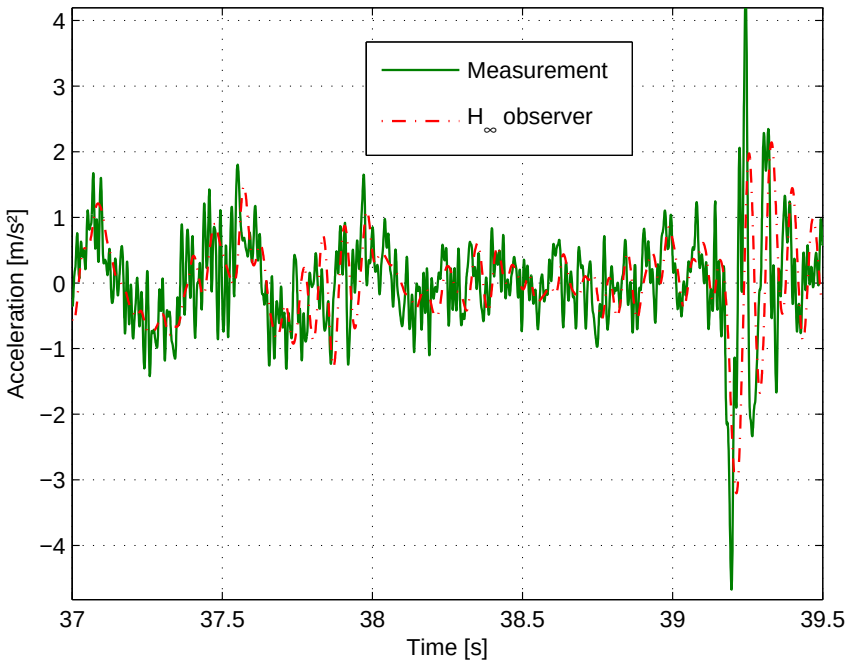

Figure 5.17: Sprung mass center of gravity vertical acceleration

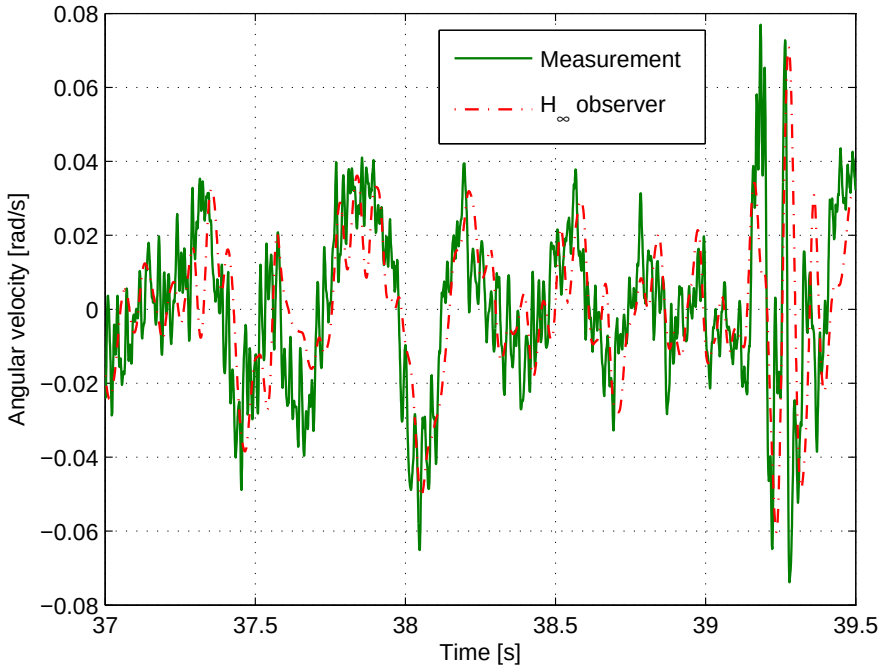

Figure 5.18: Pitch angular velocity

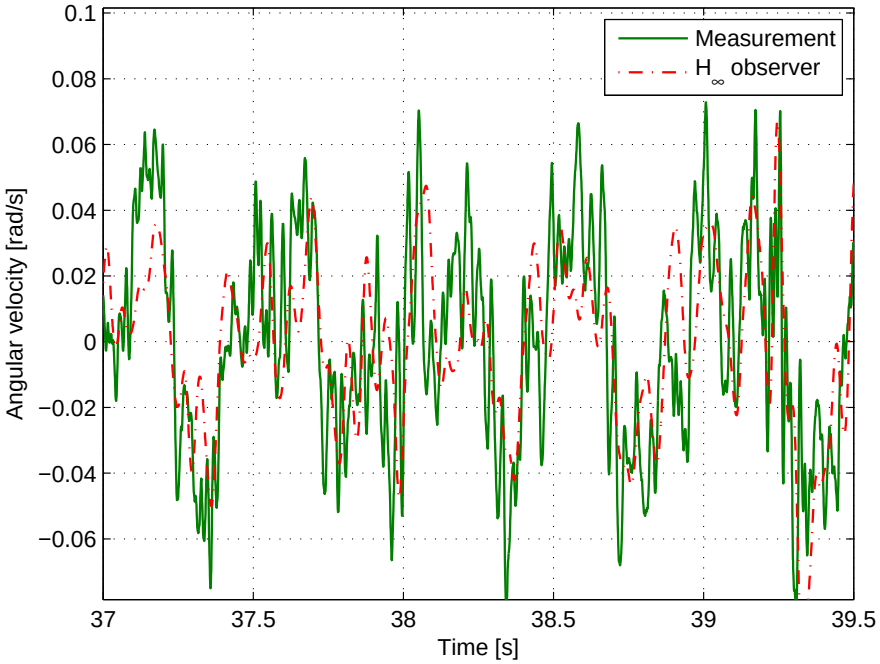

Figure 5.19: Roll angular velocity

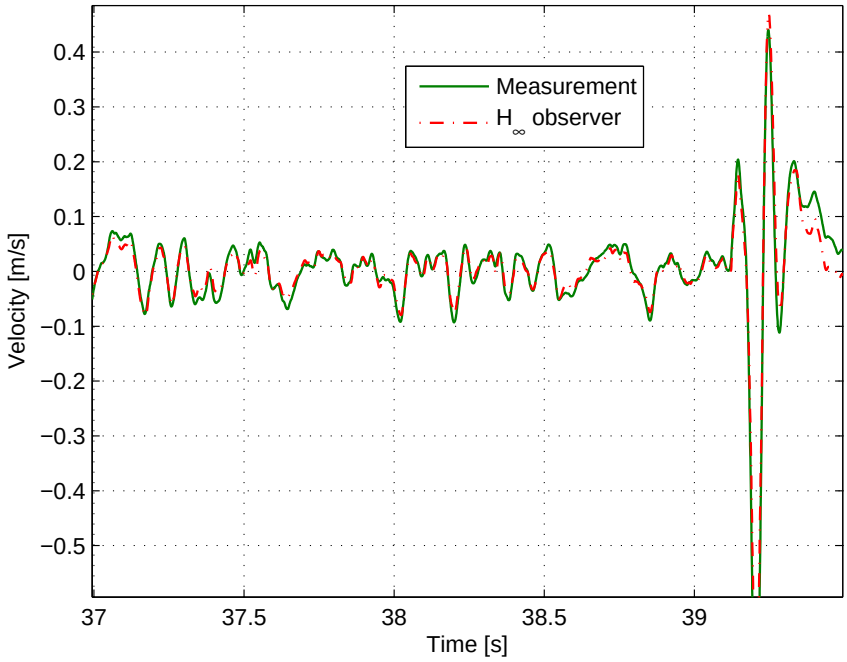

Figure 5.20: Unsprung mass 1 vertical velocity

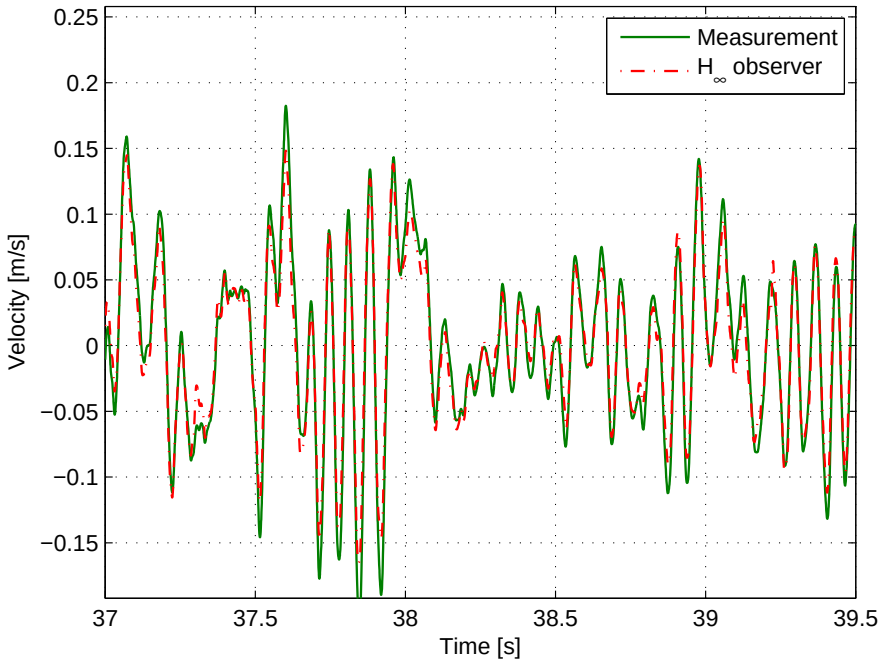

Figure 5.21: Unsprung mass 4 vertical velocity

accelerometers providing the sprung and unsprung mass vertical accelerations. The estimation is decoupled from the unknown road disturbance through an $\mathcal{H}_\infty$ minimization. The proposed synthesis method also includes a pole placement in LMI regions to avoid ill-adapted dynamics that may preclude the implementation and damage the estimation accuracy in the real embedded application. Therefore, the procedure presented in this chapter is a complete and practical observer design procedure for automotive suspension control applications. This observer has been implemented and embedded on a testing car. The experimental results emphasize the observer performance and robustness. Furthermore, the tuning of the observer is simple since only the model and the desired bandwidth of the observer have to be known.

Future works will first of all consist in designing a reduced-order observer. The observer could also be scheduled according to the damping rate c, even if this does not seem to be necessary for the considered application.

Chapter 6

Control strategy

In this chapter, a control strategy, based on the observer proposed in Chapter 5, including both a high-level vehicle controller and a local damper controller, is developed in Section 6.3 to improve the performance of the suspension in terms of comfort and road-holding, according to the criteria proposed in Section 6.2. Then some experimental results obtained with the local damper controller on a testing bench are presented in Section 6.4. Finally, some simulation results are given in the time and frequency domains and show the interest of the proposed semi-active suspension control strategy in Section 6.5. The chapter is concluded in Section 6.6.

Some of the results provided in this chapter has been presented in [Aubouet et al., 2009b, 2008].

6.1 Introduction

This section first provides a brief state of the art on on existing suspension control strategies. Then the objectives and the contribution of the chapter are described.

6.1.1 State of the art

Semi-active suspensions have been recently under study since they provide an interesting compromise between cost and performance compared to passive and active suspensions. Their industrial advantage is that classical passive damper technologies with constant damping characteristics can be transformed into semi-active dampers while adding an actuator to control the damping rate. This is economic and requires a lower amount of power compared to active suspensions. On the other hand, semi-active dampers are limited since they only can dissipate energy. Semi-active dampers indeed cannot provide

forces in the direction of the deflection elongation speed.

In the past few years, many active control laws were developed in both academic and industrial frameworks: Skyhook control [Karnopp, 1983, Sammier et al., 2003, Choia et al., 2000, Poussot-Vassal et al., 2006] improves comfort efficiently but does not suit to improve road-holding. The CRONE approach [Moreau et al., 2009, Moreau, 1995, Oustaloup and Mathieu, 1999, Oustaloup et al., 1996], consists in dealing with the open loop as a transmittance and shaping it thanks to some adjusting parameters. It can be used both to control active suspensions or optimize passive ones. $\mathcal{H}_\infty$ LTI (Linear Time Invariant) control [Gaspar et al., 2004, Rossi and Lucente, 2004, Sammier, 2001, Zin et al., 2006, 2008], or mixed $\mathcal{H}_\infty/\mathcal{H}_2$ LTI controllers [Abdellahi et al., 2000, Takahashi et al., 1998, Gaspar et al., 1998, Lu, 2004, Lu and DePoyster, 2002, Tuan et al., 2001] allow to minimize given signals on given frequency ranges and provide interesting results for suspension control applications. LPV (Linear Parameter Varying) controllers have also been addressed more recently to tackle nonlinearities, improve the robustness and adapt the vehicle behavior to given driving situations [Fialho and Balas, 2002, Zin et al., 2006, Zin, 2005, Poussot-Vassal, 2008, Savaresi et al., 2010]. However, most of the developed controllers assume active dampers, whereas active dampers are not mounted yet on mass-produced cars because of their cost and huge energy consumption. Therefore active control strategies are often saturated to control semi-active dampers, which is referred to as the "clipped" approach. Unfortunately, in this case, both performances and stability are not ensured and the results may be unpredictable (see [Canale et al., 2006]). That is why semi-active strategies have to be considered to make good use of semi-active technologies like SOBEN's one. This is currently a topic under study in both academical and industrial automotive researches.

More recently, semi-active dampers have been studied [Savaresi et al., 2010], and some control strategies have been proposed [Savaresi et al., 2005, Savaresi and Spelta, 2007] to improve comfort using switched two-state dampers, which is interesting from an industrial point of view since two-state actuators are less expensive, may consume less energy and also may have a smaller response-time than continuously adjustable actuators. However there are some limitations due to the abilities of the actuator, and these control strategies do not allow car manufacturers to tackle the compromise problem between comfort and road-holding, which is one of the main challenges to adapt the suspensions performances to the vehicle behavior intended by the customer. In [Poussot-Vassal et al., 2008, Do et al., 2010b], a semi-active control strategy has been developed using LPV techniques. Some parameters are used to adapt the performance objectives to the abilities of the damper, which ensures that the suspension's control signal remains semi-active. This method has been proposed to control a quarter-car model using an output-feedback control strategy. In [Giorgetti. et al., 2005, Canale et al., 2006], a semi-active model-predictive suspension control is proposed, but the synthesized controllers are difficult to implement since they switch between many controllers or require

on-line optimization algorithms. Furthermore, these controllers require full-state measurement and an accurate knowledge of the model. Unfortunately, these conditions are very difficult to fulfill in an industrial framework.

6.1.2 Objectives and contribution

In this section, the industrial and academic objectives of this thesis are described. As explained in the previous section, the following points have not been sufficiently developed in past studies:

1. semi-active control strategies, taking the achievable force range of the damper into account, already studied in [Poussot-Vassal, 2008],
2. control strategies for continuously variable and two-state dampers, taking the nonlinearities of the damper into account, already studied in [Do et al., 2010b, Spelta, 2008, Savaresi et al., 2010],
3. adjustable performances, according to given comfort and road-holding specifications,
4. control strategies adaptable to various sets of available sensors.

These problems prevent semi-active dampers from becoming standard and widespread since from an industrial point of view, such systems are difficult to install and repair, due to the number of sensors and cables. Furthermore the existing control strategies are not adapted to existing technologies, in terms of force range limitations, bandwidth and nonlinearities. Therefore such systems are both expensive and difficult to adjust and adapt to various types of vehicles and dampers. That is why many car manufacturers have built prototypes and never used them on mass-produced vehicles. The challenge for SOBEN is clearly to overcome these problems while developing a new easily adjustable and adaptable product combining improved performances and reduced cost.

The main contribution of this chapter, which resulted in a publication [Aubouet et al., 2009b], is a complete observer-based semi-active suspension control strategy for a full vertical car equipped with industrial semi-active dampers. The proposed architecture includes three main elements. The first one is a vehicle observer estimating the state variables of a vehicle model, presented in Chapter 5. The second one is a high-level $\mathcal{H}_\infty$/LPV static state-feedback vehicle controller that computes the four damper force references to optimize comfort and road-holding while dealing with the technological constraints. The third one is a local mixed $\mathcal{H}_\infty/\mathcal{H}_2$ LPV dynamic output-feedback controller, based on identified damper models and taking the nonlinearities of the damper into account.

The problems enumerated in the previous section have led to various methodological developments such as an observer design methodology, allowing the designer to build a vehicle observer adapted to the available sensors, to the bandwidth of the system and to the measurement noise level. A design methodology is also proposed for the vehicle controller, so that the expected performances can be simply and explicitly specified to meet the behavior intended by the customer.

The LPV-based method to ensure that the control strategy is semi-active is similar to the one described in [Poussot-Vassal et al., 2008], where a quarter-car was controlled using an output-feedback control strategy. In this chapter, this previous study is completed: the scheduling strategy is improved, the damper limitations are determined using identified models fitting the real damper. This leads to an easy-to-implement and adaptable control strategy. The performances of the vehicle can be simply specified by the designer using some adapted weighting functions, well-known in automotive industry since they correspond to existing industrial criteria for suspension control. The constraints on the actuator and the damper behavior are taken into account in the controller so that the on-line required damping rate remains semi-active through a simple scheduling strategy. Then the local $\mathcal{H}_\infty$/LPV damper force controller makes the damper provide the required damping force, ensuring robustness and performance. These damper controllers improve the robustness of the system, since for example, when the damper heats, its damping rate changes for a given control signal. The damping rate also changes because of the wearing effect of time. Furthermore mass-produced dampers have a certain disparity. All these disturbances are offset by the damper controller since the provided damping forces are controlled in real-time. As the vehicle controller is a simple static state-feedback controller, it can be scheduled by several parameters without increasing excessively the complexity of the controller to be implemented, which is one of the main interests of the observer-based control strategy developed in this chapter. Furthermore the proposed controllers take the non linearities of the system and the abilities of the damper into account. Indeed here the scheduling strategy, based on the real behavior of SOBEN damper, uses an identified damper model and allows the controller to decrease the control signal if this one is outside the achievable range. This method ensures an optimal use of the dampers in order to improve the performances of the vehicle, and can be easily adapted to all the damper technologies, even two-state adjustable dampers. Indeed a control strategy for this kind of dampers is finally proposed and tested, since this solution is very interesting from an industrial point of view.

6.2 Performance analysis and design objectives

This section presents some time and frequency-domain criteria allowing to study the behavior of the suspensions. These analysis tools can be used either to specify a given pas-

sive or semi-active suspension to be designed, or to find the optimal settings of an existing suspension, for instance. The proposed suspension performance analysis methodology has been applied to the SOBEN damper [Aubouet et al., 2008].

6.2.1 State of the art

Vehicle suspension performance evaluation is an important topic for automotive manufacturers since suspensions highly influence comfort and roadholding performances. As a result, suspensions have to be designed to meet the customer expectations, as far as possible.

Comfort can be defined as the ability of a given vehicle to isolate the passengers from the ground vibrations. But this is a subjective feeling, depending on the vehicle and on many other external parameters like noise, temperature, passenger health...

Roadholding can be defined as the ability of a given vehicle to minimize the wheel movements relative to the ground. Unlike comfort, it is not a subjective feeling, and it only results from the design and settings of the different vehicle components, like anti-roll bars, suspensions, tires, chassis...

The first step in suspension design is to define the type of vehicle and driver, and the expected vehicle behavior. Then the damper manufacturer can define the technical specifications and design the corresponding suspension. However, this step is the most complex since usual word-based specifications have to be turned into mathematical criteria. This section aims at providing some useful tools to deal with this problem.

Many works have already been published on vehicle performance evaluation, and some criteria and tests have been proposed in [Gillepsie, 1992, Wong, 2001, Miliken and Miliken, 1995] to evaluate both comfort and road-holding of ground vehicles. In this section, some frequency and time-domain criteria have been chosen to analyse the behavior of the vehicle by studying some representative variables of the vehicle dynamics. Some of these criteria have already been detailed in [Sammier et al., 2003, Aubouet et al., 2008] for the quarter-car performance evaluation and for full-car as well in [Poussot-Vassal, 2008, Poussot-Vassal et al., 2008, Zin, 2005]. It has to be noticed that these criteria are not unique. However they are used by car-manufacturers since they provide a rigorous analysis tool of the vehicle behavior.

6.2.2 Frequency-domain analysis

This section presents some analysis tools based on the frequency-response of some representative vehicle variables. Some simulation results are given and illustrate the interest

of these analysis tools.

Pseudo-Bode diagrams

In past studies, the comfort of the quarter-car has been analyzed through the relation $z_r \mapsto \ddot{z}_s$ at high frequencies and $z_r \mapsto z_s$ at low frequencies, whereas road-holding is studied using the relation $z_r \mapsto z_{us}$. The vehicle dynamical variables to be studied for vehicle performance analysis are given in [Gillepsie, 1992] for the quarter-car. These criteria are interesting for the full-car analysis too, but it is not sufficient. Indeed, the relations $M_x \mapsto \theta$ and $M_y \mapsto \phi$, from the disturbance moments to the angular positions have to be studied as well since they influence both comfort and road-holding. Indeed both roll and pitch movements are low frequency movements making the vehicle uncomfortable. Here the complete set of variables to be studied on specific frequency ranges for the full-car performance evaluation are recalled in Table 6.1.

Relation	**Frequency range**
$z_{r_i} \mapsto \ddot{z}_s$, $i \in [1,4]$	[4-20]Hz
$z_{r_i} \mapsto z_s$, $i \in [1,4]$	[0-5]Hz
$z_{r_i} \mapsto z_{us_i}$, $i \in [1,4]$	[0-20]Hz
$M_x \mapsto \theta$	[0-5]Hz
$M_y \mapsto \phi$	[0-5]Hz

Table 6.1: Performance analysis

The frequency responses of these input-output relations will be referred to as "Pseudo-Bode diagrams" in the next sections, which corresponds to the frequency response of a nonlinear system. Since the gain of such a system depends both on the frequency and on the magnitude, the pseudo-Bode diagram is the magnitude-dependent frequency response and can be seen as an extension of the well-known Bode diagram, to the nonlinear systems. These diagrams can be computed according to the following procedure, where ω denotes the pulsation of the input signal and a its amplitude:

- Send a sinusoidal input signal $w(t) = a\sin(\omega t)$ to the vehicle during N periods for $\omega = \omega_{min}$ to $\omega = \omega_{max}$), and $a = a_{min}$ to $a = a_{max}$),
- Measure and record the output signal for each pulsation and amplitude,
- Compute the discrete Fourier transform of the signal,
- Compute the magnitude for each pulsation and amplitude,
- Plot the magnitude over the pulsation and the amplitude.

Remark 6.2.1 (*Required number of periods*)

Several periods ($N > 10$ for example) are required in order to avoid transient dynamics.

Remark 6.2.2 (*Experimental pseudo-Bode diagrams*)

The pseudo-Bode diagrams can be computed both from simulated or measured variables. Indeed, a specific testing bench called "four-poster" bench, made up with four hydraulic jacks allowing to apply sinusoidal ground disturbances to each wheel of the vehicle under study can be used to analyze the frequency response of a real vehicle. Then the pseudo-Bode diagrams can be derived from the available measured variables and analyzed.

The frequencies of interest, given in Table 6.1, depend on the studied input-output relation. The amplitudes can be studied for example from 5 to 50mm. A quarter-car model of the form (4.4.1), made up with a physical nonlinear passive SOBEN damper model based on the equations (4.3.1-4.3.3) has been simulated for frequencies ranging from 0.5 to 20Hz, and input amplitude ranging from 5 to 40mm. Then the pseudo-Bode diagrams have been computed. They are presented in Figure 6.1.

The nonlinearities of the vehicle, due to the nonlinearities of the damper model appear clearly since the magnitude of each pseudo-Bode diagram highly depends on the input amplitude. The upper diagrams ($z_r \mapsto \ddot{z}_s$ and $z_r \mapsto z_s$) represent the comfort, whereas the lower ones ($z_r \mapsto \ddot{z}_{us}$ and $z_r \mapsto z_{def}$) represent the road-holding. According to the diagrams represented in Figure 6.1, the smaller the magnitudes, the higher the performances. Then some suspension specifications can be derived from these diagrams in order to design a new suspension or a suspension control strategy. These specifications can be expressed using appropriate templates for each diagram, corresponding to the expected vehicle behavior, as detailed later. The following numerical criteria can also be used for this purpose.

Power-spectral density

In order to simplify the analysis of these different pseudo-Bode diagrams on the interesting frequency ranges, the following frequency-based criterion will be used in Chapter 6 to compare various vehicles. This criterion is given by the following definition.

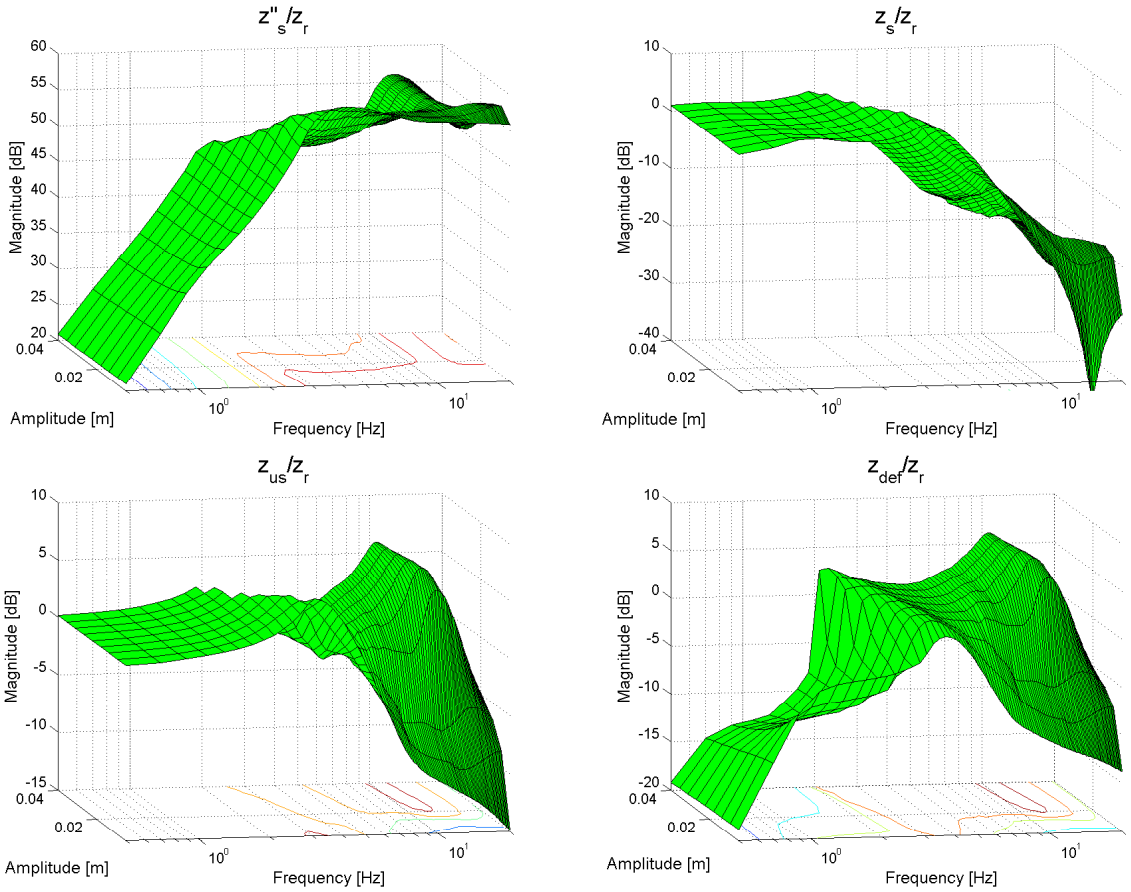

Figure 6.1: Pseudo-Bode diagrams: nonlinear quarter-car

Definition 6.2.1 (*Power Spectral Density criterion*)

The Power Spectral Density (PSD) corresponds to the integral of a given signal frequency response on given frequency and amplitude ranges, and is defined by

$$J\begin{cases} f_1 \to f_2 \\ a_1 \to a_2 \end{cases}(X(f)) = \sqrt{\int_{f_1}^{f_2}\int_{a_1}^{a_2} X^2(f,a)\cdot da \cdot df} \tag{6.2.1}$$

where f_1 and f_2 (resp. a_1, a_2) are the lower and higher frequency (resp. magnitude) bounds, respectively, and X is the magnitude.

This criterion will be used to analyze the behavior of vehicles equipped both with passive and semi-active dampers. The semi-active SOBEN damper will be referred to as a passive nominal damper if it is controlled by a mean constant control signal. The values of the criterion applied to the passive vehicle under study in this thesis, have been computed using simulations, for a vehicle model equipped with identified nominal passive damper models (4.3.4). The results are given in Table 6.2, where the criterion has been applied to the front left suspension (Suspension 1). This vehicle will be used as a reference to study the performances of various vehicles equipped with controlled suspensions in Chapter 6.

Relation	PSD value
$z_{r_1} \mapsto \ddot{z}_s$	334
$z_{r_1} \mapsto z_s$	28.9
$z_{r_1} \mapsto z_{us_1}$	3.21
$M_x \mapsto \theta$	12.8
$M_y \mapsto \phi$	21.9

Table 6.2: Passive vehicle: performance criteria

6.2.3 Time-domain analysis

Time-domain criteria have also been developed in past studies, and are sometimes used to analyze the behavior of a given vehicle. These criteria can be computed from various measured variables, recorded during various experiments such as a bad road for comfort or road-holding analysis, a change of direction for roll behavior analysis, or an acceleration or braking test for pitch behavior analysis. Here, some of them are briefly recalled, but the reader should refer to [Gillepsie, 1992, Wong, 2001, Miliken and Miliken, 1995], which are the reference works on vehicle dynamics.

RMS variables analysis

The performance of the vehicle can also be analyzed through the Root Mean Square criterion applied to given variables.

Definition 6.2.2 (*Root Mean Square criterion*)

The Root Mean Square criterion (RMS) is defined by

$$RMS_{0\to n}(x(t)) = \int_0^T \sqrt{x^2(t))} \cdot dt \tag{6.2.2}$$

Criteria	
RMS($\ddot{z}_{s_i}$), $i \in [1,4]$	High-frequency comfort
RMS(z_{s_i}), $i \in [1,4]$	Low-frequency comfort
RMS(z_{def_i}), $i \in [1,4]$	Road-holding
RMS(θ)	Road-holding, maneuverability
RMS(ϕ)	Road-holding, brake/acceleration ability

Table 6.3: RMS criteria

These criteria can easily be simulated using a vertical full-car model of the form (4.4.3). They also can be computed from measured variables if the sensors are available. Unlike the PSD criterion, no specific testing bench is required to run the corresponding experiments. Indeed, experimental results obtained while driving on any road can be used to analyze the performances, even if using a specific four-poster testing bench is better since the tests are more repeatable. However these criteria have a major disadvantage: comparing two vehicles, or two settings is possible if and only if the vehicle follows exactly the same road at the same speed. Therefore the comparison is very difficult. Furthermore, several road types should be tested since a single road is not representative of every possible ground disturbance. For example a freeway, a country road and a track should be tested.

Roll and pitch gradients analysis

Another well-known method to analyze the roll and pitch movements of a vehicle, consists in plotting the roll and pitch angles respectively over the lateral and longitudinal acceleration of the vehicle, during a given test. Since all the required variables can be measured quite easily, this tool has become quite common to study the roll and pitch movements. However the same experiment has also to be done in order to compare two vehicles, which is very difficult. Then from these results, the behavior can be analyzed:

roll overshoot during a bend, mean slope of the graph (gradient)... Some typical roll gradients [Miliken and Miliken, 1995] are given in Table 6.4.

Behavior	**Gradient** [°/g]
Very soft (Economy and basic family cars)	8.5
Soft	7.5
Semi-soft	7
Semi-firm	6
Firm	5
Very firm	4.2
Extremely firm	3
Hard (Racing cars only)	1.5

Table 6.4: Typical roll gradients

Measured variables spectrum analysis

The Fourier transform of some measured or simulated variables given in Table 6.1 can also be computed at given frequencies. For example, the natural frequencies of the wheel and of the chassis are interesting frequencies representing respectively the road-holding and the comfort. They can be analytically computed from the masses and stiffnesses of the vehicle under study. Then the amplitude of the spectrum at these particular frequencies can be used as a performance criterion. However the same experiment is also required to compare two vehicles, and furthermore, the amplitudes of the spectrum depend on the measurement noise. In particular, the natural frequency of the wheel which is in general equal to 11 or 12Hz, is corrupted by the noise resulting from the engine vibrations. Therefore these criteria are quite difficult to use in practice.

6.2.4 Conclusion

This section provides various tools to study the performances of the suspensions, both in the time and frequency domains. The method used to compute the Pseudo-bode diagrams allows damper manufacturers to study the behavior of the suspensions on the whole frequency and amplitude ranges, providing interesting informations on both comfort and road-holding that can be used to compare various suspensions. Furthermore these tests can be either simulated or measured, if a so-called four-poster testing bench is available. Time-domain criteria have also been presented. They provide interesting results too, but they describe the behavior of the suspensions only in specific cases which may not be representative. Furthermore, since the interest is to compare various

vehicles, the same experiment has to be run several times, which is not possible without a four-poster testing bench. Therefore the results may often be not representative.

6.3 Design of the control strategy

In this section, the full vertical car model presented in Section 4.4 is used to design a new semi-active control strategy improving both comfort and road-holding while taking the real damper behavior into account. Furthermore the damper model developed in Section 4.3.3 is used to design a local damper controller allowing the damper to provide the desired force reference and ensuring robustness.

6.3.1 Control strategy

The overall control architecture is presented in Figure 6.2. $V(s)$ represents the controlled vehicle model and includes both the model of the full-car given by (4.4.3) and the nonlinear dynamical identified damper model given by (4.3.9). This model is disturbed both by the ground irregularities $z_r \in \mathbb{R}^4$ under each wheel and by the moments M_x and M_y due to the load transfers. The four semi-active dampers can be controlled through the control signal $u_d \in \mathbb{R}^{n_u}$, $n_u = 4$. $O(s)$ is the full-order observer proposed in Chapter 5. This observer estimates the state variables of the full vehicle. The LPV static state-feedback vehicle controller K_v receives the estimated state variables $\hat{x}$ as an input and computes the damping forces u to be added to the nominal damping forces $c_0 z_{def}$ in order to improve the vehicle performances. This controller is scheduled by the parameter ρ_v that constraints the control signal or not, in such a way that the required forces F^* remain semi-active and adapted to each damper ability. The controllers $K_d(s)$ compute the four damper control signals u_{d_i} that allow each damper to provide the required damping forces F^*. These controllers need the real damping forces F, computed from some measurements M through a calculation procedure P that is part of confidential results. No detail can be given on this topic, but the real damper forces are assumed to be measured.

The vehicle to be controlled is given by (4.4.3) and can be rewritten as a state-space model (6.3.1).

$$\begin{cases} \dot{x} = A \cdot x + B_1 \cdot w + B_2 \cdot u \\ y = C \cdot x + D_w \cdot w + D_u u \end{cases} \tag{6.3.1}$$

where $A \in \mathbb{R}^{n \times n}$, $B_1 \in \mathbb{R}^{n \times d}$, $B_2 \in \mathbb{R}^{n \times n_u}$, $C \in \mathbb{R}^{m \times n}$, $D_u \in \mathbb{R}^{m \times n_u}$ and $D_w \in \mathbb{R}^{m \times d}$. The scalar n is the number of state variables, d the number of disturbances, n_u is the

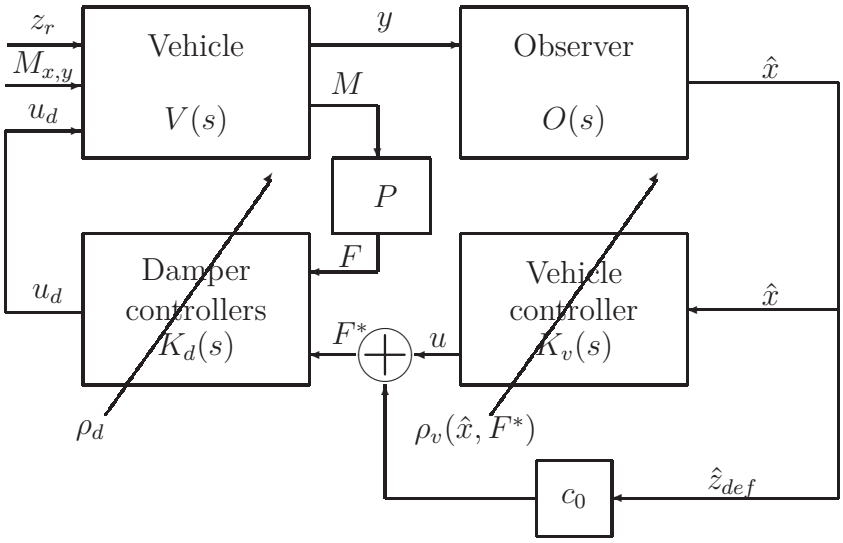

Figure 6.2: Control architecture

number of control signals and m the number of measured variables. The state vector x, the disturbance inputs w and the measured variables y, already described in Table 4.2, are given by (6.3.2). It has to be noticed that the vertical force disturbance F_z has not been taken into account in the synthesis since its influence on the vehicle behavior can be neglected compared to the influence of ground disturbances and load transfers moments.

$$\begin{cases} x &= \left(\dot{z}_s, z_s, \dot{z}_{us_1}, z_{us_1}, \dot{z}_{us_2}, z_{us_2}, \dot{z}_{us_3}, z_{us_3}, \dot{z}_{us_4}, z_{us_4}, \dot{\theta}, \theta, \dot{\phi}, \phi\right) \\ w &= (z_{r_1}, z_{r_2}, z_{r_3}, z_{r_4}, M_x, M_y) \\ y &= (\ddot{z}_{s_1}, \ddot{z}_{s_2}, \ddot{z}_{s_3}, \ddot{z}_{us_1}, \ddot{z}_{us_2}, \ddot{z}_{us_3}, \ddot{z}_{us_4}) \end{cases} \tag{6.3.2}$$

6.3.2 $\mathcal{H}_\infty$/LPV vehicle controller design

The $\mathcal{H}_\infty$ approach is interesting to handle frequency specifications. The objectives in terms of comfort and road-holding, detailed in Section 6.2, are given by some frequency-domain specifications. Therefore the proposed vehicle controller is designed in an $\mathcal{H}_\infty$ framework. LPV techniques can also be used to schedule the controller according to some measured varying parameters. This has been used in previous papers to adapt the performances specifications and to improve the robustness of the controlled system in [Zin, 2005, Fialho and Balas, 2002, Poussot-Vassal et al., 2008].

Problem statement and performance specifications

The solution proposed here aims at improving the performance criteria described in Section 6.2, using an $\mathcal{H}_\infty$/LPV controller. This work completes the preliminary results of Poussot-Vassal et al. [2008] since here a semi-active control strategy for the whole vehicle is proposed. Furthermore the proposed control strategy includes not only a dissipativity constraint, but the real damper abilities as well. The synthesized controller can also be easily implemented since it is a LPV static state-feedback controller. Indeed implementing an LPV output-feedback according to the method described in [Poussot-Vassal et al., 2008], but for the full-car control using one scheduling parameter for each suspension would imply the implementation of 16 controllers. Therefore the whole vehicle controller would have at least 320 states to be computed in real-time, which requires a important computation capacity.

The controller has been synthesized using the linear full-car model (6.3.1). The scheduling parameters are computed according to the difference between the real damping forces, computed from given confidential measurements M (see Figure 6.2) and the forces the damper can actually provide, using the identified damper models (4.3.4). This solution allows the state-feedback controller K_v presented in Figure 6.2, to compute realistic and semi-active required forces that each damper is able to provide, using an identified damper model.

The control signal amplitude is adapted on-line to each damper abilities. The required force received by each damper controller $K_{d_i}(s)$ as an input is $F_i^* = u_i + c_{0_i} \cdot \dot{z}_{def_i}$, where c_{0_i} can be seen as the nominal damping rate of the damper, and u_i as the added energy to achieve the specified performances, computed by the $\mathcal{H}_\infty$/LPV force controller. The generalized plant used for the synthesis, including the full-car model, the vehicle controller and the weighting filters is represented in Figure 6.3.

It has to be noticed that the measured variables are the state variables x of the full-car model, since a static state-feedback controller is to be synthesized in this section. Therefore a full-state measurement is assumed in the synthesis of the vehicle controller. Furthermore the weighting functions on the control signal depend on the scheduling parameter ρ_v. This scheduling strategy will be detailed later. The weighting filters are given in Table 6.5 and allow the generalized system to include the performance specifications detailed in Section 6.2. The filter W_{z_r} allow the controller to take the ground disturbance into account in the frequency range $[0 - 20]$Hz only, since higher frequencies are filtered respectively by tires and silent-blocks. The parameter dependent

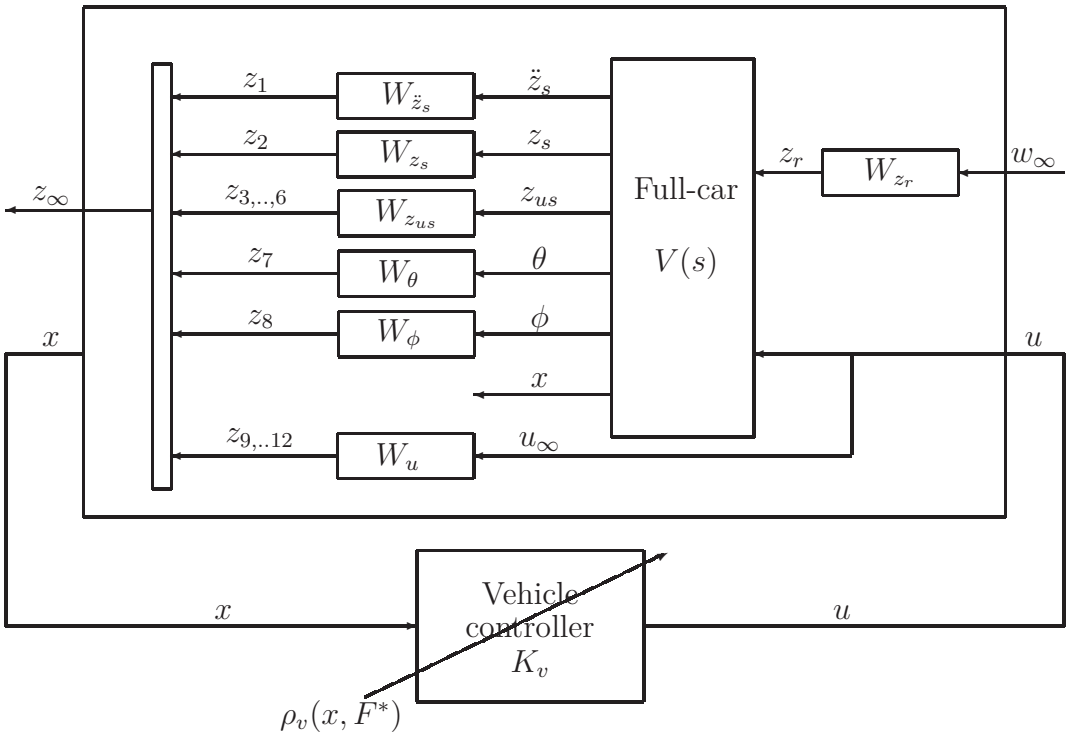

Figure 6.3: Generalized plant and weighting functions for vehicle controller design

generalized system used for the vehicle controller synthesis is given by (6.3.3).

$$\begin{pmatrix} \dot{x} \\ \dot{x}_f \\ z_\infty \end{pmatrix} = \begin{pmatrix} A & \mathcal{O} & B_1 & B_2 \\ B_f & A_f & B_{f1} & B_{f2} \\ D_f & C_f & D_{f1} & D_{f2}(\rho_v) \end{pmatrix} \begin{pmatrix} x \\ x_f \\ w_\infty \\ u \end{pmatrix} \tag{6.3.3}$$

where $w_\infty = w = (z_r, M_x, M_y) \in \mathbb{R}^{d,1}$, $z_r = (z_r)_{i=1,4}$ represents the ground disturbances and the load transfer moments M_x and M_y, $u \in \mathbb{R}^{n_u,1}$ is the control signal, corresponding to the forces to be added to the nominal damping forces. The state vector (x, x_f) includes both the state variables of the full-car (6.3.1) and the state variables of the weighting functions, given in Table 6.5, defined by their matrices A_f, B_f, B_{f1}, B_{f2} C_f, D_f, D_{f1}, $D_{f2}(\rho_v)$ and representing the performance specifications. The outputs $z_\infty \in \mathbb{R}^{n_z,1}$ are the weighted performance outputs to be minimized, and $\rho_v = [\rho_{v_1}, \rho_{v_2}, \rho_{v_3}, \rho_{v_4}]$ are the varying parameters used to schedule the controller.

These weighting functions will be taken into account in the controller synthesis using the generalized system (6.3.3) to improve the performances of the vehicle.

System	Filter (Frequency unit: Hz)	
$\ddot{z}_s \mapsto z_1$	$W_{\ddot{z}_s} = G_{\ddot{z}_s} \frac{s}{s+2\pi f_{\ddot{z}_s}}$	$f_{\ddot{z}_s} = 4$ $G_{\ddot{z}_s} = 0.01$
$z_s \mapsto z_2$	$W_{z_s} = G_{z_s} \frac{2\pi f_{z_s}}{s+2\pi f_{z_s}}$	$f_{z_s} = 5$ $G_{z_s} = 2$
$\theta \mapsto z_7$	$W_\theta = G_\theta \frac{2\pi f_\theta}{s+2\pi f_\theta}$	$f_\theta = 5$ $G_\theta = 2$
$\phi \mapsto z_8$	$W_\phi = G_\phi \frac{2\pi f_\phi}{s+2\pi f_\phi}$	$f_\theta = 5$ $G_\theta = 2$
$z_{us_i} \mapsto z_j$ $i \in [1,4]$, $j \in [3,6]$	$W_{z_{us}} = G_{z_{us}} \frac{2\pi f_{z_{us}}}{s+2\pi f_{z_{us}}}$	$f_{z_{us}} = 20$ $G_{z_{us}} = 1$
$w_\infty \mapsto z_{r_i}$ $i \in [1,4]$	$W_{z_r}^{-1} = G_{z_r} \frac{2\pi f_{z_r}}{s+2\pi f_{z_r}}$	$f_{z_{r_i}} = 20$ $G_{z_{r_i}} = 1$
$u \mapsto z_j$ $i \in [1,4]$, $j \in [9,12]$	$W_{u_i}(\rho_{v_i}) = \rho_{v_i}$	

Table 6.5: Vehicle controller weighting filters

Scheduling strategy

The method proposed in the previous work of Poussot-Vassal et al. [2008] for a quarter-car in order to fulfill the dissipativity constraint, aims at increasing or decreasing the gain of the weighting filters on the damper control signals, according to a given scheduling strategy. Indeed, if the required force computed by the controller is active, a scheduling parameter allows the controller to enhance or not the performance specifications, so that the required force remains dissipative. This method has been used to schedule the designed static state-feedback vehicle controller. Furthermore in [Poussot-Vassal et al., 2008], the actuator constraints are only two extremal linear damping rates whereas here some identified models are used to compute the scheduling parameters according to the real damper force range. The parameters ρ_v allow the controller to enhance or not the gain of the dampers, so that the required damping forces F^* remain semi-active. The scheduling parameters ρ_v are computed according to the difference between the required and achievable forces, where the required forces are the forces computed by the vehicle controller K_v and the achievable forces are given by the identified models. The four dampers indeed have been identified using experimental results obtained with the testing bench presented in Figure 4.4. Each damper has been identified for the minimal and maximal control signal as described in Experiment 1, with model (4.3.4). Therefore for each damper, two static models F_1^i and F_2^i are obtained, as given in (6.3.5). Then the minimal and maximal forces F_{min}^i and F_{max}^i are computed on-line using (6.3.6), from

the deflections and deflection velocities. It has to be noticed that due to the hysteresis of the dampers, the minimal (maximal respectively) force is not always obtained for the minimal (maximal respectively) control signal. Then the required force F_i^*, given by the vehicle controller K_v for each damper, is saturated between F_{min}^i and F_{max}^i. Therefore this saturated required force is an achievable force reference. Then, the four parameters ρ_{v_i} are computed with (6.3.8):

$$\rho_{v_i} = \begin{cases} 10^{-3} & \text{if} \quad F_{rea} = F^* \\ 10 & \text{if} \quad \mid F_{rea} - F^* \mid > \epsilon_{max} \end{cases} \tag{6.3.4}$$

If $\rho_{v_i} = 10^{-3}$, the gain of weighting function W_{u_i} is low, and thereafter the damping force u_i to be added to the nominal one is not constrained. If $\rho_{v_i} = 10$, the damping force u_i is constrained to be very small. This method allows the controller to be able to decrease the required force u_i of each damper independently as soon as one of the them forces is not achievable. The equations to compute the scheduling parameter ρ_{v_i} for the damper i are given by (6.3.5-6.3.8).

$$\begin{cases} F_1^i &= (A_1^i u_{d_{min}} + A_2^i)\tanh(A_3^i v^i + A_4^i x^i) + A_5^i v^i + A_6^i x^i + A_7^i \\ F_2^i &= (A_1^i u_{d_{max}} + A_2^i)\tanh(A_3^i v^i + A_4^i x^i) + A_5^i v^i + A_6^i x^i + A_7^i \end{cases} \tag{6.3.5}$$

where $u_{d_{min}}$ and $u_{d_{max}}$ denote respectively the minimal and maximal control signals of the dampers. A_j^i, $j = 1, .., 7$, are the identified parameters of the damper i, given in Table 4.7.

$$\begin{cases} F_{min}^i = \min(F_1^i, F_2^i) \\ F_{max}^i = \max(F_1^i, F_2^i) \end{cases} \tag{6.3.6}$$

$$F_{rea}^i = \min(\max(F_i^*, F_{min}^i), F_{max}^i) \tag{6.3.7}$$

$$\rho_{v_i} = a \cdot \frac{\min(\epsilon_{max}, \mid F_{rea} - F_i^* \mid)}{\epsilon_{max}} + b \tag{6.3.8}$$

where ϵ_{max} is a given maximal force error, F_{rea} is the projection of the required force on the achievable force range, and $a = \rho_{max} - \rho_{min} = 10^1 - 10^{-3}$, $b = \rho_{min} = 10^1$ are constant parameters so that $\rho_{v_i} \in [1, 100]$.

The achievable force range of each damper can be represented as shown in Figure 6.4. Zone 1 is active and unachievable with SOBEN damper, Zone 2 is semi-active but unachievable and Zone 3 is the achievable damper force range. The scheduling strategy described before allows the vehicle controller to compute required forces in Zone 3.

The controller $K_v(\rho)$ to be synthesized is a LPV static state-feedback. Therefore with $u = K_v(\rho) \cdot x$, where x are the state variables of the full-car given by (6.3.2), the closed-loop system can be expressed as in (6.3.9).

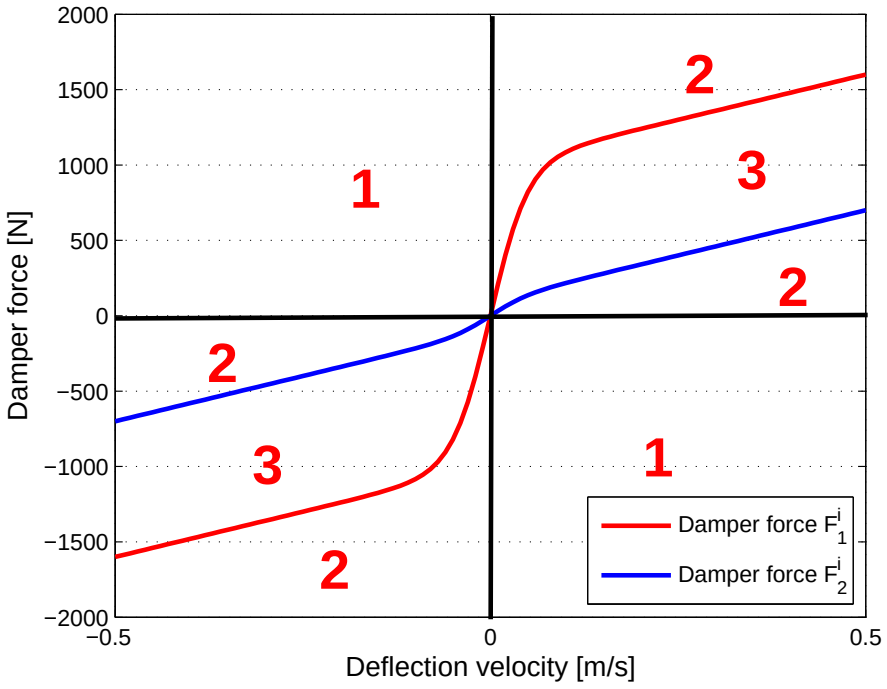

Figure 6.4: Identified SOBEN damper force range

$$\begin{pmatrix} \dot{x} \\ \dot{x}_f \\ z_\infty \end{pmatrix} = \begin{pmatrix} A + B_2 K_v & \mathcal{O} & B_f \\ B_f + B_{f2} K_v & A_f & B_{f1} \\ D_f + D_{f2} K_v & C_f & D_{f1} \end{pmatrix} \begin{pmatrix} x \\ x_f \\ w_\infty \end{pmatrix} \tag{6.3.9}$$

where $D_{f2} = D_{f2}(\rho_v)$ and $K_v = K_v(\rho_v)$ are respectively the matrix of the scheduled control signal weighting function and the scheduled vehicle controller.

Controller design solution

Here the objective consists in solving the $\mathcal{H}_\infty$ problem by minimizing, or bounding to a given level γ_∞, the system gain between $\|z_r\|_2$ and $\|z_\infty\|_2$ ($\mathcal{L}_2$ to $\mathcal{L}_2$ induced norm). The solution of this problem is given in Proposition 6.3.1.

Proposition 6.3.1

Consider the closed-loop system (6.3.9) and a positive scalar γ_∞. $K_v(\rho_v)$ is a static state-feedback $\mathcal{H}_\infty$/LPV controller ensuring that the $\mathcal{H}_\infty$-norm of the closed-loop system (6.3.9) does not exceed γ_∞ if there exist $X = X^T \succ 0$ and $U(\rho_v)$ satisfying

(6.3.10-6.3.12) at each vertex of the polytope defined by the extremal parameters: $\rho_v = [\rho_{v_1}, \rho_{v_2}, \rho_{v_3}, \rho_{v_4}]$, $\rho_{v_i} = \rho_{min}$ *or* ρ_{max}.

$$\begin{pmatrix} Q_1 + Q_1^T & B_{1a} & Q_2^T(\rho_v) \\ * & -\mathcal{I} & D_{f1}^T \\ * & * & -\gamma_\infty^2 \mathcal{I} \end{pmatrix} \prec 0 \tag{6.3.10}$$

$$\begin{cases} Q1 = \begin{pmatrix} A\mathbf{X_1} + B_2\mathbf{U}(\rho_\mathbf{v}) & \mathcal{O} \\ B_f\mathbf{X_1} + B_{f2}\mathbf{U}(\rho_\mathbf{v}) & A_f\mathbf{X_2} \end{pmatrix} \\ Q2(\rho_v) = \begin{pmatrix} D_f\mathbf{X_1} + D_{f2}(\rho_v)\mathbf{U}(\rho_\mathbf{v}) & C_f\mathbf{X_2} \end{pmatrix} \end{cases} \tag{6.3.11}$$

$$X = \begin{pmatrix} \mathbf{X_1} & \mathcal{O} \\ \mathcal{O} & \mathbf{X_2} \end{pmatrix} \quad B_{1a} = \begin{pmatrix} B_1 \\ B_{f1} \end{pmatrix} \tag{6.3.12}$$

where the decision variables are $\mathbf{X_1}$, $\mathbf{X_2}$, $\mathbf{U}(\rho_\mathbf{v})$, $*$ *and* $\mathcal{I}$ *denote respectively the symmetric element and the identity matrix of appropriate dimension.*

The control $K(\rho_v)$ *is deduced from* $K(\rho_v) = U(\rho_v)X_1^{-1}$.

Proof 6.3.1

The objective of the $\mathcal{H}_\infty$ *problem is to minimize the* $\mathcal{H}_\infty$*-norm of system (6.3.9) (input-output relation between the inputs* w_∞ *and the outputs* z_∞*), or bound it to a certain level* γ_∞*, while ensuring the internal stability (see [Boyd et al., 1994]).*

The $\mathcal{H}_\infty$ *static state-feedback synthesis problem is addressed in [Scherer et al., 1997, Scherer and Weiland, 1999], and the solution for a given system (6.3.13) is given by the matrix inequality (6.3.14) where* γ *has to be minimized.*

$$\begin{pmatrix} \dot{x} \\ z_\infty \end{pmatrix} = \begin{pmatrix} A & B_1 & B_2 \\ C_1 & D_{11} & D_{12} \end{pmatrix} \begin{pmatrix} x \\ w \\ u \end{pmatrix} \tag{6.3.13}$$

where w *is an exogenous input,* $u = K_v x$ *is the control signal given by the static state-feedback controller* K_v *to be designed.*

$$\begin{pmatrix} M_1 + M_1^T & B_1 & M_2^T \\ * & -\mathcal{I} & D_{11}^T \\ * & * & -\gamma_\infty^2 \mathcal{I} \end{pmatrix} \prec 0 \tag{6.3.14}$$

where $M_1 = (A^T + B_2 K_v)X$ *and* $M_2 = X(C_1 + D12K_v)$.

In the vehicle controller synthesis, some weighting filters have been introduced, and the system (6.3.3) has to be used in the controller synthesis. The decision variable X *has been chosen of the form (6.3.15). Therefore, the previous result (6.3.14) becomes (6.3.16).*

$$X = \begin{pmatrix} \mathbf{X_1} & \mathcal{O} \\ \mathcal{O} & \mathbf{X_2} \end{pmatrix} \quad B_{1a} = \begin{pmatrix} B_1 \\ B_{f1} \end{pmatrix} \tag{6.3.15}$$

$$\begin{pmatrix} Q_1 + Q_1^T & B_{1a} & Q_2^T \\ * & -\mathcal{I} & D_{f1}^T \\ * & * & -\gamma_\infty^2 \mathcal{I} \end{pmatrix} \prec 0 \tag{6.3.16}$$

With Q_1 and Q_2 given by

$$\begin{cases} Q1 = \begin{pmatrix} (A + B_2 K_v)\mathbf{X_1} & \mathcal{O}_{n_z} \\ (B_f + B_{f2} K_v)\mathbf{X_1} & A_f \mathbf{X_2} \end{pmatrix} \\ Q2 = \begin{pmatrix} (D_f + D_{f2} K_v)\mathbf{X_1} & C_f \mathbf{X_2} \end{pmatrix} \end{cases}$$

The obtained inequality (6.3.16) is a bilinear matrix inequality (BMI) containing some quadratic terms. The change of variable $U = KX_1$ can be introduced to transform the BMI into a solvable LMI, which leads to (6.3.10).

It is worth noting that this inequality contains a parameter ρ_v. Therefore an infinite set of LMI has to be solved. The polytopic approach detailed in [Apkarian et al., 1995] consists in finding the unknown matrices X, $U(\rho_v)$ and a scalar γ_∞ that solve a finite set of LMI. This ensures the quadratic stability of the closed-loop system using a single Lyapunov function trough the evaluation of the previous LMI (6.3.10) at each vertex of the polytope only. This polytope is defined by the extremal varying parameters. Finally, solving (6.3.10) provides an optimal solution ensuring that the $\mathcal{H}_\infty$-norm of system (6.3.13) does not exceed γ_∞. Then the LPV controller is a convex combination of the controllers computed at each vertex, as expressed in (6.3.17). In our case, there are four parameters: $\rho_v = [\rho_{v_1}, \rho_{v_2}, \rho_{v_3}, \rho_{v_4}]$, where $\rho_{v_i} \in [\rho_{min}, \rho_{max}]$, $i = 1, .., 4$.

$$K(\rho_v) = \sum_{k=1}^{2^p} \alpha_k(\rho_v) \cdot K_{v_k} \tag{6.3.17}$$

where

$$\alpha_k(\rho_v) = \frac{\prod_{j=1}^{p} \mid \rho_v(j) - \Theta_k \mid}{\prod_{j=1}^{p} \mid \rho_v^{max} - \rho_v^{min} \mid} \tag{6.3.18}$$

and

$$\sum_{k=1}^{2^p} \alpha_k(\rho_v) = 1 \tag{6.3.19}$$

where p is the number of varying parameters, $k = 2^p$ the number of vertices of the polytope, ρ_{max}, ρ_{min} are respectively the upper and lower bounds of the four parameters, and Θ_k is the kth vertex of the polytope.

This controller has not been implemented on the vehicle yet. However some simulation results are presented in Section 6.5 and the performances of the vehicle are studied using the criteria given in Section 6.2.

6.3.3 Damper controller design

In this section, the objective is to design a damper controller $K_d(s)$, made of four independent damper controllers $K_{d_i}(s)$, $i = 1, ..., 4$ and making each damper provide the required force computed by the vehicle controller. Each controller $K_{d_i}(s)$ is an $\mathcal{H}_\infty$/LPV dynamic output-feedback, based on the damper model (4.3.9).

Problem statement

The static part of this model, given by (4.3.4), can be decomposed as in (6.3.20),

$$\begin{aligned} F_i &= A_1 \tanh(A_3 v_i + A_4 x_i) \cdot u_{d_i} + A_2 \tanh(A_3 v_i + A_4 x_i) + A_5 v_i + A_6 x_i + A_7 \\ &= \rho_{d_i}(x_i, v_i) \cdot u_{d_i} + F_{0_i} \end{aligned} \tag{6.3.20}$$

where x_i, v_i and u_{d_i} are respectively the deflection, deflection velocity and control signal of the damper i. Then, as detailed in Chapter 4, this nonlinear gain can be included in the dynamics of the damper as given in (6.3.21).

$$D_i(s) = \frac{F_i(s)}{U_{d_i}(s)} = \frac{\rho_{d_i}(x_i, v_i)}{\left(\frac{s}{\omega_d}\right)^2 + 2m_d\frac{s}{\omega_d} + 1} \tag{6.3.21}$$

where ω_d and m_d represent respectively the bandwidth and the damping coefficient of the damper.

This model has been used to design a scheduled damper controller. The generalized plant including the performance objectives, and used to synthesize the $\mathcal{H}_\infty/\mathcal{H}_2$/LPV dynamic output-feedback controller, is given in Figure 6.5.

This shows the damper model $D_i(s)$ controlled by the damper controller K_{d_i}. The scheduling parameter ρ_{v_i} is used to take the nonlinearities of the damper into account. The control signal computed by the controller is u_{d_i}. The controller receives the damping

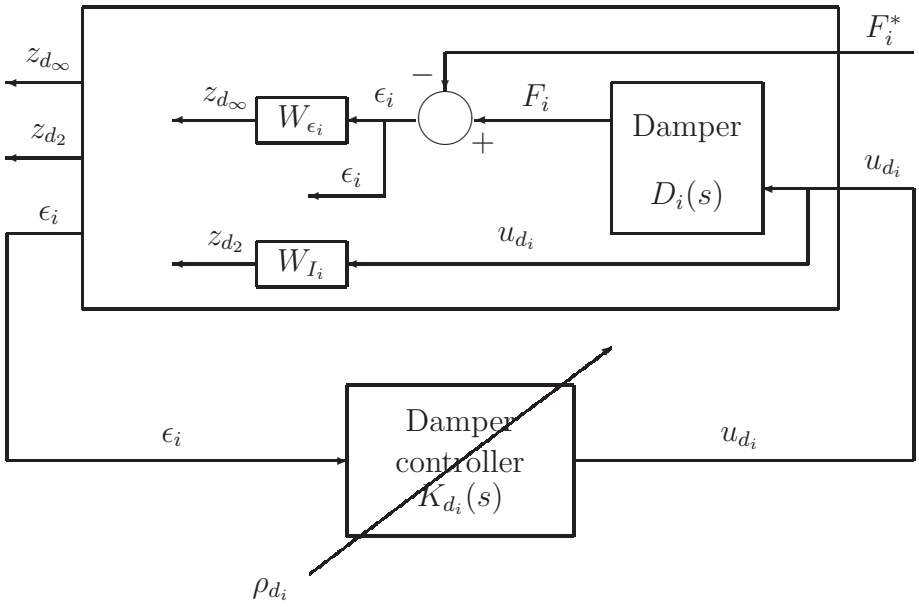

Figure 6.5: Damper controller design: generalized plant and weighting functions

force error $\epsilon_i = F_i - F_i^*$ as an input. z_{d_∞} and z_{d_2} denote the outputs to be controlled according respectively to $\mathcal{H}_\infty$ and $\mathcal{H}_2$ performance specifications, according to Definition 3.5.3. Here the aim is to design a scheduled dynamic output-feedback controller $u_{d_i} = K_{d_i}(\rho_{d_i})(s) \cdot \epsilon_i$. The design objectives given below allow to ensure tracking performances while limiting the energy of the control signal, using both $\mathcal{H}_\infty$ and $\mathcal{H}_2$ performance specifications. Thereafter, this is a multi-objective $\mathcal{H}_\infty/\mathcal{H}_2$ problem.

- the stability is ensured and the nonlinearities of the damper are taken into account through an appropriate scheduling strategy,
- the $\mathcal{H}_\infty$-norm of the system $F_i^* \mapsto z_{d_\infty}$ is bounded by a given value γ_0: force reference tracking performances,
- the $\mathcal{H}_2$-norm of the system $F_i^* \mapsto z_{d_2}$ is bounded by a given value σ_0: limited energy of the control current,
- the pole of the closed-loop system are located in a region suiting for this application: dynamics of the controller adapted to the bandwidth of the damper, identified in Section 4.3.3 (Experiment 5).

The weighting filters used for the synthesis to reach the previously described closed-loop performance objectives, represented in Figure 6.5, are given in Table 6.6.

Relation	**Filter** (Frequency unit: Hz)	
$\epsilon_i \mapsto z_{d_\infty}$	$W_{\epsilon_i} = G_{\epsilon_i} \frac{2\pi f_{\epsilon_i}}{s+2\pi f_{\epsilon_i}}$	$f_{\epsilon_i} = 20$
		$G_{\epsilon_i} = 2$
$u_{d_i} \mapsto z_{d_2}$	$W_{I_i} = G_I \frac{2\pi f_I}{s+2\pi f_I}$	$f_I = 20$
		$G_I = 0.5$

Table 6.6: Damper controller: weighting filters

The open-loop system including both the $\mathcal{H}_\infty$ and $\mathcal{H}_2$ performance specifications can be expressed as in (6.3.22).

$$\begin{pmatrix} \dot{x}_{d_a} \\ z_{d_\infty} \\ z_{d_2} \\ y \end{pmatrix} = \begin{pmatrix} A_{d_a} & B_1 & B_2 \\ C_\infty & D_{\infty 1} & D_{\infty 2} \\ C_2 & D_{21} & D_{22} \\ C_y & D_{y1} & \mathcal{O} \end{pmatrix} \cdot \begin{pmatrix} x_{d_a} \\ F_i^* \\ u_{d_i} \end{pmatrix} \tag{6.3.22}$$

where x_{d_a} contains the state variables of both the damper model and the weighting filters. The outputs z_{d_∞} and z_{d_2} represent the weighted outputs to be controlled, corresponding to the $\mathcal{H}_\infty$ and $\mathcal{H}_2$ performance specifications, F_i^* is the force reference that the damper has to provide, and u_{d_i} is the damper control signal.

Given the controller (6.3.23), the closed-loop system can be expressed as in (6.3.24).

$$K_d(\rho_d) : \begin{pmatrix} \dot{\zeta} \\ u_{d_i} \end{pmatrix} = \begin{pmatrix} A_{K_d} & B_{K_d} \\ C_{K_d} & D_{K_d} \end{pmatrix} \cdot \begin{pmatrix} \zeta \\ \epsilon_i \end{pmatrix} \tag{6.3.23}$$

where A_{K_d}, B_{K_d}, C_{K_d}, D_{K_d} represent the matrices of the damper controller to be designed, ζ are the state variables of the controller and ϵ_i is the force tracking error.

$$\begin{pmatrix} \dot{x}_{cl} \\ z_{d\infty} \\ z_{d2} \end{pmatrix} = \begin{pmatrix} A_{cl} & B_{cl} \\ C_{cl_1} & D_{cl_1} \\ C_{cl_2} & D_{cl_2} \end{pmatrix} \cdot \begin{pmatrix} x_{cl} \\ F_i^* \end{pmatrix} \tag{6.3.24}$$

Solution

Proposition 6.3.2

Consider the closed-loop system (6.3.24) and two positive scalars γ_0 and σ_0. $K_d(\rho_d)$ is a dynamic output-feedback $\mathcal{H}_\infty/\mathcal{H}_2$/LPV controller ensuring that

- *the $\mathcal{H}_\infty$-norm of the system $F_i^* \mapsto z_{d_\infty}$ is bounded by γ_0,*
- *the $\mathcal{H}_2$-norm of the system $F_i^* \mapsto z_{d_2}$ is bounded by σ_0,*
- *the poles of the closed-loop system are located in the LMI region (6.3.25)*

$$\mathcal{D} = \{z \in \mathbb{C} : L + Mz + M^T z^* \prec 0\} \tag{6.3.25}$$

with $L = L^T = \lambda_{ij}{}_{i,j\in[1,m]}$ and $M = \mu_{ij}{}_{i,j\in[1,m]}$, where λ_{ij} and μ_{ij} denote respectively the entries of $L \in \mathbb{R}^{m\times m}$ and $M \in \mathbb{R}^{m\times m}$.

if there exist $\mathbf{R}$, $\mathbf{S}$, $\mathbf{Q}$, $\mathcal{A}_{\mathbf{K_d}}$, $\mathcal{B}_{\mathbf{K_d}}$, $\mathcal{C}_{\mathbf{K_d}}$, $\mathbf{D}_{\mathbf{K_d}}$ *and* $\gamma^{\mathbf{2}}$ *satisfying (6.3.26-6.3.30).*

$$\begin{pmatrix} \mathcal{M}_{11} & \mathcal{M}_{21}^T & \mathcal{M}_{31}^T & \mathcal{M}_{41}^T \\ \mathcal{M}_{21} & \mathcal{M}_{22} & \mathcal{M}_{32}^T & \mathcal{M}_{42}^T \\ \mathcal{M}_{31} & \mathcal{M}_{32} & \mathcal{M}_{33} & \mathcal{M}_{43}^T \\ \mathcal{M}_{41} & \mathcal{M}_{42} & \mathcal{M}_{43} & \mathcal{M}_{44} \end{pmatrix} \prec 0 \tag{6.3.26}$$

where $*$ denotes the symmetric element and the matrix terms are given by,

$$\begin{aligned}
\mathcal{M}_{11} &= A\mathbf{R} + \mathbf{R}A^T + B_2\mathcal{C}_{\mathbf{K_d}} + {\mathcal{C}_{\mathbf{K_d}}}^T B_2^T \\
\mathcal{M}_{12} &= {\mathcal{A}_{\mathbf{K_d}}}^T + A + B_2\mathbf{D}_{\mathbf{K_d}}C_y \\
\mathcal{M}_{13} &= B_1 + B_2\mathbf{D}_{\mathbf{K_d}}D_{y1} \\
\mathcal{M}_{21} &= \mathcal{M}_{12}^T \\
\mathcal{M}_{22} &= A^T\mathbf{S} + \mathbf{S}A + \mathcal{B}_{\mathbf{K_d}}C_y + C_y^T\mathcal{B}_{\mathbf{K_d}} \\
\mathcal{M}_{23} &= \mathbf{S}B_1 + \mathcal{B}_{\mathbf{K_d}}D_{y1} \\
\mathcal{M}_{31} &= \mathcal{M}_{13} \\
\mathcal{M}_{32} &= \mathcal{M}_{23} \\
\mathcal{M}_{33} &= -\mathcal{I} \\
\mathcal{M}_{41} &= C_\infty\mathbf{R} + D_{\infty 2}\mathcal{C}_{\mathbf{K_d}} \\
\mathcal{M}_{14} &= \mathcal{M}_{41}^T \\
\mathcal{M}_{42} &= C_\infty + D_{\infty 2}\mathbf{D}_{\mathbf{K_d}}C_y \\
\mathcal{M}_{24} &= \mathcal{M}_{42}^T \\
\mathcal{M}_{43} &= D_{\infty 1} + D_{\infty 2}\mathbf{D}_{\mathbf{K_d}}D_{y1} \\
\mathcal{M}_{34} &= \mathcal{M}_{43}^T \\
\mathcal{M}_{44} &= -\gamma^2\mathcal{I}
\end{aligned} \tag{6.3.27}$$

$$\begin{pmatrix} \mathbf{Q} & C_2\mathbf{R} + D_{22}\mathcal{C}_{\mathbf{K_d}} & C_2 + D_{22}\mathbf{D}_{\mathbf{K_d}}C_y \\ * & \mathbf{R} & \mathcal{I} \\ * & \mathcal{I} & S \end{pmatrix} \succ 0 \tag{6.3.28}$$

$$\left[\lambda_{ij}\begin{pmatrix}\mathbf{R} & \mathcal{I}\\ \mathcal{I} & \mathbf{S}\end{pmatrix}+\mu_{ij}\begin{pmatrix}A\mathbf{R}+B_2\mathcal{C}_{\mathbf{K_d}} & A+B_2\mathbf{D}_{\mathbf{K_d}}C_y\\ \mathcal{A}_{\mathbf{K_d}} & \mathbf{S}A+\mathcal{B}_{\mathbf{K_d}}C_y\end{pmatrix}+\ldots\right.$$

$$\left.\mu_{ji}\begin{pmatrix}\mathbf{R}A^T+{\mathcal{C}_{\mathbf{K_d}}}^TB_2^T & {\mathcal{A}_{\mathbf{K_d}}}^T\\ (A+B_2\mathbf{D}_{\mathbf{K_d}}C_y)^T & A^T\mathbf{S}+C_y^T{\mathcal{B}_{\mathbf{K_d}}}^T\end{pmatrix}\right]_{i,j\in[1,m]}\prec 0 \tag{6.3.29}$$

$$\begin{gathered}Trace(\mathbf{Q})<\sigma_0^2\\ \boldsymbol{\gamma^2}<\gamma_0^2\\ D_{21}+D_{22}\mathbf{D}_{\mathbf{K_d}}D_{y1}=0\end{gathered} \tag{6.3.30}$$

Proof 6.3.2

The three design objectives can be expressed as follows:

- *$\mathcal{H}_\infty$ performance: the $\mathcal{H}_\infty$-norm of the system from $F_i^*\mapsto z_{d\infty}$ does not exceed γ if and only if [Scherer and Weiland, 1999] there exists a matrix $X_\infty=X_\infty^T\succ 0$ such that*

$$\begin{pmatrix}A_{cl}X_\infty+X_\infty A_{cl}^T & B_{cl} & X_\infty C_{cl1}^T\\ * & -\mathcal{I} & D_{cl1}^T\\ * & * & -\gamma^2\mathcal{I}\end{pmatrix}\prec 0 \tag{6.3.31}$$

- *$\mathcal{H}_2$ performance: the $\mathcal{H}_2$-norm of the system from $F_i^*\mapsto z_{d2}$ does not exceed σ if and only if [Scherer et al., 1997] $D_{cl2}=0$ and there exist two matrices $X_2=X_2^T\succ 0$ and $Q=Q^T$ such that*

$$\begin{pmatrix}A_{cl}X_2+X_2A_{cl}^T & B_{cl}\\ * & -\mathcal{I}\end{pmatrix}\prec 0 \tag{6.3.32}$$

$$\begin{pmatrix}Q & C_{cl2}X_2\\ * & X_2\end{pmatrix}\succ 0 \tag{6.3.33}$$

$$Trace(Q)\prec\sigma^2 \tag{6.3.34}$$

- *Pole placement: the closed-loop poles are located in the LMI region (6.3.25) if and only if [Chilali et al., 1999] there exists a symmetric matrix $X_{pol}=X_{pol}^T\succ 0$ such that*

$$\left[\lambda_{ij}X_{pol}+\mu_{ij}A_{cl}X_{pol}+\mu_{ij}X_{pol}A_{cl}^T\right]_{i,j\in[1,m]}\prec 0 \tag{6.3.35}$$

with the notation

$$[S_{ij}]_{i,j\in[1,m]} \begin{pmatrix} S_{11} & \cdots & S_{1m} \\ \vdots & \ddots & \vdots \\ S_{m1} & \cdots & S_{mm} \end{pmatrix}$$

Then a single Lyapunov matrix $X = X_\infty = X_2 = X_{pol}$ has to be found in order to determine a controller that fulfills these three objectives, and some changes of variable have to be performed to linearize the inequalities (6.3.31-6.3.35). X has first to be factorized according to (6.3.36).

$$\begin{cases} X = X_1 X_2^{-1} \\ X_1 = \begin{pmatrix} \mathbf{R} & \mathcal{I} \\ \mathbf{M^T} & \mathcal{O} \end{pmatrix} \quad X_2 = \begin{pmatrix} \mathcal{O} & \mathbf{S} \\ \mathcal{I} & \mathbf{N}^T \end{pmatrix} \end{cases} \tag{6.3.36}$$

And the change of controller variables (6.3.37) has to be introduced.

$$\begin{cases} \mathcal{B}_{K_d} &= N B_{K_d} + \mathbf{S} B_2 \mathbf{D_{K_d}} \\ \mathcal{C}_{K_d} &= C_{K_d} \mathbf{M^T} + \mathbf{D_{K_d}} C_y \mathbf{R} \\ \mathcal{A}_{K_d} &= \mathbf{N} A_{K_d} \mathbf{M^T} + \mathbf{N} B_{K_d} C_y \mathbf{R} + \mathbf{S} B_2 C_{K_d} \mathbf{M^T} + \mathbf{S}(A + B_2 \mathbf{D_{K_d}} C_y)\mathbf{R} \end{cases} \tag{6.3.37}$$

Then using this change of variables, the inequalities (6.3.31-6.3.35) become Linear Matrix Inequalities in the variables $\mathbf{R}$, $\mathbf{S}$, $\mathbf{Q}$, $\mathcal{A}_{K_d}$, $\mathcal{B}_{K_d}$, $\mathcal{C}_{K_d}$ and $\mathbf{D_{K_d}}$. The LMI (6.3.26-6.3.30) are obtained and solve the multi-objective damper controller synthesis problem. Finally, the matrices of the controller can be computed simply by inversing the equations (6.3.37). Such a controller has been designed to control the damper, and the results are presented in Section 6.4.

6.3.4 A two-state damper control strategy

Semi-active control strategies such as the Acceleration Driven Damper (ADD) have already been developed for two-state dampers in [Savaresi et al., 2005, Savaresi and Spelta, 2007], and improve comfort efficiently. Here a new one is proposed and allows the designer to specify the performance objectives in terms of comfort and road-holding. As already discussed in Section 6.1, two-state dampers are very interesting because of their small response-time and cost. These dampers are able to switch between the maximal nonlinear damping rate and the minimal one, and can be modeled as (6.3.38).

$$\begin{cases} F_{u_{d_{max}}} &= (A_1 + A_2)\tanh(A_3 v + A_4 x) + A_5 v + A_6 x + A_7 \text{ if } u_d = u_{d_{max}} \\ F_{u_{d_{min}}} &= (A_2 - A_1)\tanh(A_3 v + A_4 x) + A_5 v + A_6 x + A_7 \text{ if } u_d = u_{d_{min}} \end{cases} \tag{6.3.38}$$

The damper is supposed to be able to switch between these two models. Here a control strategy based on the vehicle controller designed in Section 6.3.2 is proposed to control two-state dampers and choose the most appropriate damping rate. This control strategy is given by (6.3.39).

$$\begin{cases} F_{u_{d_{max}}} &= (A_1 + A_2)\tanh(A_3 v + A_4 x) + A_5 v + A_6 x + A_7 \\ F_{u_{d_{min}}} &= (A_2 - A_1)\tanh(A_3 v + A_4 x) + A_5 v + A_6 x + A_7 \\ D_{u_{d_{max}}} &= \mid F_{max} - F_{LPV} \mid \\ D_{u_{d_{min}}} &= \mid F_{min} - F_{LPV} \mid \\ u_d &= \dfrac{u_{d_{max}} - u_{d_{min}}}{2}\tanh(p \cdot (D_{u_{d_{min}}} - D_{u_{d_{max}}})) + \dfrac{u_{d_{max}} + u_{d_{min}}}{2} \end{cases} \tag{6.3.39}$$

where F_{LPV} is the force computed by the semi-active controller designed in Section 6.3.2 and used to control the vehicle, $u_{d_{max}} = 1$ and $u_{d_{min}} = -1$ denote the extremal values of the damper control signal, $D_{u_{d_{max}}}$ and $D_{u_{d_{min}}}$ denote the distances between the required semi-active force F_{LPV} and the minimal and maximal forces of the two-state damper. Then u is computed by comparing these distances. If $D_{u_{d_{max}}} < D_{u_{d_{min}}}$, $u_{d_{max}}$ is applied to the damper, and $u_{d_{min}}$ else. The hyperbolic tangent can be seen as an approximation of the sign function. The parameter p has to be chosen according to the desired slope around zero. In this case $p = 0.2$ has been chosen. This approximation avoids chattering problems due to the noise, when the distance between the LPV force and the extremal forces are equal. Here with $p = 0.2$, the system switches as soon as the difference $D_{u_{d_{max}}} - D_{u_{d_{min}}}$ is greater than 20N.

The performances of this control strategy will be analyzed in Section 6.5 using some simulations. The results will be compared both to another two-state control strategy [Savaresi et al., 2005, Savaresi and Spelta, 2007], and to continuously controlled dampers.

6.4 Damper controller analysis

Here some results are given to emphasize the performance of the damper controller designed in Section 6.3.3. Numerical and simulation results are given in Section 6.4.1 in order to analyze the performance and robustness of the proposed damper controller. Then some closed-loop experimental results are described and analysed in Section 6.4.2.

6.4.1 Numerical and simulation results

The damper controller has been designed using Proposition 6.3.2. The achieved $\mathcal{H}_\infty$ and $\mathcal{H}_2$ performance levels are given in Table 6.7. Note that the $\mathcal{H}_2$-norm has been minimized

for a given $\mathcal{H}_\infty$ bound ($\gamma_0 = 2$) since it is not possible to minimize both norms.

	LTI controller	**LPV controller**
$\mathcal{H}_\infty$ performance	$\gamma_0 = 2$	$\gamma_0 = 2$ (fixed)
$\mathcal{H}_2$ performance	$\sigma_0 = 3.2$	$\sigma_0 = 4.3$ (fixed)

Table 6.7: Achieved $\mathcal{H}_\infty$ and $\mathcal{H}_2$ performances

Furthermore two constraints on pole placement have been used so that all the poles of the closed-loop system are in the interval $[-p_{max}, -p_{min}] = [-400, -1]$. The lower bound p_{min} ensures the stability even if the measured signal is noisy. This lower bound is not necessary if there is no measurement noise. The upper bound p_{max} allows the controller to compute control signals containing high frequencies that would damage both the performances and the servomechanism of the damper. The corresponding LMI constraints for pole placement are defined by (6.4.1) and (6.4.2), as detailed in [Chilali et al., 1999].

$$\mathcal{D}_{p_{min}} = \{z \in \mathbb{C} : z + z^* + 2p_{min} \prec 0\} \tag{6.4.1}$$

$$\mathcal{D}_{p_{max}} = \{z \in \mathbb{C} : -z - z^* - 2p_{max} \prec 0\} \tag{6.4.2}$$

The obtained poles of the LPV closed-loop system are represented in Figure 6.6, where the circles and the crosses respectively denote the poles of the closed-loop system for the maximal and minimal scheduling parameter. These results emphasize the efficiency of the pole placement method.

The synthesized damper controller has been tested in simulation. The simulated system is the nonlinear damper model given by (6.3.20-6.3.21). This damper is controlled by the controller $K_d(s)$, that computes the control signal u_d, as represented in Figure 6.7. The disturbance inputs of the damper are the deflection and the deflection velocity. The velocity has been simulated by a filtered random signal varying from 0 to 0.3m/s, which covers the most interesting velocity range. The deflection is simply the integral of this signal. The reference damping force F^* to be provided by the damper has been also simulated by some filtered (0-20Hz) steps of various amplitudes from -1000N to 1500N.

Note that the gain of the simulated damper model has been decreased of 20% in order to represent the uncertainties on the real damper gain, whereas the model used in the controller synthesis has not been changed. The force provided by the damper is assumed to be measured and corrupted by a random white noise of amplitude 10N, as represented in Figure 6.7. The cut-off frequency of the low-pass velocity filter is 20Hz, so that the simulated velocity represents the worst possible case on a vehicle. Indeed the damper does not undergo higher frequencies since they are filtered both by silent-blocks and tires. This velocity can be seen as a disturbance since it changes the gain of the damper and thereafter the provided force, for a given control signal. The interest of the

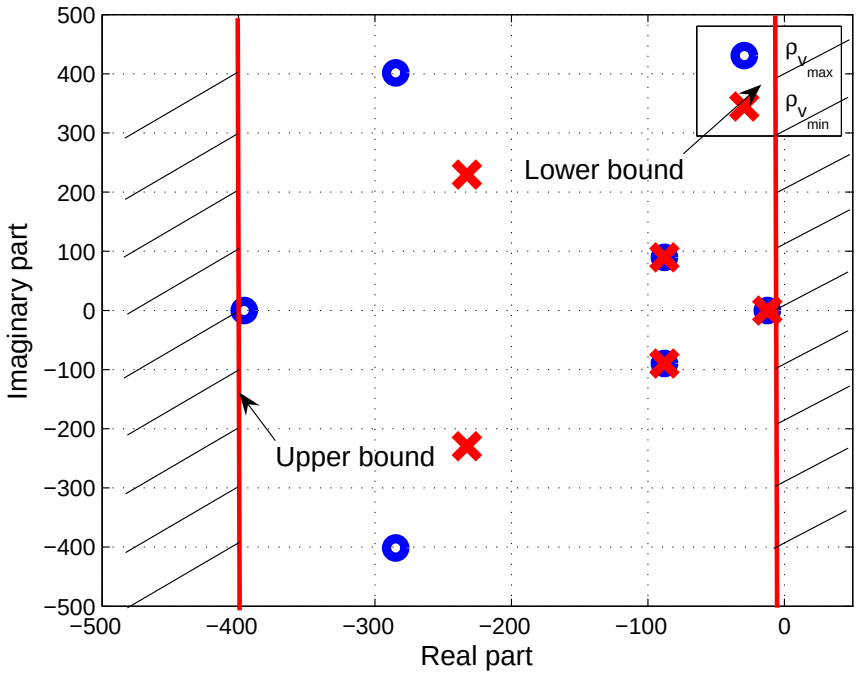

Figure 6.6: Closed-loop system poles

proposed LPV approach is to take the variations of the gain due to the nonlinearities into account. Therefore the LPV and LTI controllers have been tested and compared in Figure 6.8, for the previously described varying deflection velocity.

The Mean Relative Errors have been computed according to Definition 4.3.1, both in the LPV and LTI case. The results are given in Table 6.8.

Case	**MRE***
LTI	11%
LPV	5%
* Mean Relative Error	

Table 6.8: Simulation results: mean relative errors

The performance and robustness of the LPV controller compared to the LTI one appear clearly from these results since the disturbance attenuation is faster when the velocity changes. It has to be noticed that the same tracking errors have been achieved while performing the same simulation without the 20% uncertainty on the damper gain, which emphasizes the robustness of the designed controllers. Furthermore in both cases, the control signal has an appropriate bandwidth. The measurement noise is filtered thanks to the appropriate location of the closed-loop poles.

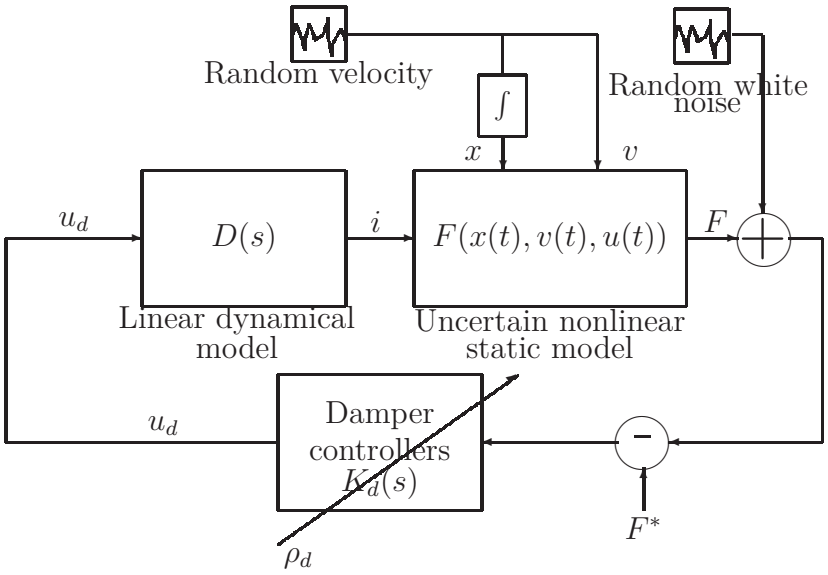

Figure 6.7: Simulations: closed-loop damper

6.4.2 Experiments and closed-loop results

Implementation

The damper controller has been implemented on a Dspace control board equipped with a PowerPC processor that processes both the acquisition of the measured analog damper force and the real-time computation of the controller. The real-time implementation of the controller is done automatically by the Dspace software. Furthermore the testing bench is equipped with an Interface strain-gage based force sensor (full scale +/-50kN) providing a 0-5V analog signal. This measured force has been used to control the damper.

Experiment and results

Some closed-loop experiments have been run. The damper has been submitted to ramp deflection profiles using SOBEN testing bench. Two different velocities have been tested for each controller: 0.05m/s and 0.1m/s in order to evaluate the performance of the proposed scheduling strategy. The LTI controller has been synthesized for a gain corresponding to a deflection velocity of 0.1m/s.

Analysis

Some high force amplitudes have been measured at constant time intervals, as represented in Figures 6.9, 6.10, 6.11 and 6.12. It corresponds to the change of velocity sign during

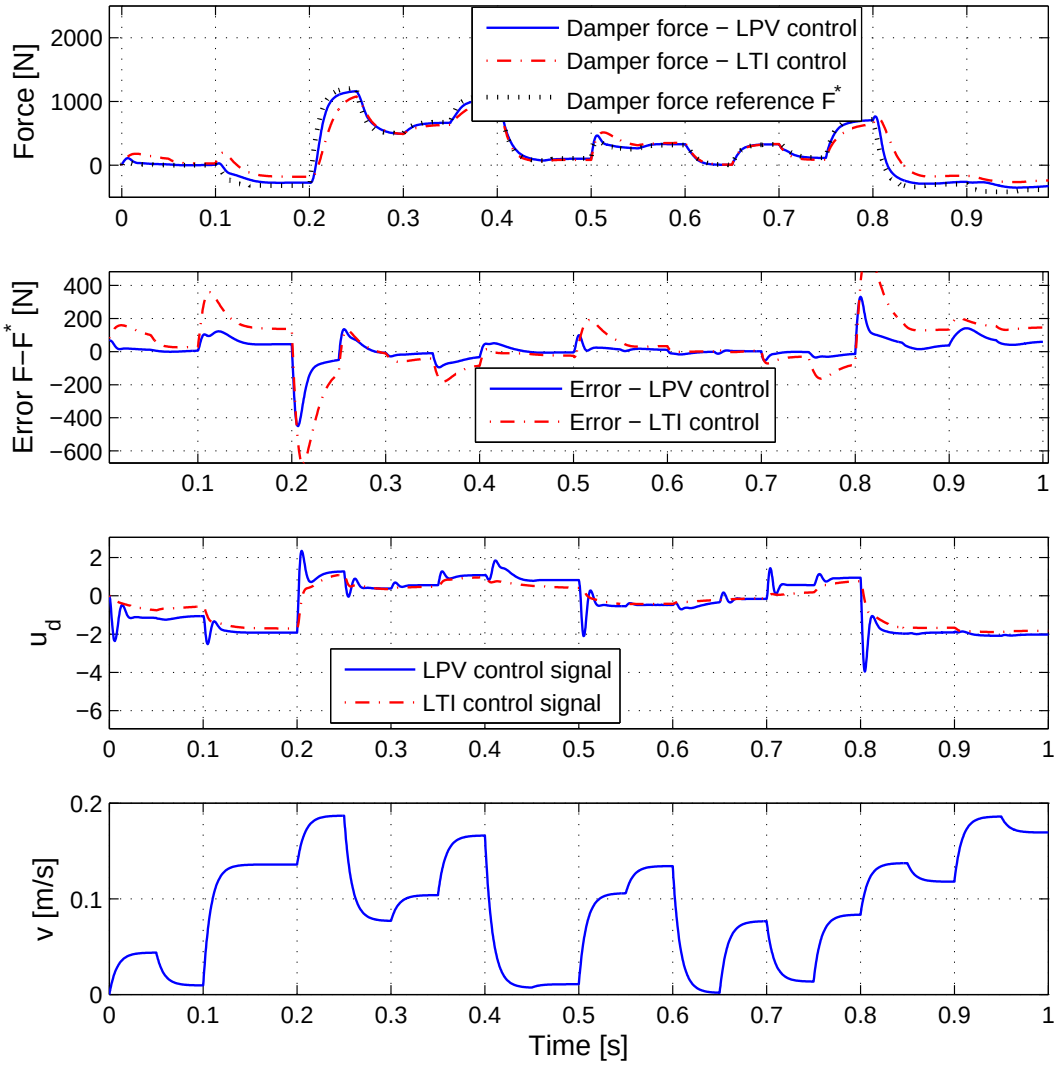

Figure 6.8: Simulation results: LTI vs LPV damper controller

the periodic triangle deflections. Indeed at these particular moments, the damper is submitted to very high accelerations and produces a high force. The results also show an important measurement noise on the damper force. The mean relative tracking errors $\epsilon(F - F^*)$ have been computed according to Definition 4.3.1 and are given in Table 6.9.

These relative errors show that the LTI controller is very efficient for the velocity where it has been designed. However these performances are not achieved for other velocities, whereas the LPV controller adapts the gain according to the deflection velocity. The LTI and LPV damper control signal (velocity 0.05m/s), given in Figures 6.10

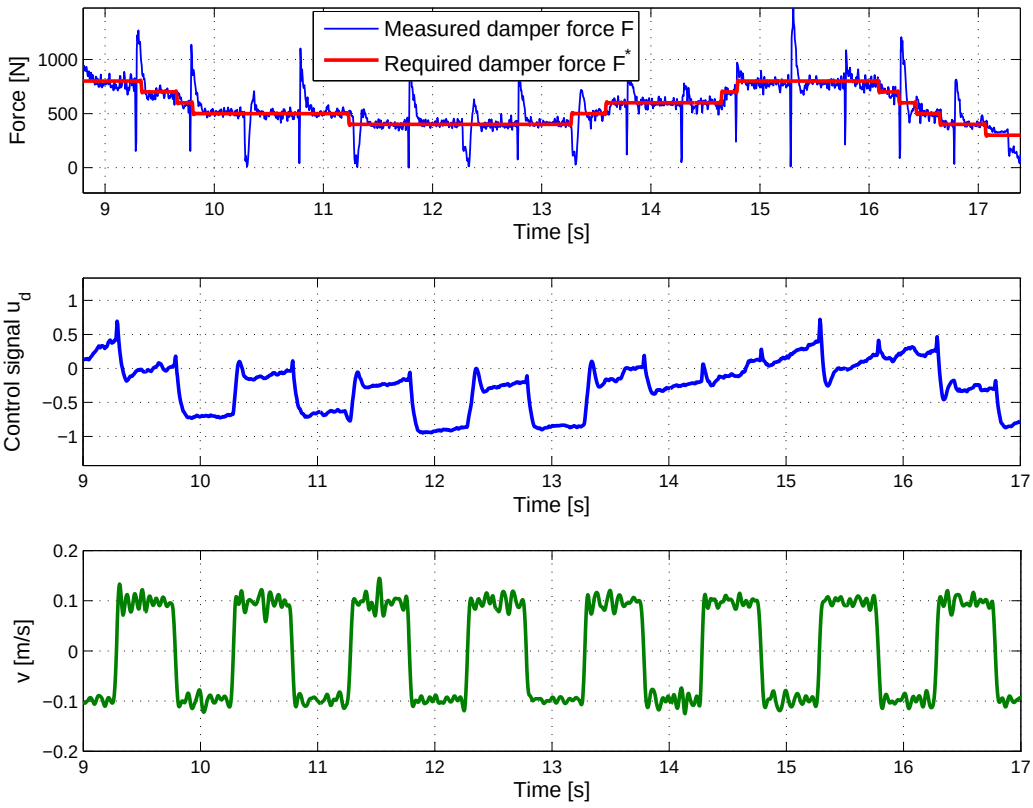

Figure 6.9: Experiments: LTI damper controller: 0.1m/s

Case	**MRE***
LTI 0.1m/s	4%
LTI 0.05m/s	17%
LPV 0.1m/s	5%
LPV 0.05m/s	6%
* Mean Relative Error	

Table 6.9: Experiment results: mean relative errors

and 6.12, have to be compared. The control signal computed by the LTI controller is slow. The disturbances, when the velocity changes, is slowly rejected, with a static error, whereas the control signal computed by the LPV controller is equivalent whatever the velocity is, and the disturbance rejection as well. This results highlight the interest of the developed LPV damper control strategy.

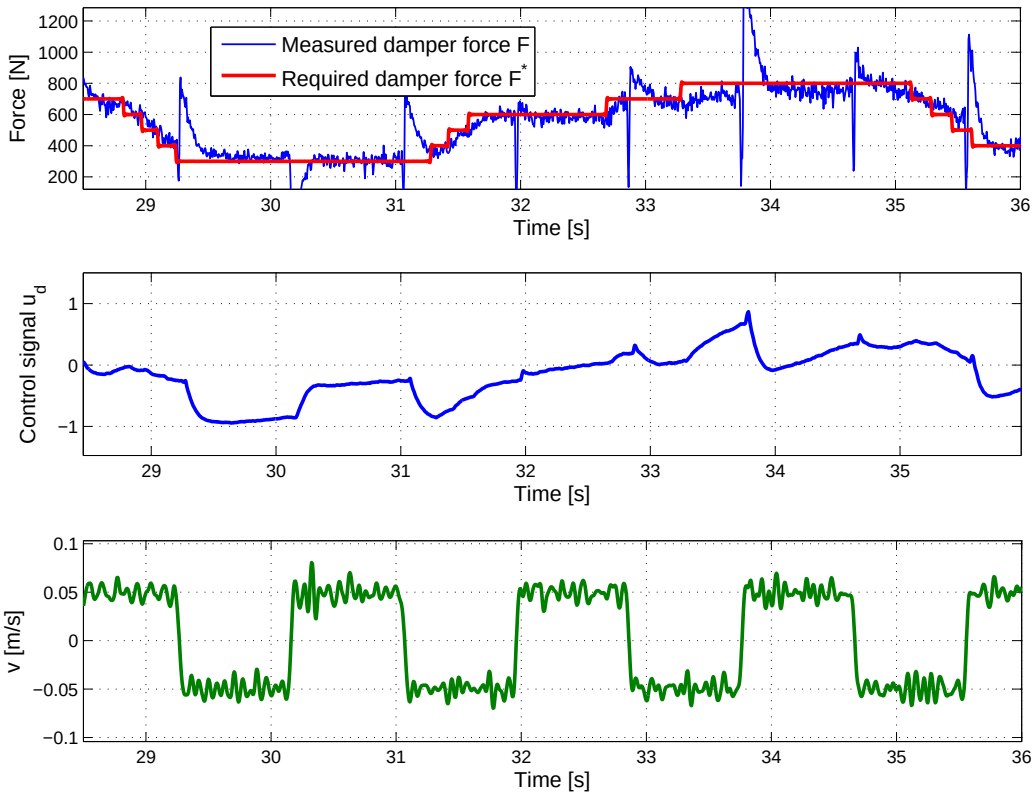

Figure 6.10: Experiments: LTI damper controller: 0.05m/s

6.5 Vehicle controller analysis

In this section, the vehicle controller designed in Section 6.3.2 is tested using some simulations. The observer proposed in Chapter 5 has been used to estimate the required state variables. The controlled system is the full vertical car model (4.4.3), equipped with dampers modeled by (4.3.9). These nonlinear models have been identified respectively for front and rear dampers. Some frequency and time simulation results are given, and the performances of both passive and controlled vehicles are analyzed using the pseudo-Bode diagrams and PSD criteria presented in Section 6.2.

6.5.1 Vehicles under study

Six different cases are under study in this section, corresponding to the following vehicles:

1. Passive linear damper with minimal damping rate,

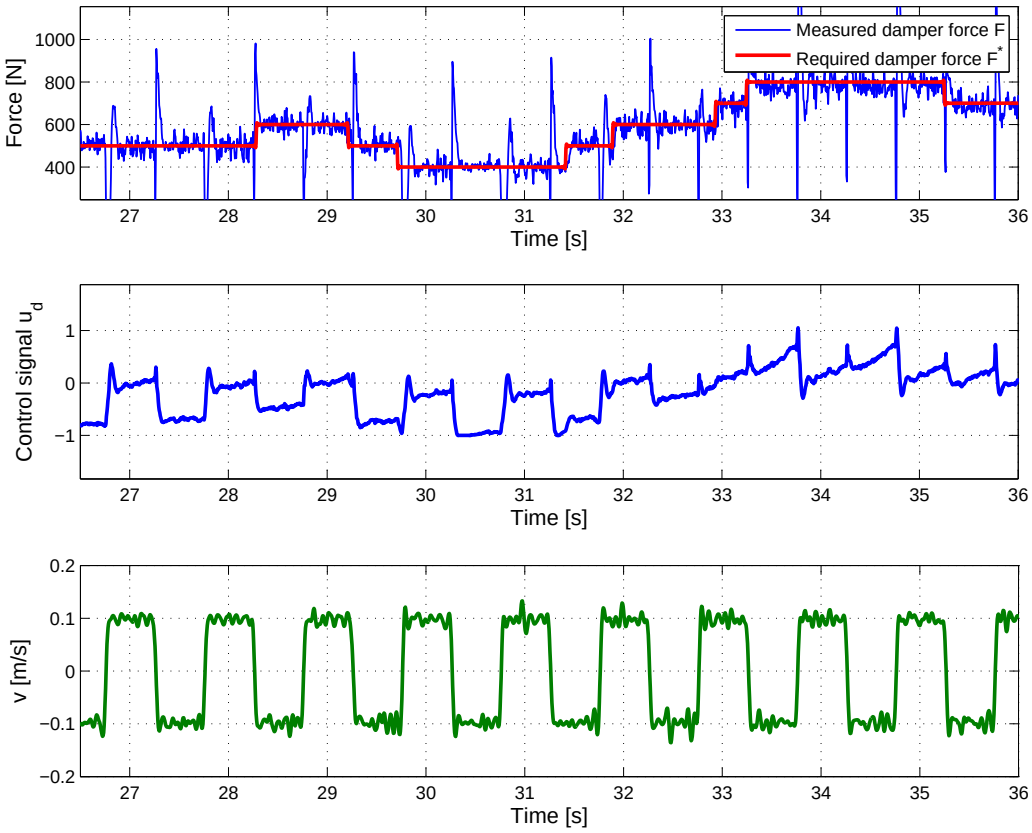

Figure 6.11: Experiments: LPV damper controller: 0.1m/s

2. Passive linear damper with maximal damping rate,
3. Active damper,
4. Semi-active LPV control,
5. Semi-active ADD control (Acceleration Driven Damper),
6. Semi-active switched control (on/off).

Case 1-2: the vehicle is equipped with non-controlled dampers. The damper model used in these simulations are the nonlinear identified models (4.3.4) for $u_d = u_{d_{min}}$ (minimal damping rate) and $u_d = u_{d_{max}}$ (maximal damping rate). These models correspond to the extremal behaviors of the damper under study.

Case 3: the controlled system is the linear full-car model (4.4.3). An active controller has been designed, corresponding to the controller designed in Section 6.3.2,

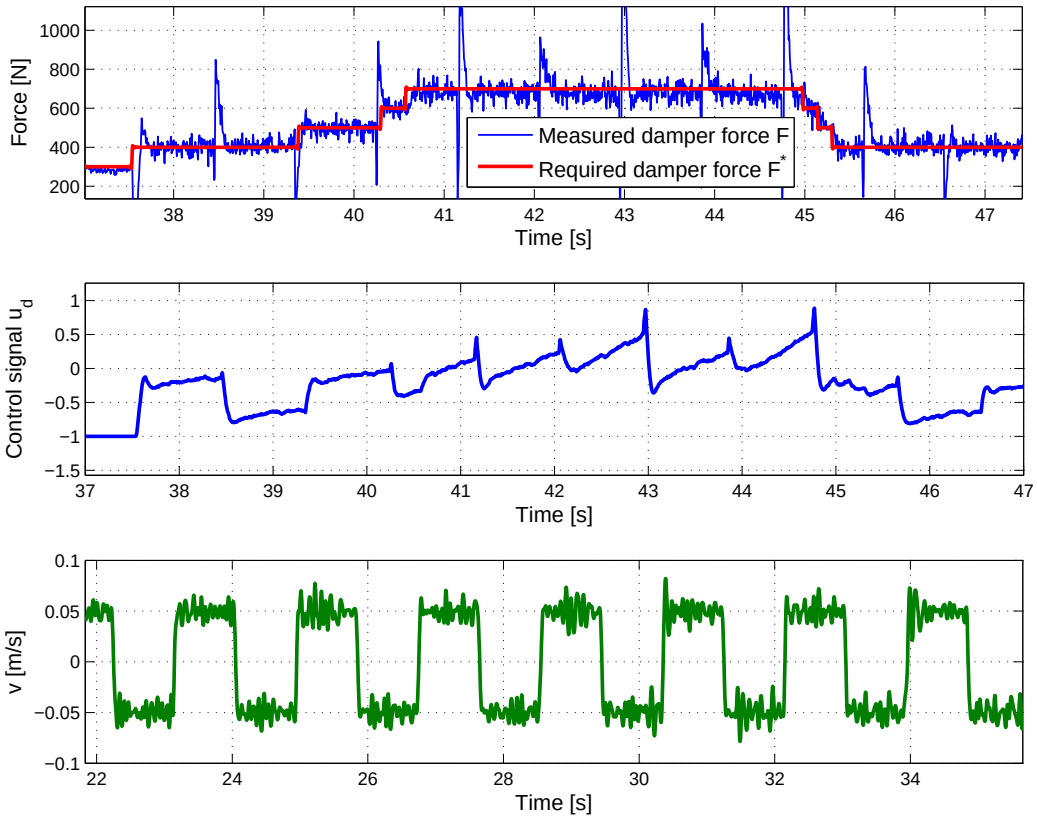

Figure 6.12: Experiments: LPV damper controller: 0.05m/s

when no constraint on the control signal u_i is considered ($\rho_v = 0$). Therefore the required damping force $F_i^* = c_{0_i} \cdot \dot{z}_{def_i} + u_i$ for each damper i may be located in Zone 1, 2 or 3 (see Figure 6.4) and all the forces $F_i^* \in \mathbb{R}$ are supposed to be achievable. Indeed in (4.4.3), the damper force u_i is exactly the force computed by the controller. This corresponds to the ideal case where no damper technological constraint is considered.

Case 4: the semi-active controller designed in Section 6.3.2 is used to control the vehicle equipped with the damper models (4.3.9). Unlike the previous case, the nonlinearities of the dampers, their response-time and their achievable force range ($u_d \in [-1, 1]$) are taken into account. Here the required force is controlled by the scheduling strategy to remain in zone 3 (see Figure 6.4). Therefore in this case, the required damping forces are realistic and can be achieved by the SOBEN damper. Each damper is controlled by the local damper controller developed in Section 6.3.3.

Case 5: the ADD semi-active two-state control strategy has been tested. This strategy uses the measurement of the sprung mass acceleration and the measurement of

the deflection. This control law is detailed in [Savaresi et al., 2005] and has been used in this section for comparison. This simple switched control strategy gives the damping rate c to be applied, as described in (6.5.1).

$$c_i = \begin{cases} c_{max} & \text{if} \quad \ddot{z}_{s_i} \cdot (\dot{z}_{s_i} - \dot{z}_{us_i}) > 0 \\ c_{min} & \text{if} \quad \ddot{z}_{s_i} \cdot (\dot{z}_{s_i} - \dot{z}_{us_i}) < 0 \end{cases} \tag{6.5.1}$$

where c_{max} and c_{min} represent respectively the maximal and minimal achievable damping rate. Then the full-car can be controlled by applying this control strategy to the four suspensions.

Case 6: the vehicle is supposed to be equipped with two-state dampers being able to switch between the maximal nonlinear damping rate to the minimal one. These two-state dampers are modeled by (6.3.38), and the strategy to control these dampers is the one presented in Section 6.3.4. Furthermore the dampers are supposed to have the same dynamics as the continuously variable active and semi-active dampers, given by (4.3.8). These two-state actuators could have a smaller response-time. However here the objective is to analyze the interest of continuously variable dampers compared to two-state ones.

6.5.2 Time-domain results

In this section, various vehicles, equipped with the following dampers, are simulated and compared:

- passive nominal dampers (mean damping rate),
- semi-active dampers continuously controlled by the LPV controller designed in Section 6.3.2,
- semi-active two-state dampers controlled by the LPV controller designed in Section 6.3.4,
- semi-active two-state dampers controlled by the ADD control strategy.

These four vehicles have been simulated, and some time-domain results are presented. The vehicles have been submitted to random ground disturbances of period 1s. Furthermore this signal has been low-pass filtered so that the spectrum of the ground disturbance contains frequencies in the range $[0, 20]$Hz only, since higher frequencies are filtered by the tires and many other parts of the vehicle.

Vehicle behavior

The sprung mass position z_s, the unsprung mass position z_{us1} of suspension one (front left) and the ground disturbance are represented in Figure 6.13.

These results show that

- the sprung mass position of the passive vehicle has larger oscillations than the controlled one and with higher amplitude. Depending on the frequency of these oscillations, the vehicle may be uncomfortable. In the semi-active LPV cases (continuous and two-state dampers), the sprung mass position is both well filtered and well damped. In the ADD case, the behavior is similar to the passive case.
- the unsprung mass position is less oscillating in the LPV continuous case, and follows better the ground disturbance, implying a better road-holding level.

The computed scheduling coefficients allowing the LPV controller (continuous case) to compute an achievable required damping force are presented in Figure 6.14. The first coefficient corresponds to the active controller providing the best performances, and the second one corresponds to the passive controller providing a very small control signal. The linear combination of these two controllers provides the achievable damping force the damper has to provide. This force has to be compared to the minimal and maximal forces the damper can provide, represented in Figure 6.15 and given by the Equation (6.3.38). They respectively correspond to the control signals $u_d = u_{min}$ and $u_d = u_{max}$ and determine the achievable force range of the damper.

From these results, the following conclusions can be drawn:

- the required force, computed by the vehicle controller, is often switching between the minimal and maximal damping forces, therefore designing a damper with a large force range is useful,
- the required force always remains in the achievable range, which means that the force is semi-active and that the SOBEN damper is able to provide this force,
- the scheduling coefficients increase or decrease the control signal as soon as the required force exceeds the achievable force bounds. Note that the coefficients are often extremal (equal to 0 or 1). Therefore the behavior is quite similar to the behavior of a two-state damper.

The vertical accelerations of the sprung mass are represented in Figure 6.16 for the four vehicles under study. Furthermore the RMS values of these variables, given in Table 6.10, have been computed for each vehicle, according to the Definition 6.2.2. The ADD

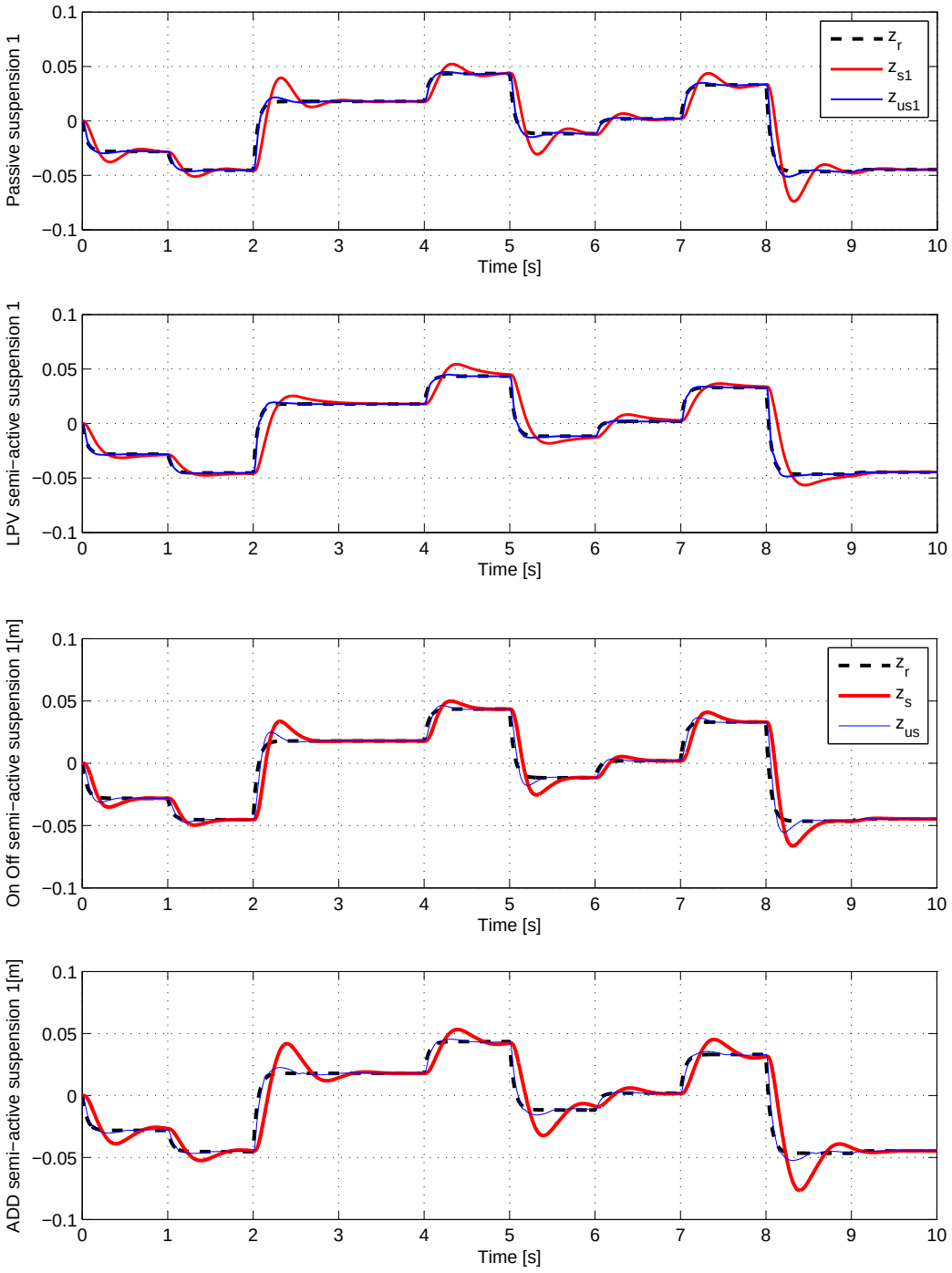

Figure 6.13: Suspension 1: sprung and unsprung mass positions (simulations)

control is the most efficient strategy to reduce the sprung mass accelerations, which is normal since this is its main goal. Note that the LPV and on/off strategies also improve this comfort criteria, compared to the nominal passive suspension.

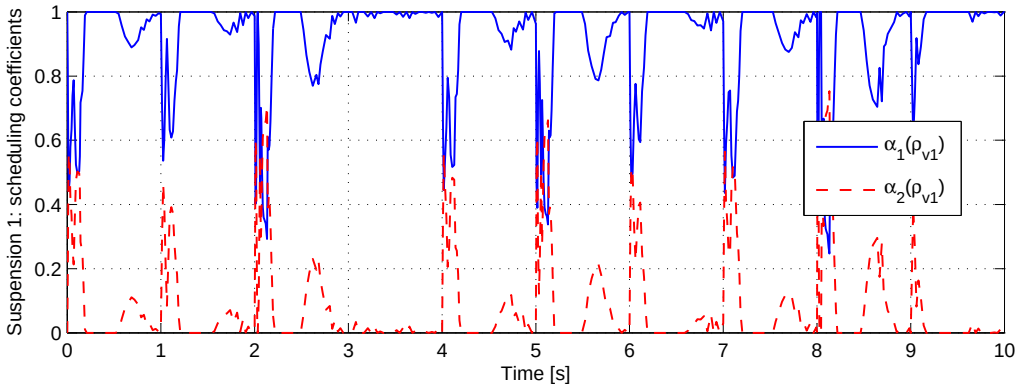

Figure 6.14: Scheduling coefficients $\alpha(\rho_{v1})$ for damper 1 (simulations)

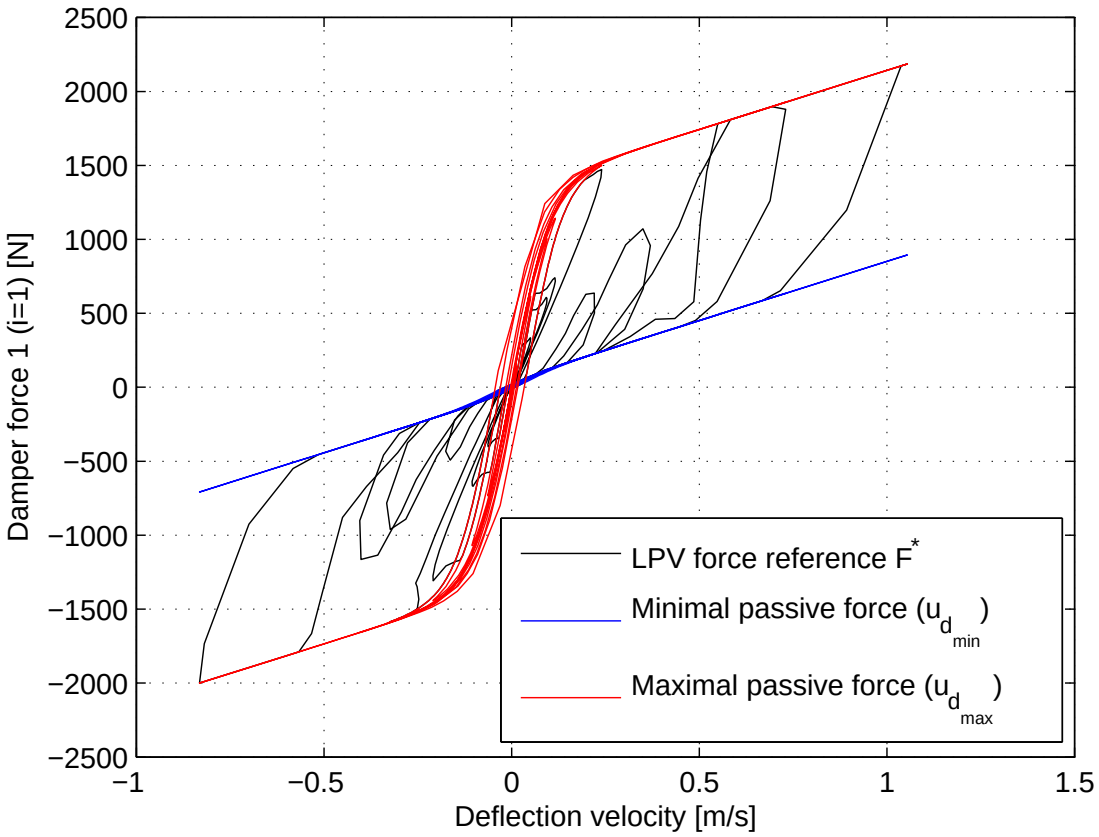

Figure 6.15: Required semi-active force and achievable force range (simulations)

In the two-state cases (ADD and LPV), the required damping coefficients and damping forces have been recorded and plotted respectively in Figures 6.17 and 6.18. They are

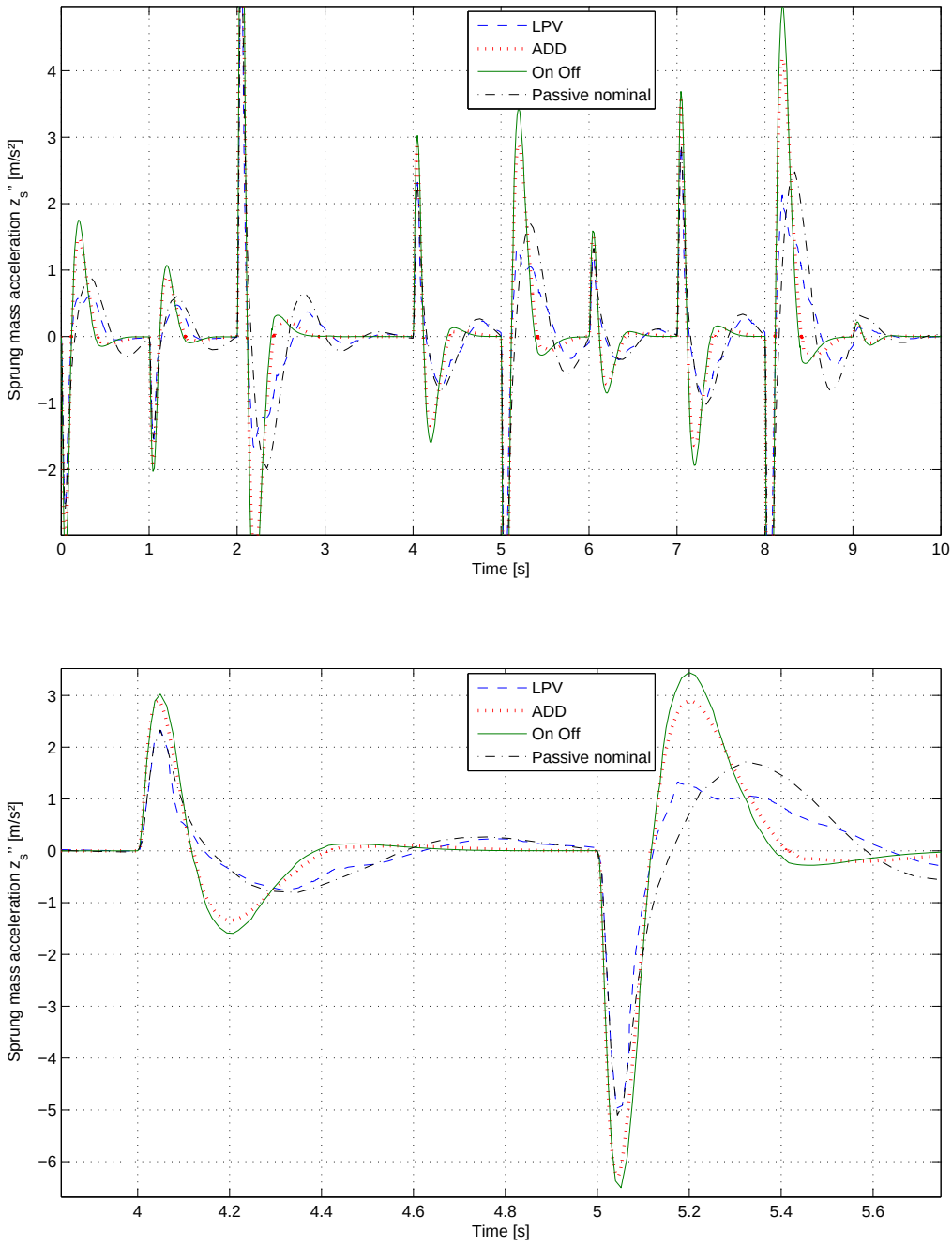

Figure 6.16: Sprung mass acceleration $\ddot{z}_s$ (top) and zoom (bottom)

quite similar. Indeed, the switching occurs at about the same moments. These results show that the proposed two-state LPV control strategy can make a vehicle as comfortable as the comfort oriented ADD control strategy, when the weighting functions used in the design of the two-state LPV controller are comfort oriented. Furthermore this con-

Vehicle	RMS($\ddot{z}_s$)
Passive nominal	212
Semi-active ADD	168
Semi-active on/off	195
Semi-active LPV	181

Table 6.10: Sprung mass acceleration - RMS criteria

troller has an important advantage: it can be adjusted according to given specifications, for example for road-holding improvement, which is not possible with the ADD control.

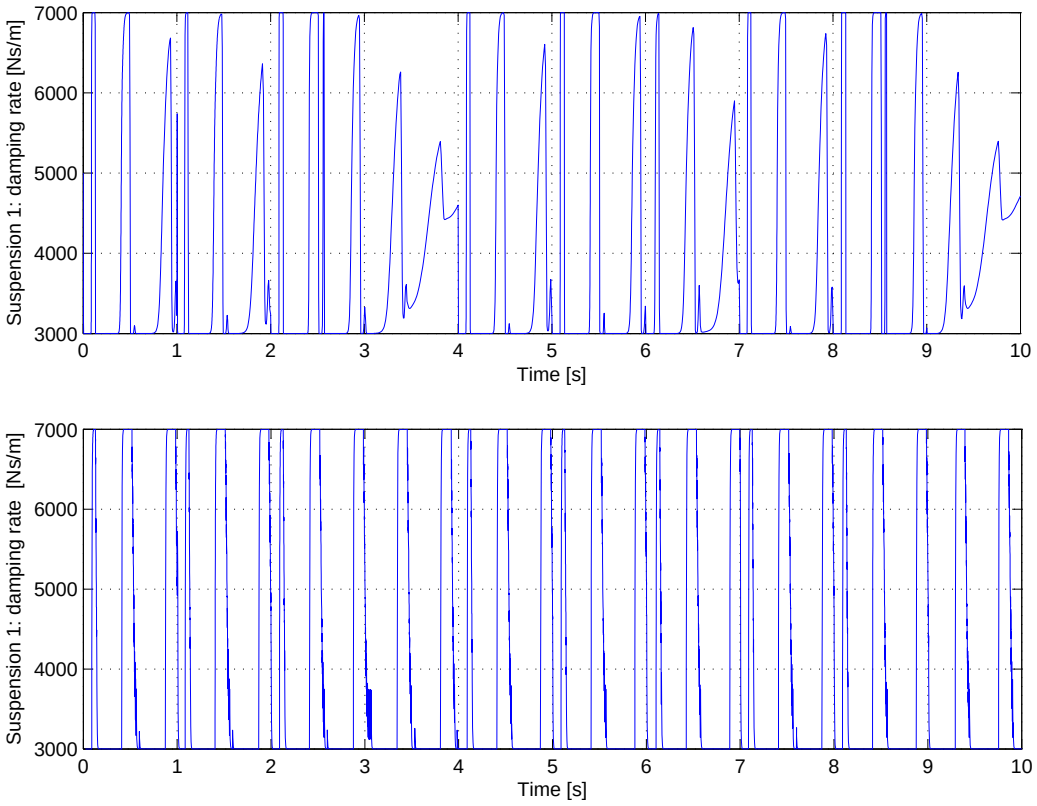

Figure 6.17: Damping coefficients (up:On/off, down:ADD) (simulations)

These results emphasize the performance of the proposed vehicle controllers. However these are only particular results obtained in a specific case. A more complete performance analysis is given in Section 6.5.3.

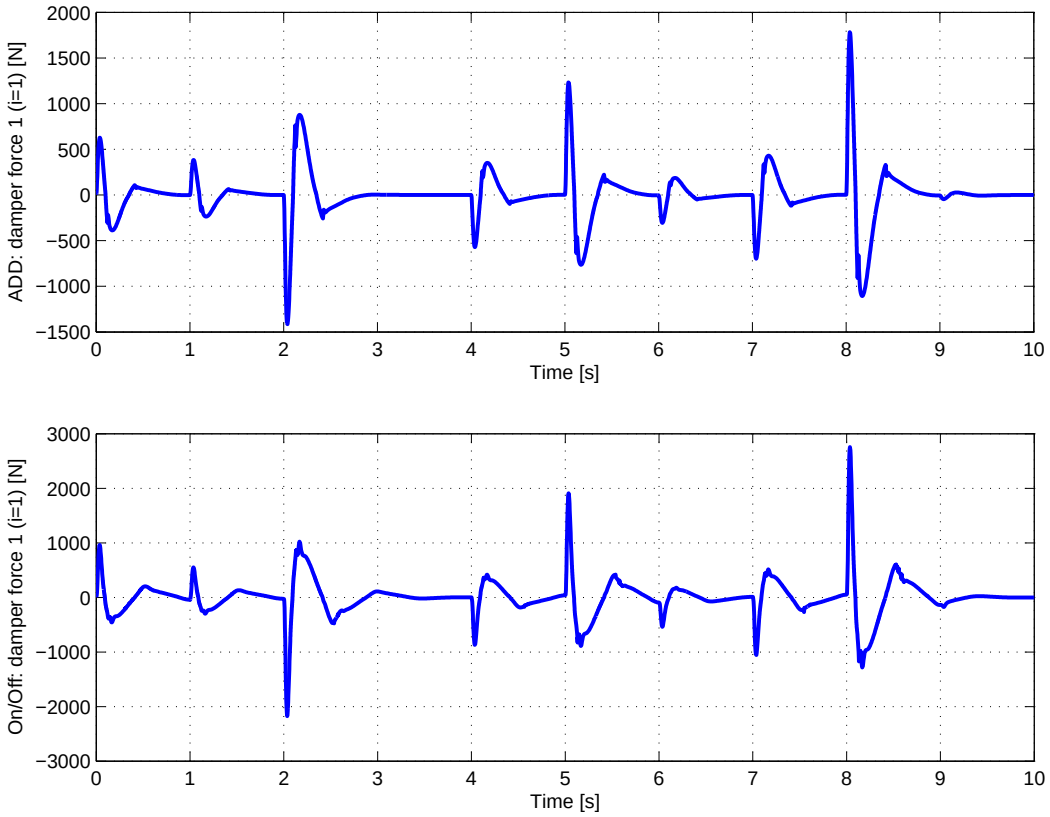

Figure 6.18: Required semi-active force (up:On/off, down:ADD) (simulations)

6.5.3 Frequency results

In this section, the six cases, given below, are studied using frequency domain results:

1. Passive linear damper with minimal damping rate,
2. Passive linear damper with maximal damping rate,
3. Active damper,
4. Semi-active LPV control,
5. Semi-active ADD control (Acceleration Driven Damper),
6. Semi-active switched control (On/Off).

These cases have been simulated and the obtained pseudo-Bode diagrams are given in Figure 6.19 and 6.20. Furthermore the performance criteria based on the power spectral

density (PSD) have been computed from these frequency results, and normalized between zero and one. They are represented graphically in Figure 6.21.

These frequency results have only been computed for the following input-output relations. Indeed, only the suspension 1 (front left suspension) is studied, but the results are equivalent for the three others.

- $z_{r_1} \mapsto \ddot{z}_s$
- $z_{r_1} \mapsto z_s$
- $z_{r_1} \mapsto \ddot{z}_{us_1}$
- $z_{r_1} \mapsto \ddot{z}_{def_1}$
- $M_x \mapsto \theta$
- $M_y \mapsto \phi$

It has to be noticed that the pseudo-Bode diagrams and the PSD criteria given in Figures 6.19 and 6.20 and 6.21 are not given over the whole range of magnitude whereas it should be, since the simulated dampers are nonlinear. Here the simulated sinusoidal ground disturbance had an amplitude of 5mm.

The following observations can be done from the pseudo-Bode diagrams and PSD criteria analysis:

High frequency comfort ($z_r \mapsto \ddot{z}_s$): the analysis of the results presented in Figure 6.19, 6.20 and 6.21 shows that the vehicle 5 (ADD) has the best high frequency comfort, from 2 to 20Hz. Then the vehicle 6, is very comfortable too. The vehicles 1, 3 and 4 are quite equivalent and less comfortable. The least comfortable vehicle is the vehicle 2.Therefore the two-state strategies improve the high frequency comfort of the vehicle, even compared to low-damped passive vehicles. The other controlled vehicles provide also a very satisfying high frequency comfort since it is equivalent to the one of the comfort-oriented low-damped vehicle 1.

Low frequency comfort ($z_r \mapsto z_s$): the active vehicle 3 is the most comfortable. Then the LPV continuously controlled vehicle 4 is almost as comfortable as the vehicle 3. It has to be noticed that the low-frequency comfort has been improved even compared to the comfort-oriented vehicle 1. The vehicles 5 (ADD) and 6 have also improved the comfort compared to the comfort-oriented vehicle, but the achieved performances are less satisfying. This criterion, which is the most important for comfort analysis,

underlines the interest of the proposed vehicle controller in terms of comfort.

Road-holding ($z_r \mapsto z_{us_1}$ and $z_r \mapsto z_{def_1}$): these two variables will be analyzed at the same time since the results are very similar. Both the pseudo-Bode diagrams and the PSD criteria given in Figures 6.19, 6.20 and 6.21 show that the vehicles 5 (ADD) and 6, equipped with switched two-state dampers provide the worst road-holding performances. Indeed the road-holding is even worst than the road-holding of the comfort-oriented low damped vehicle 1. However, the vehicle 6 has a more satisfying behavior in terms of deflection, compared to the semi-active vehicle. Furthermore the vehicles 3 and 4 do not provide a road-holding level as satisfying as the high-damped road-holding oriented vehicle 2 but, the achieved road-holding level is much better than the one of the comfort-oriented passive vehicle 1. Of course the semi-active one provides less performance than the active one.

Roll and pitch sensitivity ($M_x \mapsto \theta$ and $M_y \mapsto \phi$): The results for these two input-output relations are also very similar. The corresponding pseudo-Bode diagrams and PSD criteria show that the active vehicle 3 and the passive vehicle 2, with high damping rate, provide the best performance in terms of roll and pitch behaviors. These vehicles have the best performances compared to the others, in terms of road-holding, motivity and maneuverability since they are less sensitive than the others to roll and pitch angles for the same load transfer moments. Then, the vehicles 4 and 5 (LPV and ADD) provide almost the same level of performance, whereas the vehicles 1 and 6 (passive low damping rate and switched two-state) provide the less satisfying performances.

All these performances, summarized in Figure 6.21, show that the proposed LPV controller allows the vehicle to have improved comfort performances, even compared to a low damped passive vehicle, and road-holding performances much better than a comfort-oriented passive vehicle at the same time. As a consequence, the compromise between comfort and road-holding has been handled and overcome, thanks to the proposed vehicle controller. This performance level is not achievable with passive dampers. Therefore these results emphasize the interest of this control strategy for car manufacturers. Furthermore the gains of the weighting functions can be easily changed to adapt the behavior of the dampers to the expected behavior of the vehicle. Here the designed controller was comfort-oriented since the "Renault Laguna GT" car under study, equipped with passive mass-produced dampers, can be considered as a sport road-holding oriented car, having very poor comfort performances. It has also to be noticed that the developed two-state control strategy is also comfort-oriented. This could be easily modified by designing a more comfort-oriented active controller which is not possible with the

Acceleration Driven Damper. Therefore the proposed switched control strategy is also interesting to control two-state dampers. It has to be noticed that maximal and minimal damping rates of two-state dampers should be chosen by using some simulations and PSD analysis according to the expected vehicle behavior of the vehicle since they completely change the achieved performances. The maximal and minimal damping rates indeed can be adjusted by damper manufacturers by changing the valves inside the dampers.

6.6 Conclusion

The main contribution of this chapter is a complete and flexible suspension control design methodology. Indeed, both the performance of the closed-loop system, in terms of comfort and road-holding, and the abilities of the system, such as the achievable damper force range, or its bandwidth, can be simply specified by the designer.

A complete observer-based semi-active suspension control strategy has been proposed for a full vertical car equipped with industrial semi-active dampers. A solution has been developed both for continuously variable and two-state dampers. The proposed architecture relies on a vehicle observer, estimating on-line the state variables of a vehicle model. A high-level $\mathcal{H}_\infty$/LPV state-feedback vehicle controller computes the four damper force references. This allows to optimize comfort and road-holding of the vehicle while dealing with the damper abilities. The constraints on the actuator and the damper behavior are taken into account in the controller so that the on-line required damping rate remains semi-active through a simple scheduling strategy. Furthermore, each damper is controlled by a mixed $\mathcal{H}_\infty/\mathcal{H}_2$ LPV output-feedback controller, whose scheduling strategy is based on identified damper models allowing the controller to take the damper nonlinearities into account. Therefore the main contribution, compared to existing control strategies, is to provide a methodology to improve the performance while using few sensors, and solving many practical problems.

Some experimental results, obtained using a damper testing bench, have been described and emphasize the performance of the damper controller. Furthermore some simulation results show that the vehicle control strategy allows the suspension to optimize the behavior of the suspensions, and improves both the performance of the vehicle. For instance, the comfort can be improved without deteriorating the road-holding performances, or vice-versa, which is not possible with passive suspensions.

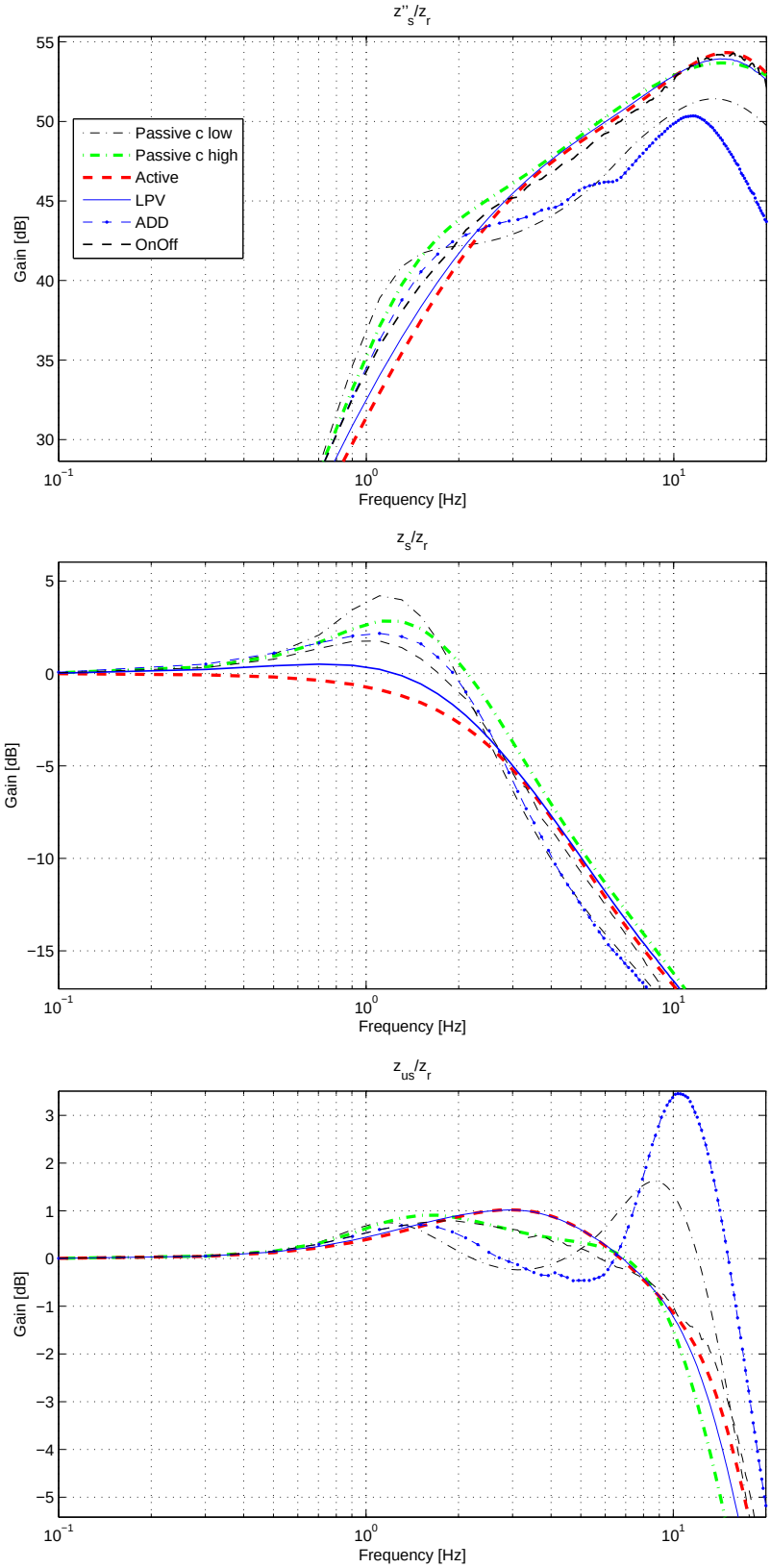

Figure 6.19: Pseudo-bode diagrams ($\ddot{z}_s$, z_s, z_{us}) (simulations)

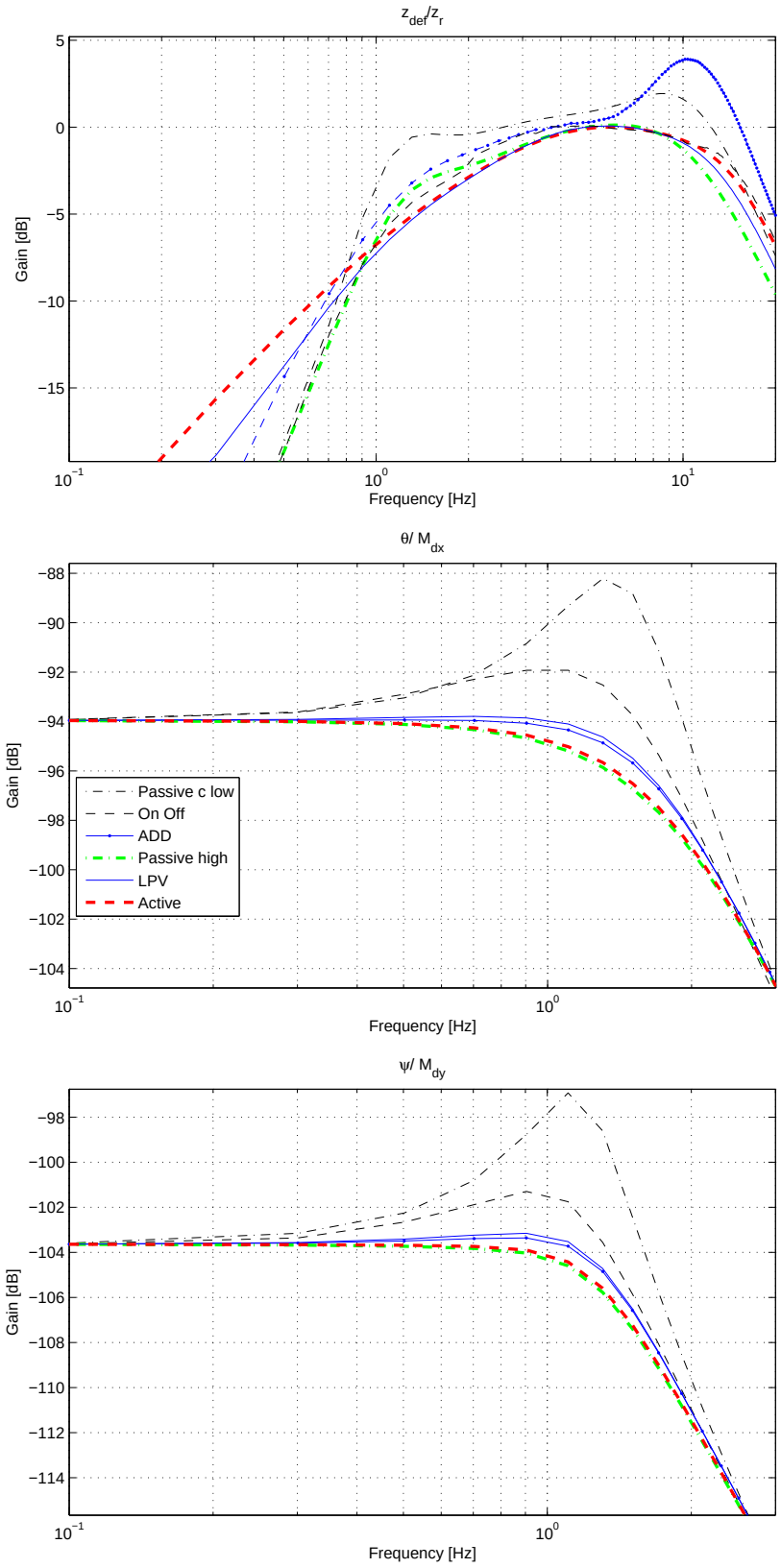

Figure 6.20: Pseudo-bode diagrams (z_{def}, θ, ϕ) (simulations)

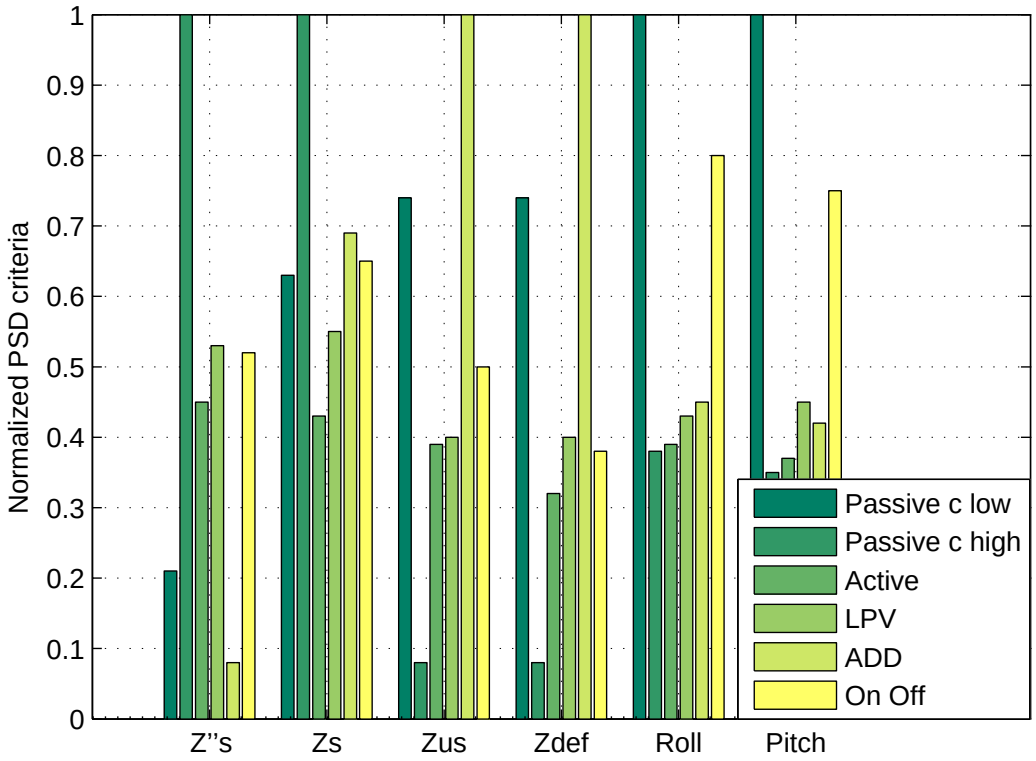

Figure 6.21: PSD criteria analysis (simulations)

Chapter 7

General conclusion and future works

7.0.1 Summary

Various topics have been studied to address the suspension control problem, such as theoretical tools, vehicle and damper models, observer design, or suspension controller design. A summary of the studied fields is given below:

- the main theoretical tools used in this thesis to design both controllers or observers have been recalled: LTI (Linear Time Invariant) and LPV (Linear Parameter Varying) systems, $\mathcal{H}_\infty$, $\mathcal{H}_2$ and mixed $\mathcal{H}_\infty/\mathcal{H}_2$ control synthesis, LPV control, pole placement in LMI regions and robustness analysis,

- the material resources, such as the testing bench, the car, or the semi-active damper have also been described. These resources have been used to run various experiments to analyze the damper behavior. An identified damper model has been proposed, based on the obtained experimental results. Finally, some well-known vehicle models, used both to control or estimate the real vehicle, have been presented,

- a methodology to design observers for vehicle estimation has been developed in order to estimate some non-measured variables, using a small number of sensors. This methodology has been applied to the vehicle and the synthesized observer has been tested experimentally using a SOBEN testing car. The experimental set-up and results are presented and analyzed. They emphasize the performance of the proposed observer,

- some performance criteria have been defined for the full-car. Then, a complete suspension control architecture including the observer, the damper controller and the vehicle controller, has been developed. Efficient controllers have been designed and tested using experiments or simulations in order to analyze their performance.

7.0.2 Contributions

This work aimed both at providing some methodological advances in suspension control, and carrying out transfers from academical research to industry. The main contributions rely on the following developments:

- **Damper models:**

  The proposed identified models can be used to represent the nonlinear dynamical behavior of many dampers. They also can be used for control or estimation purposes, since they are easily implementable in a real-time embedded application.

- **Vehicle estimation:**

  An observer design methodology has been proposed, allowing the suspension designer to build and adjust appropriate observers, estimating the non-measured variables. Various previous works on unknown input observers have been adapted to vehicle estimation. The developed methodology includes both the performance specifications in terms of unknown road disturbance decoupling, pole placement for implementation issues and measurement noise filtering. Therefore the proposed methodology is a complete observer tool allowing the suspension designer to overcome the main practical problems. This work led to some publications [Aubouet et al., 2009a, 2010].

- **Suspension control:**

  A complete suspension control design methodology has also been established. The previous results of Poussot-Vassal [2008], for semi-active suspension control, have been extended to the full vertical car, and completed with both a pole placement method, a scheduling strategy based on a damper model, and a local damper control. Indeed, the scheduling strategy has been improved using an identified damper model in order to take the real abilities of the damper into account. The expected behavior of the vehicle, for instance the roll movements, and the characteristics of the dampers, such as its bandwidth and force range, can be easily specified by the designer while following the proposed design methodology. Control solutions have been developed both for continuously

variable and switched two-state dampers, so that the most widespread types of dampers can be controlled. Finally, this methodology leads to taking the whole set of industrial constraints and technologies into account, and provides efficient and implementable controllers. This work also led to some publications [Aubouet et al., 2008, 2009b].

- **Programs and libraries:**

  The various programs and libraries resulting from this work form a complete tool that can be used by damper manufacturers to design efficient semi-active control strategies fulfilling the various specifications in terms of comfort and road-holding performance, available sensors, closed-loop bandwidth, damper abilities, robustness and measurement noise filtering.

7.0.3 Perspectives

Many perspectives can be considered to complete and improve this work. Here some possible issues are given:

Short-term perspectives

- study the performance of the vehicle controller in practice,
- design a reduced-order observer,
- discretize and implement the controllers ans observers on embedded Digital Signal Processing (DSP).

Long-term perspectives

- enhance the vehicle models while identifying the most important neglected nonlinearities, and take them into account in the controller synthesis,
- design a global attitude control strategy, including the braking and the steering system,

- design a predictive control strategy using some sensors to measure the road variations in front of the vehicle,

- develop a control strategy for a semi-active pneumatic suspension allowing to control both the damping and the stiffness,

- include a fault detection strategy. Indeed if one of the used sensors is not working anymore, the whole control strategy provides invalid control signals,

- include a supervision allowing the damping to be maximal in case of emergency.

Bibliography

E. Abdellahi, D. Mehdi, and M. M Saad. On the design of active suspension system by $\mathcal{H}_\infty$ and mixed $\mathcal{H}_2/\mathcal{H}_\infty$: An LMI approach. In *Proceedings of the American Control Conference*, pages 4041–4045, Chicago, U.S.A., june 2000.

J. Abedor, K. Nagpal, and K. Poola. Robust regulation with $\mathcal{H}_2$ performance. *System and Control Letters*, 23:431–443, 1994.

P. Apkarian, P. Gahinet, and G. Beker. Self-scheduled $\mathcal{H}_\infty$ control of linear parameter-varying systems: A design example. *Automatica*, 31(9):1251–1262, 1995.

S. Aubouet, L. Dugard, and O. Sename. $\mathcal{H}_\infty$/LPV observer for industrial semi-active suspension. In *Proceedings of the* IEEE *Multi-Conference on Systems and Control*, Saint-Petersburg, Russia, july 2009a.

S. Aubouet, L. Dugard, and O. Sename. Experimental results of an $\mathcal{H}_\infty$ observer for industrial semi-active suspension. In *Proceedings of the* IFAC *Symposium on Advances in Automotive Control (AAC)*, Munich, Germany, july 2010.

S. Aubouet, L. Dugard, O. Sename, C. Poussot-Vassal, and B. Talon. Semi-active $\mathcal{H}_\infty$/LPV control for an industrial hydraulic damper. In *Proceedings of the European Control Conference*, Budapest, Hungary, august 2009b.

S. Aubouet, O. Sename, B. Talon, C. Poussot-Vassal, and L. Dugard. Performance analysis and simulation of a new industrial semi-active damper. In *Proceedings of the* 17*th* IFAC *World Congress*, Seoul, Korea, july 2008.

R. Bambang, E. Shimemura, and K. Uchida. Mixed $\mathcal{H}_\infty/\mathcal{H}_2$ control with pole placement. In *Proceedings of the American Control Conference*, pages 2777–2779, 1993.

A. Ben-Israel and T.N.E. Greville. *Generalized inverses*. Springer-Verlag, 2003.

S. J. Benson, Y. Ye, and X. Zhang. Solving large-scale sparse semidefinite programs for combinatorial optimization. SIAM *Journal on Optimization*, 10:443–461, 1998.

S. Boyd, L. El Ghaoui, E. Feron, and V. Balakrishnan. *Linear Matrix Inequalities in System and Control Theory*, volume 15 of *Studies in Applied Mathematics*. SIAM, Philadelphia, PA, 1994. ISBN 0-89871-334-X.

M. Canale, M. Milanese, and C. Novara. Semi-active suspension control using "fast" model-predictive techniques. *IEEE Transactions on Control Systems Technology*, 14 (6):1034–1046, november 2006.

J. D. Carlson. What make a good MR fluid. *Journal of Intelligent Material Systems and Structures*, 13:431–435, 2003.

M. Chilali and P. Gahinet. $\mathcal{H}_\infty$ design with pole placement constraints: an LMI approach. *IEEE Transactions on Automatic Control*, 41(3):358–367, 1996.

M. Chilali, P. Gahinet, and P. Apkarian. Robust pole placement in LMI regions. IEEE *Transactions on Automatic Control*, 44(12):2257–2270, 1999.

S-B. Choia, H.K. Leea, and E.G. Chang. Field test results of a semi-active suspension system associated with skyhook controller. *Mechatronics*, 11(12):345–353, 2000.

P.G. Ciarlet. *Introduction à l'analyse numérique matricielle et à l'optimisation. (in French)*. 1998.

M. Darouach. Existence and design of functional observers for linear systems. IEEE *Transactions on Automatic Control*, 45(5):940–943, 2000.

M. Darouach, M. Zasadzinski, and S.J. Xu. Full-order observers for linear systems with unknown inputs. IEEE *Transactions on Automatic Control*, 39(3):606–609, 1994.

A. Do, J. J. Lozoya-Santos, L. Dugard, O. Sename, R. Morales-Menéndez, and R. A. Ramirez-Mendoza. Modelisation et commande LPV d'un amortisseur magnéto-rhéologique. In *Proceedings of the 6th Conference Internationale Francophone D'automatique (*CIFA 2010*)*, Nancy, France, June 2010a.

A. Do, O. Sename, and L. Dugard. An LPV control approach for semi-active suspension control with actuator constraints. In *Proceeding of the American Control Conference 2010*, Baltimore, U.S.A., 2010b.

J. C. Doyle. Analysis of feedback systems with structured uncertainties. IEE *Proceedings D (Control Theory and Applications)*, 129(6):242–250, november 1982.

J. C. Doyle, K. Zhou, K. Glover, and B. Bodenheimer. Mixed $\mathcal{H}_2$ and $\mathcal{H}_\infty$ performance objectives: optimal control. IEEE *Transactions on Automatic Control*, 39(8):1575–1587, 1994.

E. Eckermann. *World history of the automobile*. Society of Automotive Engineers, Inc., Warrendale,U.S.A., 2001. ISBN 0-7680-0800-X.

E. M. Elbeheiry, D. C. Karnopp, M. E. Elaraby, and A. M. Abdelraaouf. Suboptimal design of active and passive suspensions based on a full car model. *Vehicle System Dynamics*, 26:197–222, 1996.

E. Esmailzadeh and F. Fahimi. Optimal adaptive active suspensions for a full car model. *Vehicle System Dynamics*, 27:89–107, 1997.

M.K.H. Fan, A.L. Tits, and J.C. Doyle. Robustness in the presence of mixed parametric uncertainty and unmodeled dynamics. IEEE *Transactions on Automatic Control*, 36: 25–38, 1991.

I. Fialho and G. Balas. Road adaptive active suspension design using linear parameter varying gain scheduling. IEEE *Transactions on Control Systems Technology*, 10(1): 43–54, january 2002.

P. Gahinet and P. Apkarian. An linear matrix inequality approach to $\mathcal{H}_\infty$ control. *International Journal of Robust and Nonlinear Control*, 4(4):421–448, 1994.

P. Gaspar, I. Szaszi, and J. Bokor. Active suspension design using LPV control. In *Proceedings of the 1st* IFAC *Symposium on Advances in Automotive Control*, pages 584–589, Salerno, Italy, 2004.

P. Gaspar, I. Szaszi, and J.Bokor. Iterative model-based mixed $\mathcal{H}_\infty/\mathcal{H}_2$ control design. In *Proceedings of the* UKACC *international conference on control*, pages 652–657, Swansea, UK, 1998.

T. D. Gillepsie. *Fundamental of vehicle dynamics*. Society of Automotive Engineers, Inc., 1992. ISBN 978-1560911999.

N. Giorgetti., A. Bemporad., H. E. Tseng, and D. Hrovat. Hybrid model predictive control application towards optimal semi-active suspension. In *IEEE ISIE 2005*, Dubrovnik, Croatia, june 2005.

F. D. Goncalves and J. D. Carlson. Investigating the time dependence of the MR effect. *International Journal of Modern Physics B*, 21(28-29):4832–4840, August 2007.

S. Guo, S. Yang, and C. Pan. Dynamic modeling of magnetorheological damper behaviors. *Journal of Intelligent Material Systems and Structures*, 17(1):3–14, 2006.

J.K. Hedrick, R. Rajamani, and K. Yi. Observer design for electronic suspension applications. *Vehicle System Dynamics*, 23(6):413–440, 1994.

M. Hou and P. C. Muller. Disturbance decoupled observer design: A unified viewpoint. IEEE *Transactions on Automatic Control*, 32(6):1338–1341, june 1994.

L.Y. Hsu and T.L. Chen. Vehicle full-state estimation and prediction system using state observers. IEEE *Transactions on Vehicular Technology*, 58(6):2651–2662, 2009.

T. Iwasaki and R. E. Skelton. All controllers for the general $\mathcal{H}_\infty$ control problem: LMI existence conditions and state space formulas. *Automatica*, 30(8):1307–1317, 1994.

D.C. Karnopp. Semi-active control of wheel hop in ground vehicles. *Vehicle System Dynamics*, 12(6):317–330, 1983.

S. Kern. On the modeling and control of magneto-rheological dampers. Master's thesis, Grenoble INP - ENSIEG, GIPSA-lab (former LAG) & Tecnologico de Monterrey, 2008.

P.P. Khargonekar and M.A. Rotea. Mixed $\mathcal{H}_2/\mathcal{H}_\infty$ control: A convex optimization approach. *IEEE Transactions on Automatic Control*, 36(7):824–837, 1991.

D. Koenig. Observer design for unknown input nonlinear descriptor systems via convex optimization. IEEE *Transactions on Automatic Control*, 51(6):1047–1052, 2006.

D. Koenig, B. Marx, and D. Jacquet. Unknown input observers for switched nonlinear discrete time descriptor systems. IEEE *Transactions on Automatic Control*, 53(1): 373–379, 2008.

J. Lofberg. YALMIP: A toolbox for modeling and optimization in matlab. In *Proceedings of the CACSD Conference*, Taipei, Taiwan, 2004.

Lord. Lord website. technical report. `www.lord.com`, 2008.

J. J. Lozoya-Santos, R. Morales-Menendez, R. A. Ramirez-Mendoza, and E. Nino-Juarez. Frequency and current effects in a MR damper. *International Journal of Vehicle Autonomous Systems*, 7(3-4), 2009.

J. J. Lozoya-Santos, O. Sename, L. Dugard, R. Morales-Menéndez, and R. A. Ramirez-Mendoza. A semi-active control-oriented damper model for an automotive suspension. In *Proceedings of the* IFAC *Symposium Advances in Automotive Control (*AAC*)*, Munich, Germany, July 2010.

J. Lu. A frequency-adaptive multi-objective suspension control strategy. ASME *Journal of Dynamic Systems, Measurement and Control*, 126(3):700–707, 2004.

J. Lu and M. DePoyster. Multiobjective optimal suspension control to achieve integrated ride and handling performance. IEEE *Transactions on Control Systems Technology*, 10(6):807–821, 2002.

I. Masubuchi, A. Ohara, and N. Suda. LMI-based controller synthesis: A unified formulation and solution. In *Proceedings of the* IEEE *American Control Conference (*ACC*)*, pages 3473–3477, Seattle, Washington, USA, 1995.

W. F. Miliken and D. L. Miliken. *Race Car Vehicle Dynamics*. Society of Automotive Engineers, Inc., 1995. ISBN 978-1560915263.

X. Moreau. *La dérivation non entière en isolation vibratoire et son application dans le domaine de l'automobile. La suspension* CRONE *: du concept à la réalisation*. PhD thesis (in french), Université de Bordeaux I, 1995.

X. Moreau, A. Rizzo, and A. Oustaloup. Application of the crone control-design method to a low frequency active suspension system. *International Journal of Vehicle Autonomous Systems*, 7(3-4), 2009.

Y. Nesterov and A. Nemirovskii. *Interior Point Polynomial Algorithms in Convex Programming*. Studies in Applied Mathematics 13. SIAM, 1994. ISBN 978-0-898715-15-6.

A. Oustaloup and B. Mathieu. *La commande* CRONE. Hermes science publications, 1999. ISBN 2746200430.

A. Oustaloup, X. Moreau, and M. Nouillant. The CRONE suspension. *Control Engineering Practice*, 4(8):1101–1108, 1996.

A. Packard and J.C. Doyle. The complex structured singular value. *Automatica*, 29: 71–109, 1994.

C. Poussot-Vassal. *Robust Multivariable Linear Parameter Varying Automotive Global Chassis Control*. PhD thesis (in english), Grenoble INP, GIPSA-lab, Control System dpt., Grenoble, France, September 2008.

C. Poussot-Vassal, O. Sename, L. Dugard, P. Gaspar, Z. Szabo, and J. Bokor. A new semi-active suspension control strategy through LPV technique. *Control Engineering Practice*, 16(12):1519–1534, december 2008.

C. Poussot-Vassal, O. Sename, L. Dugard, R. Ramirez-Mendoza, and L. Flores. Optimal skyhook control for semi-active suspensions. In *Proceedings of the 4th IFAC Symposium on Mechatronics Systems*, pages 608–613, Heidelberg, Germany, 2006.

R. Rajamani and J.K. Hedrick. Adaptive observers for active automotive suspensions: theory and experiment. IEEE *Transactions on Control Systems Technology*, 3(1): 86–93, 1995.

R. K. Rajput. *A textbook of automobile engineering*. Laxmi Publications LTD, New Dehli, India, 2007.

C. Rossi and G. Lucente. $\mathcal{H}_\infty$ control of automotive semi-active suspensions. In *Proceedings of the 1st* IFAC *Symposium on Advances in Automotive Control (AAC)*, pages 578–583, Salerno, Italy, 2004.

M. A. Rotea. The generalized $\mathcal{H}_2$ control problem. *Automatica*, 29:373–385, 1993.

M. G. Safonov. $\mathcal{L}_\infty$ optimal sensitivity vs. stability margin. In *Proceedings of the Conference on Decision and Control*, San Antonio, Texas, 1983.

D. Sammier. *Sur la modélisation et la commande de suspensions de véhicules automobiles*. Phd thesis, Institut National Polytechnique de Grenoble, 2001.

D. Sammier, O. Sename, and L. Dugard. Skyhook and $\mathcal{H}_\infty$ control of semi-active vehicle suspensions: some practical aspects. *Vehicle System Dynamics*, 39(4):279–308, april 2003.

S. M. Savaresi, E. Siciliani, and S. Bittanti. Acceleration driven damper: an optimal control algorithm for comfort oriented semi-active suspensions. ASME *Transactions: Journal of Dynamic Systems, Measurements and Control*, 127(2):218–229, 2005.

S. M. Savaresi and C. Spelta. Mixed sky-hook and ADD: Approaching the filtering limits of a semi-active suspension. ASME *Transactions: Journal of Dynamic Systems, Measurements and Control*, 129(4):382–392, 2007.

S.M. Savaresi, C. Poussot-Vassal, C. Spelta, O. Sename, and L. Dugard. *Semi-Active Suspension Control Design for Vehicles*. Elsevier, 2010.

C. Scherer, P. Gahinet, and M. Chilali. Multiobjective output-feedback control via LMI optimization. IEEE *Transactions on Automatic Control*, 42(7):896–911, july 1997.

C. Scherer and S. Weiland. LMI *in control (lecture support, DELFT University),* `www.dcsc.tudelft.nl/∼cscherer/lmi.html`. 1999.

C.W. Scherer. An efficient solution to multi-objective control problems with LMI objectives. *System and Control Letters*, 40:43–57, 2000.

G. Scorletti. *An introduction to the* LMI *optimization in Automatic Control (in French)*. 2004.

S. Skogestad and I. Postlethwaite. *Multivariable Feedback Control: Analysis and Design*. John Wiley and Sons, 2005.

C. Spelta. *Design and applications of semi-active suspension control systems*. Phd thesis, Politecnico di Milano, dipartimento di Elettronica e Informazione, Milano, Italy, 2008.

G. Stein and J.C. Doyle. Beyond singular values and loop shapes. *Journal of Guidance and Control*, 14:5–16, 1991.

J. F. Sturm. Using sedumi 1.02, a MATLAB toolbox for optimization over symmetric cones, 1998.

R.H.C. Takahashi, J.F. Camino, D.E. Zampieri, and P.L.D. Peres. A multiobjective approach for $\mathcal{H}_2$ and $\mathcal{H}_\infty$ active suspension control. In *Proceedings of the American Control Conference*, pages 48–52, Philadelphia, U.S.A., june 1998.

C. C. Tsui. A new design approach to unknown input observers. IEEE *Transactions on Automatic Control*, 41(3):464–468, 1996.

H. D. Tuan, P. Apkarian, and S. Hosoe. Nonlinear $\mathcal{H}_\infty$ control for an integrated suspension system via parametrized linear matrix inequality characterizations. IEEE *Transactions on Control Systems Technology*, 9(1):175–185, 2001.

M.E. Valcher. State observer for discrete-time linear systems with unknown inputs. IEEE *Transactions on Automatic Control*, 44(2):397–401, 2000.

J. Y. Wong. *Theory of ground vehicles*. 3rd edition. Wiley-Interscience, 2001. ISBN 978-0471354611.

K. Yi. Design of disturbance decoupled bilinear observers. *KSME Journal*, 9(3):344–350, 1995.

K. Yi and B. Suk Song. Observer design for semi-active suspension control. *Vehicle System Dynamics*, 32(2-3), 1999.

P. M. Young, Matthew P. Newlin, and John C. Doyle. Let's get real. In *In Robust Control Theory, IMA Proceedings*, pages 143–173. Springer Verlag, 1995.

K. Zhou, J. Doyle, and K. Glover. *Robust optimal control*. Prentice Hall, Upper Saddle River, New Jersey, 1996.

A. Zin. *Sur la commande robuste de suspensions automobiles en vue du contrôle global de chassis*. Phd thesis, Institut National Polytechnique de Grenoble, Grenoble, France, 2005.

A. Zin, O. Sename, P. Gaspar, L. Dugard, and J. Bokor. Robust LPV-$\mathcal{H}_\infty$ control for active suspensions with performance adaptation in view of global chassis control. *Vehicle System Dynamics*, 46(10), 2008.

A. Zin, O. Sename, P. Gaspar, L. Dugard, and J.Bokor. An $LPV/\mathcal{H}_\infty$ active suspension control for global chassis technology: Design and performance analysis. In *Proceedings of the IEEE American Control Conference*, pages 584–589, Minneapolis, USA, june 2006.

Résumé:

Les travaux présentés dans cette thèse concernent la modélisation, la commande et l'estimation de suspensions automobiles semi-actives, dans un contexte industriel. La contribution principale concerne le développement d'une méthodologie de synthèse d'observateurs et de contrôleurs adaptés aux suspensions semi-actives. Fondée sur un observateur, un contrôleur principal et quatre contrôleurs locaux, la stratégie de commande permet d'améliorer le confort et la tenue de route du véhicule. La méthode de synthèse $\mathcal{H}_\infty$ appliquée aux systèmes Linéaires à Paramètres Variants (LPV) est utilisée pour la commande des amortisseurs, permettant ainsi de prendre en compte leurs non linéarités dans la synthèse. Différents résultats de simulation et expérimentaux sont présentés pour valider l'observateur et les lois de commande.

Mots-clefs:

Amortisseurs non linéaires semi-actifs, suspensions automobiles, observateurs, commande robuste, approche $\mathcal{H}_\infty$, systèmes linéaires à paramètres variants.

Abstract:

This thesis deals with the modeling, control and estimation of semi-active automotive suspensions in an industrial framework. The main contribution is a complete observer and controller design methodology suitable for semi-active suspensions control. Based on an observer, a main controller, and four local controllers, the proposed strategy allows optimize the comfort and road-holding of the vehicle. The $\mathcal{H}_\infty$ synthesis method, applied to Linear Parameter Varying (LPV) systems is used for the damper control, allowing to take their nonlinearities into account in the synthesis. Various experimental and simulation results are given both for the observer, and for the controllers.

Keywords:

Nonlinear semi-active damper, automotive suspensions, observers, robust control, $\mathcal{H}_\infty$ approach, linear parameter varying systems.